

Assembly of Molecular Machines in the Chloroplast

Dissertation

Zur Erlangung des Doktorgrades
der Naturwissenschaften (Dr. rer. nat.)



der Fakultät für Biologie
der Ludwig-Maximilians-Universität München

Vorgelegt von

Bennet Reiter

München, März 2020

1. Gutachter:	PD Dr. Thilo Rühle
2. Gutachter:	Prof. Dr. Jörg Nickelsen
Tag der Abgabe:	31.03.2020
Tag der mündlichen Prüfung:	15.07.2020

Eidesstattliche Erklärung:

Ich versichere hiermit an Eides statt, dass die vorgelegte Dissertation von mir selbstständig und ohne unerlaubte Hilfe angefertigt wurde. Des Weiteren erkläre ich, dass ich nicht anderweitig ohne Erfolg versucht habe, eine Dissertation einzureichen oder mich der Doktorprüfung zu unterziehen. Die folgende Dissertation liegt weder ganz noch in wesentlichen Teilen einer anderen Prüfungskommission vor.

Bennet Reiter

München, 31.03.2020

Statutory Declaration:

I declare that I have authored this thesis independently, that I have not used other than the declared sources/resources. Furthermore, I declare that I have not submitted a dissertation without success or failed to pass the oral examination. The present dissertation (neither the entire dissertation nor parts) has not been presented to another examination board.

Bennet Reiter

Munich, 31.03.2020

Contents

Abbreviations.....	VI
Publications and manuscripts originating from this thesis.....	VII
Contributions to publications and manuscripts presented in this thesis.....	VIII
Summary.....	XI
Zusammenfassung.....	XII
1 Introduction.....	1
1.1 Consequences of green endosymbiosis.....	1
1.2 The chloroplast ATP synthase.....	3
1.3 Biogenesis of the chloroplast ATP synthase.....	4
1.4 Chloroplast ribosomes.....	7
1.5 Biogenesis of chloroplast ribosomes.....	8
1.6 Identification of chloroplast auxiliary components.....	11
1.7 Aims of the thesis.....	12
2 The Arabidopsis Protein CGLD11 is Required for Chloroplast ATP Synthase Accumulation.....	13
3 CGL160 Mediates the Connection of the Chloroplast ATP Synthase Modules F ₁ and F ₀	29
4 The Arabidopsis Protein CGL20 is Required for Plastid 50S Ribosome Biogenesis.....	55
5 Chlorophyll fluorescence video imaging: A versatile tool for identifying factors related to photosynthesis.....	73
6 Discussion.....	87
6.1 Identification of auxiliary biogenesis factors.....	87
6.2 Assembly of organellar ATP synthases.....	88
6.2.1 CGLD11 is required for early CF ₁ assembly.....	88
6.2.2 CGL160 acquired a central role in the assembly of CF ₀ and linkage to CF ₁	89
6.2.3 ATP synthase regulation by night.....	91
6.3 Assembly of chloroplast ribosomes.....	93
6.3.1 Consequences of chloroplast-to-nucleus gene transfer.....	93
6.3.2 CGL20 is required for late assembly steps of chloroplast LSU.....	94
6.3.3 Adaptations to membrane targeting.....	95
6.4 Conclusion and future perspectives.....	97
References for Chapters 1 and 6.....	98
Supplemental information – Chapter 2.....	108
Supplemental information – Chapter 3.....	116

Supplemental information – Chapter 4.....	122
Danksagung	131
Curriculum Vitae	133

Abbreviations

aa	amino acid
At	<i>Arabidopsis thaliana</i>
ATP	adenosine-5'-triphosphate
BN	blue native
CDS	coding sequence
Chl	chlorophyll
CGL	conserved only in the green lineage
CGLD	conserved in the green lineage and diatoms
cpATP synthase	chloroplast ATP synthase
C-terminus	carboxy terminus
cTP	chloroplast transit peptide
DNA	deoxyribonucleic acid
ECS	electrochromic shift
EM	electron microscopy
F ₁	coupling factor 1
F _o	coupling factor oligomycin
FC	fold change
F _v /F _m	photosystem II maximum quantum efficiency
kD	kilo-daltons (atomic mass unit)
LC-MS/MS	liquid chromatography-coupled tandem mass-spectrometry
LSU	large ribosomal subunit
NPQ	non-photochemical quenching
N-terminus	amino terminus
nts	nucleotides
PAGE	polyacrylamide gel electrophoresis
<i>pmf</i>	proton motive force
PSRP	plastid specific ribosomal protein
qE	energy dependent quenching
RNA	ribonucleic acid
RP	ribosomal protein
rRNA	ribosomal RNA
SDS	sodium dodecyl sulfate
SSU	small ribosomal subunit

Publications and manuscripts originating from this thesis

Chapter 2

Grahl S*, **Reiter B***, Gügel ILL, Vamvaka E, Gandini C, Jahns P, Soll J, Leister D, Rühle T (2016) The Arabidopsis Protein CGLD11 is Required for Chloroplast ATP Synthase Accumulation. *Mol Plant* **9**: 885–899

* Authors contributed equally

Chapter 3

Reiter B, Rosenhammer L, Marino G, Leister D, Rühle T (2020) CGL160 mediates the connection of the chloroplast ATP synthase modules F₁ and F₀. Manuscript

Chapter 4

Reiter B, Vamvaka E, Marino G, Kleine T, Jahns P, Bolle C, Leister D, Rühle T (2020) The Arabidopsis Protein CGL20 is Required for Plastid 50S Ribosome Biogenesis. *Plant Physiol* **182**: 1222-1238

Chapter 5

Rühle T, **Reiter B**, Leister D (2018) Chlorophyll fluorescence video imaging: A versatile tool for identifying factors related to photosynthesis. *Front Plant Sci* **9**: 55

Contributions to publications and manuscripts presented in this thesis

Chapter 2:

S. Grahl performed organelle isolation and localization experiments, measured chloroplast/mitochondrial ATP synthase activity, and generated the CGLD11 antibody. B. Reiter performed semi-quantitative RT-PCR, RNA gel-blot analysis (Master Thesis, Reiter, 2015), polysome loading experiments (Master Thesis, Reiter, 2015), salt-wash experiments (Master Thesis, Reiter, 2015), BN-PAGE analysis, comigration analysis, and yeast two-hybrid interaction assays. I. L. Gügel performed ultra-structure analysis. E. Vamvaka performed transcription run-on assays. C. Gandini and S. Grahl performed in vivo labeling. P. Jahns performed pigment analysis. T. Rühle and S. Grahl identified the mutants. T. Rühle performed chloroplast/mitochondrial BN-PAGE analysis, PAM measurements, and immunotitration experiments. The study was conceived and supervised by J. Soll, D. Leister and T. Rühle. The manuscript was prepared by S. Grahl, B. Reiter, J. Soll, D. Leister and T. Rühle with contributions from all other authors.

Chapter 3:

B. Reiter analyzed the mutant lines, generated the AtCGL160 antibody, performed phylogenetic analysis, chlorophyll fluorescence and ECS measurements, immunotitration, native-gel assembly and comigration experiments, coimmunoprecipitation and supervised yeast two-hybrid experiments. L. Rosenhammer analyzed mutant lines, performed membrane orientation and yeast-two-hybrid-experiments. G. Marino performed the LC-MS/MS run and analyzed the data. The study was conceived by B. Reiter and T. Rühle. The manuscript was prepared by B. Reiter and T. Rühle. The study was supervised by D. Leister and T. Rühle.

Chapter 4:

B. Reiter performed localization experiments, transcriptomics and proteomics sample preparation, PAM measurements, cold treatment, in vivo labeling, polysome analysis, RNA gel-blot analysis and comigration analysis. E. Vamvaka created and analyzed the mutant and complementation lines. G. Marino performed LC-MS/MS runs and data analysis, T. Kleine performed RNA-seq data analysis, P. Jahns performed pigment analysis, C. Bolle identified the mutants. T. Rühle performed BN-PAGE and immunotitration experiments, MapMan analysis and phylogenetic analysis. The study was conceived and supervised by D. Leister and T. Rühle. The manuscript was prepared by B. Reiter and T. Rühle with contributions from all other authors.

Chapter 5:

T. Rühle prepared the figures. T. Rühle, B. Reiter, and D. Leister wrote the article.

We hereby confirm the above statements:


Bennet Reiter

Thilo Rühle

Chapter 2:

Initial characterization of mutant lines was performed by Sabine Bowman-Grahl and Thilo Rühle independently. Sabine Bowman-Grahl generated the CGLD11 antibody that was used throughout the whole study. Additionally, Sabine Bowman-Grahl established that CGLD11 is present in chloroplasts and mitochondria, but only chloroplast ATP synthase activity was diminished. Bennet Reiter analyzed the biogenesis of the chloroplast ATP synthase and could show that CGLD11 is required for posttranslational assembly steps by physical interaction with the β -subunit. Hence, both Sabine Bowman-Grahl and Bennet Reiter contributed significantly to the identification of a novel chloroplast ATP synthase CF₁ assembly factor.

We hereby confirm the above statements:



Sabine Bowman-Grahl



Bennet Reiter

Summary

Chloroplasts arose as a result of the acquisition of a cyanobacterial endosymbiont by a eukaryotic host. The transformation of autonomous prokaryotes into specialized photosynthetic organelles, tightly integrated within the context of the eukaryotic cell, has been accompanied by numerous structural and regulatory adaptations. Consequently, new auxiliary proteins evolved to ensure rapid biogenesis of the organellar complexome. In this thesis, two factors required for the chloroplast ATP synthase (cpATP synthase) and one factor for the chloroplast 70S ribosome assembly process were characterized.

CGLD11 is a soluble protein of about 33 kD and could be localized in chloroplasts and mitochondria of *Arabidopsis*. *Cgld11* mutants were growth impaired and accumulated about 20-30% of cpATP synthase, whereas other chloroplast complexes were virtually unaffected. In addition, the loss of CGLD11 impaired cpATP synthase activity but did not affect mitochondrial ATP production. CGLD11 physically interacted with chloroplast and mitochondrial β -subunits in yeast. Thus, a role for CGLD11 in chloroplast F_1 assembly was suggested, whereas its function in mitochondria might not be essential.

The membranous domain of CGL160 in *Arabidopsis* (AtCGL160), which shows sequence similarity to the bacterial F_0 biogenesis factor Atp1/Unc1, was previously shown to be required for c-ring assembly in chloroplasts. Here it could be shown that the N-terminal soluble domain has a distinct function in cpATP synthase biogenesis, since its deletion led to reduced subunit accumulation and diminished proton conductivity of the thylakoid membrane. AtCGL160 was associated with the cpATP synthase holo-complex and the stromal N-terminus specifically interacted with the membrane-proximal domain of CF_1 - β . Therefore, a central role for AtCGL160 in the assembly of the chloroplast ATP synthase by facilitating c-ring formation and joining of CF_1 to CF_0 was suggested.

Compared to AtCGLD11 or AtCGL160, deletion of AtCGL20 caused a more general disruption in chloroplast biogenesis. *Arabidopsis* plants lacking AtCGL20 proteins displayed a virescent leaf phenotype, were severely growth-retarded under ambient, and growth-arrested under low temperature. Absence of AtCGL20 resulted in reduced chloroplast translational efficiency, impaired post-maturation processing of the 23S rRNA, and abnormal accumulation of 50S ribosomal proteins in the high molecular weight fraction of stromal extracts. Since AtCGL20 was associated to 50S particles in an RNase insensitive manner, an involvement in late assembly steps of the chloroplast large ribosomal subunit was proposed.

Taken together, the factors presented in this work are examples of how the assembly of conserved chloroplast complexes has been adapted to the structural and regulatory specialization of the endosymbiont on photosynthesis and may thus help to elucidate the underlying mechanisms of organellar multi-subunit complex formation.

Zusammenfassung

Chloroplasten entstanden als Folge des Erwerbs eines cyanobakteriellen Endosymbionten durch einen eukaryotischen Wirt. Die Umwandlung von autonomen Prokaryoten in spezialisierte photosynthetische Organellen, die eng in den Kontext der eukaryotischen Zelle integriert sind, wurde von zahlreichen strukturellen und regulatorischen Anpassungen begleitet. Infolgedessen entstanden neue Hilfsproteine, um eine effiziente Biogenese der Organellen-Komplexe zu gewährleisten. Im Rahmen dieser Arbeit wurden zwei Faktoren für die Assemblierung der Chloroplasten-ATP-Synthase (cpATP-Synthase) und ein Assemblierungsfaktor für chloroplastidäre 70S-Ribosomen charakterisiert.

CGLD11 ist ein lösliches 33 kD schweres Protein, welches in Chloroplasten und Mitochondrien von Arabidopsis lokalisiert werden konnte. *Cgld11*-Mutanten waren wachstumsbeeinträchtigt und akkumulierten etwa 20-30% der cpATP-Synthase-Wildtypmenge, wohingegen andere Chloroplastenkomplexe praktisch unverändert blieben. Darüber hinaus beeinträchtigte der Verlust von CGLD11 die cpATP-Synthase-Aktivität, während die mitochondriale ATP-Generierung nicht verringert war. CGLD11 zeigte eine direkte Interaktion mit der chloroplastidären und mitochondrialen β -Untereinheit in Hefe. Daher wurde eine Rolle für CGLD11 bei der Chloroplasten- F_1 -Assemblierung vorgeschlagen, während seine Funktion in Mitochondrien möglicherweise nicht essenziell ist.

Die Membrandomäne von CGL160 in Arabidopsis (AtCGL160), die Sequenzähnlichkeit mit dem bakteriellen F_0 -Biogenesefaktor Atp1/Unc1 aufweist, wird für die Bildung von c-Ringen in Chloroplasten benötigt. Hier konnte gezeigt werden, dass die N-terminale lösliche Domäne eine spezifische Funktion in der cpATP-Synthase-Biogenese hat, da ihre Abwesenheit zu einer verringerten Anreicherung von Untereinheiten und zu einer verminderten Protonenleitfähigkeit der Thylakoidmembran führte. AtCGL160 war mit dem cpATP-Synthase-HoloKomplex assoziiert und der stromale N-Terminus interagiert spezifisch mit der membran-nahen Domäne von $CF_1\text{-}\beta$. Daher wurde eine zentrale Rolle für AtCGL160 in der Assemblierung der Chloroplasten-ATP-Synthase vorgeschlagen, in der AtCGL160 sowohl die c-Ring-Bildung als auch die Zusammenführung von CF_1 mit CF_0 unterstützt.

Im Vergleich zu AtCGLD11 oder AtCGL160 verursachte die Deletion von AtCGL20 eine allgemeine Beeinträchtigung der Chloroplasten-Biogenese. Arabidopsis-Pflanzen, denen AtCGL20-Proteine fehlten, zeigten einen vireszenten Blattphänotyp, waren bei Umgebungstemperatur stark wachstumsverzögert und das Wachstum wurde bei niedrigen Temperaturen gestoppt. Verlust von AtCGL20 führte zu einer verminderten chloroplastidären Translationseffizienz, zu einer beeinträchtigten Prozessierung der 23S rRNA und zu einer abnormalen Anreicherung von ribosomalen 50S-Proteinen in der hochmolekularen Fraktion stromaler Extrakte. Da AtCGL20 in einer RNase-unempfindlichen Weise mit 50S-Partikeln

assoziiert war, wurde eine Beteiligung an späten Assemblierungsschritten der großen ribosomalen Untereinheit in Chloroplasten vorgeschlagen.

Zusammenfassend sind die in dieser Arbeit vorgestellten Faktoren Beispiele dafür, wie die Biogenese konservierter Chloroplastenkomplexe an die strukturelle und regulatorische Spezialisierung des Endosymbionten auf die Photosynthese angepasst wurde, und können somit zur Aufklärung der zugrunde liegenden Mechanismen der Bildung von Multi-Untereinheit-Komplexen in Organellen beitragen.

1 Introduction

1.1 Consequences of green endosymbiosis

The ability to convert solar into chemical energy was one of the key inventions in the evolution of life (Hohmann-Marriott and Blankenship, 2011). Postulated the first time in 1905 by Mereschkowsky (Martin and Kowallik, 1999), it is now widely accepted that chloroplasts share one common ancestor with cyanobacteria that was engulfed by a eukaryotic cell more than 1 billion years ago in a process called primary endosymbiosis (reviewed in Archibald, 2015). Three major lineages arose from the “Archaeplastida”: Glaucophytes, Rhodophytes and Chloroplastida. The latter, with over 350.000 species the most diverse group, comprises Chlorophytes (Green algae) and Streptophytes that gave rise to land plants (Embryophytes) and is also called the “green lineage” (de Vries et al., 2016). The transformation from free-living autotrophic cells to specialized organelles was accompanied by substantial adaptations (Fig. 1; reviewed in Jensen and Leister, 2014). Early in the evolution of Archaeplastida, most of the former cyanobacterial genes were either lost or transferred to the host nucleus, presumably by the need for genetic control over the endosymbiont (Timmis et al., 2004). The majority of the ~3000 plastid-localized proteins must be imported post-translationally, with the help of N-terminal targeting sequences and an intricate protein import machinery (reviewed in Bölter and Soll, 2016). Plastids of higher plants retained around 100 protein-coding genes, which are mostly essential for photosynthesis or the endogenous plastid gene expression machinery and may represent a core set of genes that are subjected to an immediate regulatory redox control in response to changing environmental conditions (Allen, 2015). Moreover, redox control by post-translational cysteine modification plays a crucial role in the regulation of chloroplast function dependent on the light-driven generation of reduction equivalents (reviewed in Cejudo et al., 2019). Finally, chloroplasts underwent substantial structural adaptations, such as the loss of most respiratory complexes (Renato et al., 2015), the establishment of novel light harvesting antennae (reviewed in Ruban, 2014), or the rearrangement of the thylakoid membrane system to form grana stacks (reviewed in Pribil et al., 2014; Rast et al., 2015). Although the bacterial ancestry of chloroplast multi-protein complexes is apparent on the structural level, their biogenesis often differs markedly from that of bacteria because the dual genetic origin of their component requires a different mode of spatial and temporal orchestration of gene expression and assembly (Kleine and Leister, 2016). Hence, identification and characterization of new auxiliary components is crucial for understanding how cells have adapted to ensure rapid biogenesis of their organellar

complexome. In this thesis, the assembly of two ubiquitous non-pigment-containing chloroplast complexes is investigated, the thylakoid F-type ATP synthase and the chloroplast 70S ribosome.

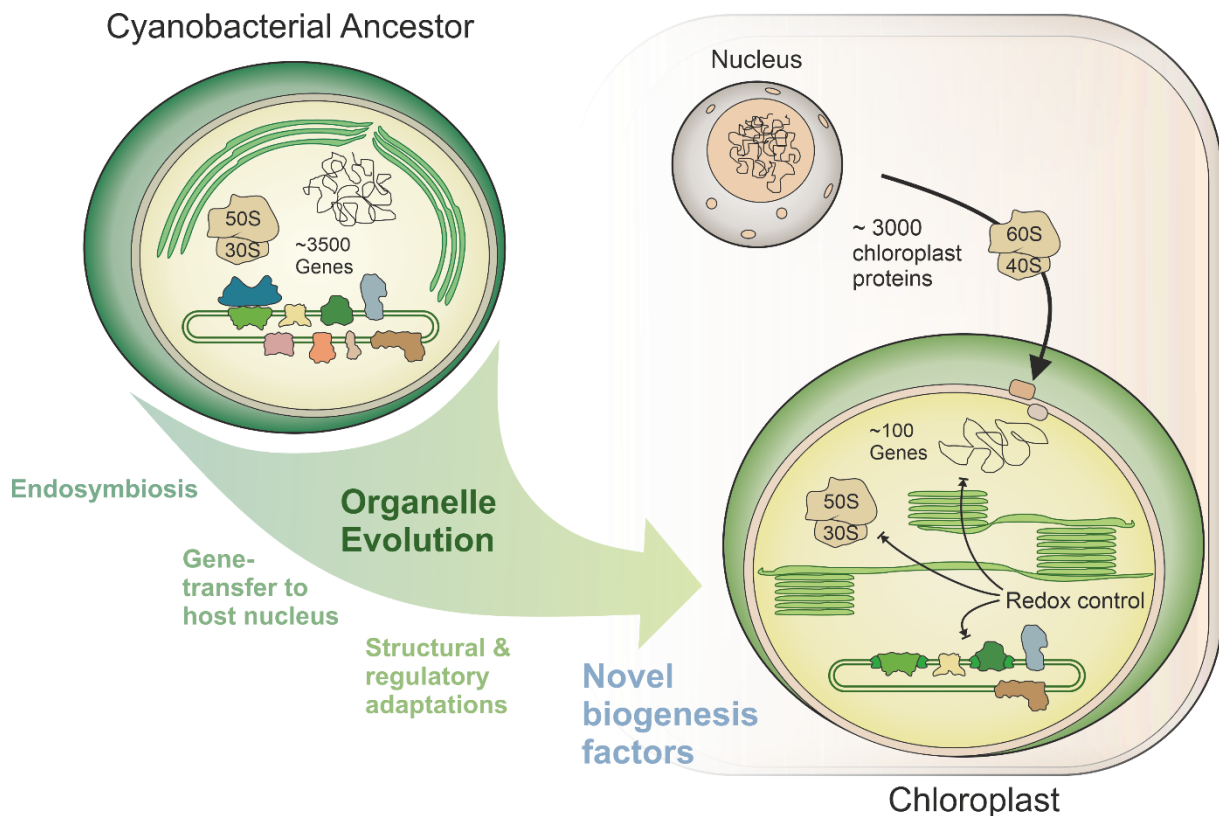


Figure 1. Consequences of green endosymbiosis. Schematic overview of the major events that may have led to adaptations in chloroplast biogenesis and acquisition of novel biogenesis factors: Most of the former cyanobacterial genes (about 3500) were either lost or transferred to the host nucleus. The majority of the ~3000 plastid-localized proteins are translated in the cytosol by 80S ribosomes and imported into the organelle. Chloroplasts of higher plants retained around 100 protein-coding genes. Structural and regulatory adaptations compared to cyanobacteria include the loss of most respiratory complexes, exchange of phycobilisomes by light harvesting complexes, acquisition of thylakoid grana stacking, and establishment of a stromal redox-regulatory system.

1.2 The chloroplast ATP synthase

F-type ATP synthases convert electrochemical potentials across membranes into chemical energy in bacteria, mitochondria, and chloroplasts. Their basic architecture is conserved and comprised of a membrane-embedded subcomplex F_o and a soluble bulky F_1 head. The chloroplast ATP synthase (cpATP synthase) utilizes the transthylakoid proton motive force (pmf) generated by the light-driven reactions of photosynthesis to convert ADP and phosphate to ATP. As a result of its protruding head, accumulation of the cpATP synthase is restricted to the non-appressed thylakoid regions and grana margins (Daum et al., 2010). The cpATP synthase is structurally similar to its bacterial ancestor (Fig. 2). Both enzymes consist of an $\alpha\beta$ -heterotrimer and a peripheral stator ab_2 that are connected via the δ -subunit. They constitute the stationary part of the ATP synthase that encloses the rotary proteolipidic c-oligomer (c_{10-15}), which is non-covalently connected to the central stalk $\gamma\epsilon$. Protons enter the rotor at a luminal a/c-interface and stay attached to the c-subunit for almost a complete rotation before they exit the membrane at the second a/c-interface (von Ballmoos et al., 2009; Okuno et al., 2011; Hahn et al., 2018). The generated torque of the γ -subunit against the stationary $\alpha_3\beta_3$ -head leads to different alternating conformations in the β -subunit (open, tight, loose), resulting in the generation of three molecules of ATP per 360° rotation of the rotor (Boyer, 1993; Junge and Nelson, 2015). The chloroplast c-ring consists of 14 subunits compared to (non-photosynthetic) bacterial c_{10} oligomers, shifting the theoretical ATP/translocated proton-ratio from ~3.33 (c_{10}) to ~4.67 (c_{14}). Moreover, cyanobacteria and chloroplasts possess two genetically distinct b-subunits (Westhoff et al., 1985). Neither b' nor b seem to be able to compensate for the loss of the other in Arabidopsis, as their respective knockouts or knockdowns led to a dramatic loss of cpATP synthase content (Kong et al., 2013; Yap et al., 2015). Bacterial ϵ -subunits are able to reach into the $\alpha\beta$ -heterotrimer (Fig. 2), thus inhibiting wasteful ATP hydrolysis (Kato-Yamada et al., 1999). Such a mechanism was also proposed for chloroplasts (Cruz et al., 1995; Shi et al., 2001; Nowak et al., 2002; Nowak and McCarty, 2004), but no ϵ -subunit in an auto-inhibitory conformation could be identified in recent high-resolution structures, suggesting a different mechanism for chloroplast ATP hydrolysis inhibition (Fig. 2; Hahn et al., 2018). Chloroplasts possess a conserved auto-inhibitory loop of the γ -subunit that is coupled to the redox state of the chloroplast stroma via thiol modification of a disulfide bond (Arana and Vallejos, 1982; Nalin and McCarty 1984; Hahn et al., 2018). This mechanism essentially accounts for inhibition of ATP hydrolysis during prolonged times of darkness but may also play a role in steady-state adjustment of ATP synthase activity in the light (Jagendorf, 2002; Kanazawa et al., 2017). Finally, the cpATP synthase is subjected to other post-translational modifications including phosphorylation and acetylation, which were shown to affect its stability and nucleotide affinity (Schmidt et al., 2013; 2017).

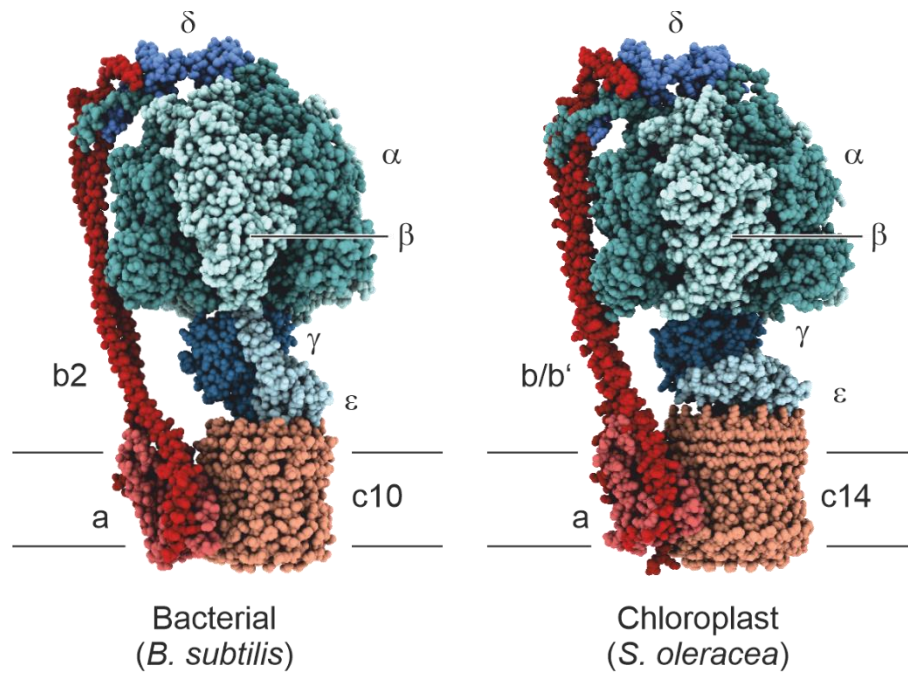


Figure 2. Comparison of bacterial and chloroplast ATP synthase structures. Cryo-EM structures of the *Bacillus subtilis* (ϵ -auto-inhibited, PDB entry: 6N2Y; Guo et al., 2019) and *Spinacia oleracea* (PDB entry: 6FKH; Hahn et al., 2018) ATP synthase. F₁-subunits α , β , γ , δ , and ϵ are colored in shades of blue. F₀-subunits a, b, and c are colored in shades of red. Bottom lines indicate the membrane position. Structures were obtained from the PDB homepage (<https://www.rcsb.org/>). Shading and coloration were performed with ChimeraX.

1.3 Biogenesis of the chloroplast ATP synthase

In bacteria, ATP synthase assembly occurs in a modular fashion with intermediates identified for the F₁-head $\alpha_3\beta_3\gamma\epsilon$ (Deckers-Hebestreit, 2013), the ab_2 -module (Hilbers et al., 2013), and the c-ring (Ballhausen et al., 2009). Since the F₁-module can hydrolyze ATP and F₀ intermediates are able to uncouple the *pmf* (Franklin et al., 2004), assembly has to be tightly regulated in order to prevent the accumulation of harmful precomplexes. F₀ assembly requires cotranslational insertion of b- and c-subunits via the signal recognition particle (SRP) pathway, the SecYEG translocon and the insertase YidC (Yi et al., 2004; van der Laan et al., 2004). Membrane insertion of F₀-a is dependent on the presence of monomeric c and mediated by SecYEG and YidC (Hermolin and Fillingame, 1995; Yi et al., 2004; Kol et al., 2009). SecYEG could also recently be copurified with intact bacterial ATP synthases, suggesting a role also in later steps of assembly (Chorev et al., 2018). Oligomerization of the c-subunit involves Atp1/Unc1 which usually precedes the structural ATP synthase genes in bacterial operons (Suzuki et al., 2007; Ozaki et al., 2008). In contrast, no bacterial F₁ assembly factor is known and F₁ assembly was shown to occur independently of auxiliary proteins in vitro (Sternweis and Smith, 1977; Sternweis, 1978). Linkage of soluble to membranous components

presumably involves the generation of an $\alpha_3\beta_3\gamma\epsilon$ -c-ring intermediate and is completed by δ -dependent addition of the stator module ab_2 (Hilbers et al., 2013).

In analogy to bacteria and mitochondria, assembly of the cpATP synthase is assumed to occur in a transient modular way (reviewed in Rühle and Leister, 2015). As in mitochondria, biogenesis is further complicated by the dual localization of genetic information in the nuclear (γ , δ , b') and organellar genomes (α , β , ϵ , a , b , c). Hence, stoichiometric availability of subunits and coordinated assembly must be tightly regulated. Indeed, several auxiliary factors were shown to be involved in cpATP synthase gene expression, mediating mRNA processing (AEF1), stability (PPR10, BFA2), and translation initiation (ATP4, TDA1) (Pfalz et al, 2009; Eberhard et al., 2011; Zoschke et al., 2012; Yap et al., 2015; Zhang et al., 2019). In contrast to bacteria and mitochondria, chloroplast F_0 (CF_0) cannot accumulate independently of chloroplast F_1 (CF_1) (Maiwald et al., 2003) and only minor amounts of CF_1 were detected in *Chlamydomonas* CF_0 mutants (Lemaire and Wollmann, 1989). A similar interdependency can also be observed in *Arabidopsis* mutants of assembly factors affecting either CF_1 or CF_0 (Rühle et al., 2014; Zhang et al., 2018). In vitro reconstitution assays suggest that chaperonin-dependent heterodimerization of α and β might be the first step of CF_1 assembly (Fig. 3; Chen and Jagendorf, 1994). Whereas, the presence of chaperonin 60 (Cpn60) in stromal chaperonin mixtures was shown to be essential for the reconstitution of active CF_1 , Cpn60 alone was not sufficient to restore ATPase activity of purified CF_1 -subunits, suggesting the involvement of additional stromal chaperones (Chen and Jagendorf, 1994). Indeed, the assembly-chaperones PAB and BFA1 were proposed to be required for the subsequent assembly of CF_1 by independently mediating the incorporation of the γ -subunit (Mao et al., 2015; Zhang et al., 2018).

CF_0 assembly involves the action of CGL160, which shares homology to Atp1/Unc1 from bacteria and is required for c-subunit oligomerization in *Arabidopsis* (Rühle et al., 2014). Split-ubiquitin assays could show that the membranous Atp1/Unc1-like domain of AtCGL160 is sufficient to interact with the CF_0 -b and -c-subunits, suggesting an additional function for the green-lineage-specific soluble domain (Rühle et al., 2014). ALB4, which shares sequence identity with bacterial YidC, was proposed to act in CF_0 -b membrane integration or ATP synthase stability (Benz et al., 2009). Recent studies rather suggest a general involvement of ALB4 in ALB3- and cpSRP-mediated thylakoid protein targeting (Trösch et al., 2015; Bédard et al., 2017). Considering the strict interdependency of CF_1 and CF_0 accumulation as well as the importance of the cpATP synthase in regulating the *pmf*, joining of the submodules is critical in the assembly of the functional complex. However, it is not clear how this process is orchestrated.

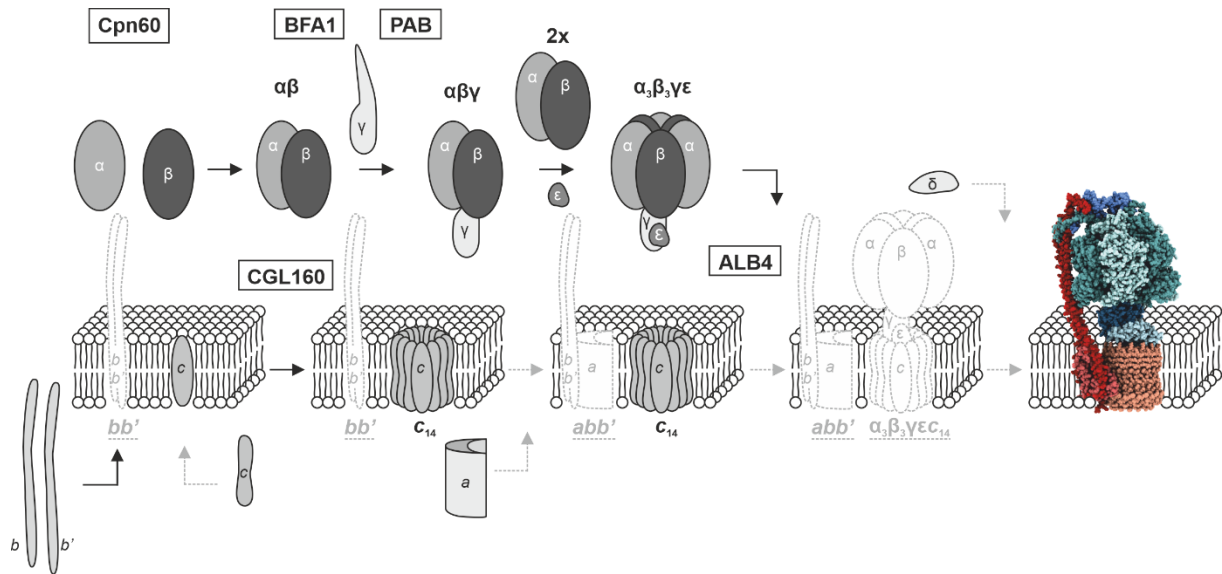


Figure 3. Schematic assembly pathway of the cpATP synthase. Assembly intermediates are mostly inferred from the bacterial model. Dotted lines indicate intermediates that have not been verified in planta. CF₁ assembly is initiated by chaperonin 60- (Cpn60) dependent heterodimerization of α - and β -subunits. The assembly-chaperones BFA1 and PAB independently assist the incorporation of the γ -subunit into $\alpha\beta$ -heterodimers. Addition of two $\alpha\beta$ -heterodimers and ϵ complete CF₁ assembly. CF₀ assembly requires CGL160, which facilitates c-subunit multimerization. Joining involves the addition of the stator module and δ , however the exact order of intermediates is not clear. Structure of the spinach cpATP synthase was obtained from the PDB homepage (<https://www.rcsb.org/>; PDB entry: 6FKH; Hahn et al., 2018). Shading and coloration were performed with ChimeraX. Figure was adapted and modified from Rühle and Leister (2015).

1.4 Chloroplast ribosomes

Ribosomes are ribonucleoprotein complexes that translate the genetic code into a polypeptide sequence. Phylogenetically they can be classified in two groups, archaeobacterial-type 80S ribosomes found also in the cytosol of eukaryotes and bacterial-type 70S ribosomes that can be also identified in their respective endosymbiotic descendants, mitochondria and plastids. Chloroplast ribosomes share with their bacterial ancestors (Fig. 4) not only their mode of action (reviewed in Zoschke and Bock, 2018), but also the basic structural organization of a small 30S (SSU) and large 50S (LSU) subunit. Both consist of catalytic ribosomal RNAs (rRNA), coated and intertwined with at least 50 ribosomal proteins (RPs). The bacterial SSU harbors a 1491 nucleotides (nts) long 16S rRNA for mRNA decoding and around 20 ribosomal proteins. The LSU consists of a large 23S rRNA (2904 nts) and a small 5S rRNA (120 nts), which provide the active sites for the formation of peptide bonds, and about 30 RPs (reviewed in Melnikov et al., 2012). Sequence and total length of the catalytic rRNA is largely conserved, but the 3' end of the 23S rRNA is represented by a separate 4.5S (103 nts) rRNA in chloroplasts (Whitfield et al., 1978; Keus et al., 1984; Leal-Klevezas et al., 2000). In addition, the higher plant 23S rRNA is subjected to post-maturation fragmentation into three parts, held together by intermolecular base pairing, thus termed hidden breaks (Kössel et al., 1985). Chloroplast ribosomal proteins are largely conserved with respect to bacteria but their total molecular mass increased by about 170 kD due to N- and C-terminal extensions, shifting the protein to RNA ratio from ~1:3 in bacterial to ~2:3 in plant chloroplasts (Yamaguchi et al., 2000; Yamaguchi and Subramanian, 2000; Yamaguchi and Subramanian, 2003; Zoschke and Bock, 2018). Furthermore, chloroplasts contain no bacterial bl25 and ul30 homologs, but five plastid-specific RPs (PSRPs) were shown to be associated in stoichiometric amounts with ribosomes (Yamaguchi et al., 2000; Yamaguchi and Subramanian, 2000; Yamaguchi and Subramanian, 2003; Sharma et al., 2010). Recently resolved cryo electron-microscopy (cryo-EM) structures of spinach chloroplast ribosomes revealed the exact positions and binding partners of the PSRPs (Ahmed et al., 2016; Bieri et al., 2017; Graf et al., 2017; Perez Boerema et al., 2018). Whereas PSRP2, PSRP3 and PSRP4 were shown to be associated with the SSU, PSRP5 and PSRP6 are part of the LSU. However, only disruption of PSRP3, PSRP4 and PSRP5 caused significant defects in ribosome biogenesis and translational capacity (Tiller et al., 2012). Presumably, they have been acquired as an adaptation to structural changes in the rRNA (Sharma et al., 2007; Tiller et al., 2012; Ahmed et al., 2016; Graf et al., 2016; Bieri et al., 2017), but also a regulatory function has been proposed (Yamaguchi and Subramanian, 2003; Manuell et al., 2007). Notably, not all RPs that are essential for chloroplast ribosome function were shown to be essential in bacteria, and some proteins non-essential in bacteria were shown to be indispensable for plants (reviewed in Tiller and Bock, 2014).

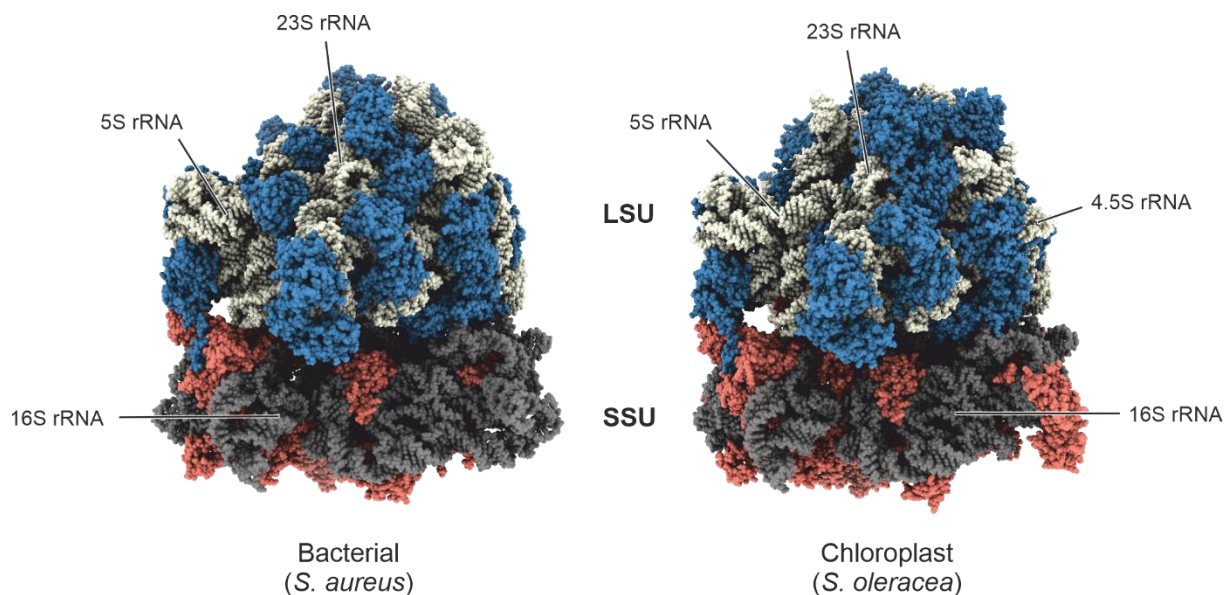


Figure 4. Structural comparison of bacterial and chloroplast 70S ribosomes. 70S ribosomes of *Staphylococcus aureus* (PDB entry: 5LI0; Khusainov et al., 2016) and *Spinacia oleracea* (PDB entry: 5MMM; Bieri et al., 2017) were resolved by cryo-EM. rRNA- and RP-components of the large subunit (LSU) are colored in beige and blue, respectively. rRNA- and RP-components of the small subunit (SSU) are colored in grey and red. Positions of the 23S, 5S and 4.5S rRNA (LSU), and 16S rRNA (SSU) are indicated. Structures were obtained from the PDB homepage (<https://www.rcsb.org/>). Shading and coloration were performed with ChimeraX.

1.5 Biogenesis of chloroplast ribosomes

Most of our knowledge about ribosome biogenesis is based on studies with bacteria (reviewed in Connolly and Culver, 2009; Shajani et al., 2011; Davis et al., 2016; Davis and Williamson, 2017). The catalytically active cores of both subunits are encoded in one rRNA operon, yielding a polycistronic primary transcript, but small and large subunits are assembled independently (Shajani et al., 2011). The secondary structure of the rRNA is mainly determined by its sequence, whereas its three-dimensional structure requires the action of RP components which shape and maintain rRNAs in their folded stage during assembly (Williamson, 2003; Duss et al., 2019). It could be shown that RPs bind to the nascent rRNAs already during their transcription (Miller et al., 1970; Gotta et al., 1991). RPs can be divided into primary binders, which bind independently from other ribosomal proteins, and secondary binders, whose binding efficiency is determined by primary binding events (Mizushima and Namura, 1970; Herold and Nierhaus, 1987). As demonstrated recently, RPs can also bind transiently to the nascent rRNA and function as folding-chaperones prior to their stable association (Duss et al., 2019). The structural elucidation of intermediates facilitated the generation of assembly maps for both subunits and established that rRNA processing, RP-assisted folding, and RP incorporation can take place sequentially and in parallel, resulting in several alternative assembly pathways (Mulder et al., 2010; Chen et al., 2012; Davis et al., 2016). It is assumed that the flexible nature of ribosome formation provides a more robust assembly process under

limited RP availability or changing environmental conditions (Davis and Williamson, 2017). Around 100 auxiliary factors have been identified in bacteria, facilitating rRNA processing, folding, modification, and integration of RPs (reviewed in Shajani et al., 2011).

Ribosome biogenesis in chloroplasts is only understood in its basic principles and no detailed maps of early or late assembly events (Fig. 5) are available. The chloroplast rRNA is encoded in the plastid genome in an rRNA operon, whereas many RPs are encoded in the nucleus and require post-translational import into the chloroplast. Cotranscriptional assembly from one rRNA-precursor as well as subsequent pre-rRNA processing were proposed to occur primarily in nucleoids, a subcompartment within plastids with high amounts of DNA (reviewed in Krupinska et al., 2013; Chai et al., 2014; Bohne, 2014). Moreover, plastid nucleoids were shown to contain RPs and other factors involved in pre-rRNA processing (Majeran et al., 2012; Bohne, 2014). This sublocalization might not only reflect the cotranslational dynamics of early ribosome biogenesis but may also provide beneficial spatial separation of immature and actively translating ribosomes (Bohne, 2014).

The early phase of chloroplast ribosome assembly is likely to be similar to bacterial ribosome assembly, because rRNA sequences are highly conserved (Bieri et al., 2017; Graf et al., 2017; Zoschke and Bock, 2018) and many pre-rRNA processing factors possess orthologs in bacteria (Komatsu et al., 2010; Fristedt et al., 2014; Liu et al., 2015; Janowski et al., 2018). Like in prokaryotes, also plastid SSU and LSU assemble independently (Walter et al., 2010). However, due to the parallel nature of alternative ribosome assembly pathways and substantial structural differences found predominantly in surface-exposed chloroplast RPs (Graf et al., 2016), subsequent assembly routes may differ considerably from the bacterial ancestor. Likewise, chloroplast-specific hidden break processing steps of the 23S rRNA and cleavage of the 4.5S rRNA-precursor were proposed to occur in later stages of ribosome assembly (Whitfeld et al., 1978; Keus et al., 1984; Leal-Klevezas et al., 2000). Consequently, factors involved in these processes are not present in bacteria (Bellaoui et al., 2003; Nishimura et al., 2010; Paieri et al., 2018). Vice versa, not all bacterial auxiliary factors have orthologs in the green lineage, and only some were shown to play a role in plastid ribosome biogenesis (reviewed in Bohne, 2014; Liu et al., 2015; Jeon et al., 2017; Janowski et al., 2018). Despite the need to orchestrate the supply of RPs of dual genetic origin and significant structural changes in chloroplast ribosomes, only few chloroplast-specific auxiliary factors have been identified (reviewed in Bohne, 2014; Wang et al., 2016; Meurer et al., 2017; Paieri et al., 2018; Pulido et al., 2018).

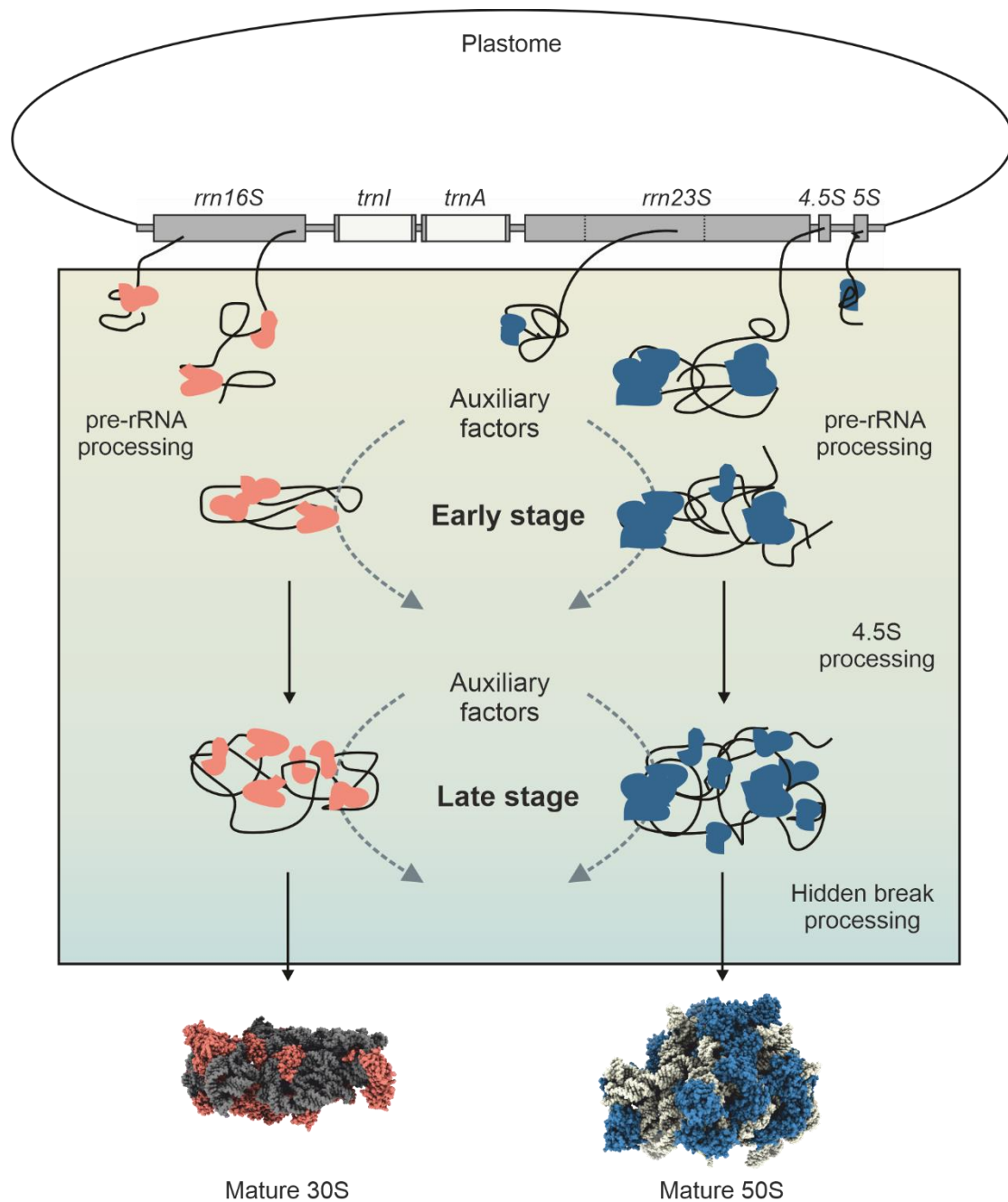


Figure 5. Schematic representation of chloroplast 70S ribosome assembly. Biogenesis is initiated by transcription of the rRNA from the plastome-encoded operon (rRNA genes are depicted as grey rectangles, 23S rRNA hidden break sites are indicated with dotted lines). Cotranslational binding and pre-rRNA processing define early assembly events. SSU and LSU are assembled independently in an ambiguous series of parallel and sequential assembly steps (omitted for clarity). Later assembly events of the LSU are defined by chloroplast-specific processing events of the 4.5S rRNA and 23S rRNA (hidden break processing). All stages of plastid ribosome assembly are mediated by auxiliary factors. Structures were obtained from the PDB homepage (<https://www.rcsb.org/>; SSU: 5MMJ; LSU: 5MMI; Bieri et al., 2017). Shading and coloration were performed with ChimeraX.

1.6 Identification of chloroplast auxiliary components

Identification and functional annotation of the chloroplast proteome advanced markedly in the last 20 years due to the increasing availability of genetic data, facilitating phylogenetic screens as well as forward and reverse genetic approaches (Gilchrist and Haughn, 2010; Fristedt, 2017; Rühle et al., 2018). However, despite progress in chloroplast research, only about 15% of the ~3000 chloroplast localized proteins can be assigned a function (Niehaus et al., 2015). Whereas much is known about structural components of the chloroplast, our understanding about the processes that regulate and assemble those macromolecular machineries is scarce. Phylogenetic analysis in combination with the increasing number of large datasets available for the model plant *Arabidopsis thaliana*, such as coregulation (Obayashi et al., 2018), comigration (Takabayashi et al., 2017), or phenotype databases (Sakurai et al., 2005; Akiyama et al., 2014), greatly improved reverse genetics approaches. Moreover, extensive collections of *Arabidopsis* insertional mutant lines including the SALK (Alonso et al., 2003), SAIL (Sessions et al., 2002), the GABI-Kat (Kleinboelting et al., 2012), or the double mutant library GABI-DUPLO (Bolle et al., 2013), have enabled fast and efficient isolation of knockout or knockdown alleles. Finally, large scale phenotyping platforms like chlorophyll a video imaging allow rapid, non-invasive screening of photosynthetic defects (Rühle et al., 2018) and provide a good starting point for further physiological or biochemical analyses.

One of those reverse genetic screens has been designed on the basis of the so-called “GreenCut2”, which describes a phylogenetic study of proteins conserved in the green lineage but not found in non-photosynthetic organisms (Merchant et al., 2007; Karpowicz et al., 2011). The GreenCut2 comprises 597 proteins, of which 311 were not functionally annotated (Karpowicz et al., 2011). It has been assumed that strictly conserved proteins are critical for chloroplast function or other plant-related processes. Indeed, GreenCut2 proteins have been shown to be involved in various aspects of chloroplast function (Fristedt et al., 2017), including protein import (Vojta et al., 2004), thylakoid biogenesis (Armbruster et al., 2013) and protein-complex assembly (Rühle et al., 2014; Fristedt et al., 2015), corroborating that the GreenCut2 is a valuable resource for identifying factors involved in essential chloroplast processes.

1.7 Aims of the thesis

The general scope of this thesis was to contribute to the current knowledge on the biogenesis of chloroplasts by functional characterization of novel putative auxiliary proteins in *Arabidopsis thaliana*.

AtCGLD11 (CONSERVED IN THE GREEN LINEAGE AND DIATOMS 11) was identified based on a phenotypic annotation in the GreenCut2 screen ("photochemical quenching affected before high light treatment", Karpowicz et al., 2011). Initial characterization and assignment of a putative role in cpATP synthase biogenesis was performed in Reiter (2015). Aim of this thesis was to reveal its function in cpATP synthase biogenesis by in-depth analysis of the assembly process and the identification of interaction partners (Chapter 2, Grahl et al., 2016).

CGL160 (CONSERVED ONLY IN THE GREEN LINEAGE 160) was previously characterized in Rühle et al., (2014). It could be shown that disruption of CGL160 in *Arabidopsis* led to drastically reduced levels of cpATP synthase and overaccumulation of monomeric c-subunits. AtCGL160 physically interacted with CF₀-b and -c, thus a function in c-ring assembly was proposed. The membranous C-terminal domain of CGL160 is distantly related to bacterial Atp1/Unc1 proteins that were demonstrated to be required for bacterial c-ring assembly (Suzuki et al., 2007; Ozaki et al., 2008). The focus of the dissertation was the characterization of the chloroplast-specific soluble domain of AtCGL160 and the investigation of its influence on the cpATP synthase assembly (Chapter 3, Reiter et al., Manuscript).

CGL20 was identified as part of the GABI-DUPLO collection (Bolle et al., 2013). Generation of mutant lines and initial characterization were performed by Vamvaka (2016). In this work, an in-depth phenotypical and biochemical characterization of CGL20 mutants in *Arabidopsis* was carried out and the putative role of CGL20 in chloroplast biogenesis was investigated (Chapter 4, Reiter et al., 2020).

2 The Arabidopsis Protein CGLD11 is Required for Chloroplast ATP Synthase Accumulation

Grahl S*, Reiter B*, Gügel IL, Vamvaka E, Gandini C, Jahns P, Soll J, Leister D, Rühle T
(2016) The Arabidopsis Protein CGLD11 is Required for Chloroplast ATP Synthase Accumulation. Mol Plant **9**: 885–899

* Authors contributed equally

DOI: <https://doi.org/10.1016/j.molp.2016.03.002>

The *Arabidopsis* Protein CGLD11 Is Required for Chloroplast ATP Synthase Accumulation

Sabine Grahl^{1,4,5}, Bennet Reiter^{2,5}, Irene Luise Gügel^{1,4}, Evgenia Vamvaka², Chiara Gandini², Peter Jahns³, Jürgen Soll^{1,4}, Dario Leister^{2,*} and Thilo Rühle²

¹Lehrstuhl für Biochemie und Physiologie der Pflanzen (Botanik), Department Biologie I, Ludwig-Maximilians-Universität München, 82152 Planegg-Martinsried, Germany

²Lehrstuhl für Molekularbiologie der Pflanzen (Botanik), Department Biologie I, Ludwig-Maximilians-Universität München, 82152 Planegg-Martinsried, Germany

³Plant Biochemistry, Heinrich-Heine-University Düsseldorf, Universitätsstrasse 1, 40225 Düsseldorf, Germany

⁴Munich Centre for Integrated Protein Science CiPSM, Ludwig-Maximilians Universität München, Butenandtstr. 5 - 13, 81377 Munich, Germany

⁵These authors contributed equally to this article.

*Correspondence: Dario Leister (leister@lrz.uni-muenchen.de)

<http://dx.doi.org/10.1016/j.molp.2016.03.002>

ABSTRACT

ATP synthases in chloroplasts (cpATPase) and mitochondria (mtATPase) are responsible for ATP production during photosynthesis and oxidative phosphorylation, respectively. Both enzymes consist of two multi-subunit complexes, the membrane-bound coupling factor O and the soluble coupling factor 1. During cpATPase biosynthesis, several accessory factors facilitate subunit production and orchestrate complex assembly. Here, we describe a new auxiliary protein in *Arabidopsis thaliana*, which is required for cpATPase accumulation. AtCGLD11 (CONSERVED IN THE GREEN LINEAGE AND DIATOMS 11) is a protein without any known functional domain and shows dual localization to chloroplasts and mitochondria. Loss of AtCGLD11 function results in reduced levels of cpATPase and impaired photosynthetic performance with lower rates of ATP synthesis. In yeast two-hybrid experiments, AtCGLD11 interacts with the β subunits of the cpATPase and mtATPase. Our results suggest that AtCGLD11 functions in F_1 assembly during cpATPase biogenesis, while its role in mtATPase biosynthesis may not, or not yet, be essential.

Key words: chloroplast, mitochondria, photosynthesis, dual targeting, ATP synthase, assembly

Grahl S., Reiter B., Gügel I.L., Vamvaka E., Gandini C., Jahns P., Soll J., Leister D., and Rühle T. (2016). The *Arabidopsis* Protein CGLD11 Is Required for Chloroplast ATP Synthase Accumulation. *Mol. Plant*. **9**, 885–899.

INTRODUCTION

ATP is synthesized by the ubiquitous F_1F_0 -ATP synthase, which is found in the energy-transducing membranes of bacteria, mitochondria and chloroplasts. The chloroplast F_1F_0 -ATP synthase/ATPase (or cpATPase) generates ATP from the light-driven electrochemical proton gradient and has a mushroom-like structure common to all F_1F_0 -ATP synthases. The cpATPase can be separated physically into two parts: a membrane-spanning subcomplex responsible for proton translocation (CF_0 , chloroplast coupling factor O) and the soluble CF_1 part (chloroplast coupling factor 1), which is peripherally attached to the membrane subcomplex and harbors the catalytic sites for reversible ATP synthesis. CF_1 is built up of the five subunits α (AtpA), β (AtpB), γ (AtpC), δ (AtpD), and ϵ (AtpE) in a stoichiometry of $\alpha_3\beta_3\gamma\delta\epsilon$ (reviewed by von Ballmoos et al., 2009). CF_0 consists of subunit b (also designated as I or AtpF), b' (II or AtpG), c (III or AtpH), and a (IV or AtpI), which are present in a stoichiometry of $abb'c_{14}$. A central stalk made up of the ϵ and γ subunits and a peripheral stator containing δ , b, and b' connect CF_1 to CF_0 . The

complete three-dimensional structure of the cpATPase is not available yet, but those of the CF_1 complex $\alpha_3\beta_3\gamma\epsilon$ (without δ) (Groth and Pohl, 2001) and the c_{14} ring of CF_0 (Vollmar et al., 2009), isolated from spinach chloroplasts, have already been determined at atomic resolution.

As is the case for all major thylakoid complexes, the subunits of the cpATPase originate from two different genetic compartments. The γ , δ , and b' subunits are encoded in the nuclear genome, while the remaining six cpATPase genes are generally organized into two operons in the plastid genome in plants. The small operon consists of *atpB* and *atpE*, and transcription is initiated from three different promoters; two are located upstream of *atpB* and one within the *atpB* coding sequence (Malik Ghulam et al., 2012). The other four cpATPase genes *atpI*, *atpH*, *atpF*, and *atpA* form the second operon together with *rps2*, which

precedes the gene cluster and codes for the plastid ribosomal protein S2. The large cpATPase operon is transcribed from several promoters, giving rise to primary transcripts that are subsequently processed into multiple poly- and monocistronic fragments (Stahl et al., 1993; Miyagi et al., 1998; Swiatecka-Hagenbruch et al., 2007; Pfalz et al., 2009; Malik Ghulam et al., 2012; Zhelyazkova et al., 2012). Thus, efficient cpATPase biogenesis depends on the orchestrated interplay of multiple cellular processes: coordinated nuclear and chloroplast gene expression, the import of γ , δ , and b' into the plastid, post-translational processing, insertion of thylakoid-embedded cpATPase subunits, and their assembly in the correct stoichiometry, $abb'c_{14}\alpha_3\beta_3\gamma\delta\epsilon$ (reviewed by Rühle and Leister, 2015).

During cpATPase biogenesis, the function of assembly factors is of particular importance, since intermediate complexes can either uncouple the proton gradient or wastefully hydrolyze ATP, and their accumulation must be avoided. The assembly of cpATPase can be divided into three major events: (i) CF₁ assembly, (ii) CF₀ assembly, and (iii) linkage of the different modules to each other. The current model for CF₁ assembly is derived from *in vitro* reconstitution studies using stromal components and purified CF₁ subunits. The chaperonins Cpn60 and Cpn20, which are related to the bacterial chaperonins GroEL and GroES, respectively, are required for the correct folding of stromal proteins (Hartl, 2002), but are also essential for CF₁ assembly (Chen and Jagendorf, 1994). Furthermore, addition of the heat-shock proteins Hsp70 and Hsp40 to reconstitution assays improves hydrolytic ATPase activity, which points to a role for Hsp70/Hsp40 in CF₁ assembly (Mao et al., 2015). Moreover, the green-lineage-specific factor PAB was shown to interact with folded cpATPase- γ and to promote the integration of this nucleus-encoded subunit into the catalytic CF₁ core downstream of Cpn60/Cpn20-mediated events (Mao et al., 2015). In contrast, CF₀ assembly depends on CGL160 (Rühle et al., 2014), which harbors a C-terminal membrane domain that is conserved in bacterial Atp1/Unc1 proteins, which are encoded by the first gene preceding the structural ATP synthase genes in the *atp* operon. Atp1/Unc1 and AtCGL160 are involved in c-ring formation, which represents the first assembled CF₀ module. Subsequent CF₀ assembly steps are unknown but, by analogy with the assembly process in bacteria, abb' might represent a second CF₀ module (Hilbers et al., 2013). Attachment of CF₁ to the membrane-embedded CF₀ module is facilitated by the Alb3 homolog Alb4 (Benz et al., 2009). The final step in cpATPase assembly is also unknown, but in bacteria the ab_2 module is joined to the $c_{10}\alpha_3\beta_3\gamma\epsilon$ module by binding of the F₁ subunit δ . In this way, undesirable bacterial ac_{10} intermediates, which can uncouple the proton-motive force (*pmf*) by mediating proton translocation without ATP generation, can be avoided (Hilbers et al., 2013).

In this study, we have identified a new auxiliary factor, AtCGLD11 (CONSERVED IN THE GREEN LINEAGE AND DIATOMS 11), which promotes cpATPase accumulation in *Arabidopsis*. As a GreenCut2 protein, AtCGLD11 is restricted to the green lineage and is absent in (cyano)bacteria (Merchant et al., 2007; Karpowicz et al., 2011). Remarkably, AtCGLD11 is targeted to both chloroplasts and mitochondria. AtCGLD11 does not contain any protein domain with a known function, but the loss of *AtCGLD11* function is associated with an overall

decrease in cpATPase activity resulted from a severe reduction in cpATPase levels. In contrast, mtATPase activity and abundance are not affected in *AtCGLD11* knockout lines. However, we show here that AtCGLD11 physically interacts with both cpATPase- β and mtATPase- β in yeast, which points to a function of AtCGLD11 in F₁ assembly of chloroplasts and a perhaps minor or emerging role in plant mitochondrial F₁ assembly.

RESULTS

Characteristics of the GreenCut Protein AtCGLD11

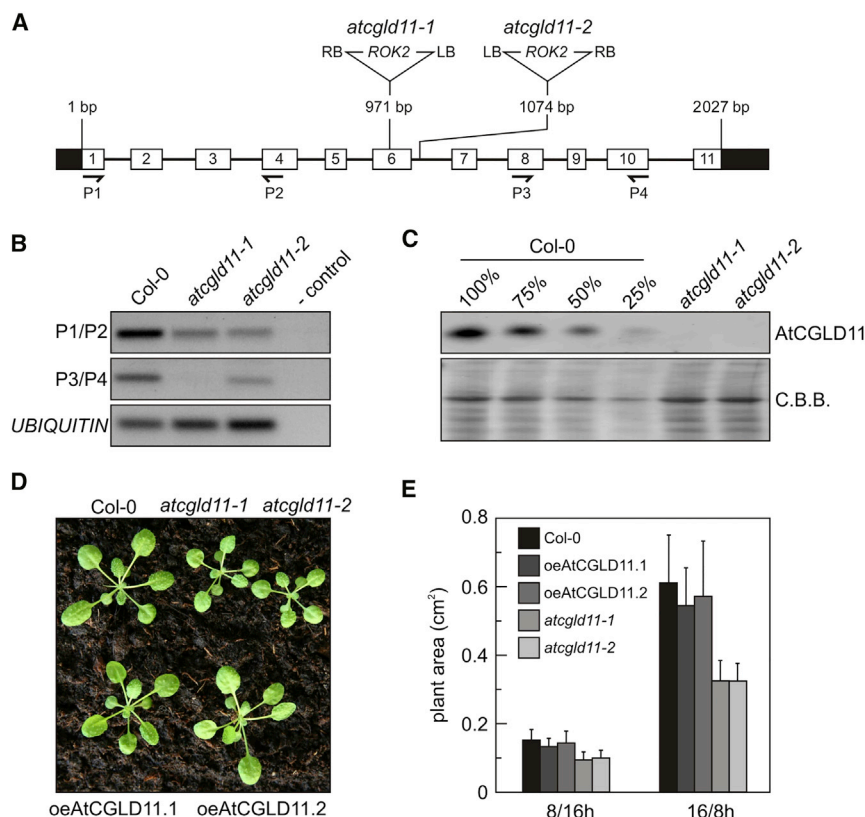
In a search for novel photosynthesis-related proteins in *Arabidopsis thaliana*, we identified AtCGLD11 (alias AT2G21385) based on its inclusion in the GreenCut set of proteins and on the nature of its mutant phenotype (see Supplemental Table 2 in Karpowicz et al., 2011: Mutant Phenotype from Chloroplast 2010 dataset: photochemical quenching affected before high light treatment).

AtCGLD11 (AT2G21385.1) codes for a protein with 330 amino acids and contains a predicted N-terminal chloroplast transit peptide (cTP) such that the mature protein should have a calculated isoelectric point of 6.0 and a calculated molecular mass of ~33 kDa. Localization to the stroma of the chloroplast has been suggested previously for AtCGLD11 and its counterpart in *Chlamydomonas reinhardtii*, based on proteomics experiments (Zybailov et al., 2008; Terashima et al., 2011), and this is in line with the absence of predicted transmembrane domains.

AtCGLD11 homologs are not found in bacteria, but a distantly related gene product was identified in *Thalassiosira pseudonana* (Supplemental Figure 1), which harbors a diatom-specific insertion at amino acid positions 236–260. A multiple alignment with representative homologs from algae, moss and vascular plants revealed 26 identical (6.8%) and 64 similar (16.6%) amino acid positions, respectively (percentages refer to an overall number of 385 amino acid positions in the alignment shown in Supplemental Figure 1). AtCGLD11 shares 59/44% and 43/26% sequence similarity/identity with its homologs in *Physcomitrella patens* and *C. reinhardtii*, respectively. AtCGLD11 does not contain any known conserved protein domain (<http://www.ncbi.nlm.nih.gov/Structure/cdd/wrpsb.cgi>). Thus, it represents a protein with few functionally suggestive features, which is moderately conserved in the green lineage and diatoms, but absent from bacteria.

AtCGLD11 Is Required for Normal Growth in *Arabidopsis*

Two *Arabidopsis* T-DNA lines for AT2G21385 were obtained from the Nottingham *Arabidopsis* Stock Centre, and sequences flanking the T-DNA insertions were amplified by PCR and sequenced. The lines *atcgld11-1* (SALK_019326) and *atcgld11-2* (SALK_006444) have insertions at position 971 bp (exon 6) and position 1074 bp (intron 6) relative to the start codon, respectively (Figure 1A). To analyze the effect of the mutations on *AtCGLD11* transcript levels, reverse transcriptase (RT)-PCR was performed and regions were amplified either upstream or downstream of each insertion (Figure 1A). A product of the 3' amplicon but not for the 5' amplicon was obtained for



expressors (*oeAtCGLD11.1* and *oeAtCGLD11.2*) according to Leister et al. (1999). Plants were grown for 14 days under 8 h light/16 h night (8/16 h) or 16 h light/8 h night (16/8 h) conditions. Values are means of 10 individual plants and standard deviations are provided.

atcglD11-1, whereas plants homozygous for the *atcglD11-2* mutation showed a PCR product for both the 3' and the 5' region (Figure 1B). To clarify whether the AtCGLD11 protein accumulates in the mutant lines, an antibody was raised against the heterologously expressed and purified AtCGLD11 (lacking the predicted cTP). Total leaf protein was isolated from *A. thaliana* ecotype Col-0 (wild type [WT]), and from *atcglD11-1* and *atcglD11-2*. Western blot analysis using the specific α -AtCGLD11 antibody demonstrated that both alleles are complete knockouts and in neither line is AtCGLD11 detectable (Figure 1C). To analyze the effects of loss of AtCGLD11 on growth behavior, knockout and WT plants were grown in climate chambers providing short-day (8/16 h) and long-day (16/8 h) exposure to a light intensity of 100 $\mu\text{mol photons m}^{-2} \text{s}^{-1}$ (Figure 1D and 1E). Leaf areas were determined (Leister et al., 1999) at 2 weeks after germination, at which time the mutant lines *atcglD11-1* and *atcglD11-2* already showed a pronounced reduction in growth rate compared with WT plants, in particular under long-day conditions (Figure 1E). To restore the WT phenotype, the coding sequence of *AT2G21385.1* was cloned under the control of the constitutive 35S promoter and transformed into *atcglD11-1*. Several BASTA-resistant plants were selected and screened for AtCGLD11 overexpression, and two lines (*oeAtCGLD11.1* and *oeAtCGLD11.2*) with 4- to 6-fold higher AtCGLD11 levels than WT were chosen for further analysis (Supplemental Figure 2A and 2B). As expected, plants overexpressing AtCGLD11 had WT-like growth rates, indicating that depletion of AtCGLD11 is responsible for the growth phenotype observed in the two mutant lines (Figure 1D).

Figure 1. Characterization of Arabidopsis *atcglD11* Knockout Mutants.

(A) Schematic representation of the *AtCGLD11* gene. Exons are numbered and depicted as white boxes, introns as thin lines, and UTR regions as black boxes. T-DNA positions relative to the start codon and their orientations (left border [LB], right border [RB]) in *atcglD11-1* and *atcglD11-2* are indicated. Primer positions for amplification of the *AtCGLD11* transcript are indicated by P1 to P4.

(B) Expression analysis of *AtCGLD11* by reverse transcriptase (RT)-PCR. Positions of primer pairs P1/P2 and P3/P4 are shown in (A). Ubiquitin mRNA levels (*UBIQUITIN*) served as controls.

(C) Total protein leaf extracts (each corresponding to 2.5 μg of Chl) of *atcglD11-1*, *atcglD11-2* and WT (100%, 75%, 50%, and 25% dilutions) were size-fractionated on SDS-PAGE, blotted and subjected to AtCGLD11 immunodetection analysis. PVDF membranes were stained with Coomassie brilliant blue G-250 (C.B.B.) to control for equal loading.

(D) Growth phenotypes of *atcglD11* knockout and AtCGLD11 overexpressor lines. WT (Col-0), mutants (*atcglD11-1* and *atcglD11-2*) and two independent AtCGLD11 overexpressing lines (*oeAtCGLD11.1* and *oeAtCGLD11.2*) were grown for 4 weeks under short-day conditions.

(E) Quantification of mean leaf area in WT (Col-0), mutants (*atcglD11-1* and *atcglD11-2*), and over-

Lack of the Dual-Targeted AtCGLD11 Affects Chloroplast and Mitochondria Structure

To clarify whether cellular ultrastructure is affected by the loss of AtCGLD11, leaves from 14-day-old *A. thaliana* seedlings grown under short-day conditions were examined with the electron microscope (Figure 2). Because the mutants *atcglD11-1* and *atcglD11-2* behaved very similarly with respect to growth phenotype and AtCGLD11 accumulation, only *atcglD11-1* was used for microscopy. Leaf sections were prepared from tissue below the tip, which contains fully developed cells. Overviews of cross-sections indicated that *atcglD11* leaves were thinner than WT (Col-0) leaves (Figure 2A and 2G). Moreover, *atcglD11-1* cells accumulated enlarged mitochondria (Figure 2E, 2F, 2K, and 2L), particularly in the palisade parenchyma (around 75% of cells affected) but also in the sponge parenchyma (around 50%; Figure 2M). Chloroplasts displayed more grana stacking (Supplemental Figure 3) and stroma lamellae were slightly bloated (Figure 2E, 2F, 2K, and 2L).

To analyze the subcellular localization of AtCGLD11, chloroplasts and mitochondria were isolated from WT and *atcglD11-1* leaves and protein extracts were subjected to western-blot analyses. Immunodetection with antibodies specific for the mitochondrial and chloroplast marker proteins Tom40 and Lhcb2, respectively, confirmed the purity of each fraction (Figure 2N). AtCGLD11 was detected in both organelles and migrated at a position corresponding to a size of about 30 kDa. Thus, AtCGLD11 is localized to chloroplasts and

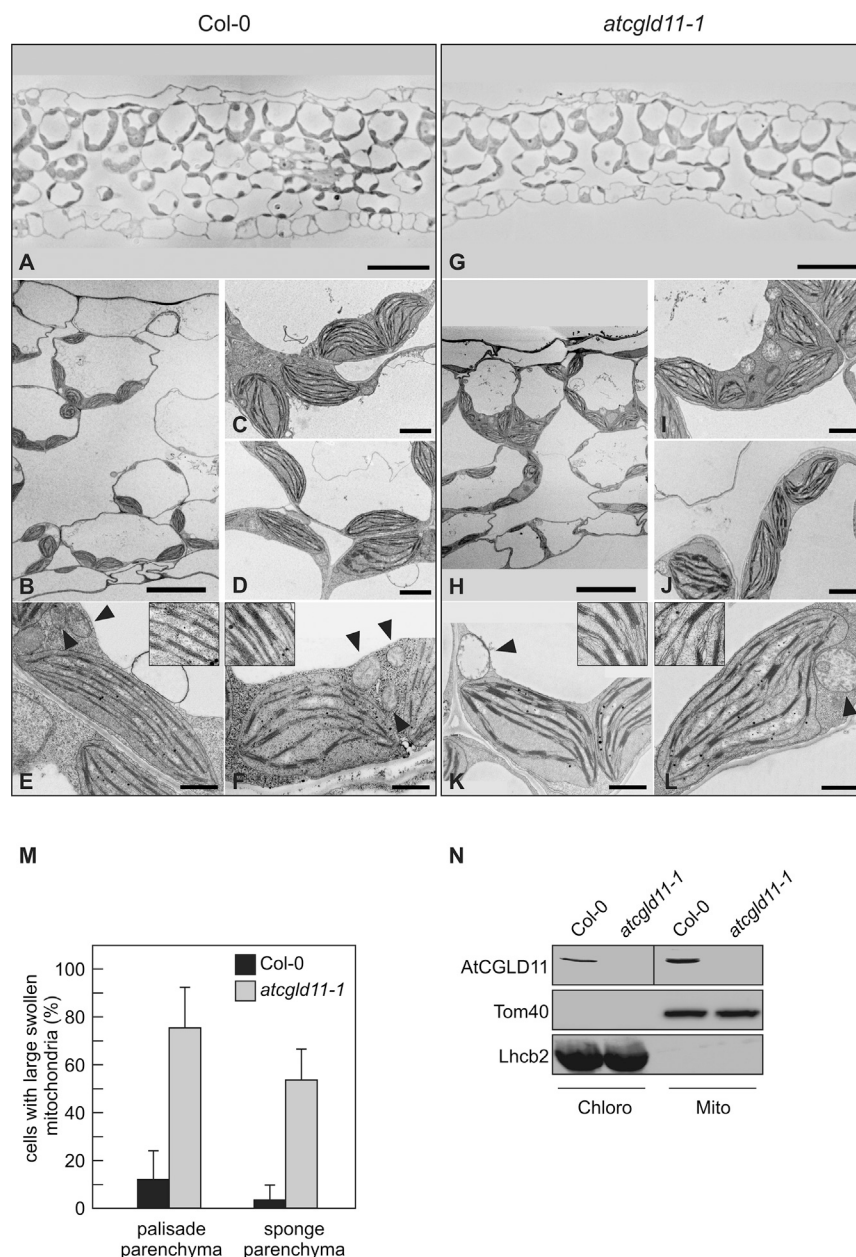


Figure 2. Ultrastructural Analysis of *atcgld11-1* Plants Grown under Short-Day Conditions, and Localization of AtCGLD11.

Col-0 (A–F) and *atcgld11-1* (G–L) were analyzed by light microscopy (A and G) and electron microscopy (B–F, H–L). Sections of palisade (C, E, I, K) and sponge parenchyma (D, F, J, L) are depicted. Mitochondria are indicated by black arrowheads. Insets show the magnification of the thylakoid structure (E, F, K, L). Scale bars are 25 μ m in (A) and (G); 10 μ m in (B) and (H); 2 μ m in (C), (D), (I), and (J); and 1 μ m in (E), (F), (K), and (L). (M) Quantification of abnormal mitochondria in WT (Col-0) and *atcgld11-1*. In total, 100 cells were analyzed from five plants (20 from each plant) of either WT (Col-0) or *atcgld11-1*. SD is shown.

(N) Mitochondrial and plastidial localization of AtCGLD11. Mitochondria (Mito) and chloroplasts (Chloro) were isolated from leaf samples taken from either Col-0 or the *atcgld11-1* mutant. Purity was analyzed by western analyses using the mitochondrial outer membrane protein Tom40 and the thylakoid-specific light-harvesting protein Lhcb2.

mitochondria, and the ultrastructure of both organelles is altered in its absence.

AtCGLD11 Is Required for Normal Rates of ATP Synthesis in Chloroplasts, but Not in Mitochondria

To screen for aberrant membrane complex levels in chloroplasts and mitochondria, two-dimensional gel analysis was carried out on organelle preparations from WT and *atcgld11-1* leaves. Thylakoid membranes and total mitochondria were solubilized in *n*-dodecyl β -D-maltoside (β -DM) and protein complexes were separated by blue native (BN) PAGE, followed by analysis of their constituent subunits by SDS-PAGE (Figure 3A and 3B). After Coomassie blue staining of thylakoid proteins, several spots were seen to be less prominent in *atcgld11-1* than in WT (Figure 3A). Based on their migration

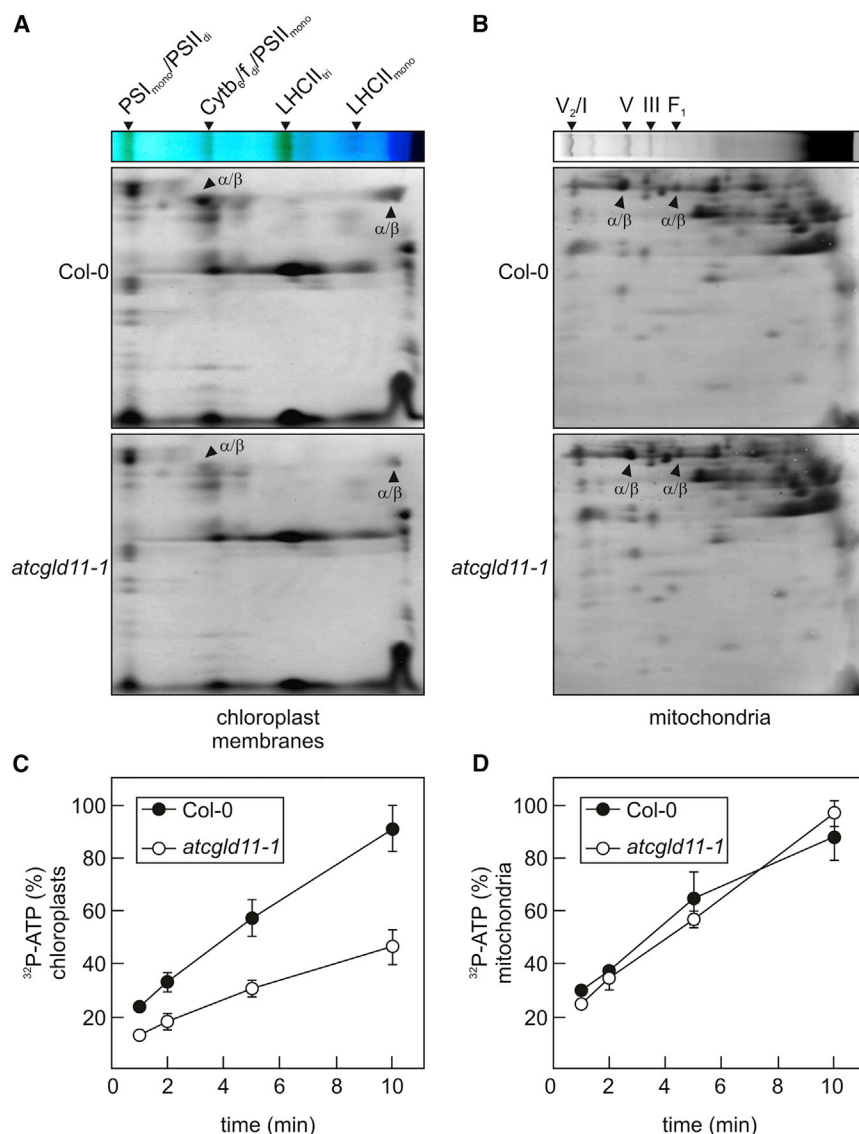
behavior on BN-PA gels and their electrophoretic mobility (50–60 kDa) in the second dimension (Rühle et al., 2014), these spots were identified as subunits α/β of the cpATPase. However, no difference in complex accumulation between *atcgld11-1* and WT mitochondria could be discerned (Figure 3B), and protein complexes attributable to mitochondrial ATP synthase accumulated to normal levels, as indicated by the presence of equal amounts of mtATPase- α/β in *atcgld11-1* and WT mitochondria (Figure 3B).

Because the cpATPase- α/β subunits were less abundant in *atcgld11-1* plants, we measured rates of ATP synthesis in isolated chloroplasts and mitochondria (Figure 3C and 3D). Indeed, the rate of ATP production in chloroplasts was reduced by

around 50% of the WT in *atcgld11-1*, but was normal in mitochondria isolated from the same mutant. Thus, we conclude that lack of the dual-targeted AtCGLD11 affects the accumulation of the cpATPase, but neither the steady-state level nor the activity of the mtATPase.

AtCGLD11 Is Specifically Required for cpATPase Accumulation

Next, we analyzed the influence of AtCGLD11 on other major thylakoid complexes. To this end, the accumulation of characteristic marker proteins in *atcgld11-1* and *atcgld11-2* was monitored by western-blot analyses (Figure 4A). In *atcgld11* knockout plants, PSII (D2, PsbP, and CP43), cytochrome *b₆f* (PetA), PSI (PsaB and PsaC), as well as light-harvesting complex II (Lhcb2) and I (Lhca1) were present to 90%–100%, 100%, 80%–90%, 70%, and 100%



of the WT levels, respectively (Figure 4A). However, a significant reduction was observed for cpATPase subunits in *atcgld11-1* and *atcgld11-2*: CF₁ subunits α, β and γ were reduced to 20% and CF₀ subunits a, b, b' and c to 20%–30% of WT levels, respectively (Figure 4A). In addition, solubilised thylakoid complexes obtained from WT, AtCGLD11 knockout and overexpressor lines were examined by BN-PAGE (Figure 4B). Levels of pigment-binding complexes, including the NDH-PSI supercomplex, were not affected in *atcgld11-1* and *atcgld11-2*. Furthermore, overexpression of AtCGLD11 had no impact on PSII, PSI, cytochrome *b₆f* or LHC accumulation (Figure 4B). In agreement with our immunotitration results (Figure 4A), amounts of the cpATPase holoenzyme (cpATPase_{holo}), as well as CF₁ levels, were reduced in both knockouts, but were restored to WT levels in the overexpressor lines, as indicated by Western analyses (Figure 4B, lower panel; Supplemental Figure S2B). From these results we conclude that AtCGLD11 specifically affects cpATPase accumulation and that minor reductions in other thylakoid complexes (Figure 4A) in *atcgld11* mutants might represent secondary effects.

Figure 3. Protein Accumulation in Chloroplasts and Mitochondria from *atcgld11-1* Plants.

(A–D) 2D BN/SDS-PAGE separation of (A) plastidial and (B) mitochondrial membrane complexes from WT (Col-0) and *atcgld11-1*. Individual lanes from BN-PA gels were analyzed on Tris-Tricine gels (10%, 4 M urea) in the presence of SDS and stained with colloidal Coomassie brilliant blue G-250. CpATPase-α/β and mtATPase-α/β subunits are indicated by black arrowheads in (A) and are annotated by their 2D gel position according to previous studies (Klodmann et al., 2011; Rühle et al., 2014). ATP synthase activity was measured in chloroplasts (C) and mitochondria (D) as described in the Methods. Spots of ³²P-ATP were quantified using ImageQuant TL. Experiments were performed in triplicate.

Loss of AtCGLD11 Function Impairs Photosynthesis

To examine the impact of AtCGLD11 on photosynthesis, we measured chlorophyll *a* fluorescence parameters (Table 1) and analyzed leaf pigment composition (Table 2) in the knockouts, as well as in the overexpressor lines. PSII functionality (F_v/F_m) was only slightly impaired in *atcgld11-1* (0.78 ± 0.02) and *atcgld11-2* (0.77 ± 0.02) compared with WT (0.8 ± 0.02), which is in line with the normal accumulation of PSII marker subunits revealed by our immunotitration analyses (Figure 4). However, effective quantum yields (ϕ_{II}) measured at 100 μmol photons m⁻² s⁻¹ in *atcgld11-1* and *atcgld11-2* were reduced to 0.44 ± 0.04 and 0.42 ± 0.06 from the WT value of 0.56 ± 0.05 . A clear difference was also observed for the non-photochemical quenching parameter NPQ. While NPQ values for the WT were 0.45 ± 0.06 , the levels of NPQ were more than doubled in both *atcgld11-1* (0.98 ± 0.28) and *atcgld11-2* (1.23 ± 0.23) leaves, indicating increased heat dissipation of absorbed light energy in the absence of AtCGLD11. To unravel the contributions of the two quenching parameters *qE* and *qI* to the NPQ phenotype, we analyzed the kinetics of dark relaxation. An increase in *qE* normally reflects the activation of Δ*pH*-dependent quenching, whereas an increase in *qI* can be attributed to photoinhibitory quenching mechanisms. Photoinhibitory quenching levels in the two mutant lines were as high as in WT, while *qE* was increased by about 4-fold in *atcgld11-1* (0.95 ± 0.12) and *atcgld11-2* (1.08 ± 0.26) compared with WT leaves (0.26 ± 0.05). The two overexpressor lines oeAtCGLD11.1 and oeAtCGLD11.2 again showed WT-like photosynthetic performance, with normal NPQ values.

To examine the effects of a lack and a surfeit of AtCGLD11 on pigment composition, we performed reverse-phase high-performance liquid chromatography analyses (Table 2) on light-adapted leaves grown under short-day conditions (80–100 μmol

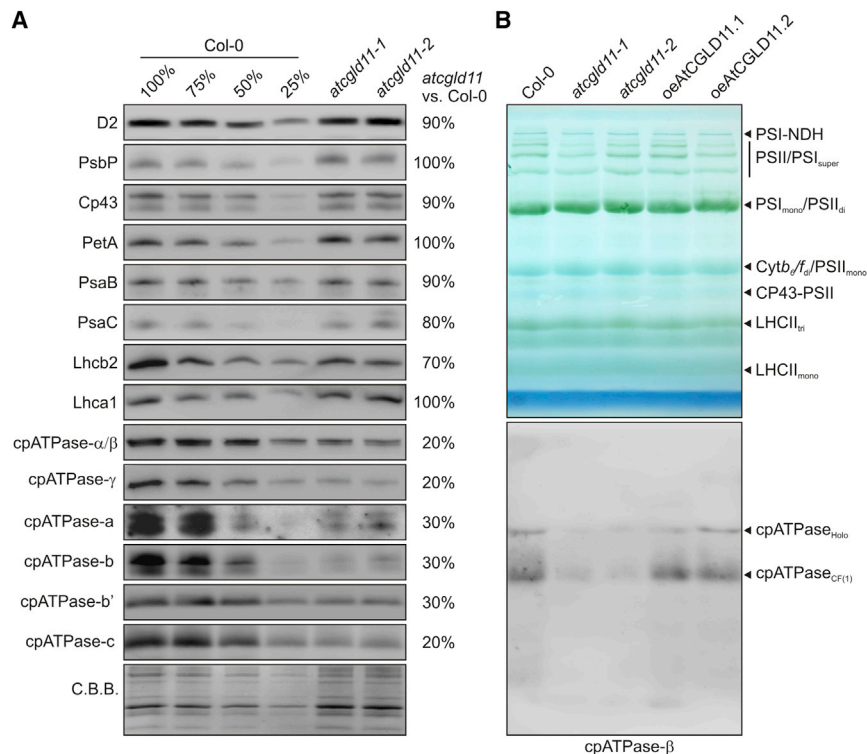


Figure 4. Immunotitration Analyses of *atcgld11* Thylakoid Proteins.

(A) Thylakoids were isolated from WT (Col-0) and the two mutant lines *atcgld11-1* and *atcgld11-2*. Dilutions of Col-0 thylakoid samples were loaded to quantify protein amounts in mutant samples. Proteins were separated by SDS-PAGE and analyzed by immunoblotting using antibodies specific for the indicated subunits. The levels of each marker subunit identified in *atcgld11* mutants are expressed relative to the corresponding WT signals.

(B) Thylakoid protein complexes from WT (Col-0), knockout lines (*atcgld11-1* and *atcgld11-2*), and overexpressors (oeAtCGLD11.1 and oeAtCGLD11.2) were analyzed by BN-PAGE. Proteins and protein complexes are labeled (upper panel) as follows: PSI-NAD(P)H dehydrogenase supercomplex (PSI-NDH), PSII/PSI supercomplexes (PSII/PSI_{super}), PSI monomers and PSII dimers (PSI_{mono} and PSII_d), PSII monomers and dimeric Cyt *b₆/f_d* (PSII_{mono} and Cyt *b₆/f_d*), CP43-free PSII monomers (CP43-PSII), trimeric LHCII (LHCII_{tr}), and monomeric LHCII (LHCII_{mono}). The BN-PAGE strip was denatured, blotted, and a specific antibody against cpATPase- β was employed to detect CF₁-containing complexes. The cpATPase holoenzyme (cpATPase_{holo}) and coupling factor 1 (cpATPase_{CF(1)}) are indicated.

photons $\text{m}^{-2} \text{s}^{-1}$). WT, knockout mutants, and overexpressor plants exhibited comparable concentrations of lutein, carotenes, and chlorophylls. However, antheraxanthin and zeaxanthin levels were clearly increased in *atcgld11* mutants at the expense of violaxanthin, which is reflected in an increase in the size of the violaxanthin + antheraxanthin + zeaxanthin pool (Col-0, $57 \pm 5 \text{ pmol mg}^{-1}$; *atcgld11-1*, $70 \pm 6 \text{ pmol mg}^{-1}$; *atcgld11-2*, $70 \pm 6 \text{ pmol mg}^{-1}$). Hence, the xanthophyll cycle is already activated at moderate light intensities in *atcgld11-1* and *atcgld11-2* leaves, as indicated by the increased levels of antheraxanthin and zeaxanthin.

AtCGLD11 Associates with Chloroplast Membranes and Is a Low-Abundance Protein

To examine whether AtCGLD11 is associated with chloroplast membranes, we separated WT chloroplasts into membrane and stroma fractions (Figure 5), the purity of which was verified by the absence of RbcL from the former and Lhcb2 from the latter. Although it does not contain any predicted membrane domain, AtCGLD11 was detected in both fractions (Figure 5A). To clarify whether AtCGLD11 is a peripherally attached membrane protein, thylakoids were isolated from WT (Col-0) and extracted with standard salt solutions (Figure 5B). Moreover, membrane-integrated (PsaA and cpATPase-c) and peripherally attached (PsaD) proteins were immunodetected in control experiments. Under all four conditions tested, most of the AtCGLD11 remained associated with the membrane fraction, but could be partially extracted into the soluble fraction by exposure to NaSCN or NaOH. Since AtCGLD11 behaved similarly to PsaD in salt-wash experiments, we concluded that AtCGLD11 is an extrinsic membrane protein (Figure 5B).

We then measured the abundance of AtCGLD11 in WT plants. Known amounts of purified His-AtCGLD11 protein and total cell extracts from WT leaves were separated by SDS-PAGE, transferred to polyvinylidene fluoride (PVDF) membranes and probed with our specific antibody (Figure 5C). Signal quantification allowed us to calculate a concentration of $0.019 \pm 0.0026 \text{ mmol per mol Chl}^{-1}$ for AtCGLD11. Thus, based on previous quantification studies (Kirchhoff et al., 2002; Mao et al., 2015), AtCGLD11 is 40–50 times less abundant than the cpATPase complex. These results suggest AtCGLD11 is a low-abundance protein that mainly associates with chloroplast membranes but also is present in the soluble chloroplast fraction.

Lack of AtCGLD11 Affects Expression of Plastid Genes for cpATPase Subunits

We next asked whether AtCGLD11 plays a role in modulating the expression of cpATPase at the transcriptional or post-transcriptional (e.g., processing or splicing) level. Northern-blot analysis of size-fractionated RNAs from WT and mutant (*atcgld11-1* and *atcgld11-2*) plants (Figure 6A and 6C) with *atpB*- and *atpE*-specific radiolabeled probes revealed seven and three bands, respectively (Figure 6A). One dicistronic transcript, which migrated in between 1.8 and 3.2 kb, was recognized by both probes and was present in excess amounts in the mutant lines, whereas other transcripts derived from the small cpATPase operon were not significantly altered. Northern-blot analyses of the large operon revealed no obvious difference in the abundance of *atpA*-containing transcripts (Figure 6C). However, levels of an *atpH/F* transcript ($\sim 1.4 \text{ kb}$) were slightly reduced. Moreover, one normally low-abundance *atpI* fragment, which migrated slightly above 3.2 kb, was absent and the levels of three *atpI* transcripts (two between 1.8 and

	WT	<i>atcgld11-1</i>	<i>atcgld11-2</i>	<i>oeAtCGLD11.1</i>	<i>oeAtCGLD11.2</i>
F_v/F_m	0.80 ± 0.02	0.78 ± 0.02	0.77 ± 0.02	0.80 ± 0.01	0.80 ± 0.01
Φ_{II}	0.56 ± 0.05	0.44 ± 0.04	0.42 ± 0.06	0.55 ± 0.02	0.59 ± 0.01
1 – qP	0.23 ± 0.04	0.29 ± 0.03	0.31 ± 0.04	0.24 ± 0.02	0.21 ± 0.02
NPQ	0.45 ± 0.06	0.98 ± 0.28	1.23 ± 0.23	0.55 ± 0.08	0.42 ± 0.10
qE	0.26 ± 0.05	0.95 ± 0.12	1.08 ± 0.26	0.41 ± 0.08	0.31 ± 0.10
qI	0.24 ± 0.04	0.23 ± 0.11	0.22 ± 0.02	0.28 ± 0.04	0.21 ± 0.02

Table 1. Chl *a* Fluorescence Parameters of WT (Col-0), *atcgld11*, and *oeAtCGLD11* Plants Grown under Short-Day Conditions.

After 20 min of dark adaptation, leaves were exposed to 100 $\mu\text{mol photons m}^{-2} \text{s}^{-1}$ for 15 min. The subsequent dark-relaxation phase was recorded for 10 min. Average values ($n = 5$) and standard deviations for the following parameters were calculated: F_v/F_m , maximum quantum yield of PSII; Φ_{II} , effective quantum yield of PSII at 100 $\mu\text{mol photons m}^{-2} \text{s}^{-1}$; 1 – qP, excitation pressure; NPQ, non-photochemical Chl fluorescence quenching; qE, energy-dependent quenching of Chl fluorescence; qI, photoinhibitory quenching.

3.2 kb in size and one at ~ 1.7 kb) were reduced in *atcgld11-1* and *atcgld11-2* (Figure 6C).

In order to explore a possible function of AtCGLD11 in the transcription of plastid genes for cpATPase subunits, we performed run-on transcription assays (Figure 6D). Denatured DNA fragments derived from the six plastome-encoded cpATPase genes, as well as two controls (*rbcL* and *psbA*), were probed with radiolabeled RNAs isolated from WT and *atcgld11-1* chloroplasts. Signal intensities for both controls (*psbA* and *rbcL*) and all tested cpATPase transcripts were unaltered in *atcgld11-1*. Thus, *de novo* transcription rates of cpATPase subunits are not affected in *atcgld11-1*.

Translation rates of cpATPase- α/β subunits in *atcgld11* mutants were examined by pulse-labeling experiments (Figure 7). Because the soluble CF₁ subunits can be easily washed off thylakoid membranes (see Figure 5B), we analyzed newly synthesized proteins in isolated chloroplasts (see Methods for further details). In the insoluble fraction, synthesis rates for thylakoid-integral PSII subunits (D1/D2) in *atcgld11* mutants were found to be equal to those in WT plants. Remarkably, in the soluble fraction, the signals for labeled cpATPase- α/β protein

levels were increased in mutant plants. This implies that, in *atcgld11* mutants, the association of cpATPase- α/β proteins with the thylakoids is perturbed (Figure 4), but not their overall rates of synthesis (Figure 7).

Since only the translation rates of cpATPase- α/β subunits could be examined in our pulse-labeling experiments, we carried out polysome-loading experiments, which permit detection of translational defects associated with low-abundance *atp* transcripts (Supplemental Figure 4). To this end, we fractionated polysomes isolated from WT and *atcgld11-1* plants on sucrose gradients, and examined the RNA patterns in the different fractions by northern-blot analyses. Generally, transcripts bound to high-molecular-weight polysomes migrate further into the gradient during centrifugation and are enriched in the denser sucrose fractions (fractions 7–12, Supplemental Figure 4), whereas unbound transcripts are found in the upper, less dense fractions (fractions 1–6, Supplemental Figure 4). Therefore, translational initiation or elongation defects can be identified by an altered RNA profile within the gradient. Distributions of cytosolic (25S and 18S) and plastid rRNAs (23S, 16S, and 4.5S) in sucrose gradients were not significantly altered in *atcgld11-1*, which indicated that overall cytosolic and

Pigment	Col-0	<i>atcgld11-1</i>	<i>atcgld11-2</i>	<i>oeAtCGLD11.1</i>	<i>oeAtCGLD11.2</i>
Nx	52 ± 3	58 ± 5	58 ± 4	54 ± 2	58 ± 4
Vx	56 ± 2	48 ± 5	49 ± 4	54 ± 3	57 ± 7
Ax	2 ± 0	15 ± 2	14 ± 1	5 ± 1	2 ± 0
Zx	0 ± 0	8 ± 2	7 ± 1	2 ± 0	0 ± 0
VAZ	57 ± 5	70 ± 6	70 ± 6	61 ± 4	59 ± 7
Lut	184 ± 11	202 ± 21	202 ± 16	187 ± 9	201 ± 22
Car	129 ± 6	139 ± 11	137 ± 10	130 ± 5	138 ± 11
Chl <i>a</i>	1365 ± 72	1462 ± 109	1461 ± 101	1385 ± 45	1488 ± 100
Chl <i>b</i>	441 ± 23	487 ± 37	485 ± 36	448 ± 15	486 ± 35
Chl <i>a + b</i>	1806 ± 95	1948 ± 146	1947 ± 137	1832 ± 59	1974 ± 134

Table 2. Pigment Analyses of WT (Col-0), *atcgld11*, and *oeAtCGLD11* Plants.

Samples were harvested from 6-week-old plants grown in a climate chamber under short-day conditions (80–100 $\mu\text{mol photons m}^{-2} \text{s}^{-1}$). Pigments were extracted and quantified as described in the Methods. Average values ($n = 5$) and standard deviations are provided and values are given in pmol per mg fresh weight. Nx, neoxanthin; Vx, violaxanthin; Ax, antheraxanthin; Lut, lutein; Zx, zeaxanthin; Chl *a*, chlorophyll *a*; Chl *b*, chlorophyll *b*; car, carotene; VAZ, violaxanthin + antheraxanthin + zeaxanthin; Chl *a + b*, total chlorophyll.

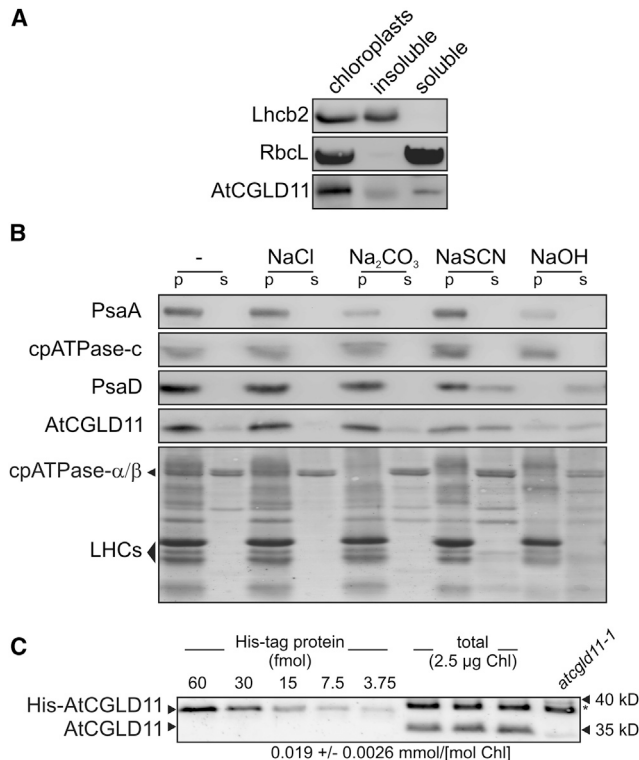


Figure 5. AtCGLD11 Membrane Association and Quantification.

(A) Chloroplasts were separated into soluble and insoluble fractions, which were analyzed for the presence of Lhcb2, RbcL, and AtCGLD11. **(B)** Membrane association of AtCGLD11. Thylakoid-enriched fractions of Col-0 chloroplasts were incubated with different salt solutions (NaCl, Na_2CO_3 , NaSCN, and NaOH) for 30 min on ice. Then the proteins remaining in the insoluble pellet fractions (p) and the proteins in the supernatants (s) were subjected to SDS-PAGE and western analyses. PsA and cpATPase-c were immunodetected as controls for membrane-integral subunits and PsAD as a control for a thylakoid-associated protein. PVDF membranes were stained with Coomassie brilliant blue G-250, and bands corresponding to LHCs and cpATPase- α/β are highlighted. **(C)** Quantification of AtCGLD11 in total leaf extract. Known amounts of purified His-AtCGLD11 and total leaf extracts corresponding to 2.5 μg Chl were separated by SDS-PAGE and subjected to western analyses using AtCGLD11-specific antibodies. The antibody also cross-reacted with a protein (marked with an asterisk), which was also present in the negative control *atcgld11-1*.

plastid translation was unaffected. Similarly, 57% of the overall signal (fraction 1–12) for *atpB/E* transcripts was detected in fractions 7–12 of *atcgld11-1* samples, compared with 53% in the WT sample. Interestingly, the dicistronic *atpB/E* transcript, which was found to overaccumulate in northern-blot analyses of *atcgld11* mutants (Figure 6A), was also enriched in the polysome-associated fractions (Supplemental Figure 4), possibly indicating that translation rates of cpATPase- β and cpATPase- ϵ might be slightly increased. With respect to the large operon, polysome-associated *atpI* (66% versus 63% in WT) and *atpH* transcript levels (59% versus 54% WT) were not dramatically changed in *atcgld11-1* samples (RNA levels are expressed relative to the overall signal for that transcript in each gradient). However, levels of one *atpH*, one *atpF*, and three *atpI*

transcripts were markedly decreased or undetectable in the polysome fractions of *atcgld11-1* samples.

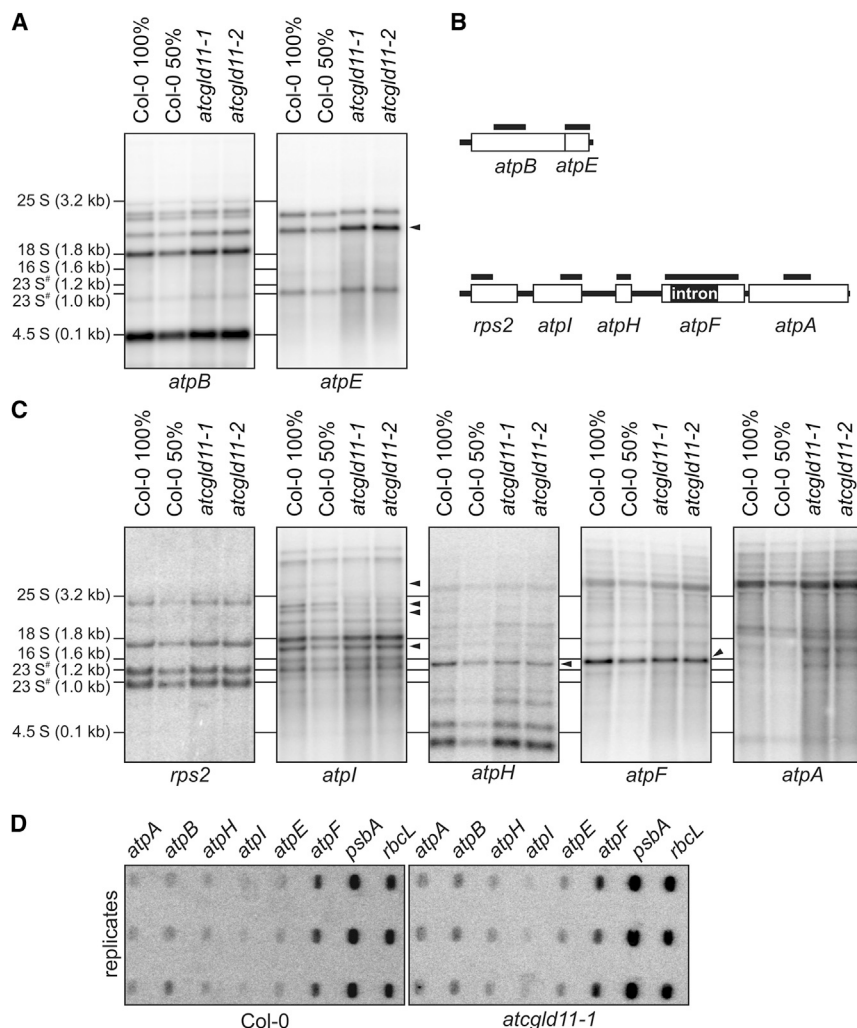
Taken together, the reduction or absence of several transcripts encoded in the large operon (Figure 6) might be explained by lower transcript stability, since *de novo* transcription of cpATPase genes was unaffected (Figure 6D). Moreover, pulse-labeling analyses showed that translation rates for the two CF_1 subunits cpATPase- α/β (Figure 7) are not perturbed, which is in line with the fact that *atpA* and *atpB* transcripts accumulate at least to WT levels (Figure 6A and 6C). No defects in translation initiation or elongation were observed for the transcripts derived from the two cpATPase operons in *atcgld11-1* (Supplemental Figure 4). However, the reduced steady-state levels of some processed transcripts are reflected in reduced association of *atpI*, *atpH*, and *atpF* with polysomes (Supplemental Figure 4), which would be expected to affect accumulation of the three chloroplast-encoded CF_0 subunits cpATPase-a, -b, and -c.

AtCGLD11 Interacts with the β Subunits of cpATPase and mtATPase

To probe whether AtCGLD11 is involved in cpATPase assembly, we examined the formation of intermediate assembly complexes by 2D gel electrophoresis and immunodetection analyses of isolated WT (Col-0) and *atcgld11-1* thylakoid membranes (Figure 8). CF_1 intermediates were visualized by immunodetection of cpATPase- α/β and γ , and CF_0 subcomplexes with antibodies against cpATPase-a, b, b', and c, respectively (Figure 8A). Subunits in the free, intermediate, and fully assembled cpATPase fractions were reduced to 20%–40% of WT in *atcgld11-1* (Figure 8B), which is in line with the results from our immunotitration analyses (Figure 4). However, no enrichment of a specific thylakoid-associated cpATPase intermediate, and thus no indication of any disruption in the membrane-associated assembly process, was observed.

Since some AtCGLD11 proteins are attached to chloroplast membranes (Figure 5A and 5B), we asked whether AtCGLD11 might be stably associated with a high-molecular-mass complex. The chloroplasts from WT (Col-0), *atcgld11-1*, and *oeAtCGLD11.1* plants were isolated, solubilized, and subjected to 2D gel and immunoblot analyses (Figure 9A). A faint signal was seen in the free protein fraction of the WT sample, which was absent in *atcgld11-1* and was more pronounced in the overexpressor line. This indicates that AtCGLD11 is not an integral part of the cpATPase, nor does it stably associate with any of its membrane-linked assembly intermediates.

To look for transient interactions of AtCGLD11 with CF_0 and CF_1 subunits, we performed split-ubiquitin and yeast two-hybrid assays, respectively. However, fusion constructs of AtCGLD11 in split-ubiquitin assays were not expressed in yeast and are for that reason not presented here. Yeast cells expressing the binding-domain fusion protein BD-AtCGLD11 were transformed with constructs coding for CF_1 subunits fused to the activation domain and plated on selective medium (lacking Leu, Trp, His, and Ade) (Figure 9B). Only cotransformants of BD-AtCGLD11 and AD- CF_1 - β were able to grow, indicating that AtCGLD11 interacts transiently with cpATPase- β . Since AtCGLD11 is a

**Figure 6. Transcript Analyses.**

(A–C) RNA samples from WT (Col-0) and the mutant lines *atcgld11-1* and *atcgld11-2* were size-fractionated by denaturing gel electrophoresis and blotted onto nylon membranes. Positions of rRNAs, which serve as molecular mass standards, are indicated (note that the two 23S rRNA breakdown products with sizes of 1.2 and 1.0 kb are depicted as 23S*). Probes specific for transcripts encoded in the (A) small (*atpB* and *atpE*) and (C) large (*rps2*, *atpI*, *atpH*, *atpF* and *atpA*) operons, respectively, are depicted as black bars in (B). Markedly altered transcript levels compared with the WT control are highlighted by black triangles. (D) Run-on transcription assays with intact, isolated WT, and *atcgld11-1* chloroplasts were carried out according to Zoschke et al. (2007). Newly synthesized RNA was labeled with ^{32}P -UTP, isolated, and hybridized to denatured DNA fragments immobilized on PVDF membranes. All plastid-encoded genes for cpATPase subunits, as well as two control genes (*psbA* and *rbcl*), were examined in three technical replicates.

dual-targeted protein (Figure 2C), we also tested AtCGLD11 interactions with mtATPase- α and - β (Figure 9C). Remarkably, yeast cells carrying BD-AtCGLD11/AD-MF $_1$ - β were also able to grow on selective medium. However, growth rates were lower than those of yeast cells expressing BD-AtCGLD11/AD-CF $_1$ - β , as became clear when cotransformants were plated in serial dilutions on selective medium (Figure 9C). Therefore, AtCGLD11 can interact with both CF $_1$ - β and, albeit apparently less strongly, with MF $_1$ - β .

DISCUSSION

Plants Lacking AtCGLD11 Exhibit a Characteristic cpATPase Deficiency Phenotype

AtCGLD11 is localized to chloroplasts and mitochondria and its loss affects the ultrastructure of both organelles (Figure 2). The changes in grana shape and stroma lamellae in *atcgld11-1* chloroplasts can be attributed to reduced cpATPase accumulation and the accompanying physiological effects. In fact, similar changes have been observed in mutants lacking the CF $_1$ assembly factor Alb4 (Benz et al., 2009) and to a greater degree in the chloroplasts of cpATPase- γ mutants, which showed swelling of the luminal space (Dal Bosco et al.,

2004). A more pronounced effect of the *atcgld11-1* mutation was observed on the morphology of mitochondria, which were significantly enlarged (Figure 2M). Several studies have shown that decreased accumulation of the mtATPase or the respiratory complex I/complex III supercomplexes cause similar effects (Lapaille et al., 2010; Pineau et al., 2013), but our analyses suggest that respiratory complexes (Figure 3B) and mtATPase activity (Figure 3D) are not altered in *atcgld11-1*. Hence, the swelling of *atcgld11*

mitochondria might either be a secondary effect of the chloroplast defect or reflect a more subtle impact of the depletion of AtCGLD11 in mitochondria, which we have not yet identified. Previous studies have demonstrated that plants with diminished levels of cpATPase are impaired in photosynthetic electron transport and trigger non-photochemical quenching mechanisms (Maiwald et al., 2003; Dal Bosco et al., 2004; Rott et al., 2011; Rühle et al., 2014). Our results corroborate these observations. In fact, the cpATPase deficiency phenotype of the *atcgld11* mutants presented here is very similar to that of the *Arabidopsis* CF $_0$ assembly mutant *atcg160* (Rühle et al., 2014). Residual cpATPase amounts (20%–30% of WT levels; Figure 4) lead to an overacidification of the lumen (indicated by the qE phenotype, Table 1). This in turn activates the xanthophyll cycle (indicated by increased antheraxanthin and zeaxanthin concentrations; Table 2) and induces non-photochemical quenching within light-harvesting proteins (reviewed by Jahns and Holzwarth, 2012). Consequently, electron transport rates are decreased (indicated by the lower ϕ_{II} ; Table 1), but efficient PSII photoprotective mechanisms are induced in *atcgld11* mutants (indicated by normal qI and F_v/F_m values; Table 1).

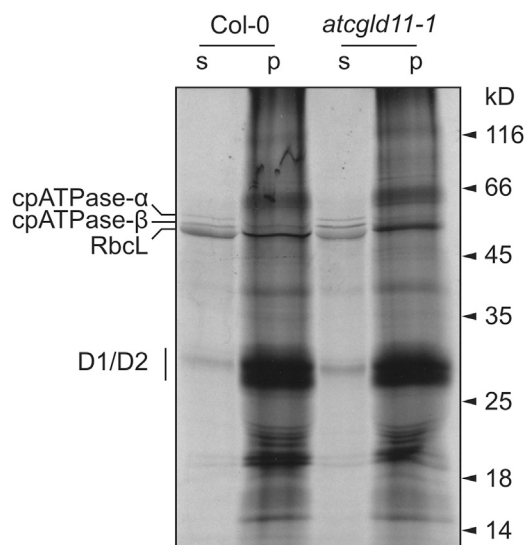


Figure 7. Rates of Translation of cpATPase- α/β .

Pulse-labeling analyses were carried out with isolated chloroplasts from WT and the knockout line *atcgld11-1*. Proteins from the soluble (s) and the insoluble fractions (p) were subjected to SDS-PAGE and signals were detected by X-ray film exposure. Positions of D1/D2, cpATPase- α , cpATPase- β , and RbcL, which are inferred from electrophoretic mobility patterns described in previous studies (Armbruster et al., 2010; Rühle et al., 2014), are highlighted.

Molecular Function of AtCGLD11 in cpATPase Biogenesis

Because lack of AtCGLD11 is associated with reduced accumulation of an active cpATPase (Figures 3C and 9), AtCGLD11 can be classified as an auxiliary, non-essential factor in cpATPase biogenesis. Other photosynthetic complexes are not markedly altered when AtCGLD11 is absent (Figure 4), implying that AtCGLD11's role is specific for cpATPase. Because steady-state levels of several RNAs encoding subunits of CF_O are specifically decreased (Figure 6A and 6C; Supplemental Figure 4) and *de novo* transcription rates of the six plastid-encoded cpATPase subunits are not affected in *atcgld11* mutants (Figure 6D), AtCGLD11 might possibly function in CF_O transcript stabilization. However, several of our findings argue against a direct role for AtCGLD11 in plastid gene expression: (i) the AtCGLD11 protein lacks a classical RNA-binding motif (e.g.,

a PPR domain) (Supplemental Figure 1); (ii) unlike RNA-binding proteins such as CSP41 (Qi et al., 2012), AtCGLD11 could not be detected in a high-molecular-mass complex (Figure 9A); (iii) we failed to pull down any *atp* transcripts in RNA immunoprecipitation analyses (data not shown); (iv) *Chlamydomonas* possesses a CGLD11 homolog (Supplemental Figure 1), but its *atp* gene organization differs significantly to that of embryophytes (Woessner et al., 1987; Maul et al., 2002). Thus, the diminished accumulation of CF_O transcripts observed in *atcgld11* mutants either represents a secondary effect of the drop in ATP synthesis or is the result of a regulatory loop that coordinates the expression of CF_O and CF₁ subunit genes, downregulating CF_O expression when CF₁ assembly is perturbed. Furthermore, the fact that some CF_O RNA species were not efficiently assembled into polysomes in *atcgld11-1* (Supplemental Figure 4) might constitute another regulatory response resulting from a CF₁ assembly defect. In this context, it is interesting to note that, in contrast to CF_O subunit expression, *atpB/atpE* expression levels are increased in *atcgld11* mutants (Figure 6). This is similar to the situation observed in the c-ring assembly mutant *atcg160-1*, which showed higher *atpH* (codes for cpATPase-c) expression levels (Rühle et al., 2014; Fristedt et al., 2015). Therefore, the up-regulation of CF₁- β transcript in *atcgld11* might represent an analogous mechanism to compensate for a defect in CF₁ assembly or instability of β in the absence of interaction with CGLD11.

Several results argue in favor of a post-translational function of AtCGLD11 in CF₁ assembly: (i) AtCGLD11 is co-regulated with the CF₁ assembly factor PAB (Mao et al., 2015) (AT4G34090; <http://atted.jp>), (ii) in the absence of AtCGLD11, CF₁- α and CF₁- β accumulate in the soluble chloroplast fraction (Figure 7), but their association with thylakoids is disturbed (Figures 4 and 8), and (iii) AtCGLD11 interacts with CF₁- β in yeast two-hybrid assays (Figure 9B). Interestingly, the mitochondrial F₁ assembly factors Atp12p (Wang et al., 2000) and Atp11p (Wang and Ackerman, 2000), which are known to interact with MF₁- α and MF₁- β in yeast, respectively, have not been identified in chloroplasts. In yeast, the absence of either of these F₁ chaperones leads to the formation of high-molecular-mass aggregates containing MF₁- α and MF₁- β (Ackerman and Tzagoloff, 1990), which are found in the form of inclusion bodies in the mitochondrial matrix (Lefebvre-Legendre et al., 2005). Based on such observations, it has been proposed that Atp11p and Atp12p act as decoys to prevent unfavorable α - α

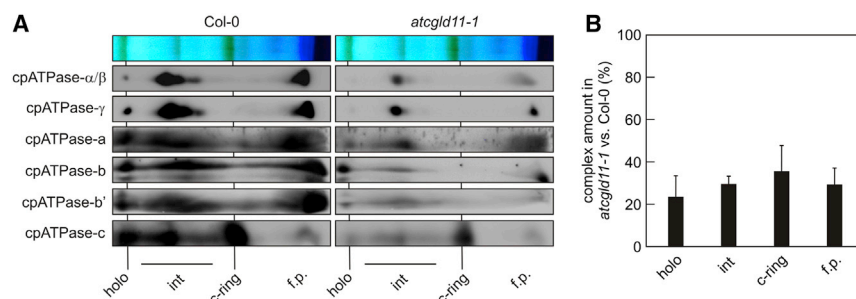


Figure 8. cpATPase Assembly Analyses.

(A) BN/SDS-PAGE and western analyses of thylakoid-associated cpATPase intermediates. Antibodies specific for individual cpATPase subunits were employed to identify CF₁- and CF_O-specific intermediates. The positions of the fully assembled cpATPase (holo), cpATPase intermediates (int), the cpATPase-c ring (c-ring), and free proteins (f.p.) are indicated.

(B) Quantification of fully assembled cpATPase (holo), cpATPase assembly intermediates (int), the c-ring, and free proteins (f.p.) was based on cpATPase- α/β , cpATPase- γ , and cpATPase-c

immunodetection assays. Chemiluminescence signals were quantified as described in the Methods, and are depicted as ratios of *atcgld11-1* to Col-0 (expressed in %). Values are averages of three biological replicates and error bars represent SDs.

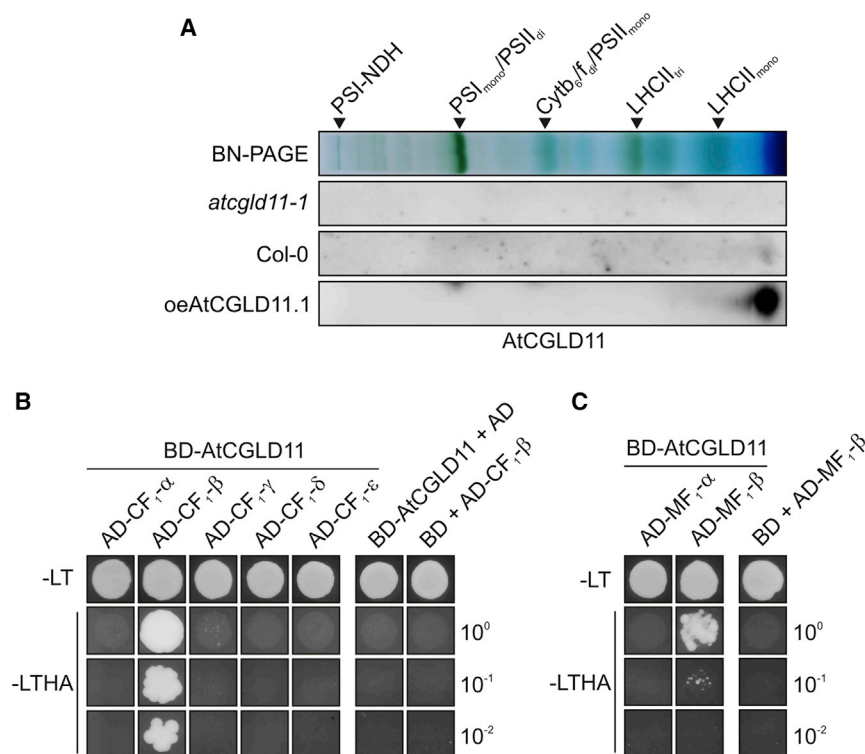


Figure 9. AtCGLD11 Comigration Analyses and Interaction Studies with ATPase Subunits in Yeast Two-Hybrid Assays.

(A) Thylakoid samples isolated from Col-0, *atcgld11-1*, and *oeAtCGLD11.1* were solubilized and subjected to 2D gel analyses. After blotting, PVDF membranes were probed with an AtCGLD11-specific antibody. The BN-PAGE pattern of solubilized WT thylakoid complexes is provided as a reference.

(B) Yeast cells carrying the BD-AtCGLD11 were transformed with constructs coding for fusions of CF₁ subunits to the activation domain AD. Control assays were carried out with cotransformed yeast cells carrying the empty vector pGADT7 (coding for the activation domain AD only) and the BD-AtCGLD11 vector or the empty vector pGBKT7 (coding for the binding domain BD only) and the AD-CF_{1-β} vector.

(C) Interaction of MF_{1-α} and -β with CGLD11 was tested by cotransformation of BD-AtCGLD11 and AD-MF_{1-α} or AD-MF_{1-β} constructs. As control, the AD-MF_{1-β} construct was transformed into yeast cells carrying the empty vector pGBKT7. Successful transformation was checked by plating on permissive medium lacking Leu and Trp (-LT). Interactions were then tested on selective medium (-Leu/-Trp/-His/-Ade) by plating equal numbers of yeast cells in serial dilutions (10⁰, 10⁻¹, and 10⁻²).

or β-β dimerization. Although AtCGLD11 does not show any sequence similarity to Atp11p, it might have acquired a similar role in chloroplasts by convergent evolution, namely the integration of cpATPase-β into a functional complex during early CF₁ assembly steps.

AtCGLD11, a Green-Lineage-Specific ATPase Biogenesis Factor Shared between Plastids and Mitochondria?

The fact that AtCGLD11 is required for efficient cpATPase accumulation and is also targeted to mitochondria raises the question whether AtCGLD11 is also involved in mtATPase biogenesis. However, mtATPase accumulation and activity were not impaired in the mutant (Figure 3), even though AtCGLD11 physically interacts with mtATPase-β (Figure 9C), which is highly similar to cpATPase-β. Based on these data, AtCGLD11 function seems to be less critical for MF₁ biosynthesis. Indeed, this is corroborated by the weaker interaction of AtCGLD11 with mtATPase-β identified in yeast two-hybrid assays (Figure 9C). Moreover, Atp11p and/or Atp12p homologs that are present in plant mitochondria (Pícková et al., 2005), or other unknown MF₁ auxiliary factors, might compensate for a functional defect in AtCGLD11. Thus, AtCGLD11 represents an invention of the green lineage, which localizes to chloroplasts and mitochondria, interacts with the same subunit of the ATP synthase complexes in both organelles, and clearly has a function in ATP synthase assembly in chloroplasts. Its innocuous mutant phenotype with regard to mtATPase assembly might be attributable to functional redundancy, because mitochondria contain additional assembly factors not found in chloroplasts. Alternatively, the mitochondrial targeting of AtCGLD11 might be a relatively new evolutionary invention,

such that its function in mtATPase assembly is in the process of being fully established.

METHODS

Plant Material and Growth Conditions

The *atcgld11-1* (SALK_019326C) and *atcgld11-2* (SALK_006444C) T-DNA lines, both in the Col-0 background, were obtained from the SALK collection (Alonso et al., 2003). *Arabidopsis thaliana* plants were grown under controlled greenhouse conditions (70–90 μmol photons m⁻² s⁻¹, 16/8 h light/dark cycles) as described in Rühle et al. (2014). For biochemical and physiological analyses, plants were grown in climate chambers under short-day (8/16 h light/dark) or long-day (16/8 h) conditions. For complementation experiments, the *AtCGLD11* coding region (gene model AT2G21385.1 according to TAIR) was cloned into the binary Gateway destination vector pB2GW7 (Karimi et al., 2002), placing the gene under the control of the 35S promoter derived from the Cauliflower Mosaic Virus. Construct transformation into *atcgld11-1* plants and BASTA selection were carried out as described in Rühle et al. (2014). Levels of AtCGLD11 were determined from western blots, and complementation of the *atcgld11-1* mutant phenotype was assessed by measuring leaf surface areas from 14-day-old plants grown under short-day or long-day conditions (Figure 2) and by NPQ analysis (Supplemental Figure 2A).

Ultrastructural Analysis of *atcgld11-1*

A. thaliana seedlings for transmission electron microscopy studies were grown on soil (14 days) under short-day conditions. Plants were harvested in the dark and immediately prefixed in 2.5% (w/v) glutaraldehyde in 75 mM cacodylate buffer (pH 7.0). Five independent plants were analyzed. Distal pieces (approximately 1 mm² segments, standardized area) of pre-fixed vegetative leaf 2 were then rinsed in cacodylate buffer and fixed in 1% (w/v) osmium tetroxide in the same buffer for 2.5 h at room temperature. The specimens were stained *en bloc* with 1% (w/v) uranyl acetate in 20% acetone, dehydrated in a graded acetone series and embedded in Spurr's low-viscosity epoxy resin (Spurr, 1969). Semi-thin sections

(500 nm thick) for overviews (400×) were analyzed by light microscopy. Ultrathin sections (40–55 nm thick) were cut with a diamond knife on an Ultramicrotome Leica EM UC6, and post-stained with lead citrate (Reynolds, 1963). Micrographs were taken at 1800× (overviews) and 7100×, 22 000× and 44 000× (details) at 80 kV on a Fei Morgagni 268 electron microscope.

ATPase Synthase Activity Measurements

Mitochondria and chloroplasts were isolated from 14-day-old plants grown on soil as described previously (Lister et al., 2007; Benz et al., 2009). Photophosphorylation assays using radiolabeled inorganic phosphate (^{32}P) and 5 μg of either mitochondrial or plastidial protein were performed according to Benz et al. (2009), and stopped by addition of EDTA after 1, 2, 5, or 10 min. After centrifugation, 0.5- μl aliquots of the supernatant were spotted onto a PEI Cellulose thin-layer chromatography plate (Merck, Germany), which was developed in 1 M KH_2PO_4 . Radioactivity was recorded on X-ray film and spots were quantified using ImageQuant TL (GE Healthcare, USA).

Chl a Fluorescence Measurements

Chl a fluorescence measurements on single leaves and whole plants were carried out with the Dual-PAM 101/103 fluorometer (Walz, Effeltrich, Germany) and an imaging Chl a fluorometer (Walz Imaging PAM; Walz), respectively, as described in Rühle et al. (2014). Non-photochemical Chl fluorescence quenching of whole plants ($\text{NPQ}/4 = (\text{Fm} - \text{Fm}')/\text{Fm}'/4$) was calculated as described in Bilger and Björkman (1990).

Nucleic Acid Analyses

Genomic DNA was isolated from *Arabidopsis* rosette leaves as described in Ihnawicz et al. (2004). T-DNA insertion sites for *atcglD11-1* and *atcglD11-2* were identified by PCR using gene-specific and insertion-specific primer combinations (see Supplemental Table 1). Total RNA was isolated from fresh leaves using TRIzol reagent (Invitrogen, Karlsruhe, Germany). Reverse transcription was carried out with Superscript III reverse transcriptase (Invitrogen) according to the manufacturer's instructions. *AtCGLD11* transcripts were quantified by PCR using primer sets flanking the up- or downstream regions of the T-DNA insertion sites (for primer information, see Supplemental Table 1).

Northern analyses and polysome analyses were done as described previously (Rühle et al., 2014). The primer sequences used for probe generation are listed in Supplemental Table 1. DNA fragments amplified from cDNA were labeled with radioactive [α - ^{32}P]dCTP and signals were detected with the Typhoon Phosphor Imager System (GE Healthcare).

Run-on assays were performed according to Zoschke et al. (2007). Intact chloroplasts were isolated from 10-g samples of leaves in a Percoll gradient (40/70%) according to Grisse et al. (1986). For *in vitro* transcription, 3×10^7 chloroplasts were used for each genotype. The reaction was performed at 25°C for 15 min in 50 mM 2-amino-2-(hydroxymethyl)-1,3-propane diol (TRIS)-HCl (pH 8.0), 10 mM MgCl_2 , 10 mM β -mercaptoethanol, 40 U RNase inhibitor, 0.2 mM ATP, GTP, CTP, and 10 $\mu\text{Ci}/\mu\text{l}$ [α - ^{32}P]UTP. Transcription was terminated by adding 5% sodium-lauroylsarcosine, 50 mM (TRIS)-HCl (pH 8.0) and 25 mM EDTA. The radiolabeled RNAs were isolated, and hybridized to 1- μg samples of DNA fragments which were spotted on a nylon membrane in triplicate. The signals were detected with the Typhoon Phosphor Imager System (GE Healthcare).

Leaf Pigment Analysis

Leaves from plants grown under short-day conditions (6 weeks) were harvested 4 h after the onset of the light phase and ground in liquid nitrogen. After treating leaf material with 100% acetone, cell debris were eliminated by centrifugation (16,000 g, 20 min at 4°C) and pigments in the supernatants were analyzed as described in Färber et al. (1997).

Thylakoid Membrane Isolation, Immunotitrations, and BN/SDS-PAGE

Thylakoid membrane isolation, immunotitrations and BN/SDS-PAGE analyses were carried out with leaves from 6-week-old plants grown under short-day conditions as described previously in Rühle et al. (2014). For BN-PAGE of solubilized mitochondria, samples (50 μg protein) were treated with solubilization buffer (1% (w/v) β -D-maltoside (β -DM), 20% (w/v) glycerol, 25 mM BisTris pH 7.0) for 10 min on ice. After centrifugation (16 000 g, 20 min, 4°C), supernatants were supplemented with 1/10 volume of BN sample buffer (100 mM BisTris/HCl [pH 7.0], 750 mM ϵ -aminocaproic acid, 5% (w/v) Coomassie G-250). BN-PAGE gels (4–16%) were cast according to Schagger et al. (1994). Solubilized thylakoid and mitochondria samples corresponding to 20 μg Chl or 50 μg protein, respectively, were loaded per lane and complexes were separated at 4°C overnight. Chlorophyll and protein concentrations were determined according to Porra et al. (1989) and with the Bradford method (Bio-Rad), respectively. BN-PAGE strips were incubated in denaturing buffer (0.5 M Na_2CO_3 , 2% [w/v] SDS, 0.7% [v/v] β -mercaptoethanol) for 30 min at room temperature, and complexes were either transferred directly onto PVDF membranes or separated into their subunits on denaturing PAGE gels. To this end, BN strips were loaded onto Tricine-SDS-PA gels (10% gels supplemented with 4 M urea), which were cast according to Schagger (2006). After electrophoresis, gels were stained with colloidal Coomassie blue (Dyballa and Metzger, 2009) or subjected to immunoblot analysis as described below.

Chloroplast Isolation and Salt-Wash Treatment of Thylakoids

Chloroplast isolation was performed according to Kunst (1998) and is described in detail in Rühle et al. (2014). Salt-wash treatments were performed as described by Karnauchov et al. (1997). In brief, isolated WT thylakoid membranes were incubated with either 2 M NaCl, 0.1 M Na_2CO_3 , 2 M NaSCN, or 0.1 M NaOH for 30 min on ice. Then insoluble and soluble membrane proteins were separated by centrifugation at 16 000 g for 10 min at 4°C. Pelleted proteins, and soluble proteins that had been acetone-extracted from the supernatants, were solubilized, fractionated on Tricine-SDS-PAGE gels (10%), and subjected to immunoblot analysis using antibodies specific for PsA (Agrisera; Vännäs, Sweden), PsD (Agrisera), cpATPase-c (Agrisera) and AtCGLD11.

Immunoblot Analyses

Proteins fractionated by gel electrophoresis were blotted onto PVDF membranes (Immobilon-P; Millipore, Eschborn, Germany) using a semi-dry blotting apparatus (Bio-Rad) as described in the manufacturers' instructions. After blocking with TBST (10 mM Tris [pH 8.0], 150 mM NaCl, and 0.1% Tween-20) supplemented with 3% milk, the membranes were incubated with antibodies directed against subunits of PSII (Agrisera), PSI (Agrisera), Cyt *b₆/f* (Agrisera), cpATPase subunits (Agrisera) or obtained from Jörg Meurer, University of Munich), or against AtCGLD11 at 4°C overnight. An antibody against Tom40 was provided by Chris Carrie (University of Munich). Rabbit antibodies were generated against AtCGLD11, which had been heterologously expressed in *Escherichia coli*, and purified. To this end, AtCGLD11₇₉₋₃₃₀ was cloned into the pET51b(+) vector (Novagen) using *Sal*I and *Not*I restriction sites, yielding an N-terminal fusion with a Strep-tag and a C-terminal fusion with a His₁₀-tag. The Strep-AtCGLD11₇₉₋₃₃₀-His₁₀ protein was purified using Ni-NTA Agarose (Qiagen) followed by purification with Strep-Tactin Sepharose (Iba-lifescience, Göttingen, Germany) according to the manufacturer's instructions. The protein was injected into rabbits for antibody production (Pineda, Berlin, Germany), and antiserum was employed at a dilution of 1:1000. Signals were detected by enhanced chemiluminescence (ECL kit, Amersham Bioscience) using an ECL reader system (Fusion FX7; PeqLab, Erlangen, Germany) and quantified with Bioprofile software (PeqLab).

In Vivo Translation in Chloroplasts

Plants were grown on 0.5× Murashige and Skoog medium in the presence of 1% (w/v) sucrose for 14 days under long-day conditions. Chloroplasts

were isolated according to Benz et al. (2009). Protein concentration was measured (Lowry et al., 1951) and chloroplasts corresponding to a protein content of 100 µg were employed for *in vivo* translation assays. Translation was performed in translation buffer (50 mM HEPES-KOH [pH 8.0], 2 mM ATP, 0.2 mM GTP, 8 mM Mg-acetate, 118 mM K-acetate, 10 mM DTT, 100 µM amino acid mix without methionine) and [³⁵S]methionine for 15 min at room temperature and a light intensity of 500 µmol photons m⁻² s⁻¹. A chase was performed for 30 min in translation buffer and 10 mM methionine. Chloroplasts were pelleted and subjected to lysis buffer (50 mM Tris [pH 7.5], 5 mM MgCl₂, 10 mM DTT). After incubation on ice for 10 min, soluble and insoluble fractions were separated by centrifugation (13 000 g, 10 min, 4°C). Proteins were analyzed by SDS-PAGE and X-ray films.

Yeast Two-Hybrid Assay

Yeast two-hybrid assays were carried out using the Matchmaker Two-Hybrid System Kit (Clontech). The AT2G21385.1 CDS without the signal peptide coding sequence (see Supplemental Table 1 for primer information) was cloned into the bait vector pGBKT7 (named BD-AtCGLD11), whereas the coding sequences of CF₁-α, -β, -γ, -δ, -ε, as well as MF₁-α and -β, were cloned into the prey vector pGADT7 (named AD-CF₁-α, -β, -γ, -δ, -ε, and AD-MF₁-β). As in the case of AtCGLD11, signal peptide sequences were omitted from the nucleus-encoded subunits CF₁-γ, CF₁-δ, and MF₁-β. Bait and prey vectors were cotransformed into the AH109 yeast strain (Clontech) following the manufacturer's instructions. As controls, yeast cells carrying the empty vector pGADT7 were transformed with BD-AtCGLD11, and yeast cells bearing the empty vector pGBKT7 with AD-CF₁-β and AD-MF₁-β, respectively. Cotransformants were selected on synthetic dropout (SD) medium (Clontech) lacking leucine and tryptophan (-LT). In order to identify protein interactions, double transformants were grown on SD medium lacking leucine, tryptophan, histidine, and adenine (-LTHA).

Bioinformatics Sources

Gene and protein sequences were obtained from the National Center for Biotechnology Information server (NCBI; <http://www.ncbi.nlm.nih.gov/>), the *Arabidopsis* Information Resource server (TAIR; <http://www.Arabidopsis.org>), and Phytozome (<http://phytozome.jgi.doe.gov>). Protein sequences were aligned using the Vector NTI software (Invitrogen). Chloroplast transit peptides were predicted by ChloroP (<http://www.cbs.dtu.dk/services/ChloroP/>). Alignments were formatted using Boxshade (http://www.ch.embnet.org/software/BOX_form.html).

ACCESSION NUMBERS

Sequence identifiers for AtCGLD11.1 (GI: 330252075) homologs in eukaryotes are: *Vitis vinifera* (GI: 731383153), *Oryza sativa* (GI: 115480319), *Zea mays* (GI: 195648404), *Picea sitchensis* (GI: 116794136), *Physcomitrella patens* (Phpat.022G017100.1, Phytozome), *Selaginella moellendorffii* (GI: 302761380), *Chlamydomonas reinhardtii* (Cre08.g372000.t1.2, Phytozome), and *Thalassiosira pseudonana* (GI: 223995093).

SUPPLEMENTAL INFORMATION

Supplemental Information is available at *Molecular Plant Online*.

FUNDING

Financial support by the Deutsche Forschungsgemeinschaft (grant LE 1265/30-1) is gratefully acknowledged.

AUTHOR CONTRIBUTIONS

S.G., B.R., J.S., D.L., and T.R. designed the research. S.G., B.R., I.L.G., E.V., C.G., P.J., and T.R. performed the research. S.G., B.R., J.S., D.L., and T.R. prepared the article. J.S., D.L., and T.R. supervised the whole study.

ACKNOWLEDGMENTS

We would like to thank Ilona Kutschka, Felix Zierhut, and Benjamin Schwarz for excellent technical assistance. We thank Paul Hardy for critical comments on the manuscript. No conflict of interest declared.

Received: January 18, 2016

Revised: February 29, 2016

Accepted: March 7, 2016

Published: March 11, 2016

REFERENCES

- Ackerman, S.H., and Tzagoloff, A. (1990). Identification of two nuclear genes (ATP11, ATP12) required for assembly of the yeast F₁-ATPase. *Proc. Natl. Acad. Sci. USA* **87**:4986–4990.
- Alonso, J.M., Stepanova, A.N., Leisse, T.J., Kim, C.J., Chen, H., Shinn, P., Stevenson, D.K., Zimmerman, J., Barajas, P., Cheuk, R., et al. (2003). Genome-wide insertional mutagenesis of *Arabidopsis thaliana*. *Science* **301**:653–657.
- Armbruster, U., Zühlke, J., Rengstl, B., Kreller, R., Makarenko, E., Rühle, T., Schünemann, D., Jahns, P., Weisshaar, B., Nickelsen, J., et al. (2010). The *Arabidopsis* thylakoid protein PAM68 is required for efficient D1 biogenesis and photosystem II assembly. *Plant Cell* **22**:3439–3460.
- Benz, M., Bals, T., Gügel, I.L., Piotrowski, M., Kuhn, A., Schünemann, D., Soll, J., and Ankele, E. (2009). Alb4 of *Arabidopsis* promotes assembly and stabilization of a non chlorophyll-binding photosynthetic complex, the CF₁CF₀-ATP synthase. *Mol. Plant* **2**:1410–1424.
- Bilger, W., and Björkman, O. (1990). Role of the xanthophyll cycle in photoprotection elucidated by measurements of light-induced absorbance changes, fluorescence and photosynthesis in leaves of *Hedera canariensis*. *Photosynth. Res.* **25**:173–185.
- Chen, G.G., and Jagendorf, A.T. (1994). Chloroplast molecular chaperone-assisted refolding and reconstitution of an active multisubunit coupling factor CF₁ core. *Proc. Natl. Acad. Sci. USA* **91**:11497–11501.
- Dal Bosco, C., Lezhneva, L., Biehl, A., Leister, D., Strotmann, H., Wanner, G., and Meurer, J. (2004). Inactivation of the chloroplast ATP synthase gamma subunit results in high non-photochemical fluorescence quenching and altered nuclear gene expression in *Arabidopsis thaliana*. *J. Biol. Chem.* **279**:1060–1069.
- Dyballa, N., and Metzger, S. (2009). Fast and sensitive colloidal coomassie G-250 staining for proteins in polyacrylamide gels. *J. Vis. Exp.*, 2–5.
- Färber, A., Young, A.J., Ruban, A.V., Horton, P., and Jahns, P. (1997). Dynamics of xanthophyll-cycle activity in different antenna subcomplexes in the photosynthetic membranes of higher plants (the relationship between zeaxanthin conversion and nonphotochemical fluorescence quenching). *Plant Physiol.* **115**:1609–1618.
- Fristedt, R., Martins, N.F., Strenkert, D., Clarke, C.A., Suchoszek, M., Thiele, W., Schöttler, M.A., and Merchant, S.S. (2015). The thylakoid membrane protein CGL160 supports CF₁CF₀ ATP synthase accumulation in *Arabidopsis thaliana*. *PLoS One* **10**:e0121658.
- Groth, G., and Pohl, E. (2001). The structure of the chloroplast F₁-ATPase at 3.2 Å resolution. *J. Biol. Chem.* **276**:1345–1352.
- Gruissem, W., Greenberg, B.M., Zurawski, G., and Hallick, R.B. (1986). Chloroplast gene expression and promoter identification in chloroplast extracts. *Methods Enzymol.* **118**:253–270.
- Harti, F.U. (2002). Molecular chaperones in the cytosol: from nascent chain to folded protein. *Science* **295**:1852–1858.
- Hilbers, F., Eggers, R., Pradela, K., Friedrich, K., Herkenhoff-Hesselmann, B., Becker, E., and Deckers-Hebestreit, G. (2013). Subunit δ is the key player for assembly of the H⁺-translocating unit

- of *Escherichia coli* F₀F₁ ATP synthase. J. Biol. Chem. **288**:25880–25894.
- Ihnatowicz, A., Pesaresi, P., Varotto, C., Richly, E., Schneider, A., Jahns, P., Salamini, F., and Leister, D. (2004). Mutants for photosystem I subunit D of *Arabidopsis thaliana*: effects on photosynthesis, photosystem I stability and expression of nuclear genes for chloroplast functions. Plant J. **37**:839–852.
- Jahns, P., and Holzwarth, A.R. (2012). The role of the xanthophyll cycle and of lutein in photoprotection of photosystem II. Biochim. Biophys. Acta **1817**:182–193.
- Karimi, M., Inzé, D., and Depicker, A. (2002). GATEWAY vectors for *Agrobacterium*-mediated plant transformation. Trends Plant Sci. **7**:193–195.
- Karnauchov, I., Herrmann, R.G., and Klösken, R.B. (1997). Transmembrane topology of the Rieske Fe/S protein of the cytochrome *b₆/f* complex from spinach chloroplasts. FEBS Lett. **408**:206–210.
- Karpowicz, S.J., Prochnik, S.E., Grossman, A.R., and Merchant, S.S. (2011). The GreenCut2 Resource, a phylogenomically derived inventory of proteins specific to the plant lineage. J. Biol. Chem. **286**:21427–21439.
- Kirchhoff, H., Mukherjee, U., and Galla, H.-J. (2002). Molecular architecture of the thylakoid membrane: lipid diffusion space for plastoquinone. Biochemistry **41**:4872–4882.
- Klodmann, J., Senkler, M., Rode, C., and Braun, H.-P. (2011). Defining the protein complex proteome of plant mitochondria. Plant Physiol. **157**:587–598.
- Kunst, L. (1998). Preparation of physiologically active chloroplasts from *Arabidopsis*. Methods Mol. Biol. **82**:43–48.
- Lapaille, M., Thiry, M., Perez, E., González-Halphen, D., Remacle, C., and Cardol, P. (2010). Loss of mitochondrial ATP synthase subunit beta (Atp2) alters mitochondrial and chloroplastic function and morphology in *Chlamydomonas*. Biochim. Biophys. Acta **1797**:1533–1539.
- Lefebvre-Legendre, L., Salin, B., Schaëffer, J., Brêthes, D., Dautant, A., Ackerman, S.H., and di Rago, J.-P. (2005). Failure to assemble the $\alpha_3\beta_3$ subcomplex of the ATP synthase leads to accumulation of the α and β subunits within inclusion bodies and the loss of mitochondrial cristae in *Saccharomyces cerevisiae*. J. Biol. Chem. **280**:18386–18392.
- Leister, D., Varotto, C., Pesaresi, P., Niwergall, A., and Salamini, F. (1999). Large-scale evaluation of plant growth in *Arabidopsis thaliana* by non-invasive image analysis. Plant Physiol. Biochem. **37**:671–678.
- Lister, R., Carrie, C., Duncan, O., Ho, L.H.M., Howell, K.A., Murcha, M.W., and Whelan, J. (2007). Functional definition of outer membrane proteins involved in preprotein import into mitochondria. Plant Cell **19**:3739–3759.
- Lowry, O.H., Rosebrough, N.J., Farr, A.L., and Randall, R.J. (1951). Protein measurement with the Folin phenol reagent. J. Biol. Chem. **193**:265–275.
- Maiwald, D., Dietzmann, A., Jahns, P., Pesaresi, P., Joliot, P., Joliot, A., Levin, J.Z., Salamini, F., and Leister, D. (2003). Knock-out of the genes coding for the rieske protein and the ATP-synthase δ -subunit of *Arabidopsis*. Effects on photosynthesis, thylakoid protein composition, and nuclear chloroplast gene expression. Plant Physiol. **133**:191–202.
- Malik Ghulam, M., Zghidi-Abouzid, O., Lambert, E., Lerbs-Mache, S., and Merendino, L. (2012). Transcriptional organization of the large and the small ATP synthase operons, *atp1/H/F/A* and *atpB/E*, in *Arabidopsis thaliana* chloroplasts. Plant Mol. Biol. **79**:259–272.
- Mao, J., Chi, W., Ouyang, M., He, B., Chen, F., and Zhang, L. (2015). PAB is an assembly chaperone that functions downstream of chaperonin 60 in the assembly of chloroplast ATP synthase coupling factor 1. Proc. Natl. Acad. Sci. USA **112**:4152–4157.
- Maul, J.E., Lilly, J.W., Cui, L., DePamphilis, C.W., Miller, W., Harris, E.H., and Stern, D.B. (2002). The *Chlamydomonas reinhardtii* plastid chromosome: islands of genes in a sea of repeats. Plant Cell **14**:2659–2679.
- Merchant, S.S., Prochnik, S.E., Vallon, O., Harris, E.H., Karpowicz, S.J., Witman, G.B., Terry, A., Salamov, A., Fritz-Laylin, L.K., Maréchal-Drouard, L., et al. (2007). The *Chlamydomonas* genome reveals the evolution of key animal and plant functions. Science **318**:245–250.
- Miyagi, T., Kapoor, S., Sugita, M., and Sugiura, M. (1998). Transcript analysis of the tobacco plastid operon *rps2/atp1/H/F/A* reveals the existence of a non-consensus type II (NCII) promoter upstream of the *atp1* coding sequence. Mol. Gen. Genet. **257**:299–307.
- Pfalz, J., Bayraktar, O.A., Prikryl, J., and Barkan, A. (2009). Site-specific binding of a PPR protein defines and stabilizes 5' and 3' mRNA termini in chloroplasts. EMBO J. **28**:2042–2052.
- Pícková, A., Potocký, M., and Houstek, J. (2005). Assembly factors of F₁F₀-ATP synthase across genomes. Proteins **59**:393–402.
- Pineau, B., Bourge, M., Marion, J., Mauve, C., Gilard, F., Maneta-Peyret, L., Moreau, P., Satiat-Jeunemaitre, B., Brown, S.C., De Paepe, R., et al. (2013). The importance of cardiolipin synthase for mitochondrial ultrastructure, respiratory function, plant development, and stress responses in *Arabidopsis*. Plant Cell **25**:4195–4208.
- Porra, R.J., Thompson, W.A., and Kriedemann, P.E. (1989). Determination of accurate extinction coefficients and simultaneous equations for assaying chlorophylls a and b extracted with four different solvents: verification of the concentration of chlorophyll standards by atomic absorption spectroscopy. Biochim. Biophys. Acta **975**:384–394.
- Qi, Y., Armbruster, U., Schmitz-Linneweber, C., Delannoy, E., de Longevialle, A.F., Rühle, T., Small, I., Jahns, P., and Leister, D. (2012). *Arabidopsis* CSP41 proteins form multimeric complexes that bind and stabilize distinct plastid transcripts. J. Exp. Bot. **63**:1251–1270.
- Reynolds, E.S. (1963). The use of lead citrate at high pH as an electron-opaque stain in electron microscopy. J. Cell Biol. **17**:208–212.
- Rott, M., Martins, N.F., Thiele, W., Lein, W., Bock, R., Kramer, D.M., and Schöttler, M.A. (2011). ATP synthase repression in tobacco restricts photosynthetic electron transport, CO₂ assimilation, and plant growth by overacidification of the thylakoid lumen. Plant Cell **23**:304–321.
- Rühle, T., and Leister, D. (2015). Assembly of F₁F₀-ATP synthases. Biochim. Biophys. Acta **1847**:849–860.
- Rühle, T., Razeghi, J.A., Vamvaka, E., Viola, S., Gandini, C., Kleine, T., Schünemann, D., Barbato, R., Jahns, P., and Leister, D. (2014). The *Arabidopsis* protein CONSERVED ONLY IN THE GREEN LINEAGE160 promotes the assembly of the membranous part of the chloroplast ATP synthase. Plant Physiol. **165**:207–226.
- Schägger, H. (2006). Tricine-SDS-PAGE. Nat. Protoc. **1**:16–22.
- Schägger, H., Cramer, W.A., and Vonjagow, G. (1994). Analysis of molecular masses and oligomeric states of protein complexes by blue native electrophoresis and isolation of membrane protein complexes by two-dimensional native electrophoresis. Anal. Biochem. **217**:220–230.
- Spurr, A.E. (1969). A low-viscosity epoxy resin embedding medium for electron microscopy. J. Ultrastruct. Res. **26**:31–43.
- Stahl, D.J., Rodermer, S.R., Bogorad, L., and Subramanian, A.R. (1993). Co-transcription pattern of an introgressed operon in the maize chloroplast genome comprising four ATP synthase subunit genes and the ribosomal *rps2*. Plant Mol. Biol. **21**:1069–1076.

- Swiatecka-Hagenbruch, M., Liere, K., and Börner, T. (2007). High diversity of plastidial promoters in *Arabidopsis thaliana*. *Mol. Genet. Genomics* **277**:725–734.
- Terashima, M., Specht, M., and Hippler, M. (2011). The chloroplast proteome: a survey from the *Chlamydomonas reinhardtii* perspective with a focus on distinctive features. *Curr. Genet.* **57**:151–168.
- Vollmar, M., Schlieper, D., Winn, M., Büchner, C., and Groth, G. (2009). Structure of the c_{14} rotor ring of the proton translocating chloroplast ATP synthase. *J. Biol. Chem.* **284**:18228–18235.
- von Ballmoos, C., Wiedenmann, A., and Dimroth, P. (2009). Essentials for ATP synthesis by F_1F_0 ATP synthases. *Annu. Rev. Biochem.* **78**:649–672.
- Wang, Z.G., and Ackerman, S.H. (2000). The assembly factor Atp11p binds to the β -subunit of the mitochondrial F_1 -ATPase. *J. Biol. Chem.* **275**:5767–5772.
- Wang, Z.G., Sheluho, D., Gatti, D.L., and Ackerman, S.H. (2000). The α -subunit of the mitochondrial F_1 ATPase interacts directly with the assembly factor Atp12p. *EMBO J.* **19**:1486–1493.
- Woessner, J.P., Gillham, N.W., and Boynton, J.E. (1987). Chloroplast genes encoding subunits of the H^+ -ATPase complex of *Chlamydomonas reinhardtii* are rearranged compared to higher plants: sequence of the *atpE* gene and location of the *atpF* and *atpI* genes. *Plant Mol. Biol.* **8**:151–158.
- Zhelyazkova, P., Sharma, C.M., Forstner, K.U., Liere, K., Vogel, J., and Börner, T. (2012). The primary transcriptome of barley chloroplasts: numerous noncoding RNAs and the dominating role of the plastid-encoded RNA polymerase. *Plant Cell* **24**:123–136.
- Zoschke, R., Liere, K., and Börner, T. (2007). From seedling to mature plant: *Arabidopsis* plastidial genome copy number, RNA accumulation and transcription are differentially regulated during leaf development. *Plant J.* **50**:710–722.
- Zybailov, B., Rutschow, H., Friso, G., Rudella, A., Emanuelsson, O., Sun, Q., and van Wijk, K.J. (2008). Sorting signals, N-terminal modifications and abundance of the chloroplast proteome. *PLoS One* **3**:e1994.

3 CGL160 Mediates the Connection of the Chloroplast ATP Synthase Modules F₁ and F₀

Manuscript

Bennet Reiter, Lea Rosenhammer, Giada Marino, Dario Leister, Thilo Rühle[§]

Plant Molecular Biology Faculty of Biology I, Ludwig-Maximilians-Universität Munich,
D-82152 Planegg-Martinsried, Germany (B.R., L.R., G.M., D.L., T.R.)

[§] To whom correspondence should be addressed. E-mail: thilo.ruehle@biologie.uni-muenchen.de

Running title: AtCGL160 is required for CF₁-CF₀ joining

Abstract

ATP synthases couple the generation of chemical energy to a transmembrane electrochemical potential in bacteria, mitochondria, and chloroplasts. The chloroplast ATP synthase (cpATP synthase) consists of two multi-subunit complexes, the membrane-bound coupling factor O (CF_O) and the soluble coupling factor 1 (CF₁). During cpATP synthase biogenesis, several auxiliary factors facilitate complex assembly. Previously, it could be shown that the *Arabidopsis* thylakoid-integral protein CONSERVED ONLY IN THE GREEN LINEAGE 160 (AtCGL160) mediates the formation of the proton-translocating c-ring. However, the function of its chloroplast-specific soluble N-terminal domain (AtCGL160N) remained unclear. In this study we show that plants lacking AtCGL160N exhibited a cpATP synthase deficiency phenotype demonstrated by a decreased proton conductivity of the thylakoid membrane, elevated proton motive force and increased non-photochemical quenching parameters. C-ring formation was not disturbed, but cpATP synthase complexes accumulated only to ~65% of wild-type levels. CF_O-, as well as CF₁-subunits, coimmunoprecipitated with AtCGL160, which could also be crosslinked to the cpATP synthase holo-complex. The interaction-site of AtCGL160N and CF₁ was narrowed down to the membrane-proximal domain of subunit β in yeast two-hybrid experiments. Thus, AtCGL160 is also involved in late cpATP synthase assembly and facilitates the connection of the CF₁ and CF_O modules in an AtCGL160N-dependent manner.

Keywords: chloroplast, photosynthesis, ATP synthase, thylakoid complex, assembly, CF₁-CF_O

Introduction

F-type ATP synthases of bacteria, mitochondria, and chloroplasts utilize chemiosmotic membrane potentials to generate ATP. They share an overall conserved structure and consist of a soluble F_1 and a membranous F_0 moiety. (Cyano)bacterial and chloroplast ATP synthases (cpATP synthases) are more closely related with respect to size and subunit composition (Groth and Pohl, 2001; Vollmar et al., 2009; Hahn et al., 2018) and, in contrast to the occurrence of dimeric mitochondrial ATP synthases, are only present as monomers (Daum et al., 2010). In higher plant chloroplasts, cpATP synthases reside exclusively in stroma lamellae and grana end membranes, because the ~16 nm stromal extension of chloroplast F_1 (CF_1) prevents migration into the tightly packed grana stacks (Daum et al., 2010).

During photophosphorylation, cpATP synthases couple the light-driven generation of the trans-thylakoid proton motive force (pmf) to ADP phosphorylation. The membrane-embedded proteolipidic c_{14} -ring together with the non-covalently bound central stalk $\gamma\epsilon$ form the motor unit and drive rotary catalysis of CF_1 . The peripheral stator consists of a , b and b' and is connected to the $\alpha\beta$ -heterotrimer by the δ -subunit, which acts as a flexible hinge between CF_1 and chloroplast F_0 (CF_0) (Murphy et al., 2019). Protons are translocated from the luminal to the stromal side through two aqueous channels in the a -subunit. During translocation, each proton enters the access-channel and binds to a conserved glutamate residue in subunit c . The c_{14} -motor fulfills almost a complete rotation before it releases the proton into the stroma through the exit-channel (Hahn et al., 2018). The counterclockwise rotation of the central stalk in the vicinity of the hexamer triggers alternating nucleotide binding affinities in the β -subunits that ultimately drive ATP generation (reviewed in Von Ballmoos et al., 2009; Junge and Nelson, 2015).

As a result of extensive organellar gene transfer during plant evolution, three cpATP synthase subunits (b' , γ , δ) are encoded in the nuclear genome, whereas the remaining cpATP synthase genes are organized in two plastid operons. Consequently, two different expression apparatuses and the chloroplast protein import machinery have to be tightly coordinated for efficient cpATP synthase biogenesis. Several cpATP synthase auxiliary factors involved in plastid gene expression have been identified, including mRNA processing (AEF1), mRNA stabilization (PPR10, BFA2), or translation initiation (ATP4, TDA1) (Pfalz et al., 2009; Eberhard et al., 2011; Zoschke et al., 2012; Yap et al., 2015; Zhang et al., 2019). Moreover, cpATP synthase assembly factors ensure a correct complex stoichiometry, but also the avoidance of dead-end products or harmful intermediates that could lead to wasteful ATP hydrolysis or pmf dissipation.

As derived from the bacterial assembly model, cpATP synthases are constructed from different intermediates or modules (reviewed in Rühle and Leister, 2015). CF₁ assembly was first examined in in vitro reconstitution assays and was shown to be initiated by α/β -dimerization in a chaperone-assisted process (Chen and Jagendorf, 1994). Known mitochondrial F₁ assembly factors such as Atp11 or Atp12 could not be identified in chloroplasts, but CF₁ formation depends on the green-lineage-specific factor CGLD11/BFA3 (Grahl et al., 2016, Zhang et al., 2016). CGLD11/BFA3 interacts with the hydrophobic catalytic site of the β -subunit (Zhang et al., 2016) and might prevent aggregation or formation of unfavorable homodimers. Moreover, PAB (Mao et al., 2015) and BFA1 (Zhang et al., 2018) were proposed to be required for efficient incorporation of the γ -subunit into CF₁.

In contrast to CF₁ formation, less is known about CF₀ assembly and only the assembly factor CONSERVED ONLY IN THE GREEN LINEAGE 160 (CGL160) has been identified so far (Rühle et al., 2014). CGL160 was defined as a green-lineage-specific protein (Karpowicz et al., 2011), but protein sequence alignments revealed a moderate similarity between its membrane domain and Atp1/Uncl (Rühle et al., 2014), which is encoded by the first gene in the bacterial operon *atp1*. The absence of CGL160 in *Arabidopsis thaliana* (AtCGL160) led to a significant reduction of cpATP synthase levels (10-30% wild-type levels) and c-subunits accumulated as monomers in *atcgl160*. Moreover, split-ubiquitin assays provided evidence that AtCGL160 interacts with CF₀-c and CF₀-b. We concluded that CGL160 is required for efficient formation of the c-ring in chloroplasts and shares the same function with its distantly related bacterial counterpart Atp1/Uncl (Suzuki et al., 2007; Ozaki et al., 2008).

In this study, the function of the N-terminal domain conserved in all CGL160 proteins from the green lineage was investigated in *Arabidopsis*. The results demonstrated that AtCGL160N mediates the connection of CF₁ and CF₀ modules via interaction of the N-terminal domain of AtCGL160 and subunit β . Thus, CGL160 emerges as a key auxiliary factor that not only promotes CF₀ formation but is also involved in late cpATP synthase assembly steps.

Results

Deletion of AtCGL160N affects cpATP synthase activity

To investigate CGL160N-specific protein properties, N-terminal sequences of green algae, bryophytes and higher plant homologs were compared in a multiple alignment (Supplemental Fig. S1). CGL160N sequences across the green lineage comprise about 150-200 amino acids (aa) and contain no predicted functional or conserved protein domain. However, AtCGL160N was found to be phosphorylatable (Reiland et al., 2009) and two putative phosphorylation sites are conserved throughout all sequences (Supplemental Fig. S1).

To dissect the function of the soluble domain in higher plants, coding sequences of AtCGL160₁₋₃₅₀ (oeAtCGL160), AtCGL160₁₋₂₀₆ (oeAtCGL160N) or the membranous C-terminus AtCGL160₂₀₇₋₃₅₀ fused to the manually annotated transit peptide of 46 aa (oeAtCGL160C) were overexpressed in the *atcgl160* knockout background (Fig. 1A). The mutant phenotype could be completely rescued by overexpression of the full-length *AtCGL160* cDNA, as wild-type (WT)-like growth rates under short-day conditions and a normal leaf phenotype were observed (Fig. 1B, C). In contrast, overexpression of AtCGL160N in the *atcgl160* background could not restore the WT phenotype, since AtCGL160N was only detectable on the transcriptional, but not on the protein level (Supplemental Fig. 2A, B). Overexpression of AtCGL160C led to a significant increase in leaf area compared to *atcgl160*. However, oeAtCGL160C plants were slightly growth retarded relative to the WT and displayed a variegated leaf phenotype, which was observed for *atcgl160* but not for the CF₁ assembly mutant *atcgl11* (Fig. 1B, C).

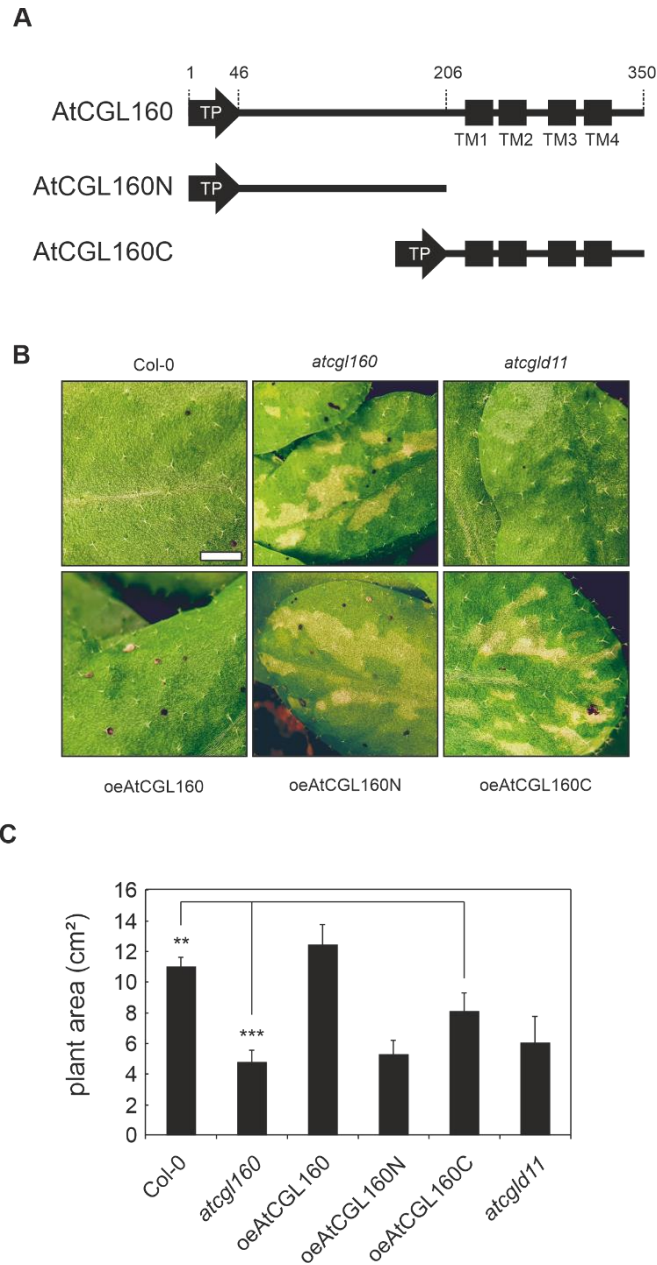


Figure 1. Impact of AtCGL160 truncations on leaf phenotype and plant growth. A, *Atcgl160* plants were transformed with constructs coding for the full-length sequence (oeAtCGL160), the soluble N-terminal domain (oeAtCGL160N), or the membranous C-terminus (oeAtCGL160C), which were all placed under transcriptional control of the 35S CaMV promoter. B, Leaf sections of Col-0, *atcgl160*, *atcgl160C*, oeAtCGL160, oeAtCGL160N and oeAtCGL160C plants. White bar indicates ~2 mm. C, Leaf area measurements of the genotypes grown under short-day conditions for 4 weeks. Means and standard deviations were calculated from 6 individual plants per genotype. Asterisks indicate p-values (* <0.05 , ** <0.01 , *** <0.001) according to two-sided Student's t-test.

Impairment of the cpATP synthase affects the dynamics of the thylakoid proton motive force (pmf), as it is the major contributor to the proton efflux from the luminal to the stromal side (Armbruster et al., 2017). Perturbations of the cpATP synthase can be investigated by measurements of the reversible energy-dependent quenching parameter qE , which is the major component of non-photochemical quenching (NPQ) and sensitive to changes in luminal proton concentration under moderate light intensities (Rott et al., 2011; Carrillo et al., 2016). To test whether disruption of AtCGL160N leads to increased luminal acidification, steady-state transient NPQ was determined for Col-0, *atcgl160*, *oeAtCGL160*, *oeAtCGL160N*, and *oeAtCGL160C* plants under moderate light intensities (Fig. 2A, B). As expected, NPQ values of *atcgl160* and *oeAtCGL160N* were increased (Fig. 3A). Interestingly, also *oeAtCGL160C* showed a significant increase in transient NPQ compared to WT or *oeAtCGL160* but were lowered compared to *atcgl160* or *oeAtCGL160N* plants.

Whereas NPQ parameters only indirectly reflect the pmf status, electrochromic shift (ECS) measurements are a more direct way to determine proton fluxes across the thylakoid membrane (reviewed in Baker et al., 2007). Measuring of dark induced relaxation kinetics (DIRK) of the ECS signal, allows estimations of the pmf during steady-state photosynthesis (Cruz et al., 2001; Kramer et al., 2003). In line with the increased NPQ levels, also the total change in ECS signal (ECS_t) was increased significantly in *oeAtCGL160C* relative to WT and *oeAtCGL160* plants, but decreased compared to *atcgl160*, *atcgld11*, and *oeAtCGL160N* (Fig. 2C).

When ECS_t is resolved in the millisecond range, estimations on the activity of the cpATP synthase can be made, as the rate of signal decrease is reciprocally proportional to the efflux of protons from the lumen to the stroma, or proton conductivity (gH^+) (Cruz et al., 2001; Kanazawa and Kramer, 2002). Remarkably, also gH^+ was decreased significantly in *oeAtCGL160C* plants, compared to WT and *oeAtCGL160*, indicating that the increase in pmf and the subsequent higher quenching of excitation energy is caused by decreased ATP synthase activity (Fig. 2D). Taken together, disruption of AtCGL160N led to decreased proton conductivity of the thylakoid membrane, increased pmf and NPQ parameters, as well as reduced plant growth compared to WT or *oeAtCGL160*. We thus concluded that the chloroplast-specific soluble N-terminus impacts cpATP synthase activity.

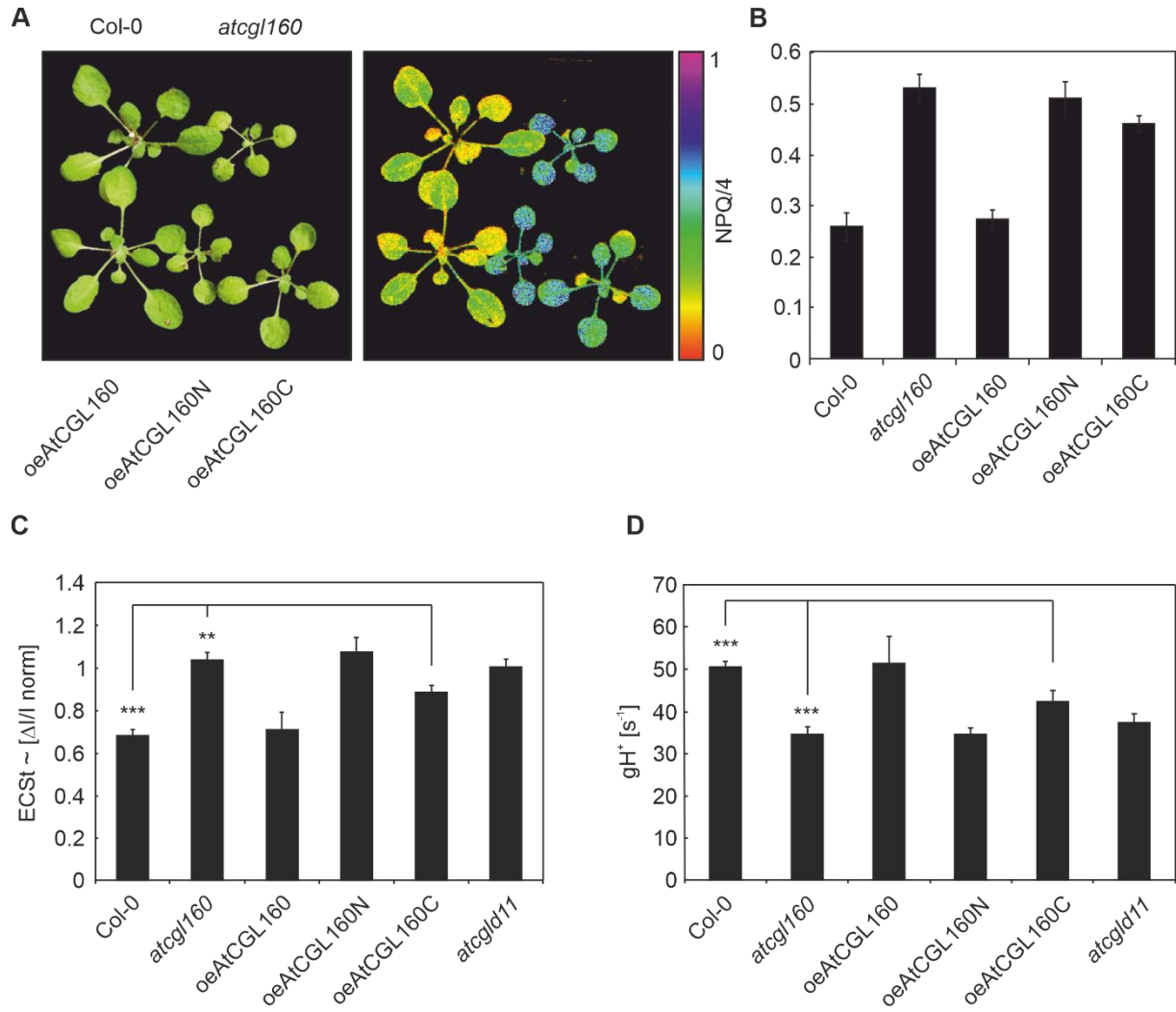


Figure 2. Analysis of *pmf* and *cpATP* synthase activity. A, Chlorophyll *a* video imaging of steady-state NPQ values of Col-0, *atcg160*, oeAtCGL160, oeAtCGL160N, and oeAtCGL160C grown under short-day conditions were measured under moderate light intensity ($145 \mu\text{mol photons m}^{-2} \text{s}^{-1}$). NPQ values ranging from 0 to 1 are displayed in false colors. B, Quantification of NPQ values from measurements shown in A. Means and standard deviations were calculated from 5 leaf areas. C, Dark interval relaxation kinetics (DIRK) after 10 minutes of illumination. The total amplitude of the P515 differential absorption signal (ECS_t) was normalized to a single turnover flash. Means and standard deviations were calculated from 6 individual plants grown under short-day conditions. D, Proton conductivity of the thylakoid membrane. The rate of ECS signal relaxation was measured in ms resolution and fitted to a first-order decay function. Means and standard deviations were calculated from 6 individual plants grown under short-day conditions. Asterisks indicate p-values (* <0.05 , ** <0.01 , *** <0.001) according to two-sided Student's t-test.

Disruption of AtCGL160N affects cpATP synthase assembly but not c-ring formation

To assess whether the decreased thylakoid proton conductivity of *oeAtCGL160C* plants could be attributed to reduced cpATP synthase amounts, we analyzed steady-state levels of CF₁- and CF₀-subunits in the WT, *atcgl160*, *atcgl11*, and the overexpression lines (Fig. 3A, B). Indeed, the marker proteins CF₁-β, -γ as well as CF₀-b and -c were reduced to about 60-65 % in *oeAtCGL160C* thylakoid preparations compared to WT and *oeAtCGL160*.

To investigate the influence of AtCGL160N on cpATP synthase assembly, we performed Blue Native (BN)/ SDS-PAGE analysis with isolated thylakoids of *oeAtCGL160* and *oeAtCGL160C* plants grown under short-day conditions. Consistent with the accumulation of steady-state cpATP synthase levels, signals of CF₁-γ, CF₀-b, and CF₀-c were reduced in *oeAtCGL160C* compared to plants overexpressing the full-length cDNA (Fig. 3C). Furthermore, no accumulation of precomplexes could be observed, since signals for free proteins, the c-ring, CF₁, and the holo-complex were all reduced to a similar extent. Moreover, CF₀-c subunits did not overaccumulate in their monomeric form, as has been shown previously for *atcgl160* mutant plants (Rühle et al., 2014). To study the assembly status of the c-ring in more detail, we performed BN/SDS-PAGE with higher amounts of *atcgl160* and *oeAtCGL160C* thylakoids (Fig. 3D). Remarkably, the c-ring levels were clearly increased in *oeAtCGL160C* compared to *atcgl160*. We concluded that introduction of the membranous Atp1/Unc1-like domain of AtCGL160 restored efficient c-ring formation, but not overall cpATP synthase levels.

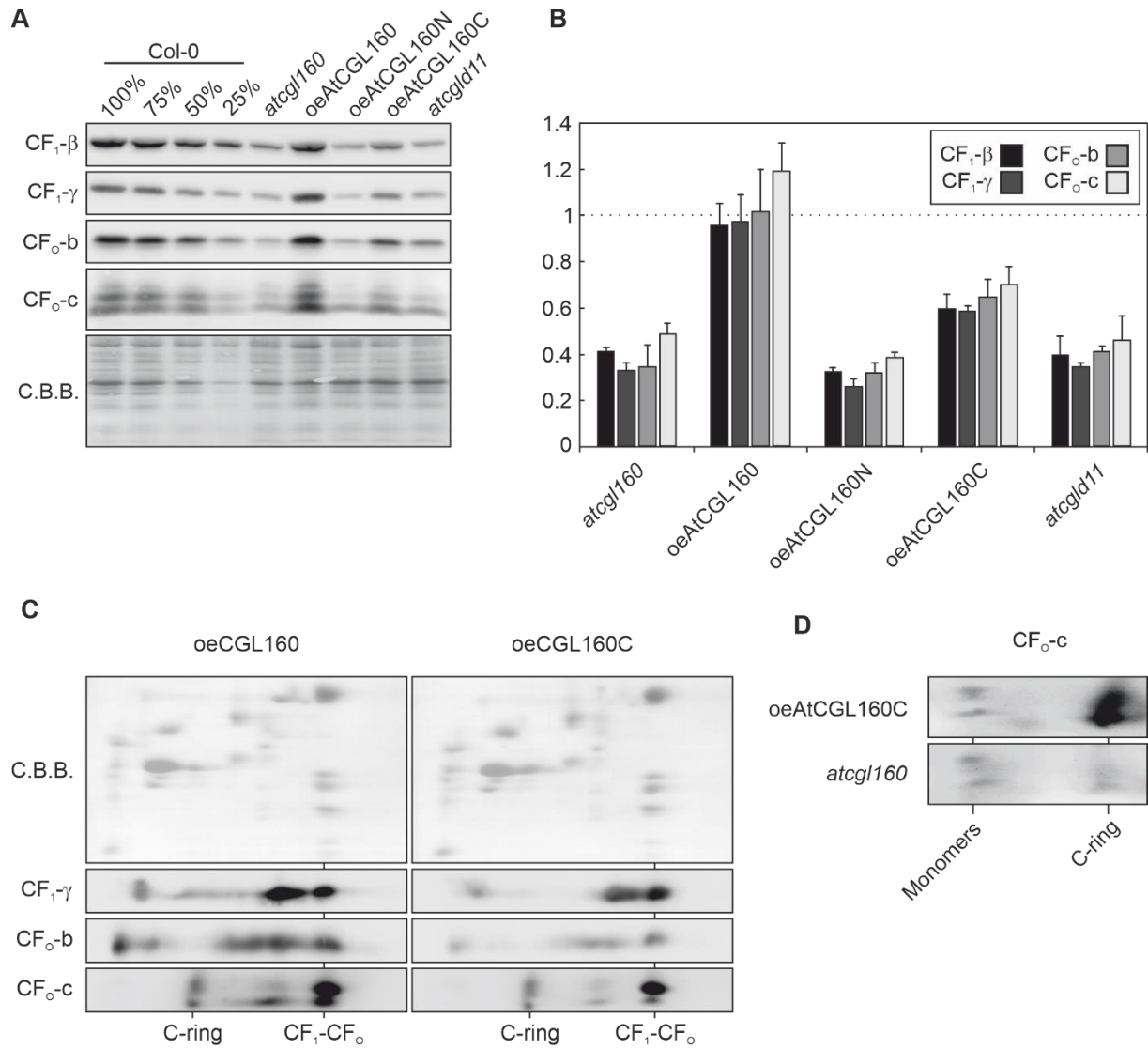


Figure 3. Assembly of the cpATP synthase. A, Steady-state levels of cpATP synthase marker subunits in thylakoids of Col-0, *atcg1160*, *oeAtCGL160*, *oeAtCGL160N*, *oeAtCGL160C*, and *atcgld11*. Samples were separated by SDS-PAGE and blotted onto polyvinylidene difluoride (PVDF) membranes, which were decorated with antibodies against CF₁-β, CF₁-γ, CF_o-b, and CF_o-c. Coomassie brilliant blue (C.B.B.) staining is shown as loading control. B, Quantification of signals shown in A. Values were normalized to Col-0 (1). Means and standard deviations were calculated from 4 technical replicates. C, Steady-state levels of cpATP synthase intermediates. Solubilized thylakoid complexes of *oeAtCGL160* and *oeAtCGL160C* were separated by BN/SDS-PAGE and blotted onto PVDF membranes. Immunoblots were decorated with antibodies against CF₁-γ, CF_o-b, and CF_o-c. Positions of the cpATP synthase holo-complex (CF₁-CF_o) and the c-ring are indicated. C.B.B. staining is shown as loading control. D, C-ring assembly in *atcg1160* and *oeAtCGL160C*. Increased amounts of *atcg1160* and *oeAtCGL160C* thylakoids were separated by BN/SDS-PAGE. Blots were probed with a CF_o-c antibody. Positions of free c-monomers and the assembled c-ring are indicated.

AtCGL160 is associated to the cpATP synthase holo-complex

In a previous study, AtCGL160 could be immunodetected in CF₁-containing fractions in the presence of the crosslinker dithiobis(succinimidyl propionate) (DSP) (Fristedt et al., 2015). However, the antibody (Agrisera AS12 1853) used in that study cross-reacts with CF₁- β (Supplemental Fig. S2B) and was therefore unsuitable for one-dimensional comigration or coimmunoprecipitation experiments. Thus, a new antibody against AtCGL160N was generated (see Materials and Methods for details), which detects specifically AtCGL160 without any cross-reactions in immunodetection assays with isolated thylakoids (Supplemental Fig. S2B).

To identify new AtCGL160 interaction partners, the generated antibody was employed for coimmunoprecipitation (coIP) coupled to LC-MS/MS analysis with NP40 solubilized thylakoids of *oeAtCGL160* and *oeAtCGL160C* plants grown under short-day conditions (Fig. 4A, Supplemental Fig. S3, Supplemental Table S1). Strikingly, besides AtCGL160 (\log_2 FC ~6.5), peptides of all subunits of the cpATP synthase were significantly enriched (\log_2 FC >2.8) in the IP fraction of *oeAtCGL160* compared to *oeAtCGL160C* (Fig. 4A). No specific enrichment of either CF₀- or CF₁-subunits was observed. Moreover, when the IP fractions of *oeAtCGL160* and *oeAtCGL160C* were separated on SDS-PAGE, CF₁- β and CF₁- γ were only detectable in *oeAtCGL160* samples (Supplemental Fig. S3). Other known cpATP synthase assembly factors could not be identified in the coIP fractions (Supplemental Table S1).

To confirm the coIP results, BN/SDS-PAGE analysis with isolated thylakoids of the WT, treated with the crosslinking agent DSP, were compared to untreated thylakoids and blots were decorated with AtCGL160- and CF₀-b-specific antibodies (Fig. 4B). In untreated samples, the AtCGL160 signal was predominantly present in the monomer fraction. After crosslinking with DSP, a large portion of the AtCGL160 signal shifted to the higher molecular weight fraction (>520 kD) and comigrated with the cpATP synthase holo-complex (Fig. 4B). Taken together, these results indicated that AtCGL160 might be associated to late assembly stages or with holo-complexes of the cpATP synthase.

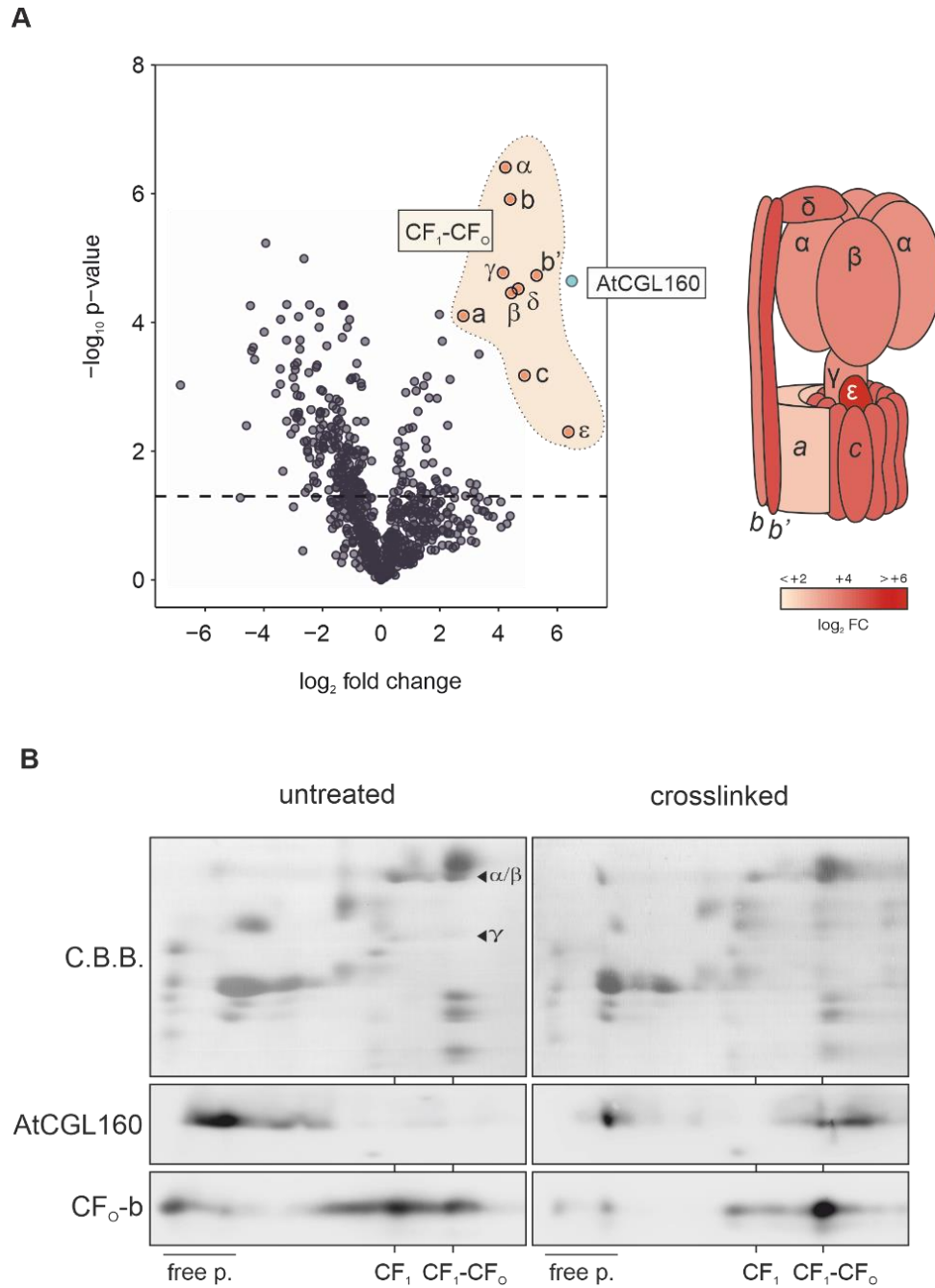


Figure 4. Association studies of AtCGL160 with the cpATP synthase. A, Volcano-plot of differentially enriched proteins in coimmunoprecipitation fractions of oeAtCGL160 versus oeAtCGL160C lines using the AtCGL160N antibody. Y-axis: negative log₁₀ p-value (Benjamini-Hochberg corrected) of three biological replicates. Dashed line represents a -log₁₀ p-value-threshold of 1.5. X-axis: log₂ fold change (FC) of peptide abundance in oeAtCGL160 versus oeAtCGL160C. Blue dot marks peptides of AtCGL160. Red dots mark signals of cpATP synthase subunits. B, Schematic representation of enriched cpATP synthase subunits of A. Color scheme of log₂-FC of oeAtCGL160 versus oeAtCGL160C ranges from beige (log₂ FC < 2) to dark red (log₂ FC > 6). C, Comigration of AtCGL160 with the cpATP synthase holo-complex. Untreated thylakoid extracts of the WT (Col-0) were compared to extracts crosslinked with DSP on BN/SDS-PAGE analysis. Blots of the second dimension were decorated with antibodies against AtCGL160 and CF₀-b. Positions of the cpATP synthase holo-complex (CF₁-CF₀), the CF₁-intermediate, and the free protein fraction are indicated based on the signals of CF₁-α/β and -γ on the C.B.B. staining.

The stroma-exposed N-terminus specifically interacts with CF₁-β

It could already be demonstrated that AtCGL160 is an integral thylakoid membrane protein (Rühle et al., 2014; Fristedt et al., 2015). To investigate whether the N-terminal domain is exposed to either the stromal or luminal side of the thylakoid membrane, isolated WT thylakoids were mildly treated with trypsin, such that only stroma-exposed peptides were accessible for the protease. Samples were separated by SDS-PAGE, blotted, and immunodetections were carried out with antibodies against AtCGL160, the lumen-facing PSII subunit PsbO, and the stroma-exposed PsaD (Fig. 5A). As expected, the luminal PsbO was unaffected by trypsin digestion, whereas PsaD was susceptible to the proteolytic treatment. AtCGL160N was efficiently digested without leaving any detectable proteolytic cleavage product, indicating that the N-terminal domain is exposed to the chloroplast stroma.

The association of AtCGL160 to CF₁-containing complexes and the stromal-exposed topology of the N-terminus suggested that the soluble domain of AtCGL160 might physically interact with soluble parts of the cpATP synthase. Thus, yeast two-hybrid (Y2H) experiments were carried out with AtCGL160N (aa 29-206) fused to the binding domain (BD) and all CF₁-subunits ($\alpha, \beta, \gamma, \delta, \epsilon$), the soluble parts of the stator (b, b'), AtCGL160N, as well as the CF₁ assembly factor AtCGLD11 fused to the activation domain (AD). Only yeast cells carrying AD-CF₁-β together with BD-AtCGL160N were able to grow on restrictive medium, lacking histidine and adenine (Fig. 5B), suggesting that the soluble domain of AtCGL160 physically interacts with CF₁-β in yeast. Moreover, neither homodimerization nor an interaction with AtCGLD11 could be detected for AtCGL160N.

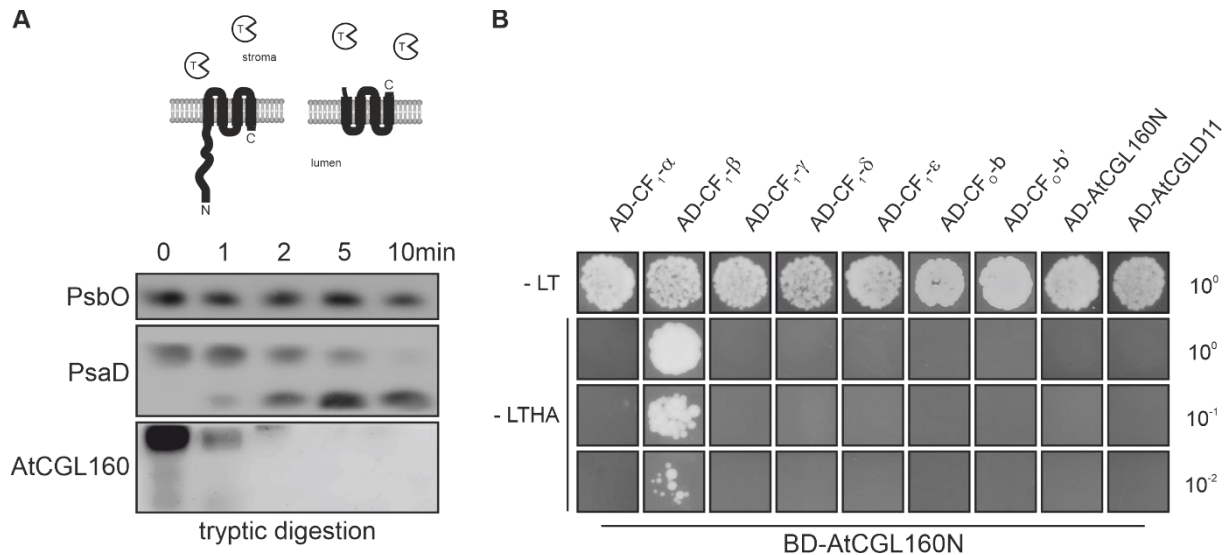


Figure 5. AtCGL160N topology and its physical interaction with the peripheral stator or CF₁ module. A, Immunoblot analyses of trypsin-treated (0, 1, 2, 5, and 10 min) WT (Col-0) thylakoids. After SDS-PAGE and transfer to PVDF membranes, blots were decorated with antibodies against PsbO, PsaD and AtCGL160. Possible membrane orientations of AtCGL160 are depicted schematically. B, Interaction of AtCGL160N with itself, CF₁-subunits, membrane domain-truncated b/b'-subunits and the CF₁ assembly factor AtCGLD11. Interactions were tested by cotransformation of a construct coding for an AtCGL160N fusion to the GAL4 binding domain (BD-AtCGL160N) and constructs coding for fusions with the GAL4 activation domain (AD). Successful cotransformations were verified by plating yeast cells on permissive medium lacking Leu and Trp (-LT). Interactions were tested on restrictive medium lacking Leu, Trp, His and Ade (-LTHA) by plating equal numbers of yeast cells in serial dilutions (10⁰, 10⁻¹, and 10⁻²).

The CF₁- β -subunit can be subdivided into three structural domains (Groth and Pohl, 2001). Domain I comprises the membrane-distal beta-barrel structure, domain II includes the nucleotide binding pockets, and the membrane-proximal domain III is organized by alpha-helical structures (Fig. 6A). To test whether the interaction with AtCGL160N can be assigned to a structural domain of CF₁- β , the three domains were cloned into the AD vector and tested for interaction with BD-AtCGL160N (Fig. 6A). Only cells carrying constructs for AD-CF₁- β III together with BD-AtCGL160N showed growth on restrictive medium, whereas yeast cells transformed with constructs for AD-CF₁- β II, or AD-CF₁- β I grew slowly or not at all. In a reciprocal approach, coding sequences of the CGL160 N-terminus (aa 29-74, aa 75-105, aa 106-134, aa 135-160, and aa 161-206) were omitted from the BD-AtCGL160N vector and the resulting truncated N-termini were tested for interaction with AD-CF₁- β in yeast (Fig. 6B). Remarkably, only the N-terminal amino acids 29-105 were necessary for the interaction, since their deletion led to abolished growth on restrictive medium, whereas strains carrying BD-AtCGL160N vectors with deleted amino acids 106-206 were still able to grow (Fig. 6B). Taken together, AtCGL160N is exposed to the stromal side of the thylakoid membrane and its N-terminal region interacts with the membrane-proximal domain of CF₁- β in yeast.

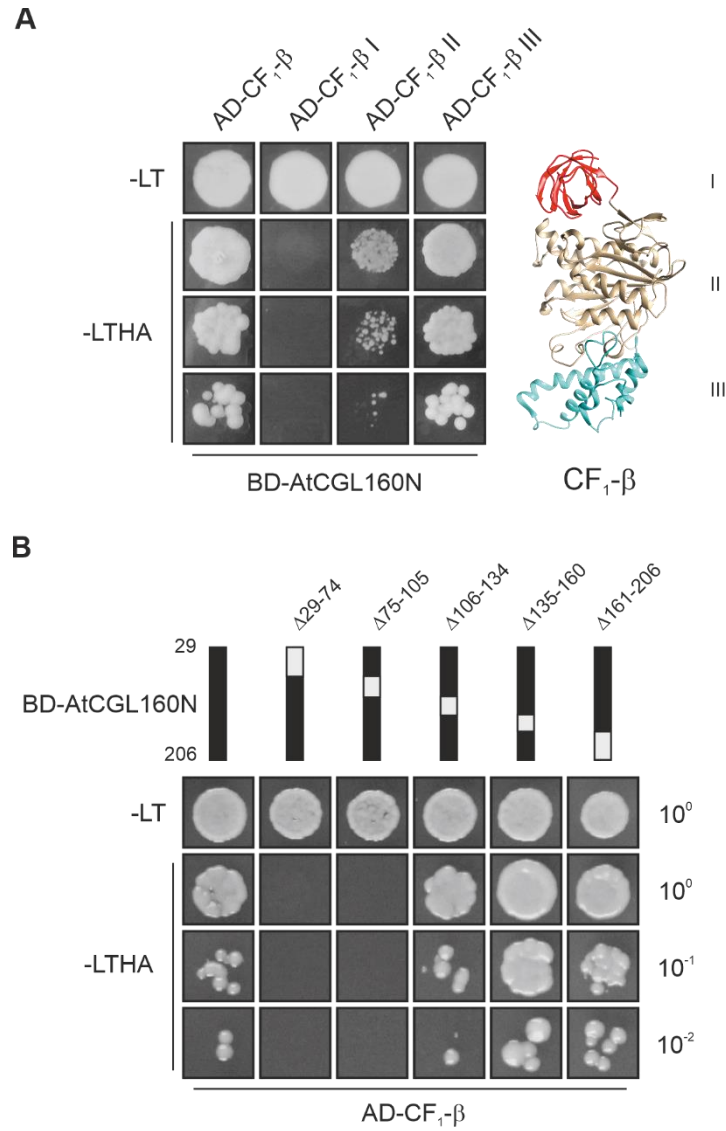


Figure 6. Mapping of AtCGL160N and CF₁-β interaction sites. A, Interaction of AtCGL160N with structural domains of CF₁-β. Yeast cells were cotransformed with constructs coding for AD-CF₁-β I, AD-CF₁-β II, AD-CF₁-β III and BD-AtCGL160N and plated on permissive (-LT) and restrictive (-LTHA) growth medium. Structural domains of the CF₁-β are colored in red (Domain I), beige (Domain II), and blue (Domain III). Structural data were obtained from the PDB database (ID: 1FX0; Groth and Pohl, 2001). B, Mapping of AtCGL160N interaction domains. Several deletion constructs (grey boxes) of the soluble AtCGL160N were tested in cotransformation assays with AD-CF₁-β in yeast.

Discussion

AtCGL160N promotes ATP synthase assembly

Atp1/Unc1 are small transmembrane proteins that are usually encoded by the first gene of the large bacterial ATP synthase operon and assist in the formation of the proteolipidic c-ring (Suzuki et al., 2007; Ozaki et al., 2008). The membranous C-terminal part of the green-lineage-specific CGL160 is distantly related to Atp1/Unc1, but eukaryotic CGL160 proteins additionally harbor an N-terminal soluble domain (CGL160N). Arabidopsis plants lacking CGL160 were growth retarded and contained only about 10-30% of cpATP synthase, whereas monomeric c-subunits overaccumulated compared to WT (Rühle et al., 2014). Since the membranous domain physically interacted with CF₀-b and -c, we concluded that CGL160 is required for c-ring assembly in chloroplasts. However, the mild effects of Atp1/Unc1 disruption on ATP synthase function in bacteria (Gay, 1984; Liu et al., 2013) raised the question whether the N-terminal chloroplast-specific domain could have acquired an additional role in cpATP synthase assembly in the green lineage. Indeed, reintroduction of the membranous domain into the *atcgl160* mutant background (oeAtCGL160C) restored efficient formation of the c-ring but failed to fully reconstitute cpATP synthase amounts to WT levels (Fig. 3), resulting in reduced cpATP synthase activity (Fig. 2D). Consequently, oeAtCGL160C-lines exhibited a typical cpATP synthase deficiency phenotype (Maiwald et al., 2003; Dal Bosco et al., 2004), observable by elevated *pmf* and NPQ values (Fig. 2). Hence, disruption of c-ring formation, observed in mutants of eukaryotic CGL160, might not fully account for the strong reduction of cpATP synthase amounts compared to bacteria, suggesting a separate function of the chloroplast-specific soluble domain in promoting cpATP synthase assembly.

AtCGL160 is involved in later stages of assembly

Fristedt et al. (2015) proposed that AtCGL160 might predominantly interact with the CF₁-subcomplex, based on the observation that AtCGL160 comigrated with CF₁ in BN-PAGE analysis and crosslinking SDS-PAGE. Since the antibody used in the study additionally recognizes CF₁- β (Supplemental Fig. S2B), it is not possible to unambiguously assess an association of AtCGL160 to CF₁ in immunoblots of one-dimensional gel electrophoresis. The AtCGL160 signal was also shown to comigrate with CF₁ in two-dimensional BN/SDS-PAGE analysis (Fristedt et al., 2015). However, we failed to reproduce an association of AtCGL160 with CF₁ subcomplexes in BN/SDS-PAGE analysis, as we found the AtCGL160 signal mostly in the monomeric fraction in untreated thylakoid preparations (Rühle et al., 2014; Fig. 4B). Only when thylakoids were crosslinked with DSP, the AtCGL160 signal comigrated with the cpATP synthase holo-complex and complexes of higher MW (>520 kD), but it was absent in the CF₁

fraction (Fig. 4B). Moreover, when we conducted colP experiments with an antibody that solely recognized AtCGL160 in thylakoid extracts (Supplemental Fig. S2B), all subunits of the cpATP synthase were enriched significantly in the IP fraction (Fig. 4A). This is in contrast to other cpATP synthase assembly factors, where colP was mostly restricted to the primary target or assembly intermediate (Mao et al., 2015; Zhang et al., 2016; 2018), and interaction partners were only pulled-down after chemical crosslinking (Zhang et al., 2016; 2018). Whereas CGLD11/BFA3 could be identified in colP fractions of BFA1 (Zhang et al., 2018), no other known assembly factors were present in the oeAtCGL160 IP-fraction (Supplemental Table S1). AtCGL160 has already been shown to be present sub-stoichiometrically and thus does not qualify as a bona fide component of the cpATP synthase (Rühle et al., 2014). Hence, whereas AtCGL160 might not predominantly be associated to a CF₁-intermediate, comigration with the cpATP synthase holo-complex and coimmunoprecipitation of all subunits, suggest an association to a CF₀-CF₁ containing intermediate. The absence of other known (CF₁) assembly factors further support that AtCGL160 might be involved in later stages of assembly.

ALB4, which shares sequence similarity with bacterial YidC and mitochondrial Oxa1p was proposed to be involved joining of the ATP synthase submodules, based on the observation that ALB4 physically interacted with CF₀-b and associated to CF₁-β (Benz et al., 2009). Moreover, mutant plants lacking ALB4 accumulated reduced amounts of cpATP synthase subunits. However, studies with its closest homolog in Arabidopsis, the well characterized membrane insertase ALB3 (reviewed in Wang and Dalbey, 2011), revealed that ALB3 and ALB4 physically interact and showed significant functional overlap in the membrane insertion of Cytochrome *b6f* complex subunits (Trösch et al., 2015). Moreover, ALB4 and STIC2 were shown to act together in thylakoid protein targeting in a common pathway that also involves cpSRP54 and cpFtsY (Bédard et al., 2017). Finally, we could not identify ALB4 among the proteins that were enriched in colP experiments with AtCGL160 (Supplemental Table S1), suggesting that ALB4 and AtCGL160 do not act concertedly in late stages of cpATP synthase assembly.

AtCGL160N might have evolved to regulate the joining of the subcomplexes

Joining of CF₀ to CF₁ is a critical step in the biogenesis of the bacterial ATP synthase, since incorrect or premature formation of the proton-conducting channel between the c-ring and the a-subunit leads to uncontrolled dissipation of the transmembrane *pmf* (Birkenhäger et al., 1999; Franklin et al., 2004). Likewise, in mitochondria, joining of subcomplexes is considered critical and tightly regulated in order to prevent uncoupled dissipation of the *pmf* (reviewed in Song et al., 2018). In yeast, the INA complex (INAC) physically interacts with the c-ring (ATP9) and a preformed F₁-Stator module (Naumenko et al., 2017). In later stages of assembly, INAC

connects both modules and promotes the formation of the proton-translocating unit between ATP6 (α -subunit) and ATP9. Similar to INAC, AtCGL160 interacted with subunits of the c-ring as well as the peripheral stator (Rühle et al., 2014) and has acquired a stroma-exposed soluble domain that interacted with CF₁- β in yeast (Fig. 5). Whereas the CF₁ assembly factors AtCGLD11/BFA3 and BFA1 were both shown to interact with the catalytic site containing hydrophobic domain II (Grahl et al., 2016; Zhang et al., 2016; 2018), AtCGL160 preferably interacted with the membrane-proximal domain III of CF₁- β (Fig. 6A). Domain III is organized α -helical and contains the conserved “DELSEED” motif, required for the CF₁- γ/ϵ -dependent regulation of the CF₁ ATP-hydrolysis function and ATP synthase activity (Kanazawa et al., 2017; Hahn et al., 2018). In-depth characterization of the soluble AtCGL160 domain in yeast two-hybrid experiments revealed that only the first 29-105 aa were required for the interaction with CF₁- β (Fig. 6B). Our results thus further support the notion that AtCGL160 might interact with components of CF₁ and CF₀ simultaneously and, like INAC in yeast, physically connects F₀ and F₁ during later stages of the assembly process.

In contrast to bacteria, the chemiosmotic potential across the chloroplast thylakoid membrane regulates photosynthetic electron transport in response to the redox poise of the stroma (reviewed in Takagi et al., 2017). Conceivably, this increased regulatory importance of the *pmf* selected for a more tightly orchestrated assembly of the thylakoid-bound ATP synthase. Indeed, whereas precomplexes have been identified in bacteria, accumulation of CF₀ was found to be strictly dependent on CF₁ in plants (Lemaire and Wollman, 1989), indicating that joining of the subcomplexes might be crucial. CGL160 may have evolved from a sole CF₀ assembly factor to a central mediator of cpATP synthase assembly as a response to the increased significance of maintaining control over the *pmf*. Moreover, CGL160 itself could be target for regulatory modulation, since the green-lineage-specific domain contains conserved phosphorylation sites adjacent to the proposed interaction domain (Supplemental Fig. S1), which were identified to be phosphorylated in Arabidopsis (Reiland et al., 2009). However, further genetic and biochemical studies must be conducted in order to dissect a possible regulatory role for CGL160.

Materials and methods

Bioinformatics sources

Protein and gene sequences were downloaded from the Arabidopsis Information Resource server (TAIR; <http://www.arabidopsis.org>), Phytozome (<https://phytozome.jgi.doe.gov/pz/portal.html>), and the National Center for Biotechnology Information server (NCBI; <http://www.ncbi.nlm.nih.gov/>). Transit peptides were predicted by ChloroP (<http://www.cbs.dtu.dk/services/ChloroP/>). Structural data were obtained from the PDB homepage (<https://www.rcsb.org/>).

Plant material and growth conditions

T-DNA lines for *atcgl160* (SALK_057229, Col-0 background) and *atcgl11* (SALK_019326C, Col-0 background) were obtained from the SALK collection (Alonso et al., 2003). Plants were grown on potting soil (A210, Stender) under controlled greenhouse conditions (70-90 $\mu\text{mol photons m}^{-2} \text{ s}^{-1}$, 16/8 h light/dark cycles), or for biochemical and physiological analyses in climate chambers using an 8h light/16h dark cycle (short-day). Fertilizer was added to plants grown under greenhouse conditions according to the manufacturer's recommendations (Osmocote Plus; 15% nitrogen [w/v], 11% [w/v] P_2O_5 , 13% [w/v] K_2O , and 2% [w/v] MgO; Scotts Deutschland). For domain-specific complementation assays, either the complete coding region of AtCGL160 (oeAtCGL160) or parts of the CDS corresponding to aa 1-206 (oeAtCGL160N) and aa 1-46 fused to aa 207-350 (oeATCGL160C) were cloned into the binary Gateway vector pB2GW7 (Karimi et al., 2002), placing the genes under control of the 35S CaMV promoter (see Supplemental Table S2 for primer information). The constructs were first transformed into *Agrobacterium tumefaciens* strain GV3101 and then into *atcgl160-1* plants by the floral-dip method (Clough and Bent, 1998). T1 plants were selected by screening for glufosinate (Basta, Bayer Crop Science) resistance. Basta-resistant plants were screened by RNA gel-blot hybridization for equal amounts of *AtCGL160* transcript as described below. Growth parameters of WT and mutant lines were analyzed on the basis of leaf area, which was determined from photographs taken at 4 weeks after germination in short-day conditions and quantified using the ImageJ software (Schneider et al., 2012).

Chlorophyll a fluorescence measurement

In vivo Chlorophyll a fluorescence of whole plants was measured using an imaging Chl fluorometer (Imaging PAM; Walz). Plants were dark-adapted for 20 minutes and exposed to a pulsed, blue measuring beam (4 Hz, intensity 3, gain 3, damping 2; F_0) and a saturating light flash (intensity 10) to calculate F_v/F_m . Transient NPQ induction was measured at 155 s after the switch from dark to illumination with $145 \mu\text{mol photons m}^{-2} \text{s}^{-1}$.

ECS measurements

ECS measurements were performed using the Dual-PAM-100 equipped with a P515/535 emitter-detector module (Walz; Schreiber and Klughammer, 2008). The measurement was carried out at 23°C under ambient CO_2 conditions. Plants grown in short-day conditions for four weeks were light-adapted, and detached leaves were illuminated for at least 10 min with $129 \mu\text{mol photons m}^{-2} \text{s}^{-1}$ red light. After illumination, dark interval relaxation kinetics (DIRK) were measured in the ms to s range. Briefly, the total amplitude of the inverse electrochromic band-shift kinetic (ECS_t) was measured and normalized to a single saturating P515 pulse, applied after 4 minutes of dark incubation. For proton conductivity (gH^+), electrochromic band-shift kinetics were recorded in the millisecond-range for 2 seconds for 5 consecutive times with light intervals of 30 seconds, respectively. The combined signals were fitted to a first order exponential decay function and the reciprocal value of the lifetime was used to estimate the proton conductivity (Kanazawa and Kramer, 2002). ECS_t and gH^+ were calculated as described in Cruz et al. (2001). Values and standard deviations were calculated from 6 biological replicates.

Nucleic acid analysis

Total RNA from snap-frozen leaves was extracted with the RNeasy Plant Mini Kit (Qiagen) according to the supplier's instructions. Samples equivalent to 20 μg total RNA were fractionated by electrophoresis in formaldehyde-containing agarose gels (1.2% [w/v]), blotted onto nylon membranes (Hybond-N+, Amersham Bioscience) and fixed by UV radiation (Stratalinker® UV Crosslinker 1800). To control equal loading, abundant RNAs on nylon membranes were stained with methylene blue solution (0.02% [w/v] methylene blue, 0.3 M sodium acetate pH 5.5). To detect gene-specific transcripts, amplified DNA fragments from cDNA were labeled with radioactive [$\alpha\text{-}^{32}\text{P}$]dCTP and subsequently used as probes in hybridization experiments (see Supplemental Table S2 for primer information). Signals were detected with the Typhoon Phosphor Imager System (GE Healthcare).

Protein analysis

Leaves from four-week-old plants grown under short-day conditions were harvested shortly after the onset of the light period and thylakoid membrane-enriched samples were isolated according to Rühle et al. (2014). Crosslinking of thylakoid proteins was performed by incubation with 2.5 mM dithiobis(succinimidyl propionate) (DSP, Thermo Scientific). After incubation for 20 min on ice, crosslinking was quenched with 60 mM Tris/HCl (pH 7.5). Chl concentrations were determined as described in Porra et al. (1989). For immunotitrations, thylakoid membrane pellets were resuspended in loading buffer (100 mM Tris-HCl pH 6.8, 50 mM DTT, 8% [w/v] SDS, 24% [w/v] glycerol and 0.02% [w/v] bromophenol blue). Denaturation for 5 min at 70°C and protein fractionation on Tricine-SDS-PAGE gels (10% [w/v] acrylamide gels supplemented with 4M urea) was carried out according to Schägger (2006). Immunodetections were performed as described below. Sample preparation for BN-PAGE was performed as described in Peng et al. (2008) with freshly prepared thylakoids. First, membranes were washed two times in washing buffer (20% [w/v] glycerol, 25 mM BisTris/HCl pH 7.0). Then, samples were treated with wash buffer including 1% (w/v) n-dodecyl β -D-maltoside and adjusted to 1 mg ml⁻¹ Chl for 10 min on ice. After centrifugation (16,000 g, 20 min, 4°C), supernatants were supplemented with 1/10 volume of BN sample buffer (100 mM BisTris/HCl pH 7.0, 750 mM ϵ -aminocaproic acid, 5% (w/v) Coomassie G-250). BN-PAGE gels (4-12% gradient) were prepared as described in Schägger et al. (1994). Solubilized samples corresponding to 60 μ g Chl were loaded per lane and gels were run at 4°C overnight. To separate complexes into their subunits, BN-PAGE strips were treated with denaturing buffer (0.2 M Na₂CO₃, 5% [w/v] SDS, 50 mM DTT) for 30 min at room temperature and loaded on Tricine-SDS-PAGE gels. Gels were subsequently subjected to immunoblot analysis with antibodies against cpATP synthase subunits and AtCGL160 as described below.

Immunoblot analysis

Proteins fractionated by gel electrophoresis were transferred to polyvinylidene difluoride membranes (PVDF) (Immobilon®-P, Millipore) using a semi-dry blotting system (Biorad) as described in the supplier's instructions. After blocking with TBST (10 mM Tris pH 8.0, 150 mM NaCl and 0.1% [w/v] Tween-20) supplemented with 3% milk, the membranes were incubated with antibodies at 4°C overnight. Signals were detected by enhanced chemiluminescence (Pierce™ ECL Western Blotting Substrate, Thermo Scientific) using an ECL reader system (Fusion FX7; PeqLab, Erlangen, Germany). Antibodies used in this study were obtained from Agrisera (CF₁- β : AS05 085, 1:5000; CF₁- γ : AS08 312, 1:5000; CF_O-b: AS10 1604, 1:5000; CF_O-c: AS09 591, 1:3000; and AtCGL160: AS12 1853, 1:1000).

AtCGL160N antibody generation

The coding sequence of AtCGL160N (aa 29-206) was cloned into the pMal-c5x vector (NEB) and purification was carried out with amylose columns (NEB) according to manufacturer's instructions. The protein was injected into rabbits for antibody production (Pineda, Berlin, Germany). To reduce epitope cross-reactions, the antiserum was purified on columns crosslinked with heterologously expressed AtCGL160N (aa 29-206), fused to the glutathion s-transferase tag (pDest15, Invitrogen). Purified antibody was employed in a dilution of 1:1000.

Yeast two-hybrid experiments

Yeast two-hybrid assays were carried out using the Matchmaker Two-Hybrid Kit (Clontech). The AtCGL160 CDS without the cTP (see Supplemental Table S2 for primer information) was cloned into the bait vector pGBKT7 (BD-AtCGL160), whereas the coding sequences of CF₁- α , - β , - γ , - δ , - ϵ , as well as the soluble parts of CF_O-b and -b', AtCGL160 and the CF₁ assembly factor AtCGLD11/BFA3 were cloned into the prey vector pGADT7 (named AD-CF₁- α , - β , - γ , - δ , - ϵ ; -CF_O-b, -b'; -AtCGL160, -AtCGLD11). As in the case of AtCGL160, cTP sequences were omitted from the nucleus-encoded subunits CF₁- γ , CF₁- δ , CF_O-b' and AtCGLD11. For the binding domain analysis of CF₁- β , the respective CDS was sub-divided into three parts (I: aa 1-96, II: aa 97-377, III: aa 378-498), according to Zhang et al. (2016) and cloned into pGADT7. In the case of the binding-site analysis of AtCGL160N, nucleotides coding for aa 29-74, aa 75-105, aa 106-134, aa 135-160, and aa 161-206 were deleted from the BD-AtCGL160 vector using the Q5 site-directed mutagenesis kit (NEB) and primers listed in Supplemental Table S2. Bait and prey vectors were cotransformed into the AH109 yeast strain (Clontech) following the manufacturer's instructions. Cotransformants were selected on synthetic dropout (SD) medium (Clontech) lacking leucine and tryptophan (-LT). In order to identify protein interactions, double transformants were grown on SD medium lacking leucine, tryptophan, histidine, and adenine (-LTHA).

Coimmunoprecipitation

Freshly extracted thylakoids corresponding to ~5 mg chlorophyll were resuspended in 500 μ L extraction buffer (50 mM Tris/HCl pH 7.5, 150 mM NaCl, 1mM MgCl₂, 5% [w/v] glycerol, 1% [v/v] Nonidet P40, 0.2 mM PMSF) and solubilized for 30 min on ice. After centrifugation at 35,000 g for 30 min and 4°C, the supernatant was added to 20 μ L Dynabeads™ (Thermo Scientific), equilibrated with (50 mM Tris/HCl pH 7.5, 150 mM NaCl, 5% [w/v] glycerol, 0.05% [v/v] Nonidet P40), and labeled with AtCGL160 antibody according to manufacturer's instructions. The suspension was incubated with rotation for 3 hours at 4° C, washed three times with equilibration buffer including, and two times with buffer excluding NP40. Proteins

were eluted with 100 µL 0.1 M Glycine pH 2.0 for 10 minutes and neutralized with 100 µL 0.1 M ammonium bicarbonate. After treatment with 10 µL 45 mM DTT and 10 µl of 0.1 M iodoacetamide, samples were digested with 1.5 µg trypsin at 37°C over-night. Peptides were desalted on home-made C₁₈ stage tips (Rappsilber et al., 2003), vacuum dried to near dryness, and stored at –80°C. LC-MS/MS run and data analysis was performed as described in Reiter et al. (2020).

Author contributions

B.R. and T.R. designed research. B.R., L.R., G.M., and T.R. performed research. B.R. and T.R. prepared the article. D.L. and T.R. supervised the whole study.

Acknowledgments

We thank Benjamin Schwarz, Tim Scheibenbogen, Michael Berger, and Tanja Neufeld for technical assistance with Yeast two-hybrid experiments as well as Tim Dreißig for technical assistance with heterologous expression of AtCGL160N.

Funding

This work was supported by the Deutsche Forschungsgemeinschaft, FOR2092 project no. 239484859.

References

- Alonso JM, Stepanova AN, Leisse TJ, Kim CJ, Chen HM, Shinn P, Stevenson DK, Zimmerman J, Barajas P, Cheuk R, et al. (2003) Genome-wide insertional mutagenesis of *Arabidopsis thaliana*. *Science* **301**: 653–657.
- Armbruster U, Correa Galvis V, Kunz HH, Strand DD (2017) The regulation of the chloroplast proton motive force plays a key role for photosynthesis in fluctuating light. *Curr Opin Plant Biol* **37**: 56–62
- Baker NR, Harbinson J, Kramer DM (2007) Determining the limitations and regulation of photosynthetic energy transduction in leaves. *Plant, Cell Environ* **30**: 1107–1125
- von Ballmoos C, Wiedenmann A, Dimroth P (2009) Essentials for ATP Synthesis by F_1F_0 ATP Synthases. *Annu Rev Biochem* **78**: 649–672
- Bédard J, Trösch R, Wu F, Ling Q, Flores-Pérez Ú, Töpel M, Nawaz F, Jarvis P (2017) Suppressors of the chloroplast protein import mutant *tic40* reveal a genetic link between protein import and thylakoid biogenesis. *Plant Cell* **29**: 1726–1747
- Benz M, Bals T, Gügel IL, Piotrowski M, Kuhn A, Schünemann D, Soll J, Ankele E (2009) Alb4 of *Arabidopsis* promotes assembly and stabilization of a non chlorophyll-binding photosynthetic complex, the CF_1CF_0 -ATP synthase. *Mol Plant* **2**: 1410–1424
- Birkenhäger R, Greie JC, Altendorf K, Deckers-Hebestreit G (1999) F_0 complex of the *Escherichia coli* ATP synthase: Not all monomers of the subunit c oligomer are involved in F_1 interaction. *Eur J Biochem* **264**: 385–396
- Carrillo LR, Froehlich JE, Cruz JA, Savage LJ, Kramer DM (2016) Multi-level regulation of the chloroplast ATP synthase: the chloroplast NADPH thioredoxin reductase C (NTRC) is required for redox modulation specifically under low irradiance. *Plant J* **87**: 654–663
- Chen GG, Jagendorf AT (1994) Chloroplast molecular chaperone-assisted refolding and reconstitution of an active multisubunit coupling factor CF_1 core. *Proc Natl Acad Sci U S A* **91**: 11497–11501
- Clough SJ, Bent AF (1998) Floral dip: A simplified method for *Agrobacterium*-mediated transformation of *Arabidopsis thaliana*. *Plant J* **16**: 735–743
- Cruz JA, Sacksteder CA, Kanazawa A, Kramer DM (2001) Contribution of electric field ($\Delta\psi$) to steady-state transthylakoid proton motive force (*pmf*) in vitro and in vivo. Control of *pmf* parsing into $\Delta\psi$ and ΔpH by ionic strength. *Biochemistry* **40**: 1226–1237
- Dal Bosco C, Lezhneva L, Bieh A, Leister D, Strotmann H, Wanner G, Meurer J (2004) Inactivation of the Chloroplast ATP Synthase γ Subunit Results in High Non-photochemical Fluorescence Quenching and Altered Nuclear Gene Expression in *Arabidopsis thaliana*. *J Biol Chem* **279**: 1060–1069
- Daum B, Nicastro D, Austin J, Richard McIntosh J, Kühlbrandt W (2010) Arrangement of photosystem II and ATP synthase in chloroplast membranes of spinach and pea. *Plant Cell* **22**: 1299–1312
- Eberhard S, Loiselay C, Drapier D, Bujaldon S, Girard-Bascou J, Kuras R, Choquet Y, Wollman FA (2011) Dual functions of the nucleus-encoded factor TDA1 in trapping and translation activation of *atpA* transcripts in *Chlamydomonas reinhardtii* chloroplasts. *Plant J* **67**: 1055–1066
- Franklin MJ, Brusilow WSA, Woodbury DJ (2004) Determination of proton flux and conductance at pH 6.8 through single F_0 sectors from *Escherichia coli*. *Biophys J* **87**: 3594–3599
- Fristedt R, Martins NF, Strenkert D, Clarke CA, Suchoszek M, Thiele W, Schöttler MA, Merchant SS (2015) The Thylakoid Membrane Protein CGL160 Supports CF_1CF_0 ATP Synthase Accumulation in *Arabidopsis thaliana*. *PLoS One* **10**: e0121658
- Gay NJ (1984) Construction and characterization of an *Escherichia coli* strain with a *unc1* mutation. *J Bacteriol* **158**: 820–825

- Grahl S, Reiter B, Gügel ILL, Vamvaka E, Gandini C, Jahns P, Soll J, Leister D, Rühle T** (2016) The Arabidopsis Protein CGLD11 Is Required for Chloroplast ATP Synthase Accumulation. *Mol Plant* **9**: 885–899
- Groth G, Pohl E** (2001) The structure of the chloroplast F₁-ATPase at 3.2 Å resolution. *J Biol Chem* **276**: 1345–1352
- Hahn A, Vonck J, Mills DJ, Meier T, Kühlbrandt W** (2018) Structure, mechanism, and regulation of the chloroplast ATP synthase. *Science* **360**: 4318
- Junge W, Nelson N** (2015) ATP synthase. *Annu Rev Biochem* **84**: 631–557
- Kanazawa A, Kramer DM** (2002) *In vivo* modulation of nonphotochemical exciton quenching (NPQ) by regulation of the chloroplast ATP synthase. *Proc Natl Acad Sci U S A* **99**: 12789–12794
- Kanazawa A, Ostendorf E, Kohzuma K, Hoh D, Strand DD, Sato-Cruz M, Savage L, Cruz JA, Fisher N, Froehlich JE, et al** (2017) Chloroplast ATP synthase modulation of the thylakoid proton motive force: implications for photosystem I and photosystem II photoprotection. *Front Plant Sci* **8**: 1–12
- Karimi M, Inzé D, Depicker A** (2002) GATEWAY™ vectors for Agrobacterium-mediated plant transformation. *Trends Plant Sci* **7**: 193–195
- Karpowicz SJ, Prochnik SE, Grossman AR, Merchant SS** (2011) The GreenCut2 resource, a phylogenomically derived inventory of proteins specific to the plant lineage. *J Biol Chem* **286**: 21427–21439
- Kramer DM, Cruz JA, Kanazawa A** (2003) Balancing the central roles of the thylakoid proton gradient. *Trends in Plant Science* **8**: 27–32.
- Lemaire C, Wollman F** (1989) The Chloroplast ATP Synthase in *Chlamydomonas reinhardtii*. *Biochemistry* **264**: 10235–10242
- Liu J, Hicks DB, Krulwich TA** (2013) roles of Atpl and two YidC-type proteins from alkaliphilic *Bacillus pseudofirmis* OF4 in ATP synthase assembly and nonfermentative growth. *J Bacteriol* **195**: 220–230
- Maiwald D, Dietzmann A, Jahns P, Pesaresi P, Joliot P, Joliot A, Levin JZ, Salamini F, Leister D** (2003) Knock-out of the genes coding for the rieske protein and the ATP-synthase δ -subunit of Arabidopsis. Effects on photosynthesis, thylakoid protein composition, and nuclear chloroplast gene expression. *Plant Physiol* **133**: 191–202
- Mao J, Chi W, Ouyang M, He B, Chen F, Zhang L** (2015) PAB is an assembly chaperone that functions downstream of chaperonin 60 in the assembly of chloroplast ATP synthase coupling factor 1. *Proc Natl Acad Sci USA* **112**: 4152–4157
- Murphy BJ, Klusch N, Langer J, Mills DJ, Yildiz Ö, Kühlbrandt W** (2019) Rotary substates of mitochondrial ATP synthase reveal the basis of flexible F₁-F_o coupling. *Science* **364**: 1155
- Naumenko N, Morgenstern M, Rucktäschel R, Warscheid B, Rehling P** (2017) INA complex liaises the F₁F_o-ATP synthase membrane motor modules. *Nat Commun* **8**: 1237
- Ozaki Y, Suzuki T, Kuruma Y, Ueda T, Yoshida M** (2008) Unc1 protein can mediate ring-assembly of c-subunits of F₀F₁-ATP synthase *in vitro*. *Biochem Biophys Res Commun* **367**: 663–666.
- Pfalz J, Bayraktar OA, Prikryl J, Barkan A** (2009) Site-specific binding of a PPR protein defines and stabilizes 5' and 3' mRNA termini in chloroplasts. *EMBO J* **28**: 2042–2052
- Porra RJ, Thompson WA, Kriedemann PE** (1989) Determination of accurate extinction coefficients and simultaneous equations for assaying chlorophylls *a* and *b* extracted with four different solvents: verification of the concentration of chlorophyll standards by atomic absorption spectroscopy. *Biochim Biophys Acta* **975**: 384–394.
- Rappsilber J, Ishihama Y, Mann M** (2003) Stop and go extraction tips for matrix-assisted laser desorption/ionization, nanoelectrospray, and LC/MS sample pretreatment in proteomics. *Anal Chem* **75**: 663–70

- Reiland S, Messerli G, Baerenfaller K, Gerrits B, Endler A, Grossmann J, Grussem W, Baginsky S** (2009) Large-scale Arabidopsis phosphoproteome profiling reveals novel chloroplast kinase substrates and phosphorylation networks. *Plant Physiol* **150**: 889–903
- Reiter B, Vamvaka E, Marino G, Kleine T, Jahns P, Bolle C, Leister D, Rühle T** (2020) The Arabidopsis Protein CGL20 is Required for Plastid 50S Ribosome Biogenesis. *Plant Physiol* **182**: 1222–1238
- Rott M, Martins NF, Thiele W, Lein W, Bock R, Kramer DM, Schöttler MA** (2011) ATP synthase repression in tobacco restricts photosynthetic electron transport, CO₂ assimilation, and plant growth by overacidification of the thylakoid lumen. *Plant Cell* **23**: 304–321
- Rühle T, Leister D** (2015) Assembly of F₁F₀-ATP synthases. *Biochim Biophys Acta* **1847**: 849–860
- Rühle T, Razeghi JA, Vamvaka E, Viola S, Gandini C, Kleine T, Schunemann D, Barbato R, Jahns P, Leister D** (2014) The Arabidopsis Protein CONSERVED ONLY IN THE GREEN LINEAGE160 Promotes the Assembly of the Membranous Part of the Chloroplast ATP Synthase. *Plant Physiol* **165**: 207–226
- Rühle T, Reiter B, Leister D** (2018) Chlorophyll fluorescence video imaging: A versatile tool for identifying factors related to photosynthesis. *Front Plant Sci* **9**: 55
- Schneider CA, Rasband WS, Eliceiri KW** (2012) NIH Image to ImageJ: 25 years of image analysis. *Nature Methods* **9**: 671–675
- Schreiber U, Klughammer C** (2008) New accessory for the DUAL-PAM-100 : The P515 / 535 module and examples of its application. **10**: 1–10
- Song J, Pfanner N, Becker T** (2018) Assembling the mitochondrial ATP synthase. *Proc Natl Acad Sci U S A* **115**: 2850–2852
- Suzuki T, Ozaki Y, Sone N, Feniouk BA, Yoshida M** (2007) The product of *uncl* gene in F₁F₀-ATP synthase operon plays a chaperone-like role to assist c-ring assembly. *Proc Natl Acad Sci U S A* **104**: 20776–20781
- Takagi D, Amako K, Hashiguchi M, Fukaki H, Ishizaki K, Goh T, Fukao Y, Sano R, Kurata T, Demura T, et al** (2017) Chloroplastic ATP synthase builds up a proton motive force preventing production of reactive oxygen species in photosystem I. *Plant J* **91**: 306–324
- Trösch R, Töpel M, Flores-Pérez Ú, Jarvis P** (2015) Genetic and physical interaction studies reveal functional similarities between ALBINO3 and ALBINO4 in Arabidopsis. *Plant Physiol* **169**: 1292–1306
- Vollmar M, Schlieper D, Winn M, Büchner C, Groth G** (2009) Structure of the c₁₄ rotor ring of the proton translocating chloroplast ATP synthase. *J Biol Chem* **284**: 18228–18235
- Wang P, Dalbey RE** (2011) Inserting membrane proteins: The YidC/Oxa1/Alb3 machinery in bacteria, mitochondria, and chloroplasts. *Biochim Biophys Acta - Biomembr* **1808**: 866–875
- Yap A, Kindgren P, Colas Des Francs-Small C, Kazama T, Tanz SK, Toriyama K, Small I** (2015) AEF1/MPR25 is implicated in RNA editing of plastid *atpF* and mitochondrial *nad5*, and also promotes *atpF* splicing in Arabidopsis and rice. *Plant J* **81**: 661–669
- Zhang L, Duan Z, Zhang J, Peng L** (2016) BIOGENESIS FACTOR REQUIRED FOR ATP SYNTHASE 3 Facilitates Assembly of the Chloroplast ATP Synthase Complex in Arabidopsis. *Plant Physiol* **171**: 1291–1306
- Zhang L, Pu H, Duan Z, Li Y, Liu B, Zhang Q, Li W** (2018) Nucleus-Encoded Protein BFA1 Promotes Efficient Assembly of the Chloroplast ATP Synthase Coupling Factor 1. *Plant Cell* **30**: 1770–1788
- Zhang L, Zhou W, Che L, Rochaix JD, Lu C, Li W, Peng L** (2019) PPR protein BFA2 is essential for the accumulation of the *AtpH/F* transcript in chloroplasts. *Front Plant Sci* **10**: 1–12
- Zoschke R, Kroeger T, Belcher S, Schöttler MA, Barkan A, Schmitz-Linneweber C** (2012) The pentatricopeptide repeat-SMR protein ATP4 promotes translation of the chloroplast *atpB/E* mRNA. *Plant J* **72**: 547–558

4 The Arabidopsis Protein CGL20 is Required for Plastid 50S Ribosome Biogenesis

Reiter B, Vamvaka E, Marino G, Kleine T, Jahns P, Bolle C, Leister D, Rühle T (2020) The Arabidopsis Protein CGL20 is Required for Plastid 50S Ribosome Biogenesis. *Plant Physiol* **182**: 1222-1238

DOI: <https://doi.org/10.1104/pp.19.01502>

The Arabidopsis Protein CGL20 Is Required for Plastid 50S Ribosome Biogenesis¹[OPEN]

Bennet Reiter,^a Evgenia Vamvaka,^a Giada Marino,^a Tatjana Kleine,^a Peter Jahns,^b Cordelia Bolle,^a Dario Leister,^a and Thilo Rühle^{a,2,3}

^aPlant Molecular Biology Faculty of Biology I, Ludwig-Maximilians-Universität, D-82152 Planegg-Martinsried, Germany

^bInstitute of Plant Biochemistry, Heinrich-Heine University, 40225 Duesseldorf, Germany

ORCID IDs: 0000-0002-6526-9727 (B.R.); 0000-0002-1525-4244 (G.M.); 0000-0001-6455-3470 (T.K.); 0000-0002-5340-1153 (P.J.); 0000-0002-4399-0070 (C.B.); 0000-0003-1897-8421 (D.L.); 0000-0003-0155-2168 (T.R.).

Biogenesis of plastid ribosomes is facilitated by auxiliary factors that process and modify ribosomal RNAs (rRNAs) or are involved in ribosome assembly. In comparison with their bacterial and mitochondrial counterparts, the biogenesis of plastid ribosomes is less well understood, and few auxiliary factors have been described so far. In this study, we report the functional characterization of CONSERVED ONLY IN THE GREEN LINEAGE20 (CGL20) in *Arabidopsis* (*Arabidopsis thaliana*; AtCGL20), which is a Pro-rich, ~10-kD protein that is targeted to mitochondria and chloroplasts. In *Arabidopsis*, CGL20 is encoded by segmentally duplicated genes of high sequence similarity (AtCGL20A and AtCGL20B). Inactivation of these genes in the *atcgl20ab* mutant led to a visible virescent phenotype and growth arrest at low temperature. The chloroplast proteome, pigment composition, and photosynthetic performance were significantly affected in *atcgl20ab* mutants. Loss of AtCGL20 impaired plastid translation, perturbing the formation of a hidden break in the 23S rRNA and causing abnormal accumulation of 50S ribosomal subunits in the high-molecular-mass fraction of chloroplast stromal extracts. Moreover, AtCGL20A-eGFP fusion proteins comigrated with 50S ribosomal subunits in Suc density gradients, even after RNase treatment of stromal extracts. Therefore, we propose that AtCGL20 participates in the late stages of the biogenesis of 50S ribosomal subunits in plastids, a role that presumably evolved in the green lineage as a consequence of structural divergence of plastid ribosomes.

The vast majority of the ~3,000 chloroplast proteins are encoded in the nuclear genome, and only ~120 genes have been retained in a small, ~150-kb plastid genome of cyanobacterial origin (Leister, 2003). Plastid genes are either transcribed by a plastid-encoded, bacteria-type or a nucleus-encoded, phage-type RNA polymerase (for review, see Pfannschmidt et al., 2015). Several plastid genes are organized in operons, and polycistronic transcripts undergo a variety of processing steps, including splicing, editing, and endonucleolytic cleavage (for review, see Germain et al., 2013). Despite the complexity of posttranscriptional RNA

metabolism in the organelle, plastid gene expression is considered to be controlled mainly at the translational level (Sun and Zerges, 2015; Zoschke and Bock, 2018) and therefore depends on the activity of plastid ribosomes. Like those of their bacterial ancestors, plastid ribosomes are made up of a small 30S (SSU) and a large 50S (LSU) subunit and contain catalytic ribosomal RNAs (rRNA) as well as at least 50 ribosomal proteins (RPs). The overall length of the unprocessed chloroplast rRNA corresponds approximately to that of rRNAs found in bacteria; however, the 3' end of the 23S plastid rRNA is further processed to yield a 4.5S fragment after LSU maturation (Keus et al., 1984; Leal-Klevezas et al., 2000). In higher plants, the 23S rRNA is additionally subjected to postmaturation processing resulting in three fragments, separated by so-called hidden breaks (Kössel et al., 1985). In comparison with bacterial ribosomes, chloroplast ribosomes show differences in RP composition, and some harbor additional extensions, leading to an overall increase in molecular mass of about 170 kD (Yamaguchi et al., 2000; Yamaguchi and Subramanian, 2000, 2003). No homologs of the bacterial subunits bl25 and ul30 have been identified in chloroplasts, but five plastid-specific ribosomal proteins (PSRPs) are associated with chloroplast ribosomes in stoichiometric amounts (Yamaguchi et al., 2000; Yamaguchi and Subramanian, 2000, 2003; Sharma et al., 2010).

¹This work was supported by the Deutsche Forschungsgemeinschaft (project no. 197471519, FOR2092 project no. 239484859, SFB-TRR175 C01 project no. 317553531, and SFB-TRR175 C05 project no. 317556510).

²Author for contact: thilo.ruehle@biologie.uni-muenchen.de.

³Senior author.

The author responsible for distribution of materials integral to the findings presented in this article in accordance with the policy described in the Instructions for Authors (www.plantphysiol.org) is: Thilo Rühle (thilo.ruehle@biologie.uni-muenchen.de).

B.R., E.V., D.L., and T.R. designed research; B.R., E.V., G.M., T.K., C.B., P.J., and T.R. performed research; B.R., E.V., G.M., T.K., P.J., C.B., D.L., and T.R. analyzed data; the article was written by B.R., D.L., and T.R. with contributions from all other authors.

[OPEN] Articles can be viewed without a subscription.

www.plantphysiol.org/cgi/doi/10.1104/pp.19.01502

Recently, structures of chloroplast ribosomes from spinach (*Spinacia oleracea*) have been determined at high resolution (Ahmed et al., 2016; Bieri et al., 2017; Graf et al., 2017; Perez Boerema et al., 2018), revealing the exact positions and binding partners of PSRPs. PSRP2, PSRP3, and PSRP4 form part of the SSU, whereas PSRP5 and PSRP6 associate with the LSU. Moreover, only the loss of PSRP3, PSRP4, or PSRP5 significantly disrupts ribosome biogenesis and translation (Tiller et al., 2012). Hence, as in bacteria, not all RPs are essential for chloroplast ribosome function or biogenesis, whereas some nonessential proteins in bacteria have been shown to be indispensable for plants (for review, see Tiller and Bock, 2014).

Biogenesis of bacterial ribosomes has been studied extensively (for review, see Shajani et al., 2011; Davis and Williamson, 2017), but the corresponding process in chloroplasts is less well understood. The rRNAs are encoded in a single plastid operon, whereas the majority of RPs are encoded in the nucleus and imported posttranslationally into the chloroplast. As expected from the bacterial model, chloroplast ribosome biogenesis is initiated by rRNA transcription and cotranscriptional binding of RPs (Miller et al., 1970). Subsequent rRNA processing and RP-assisted folding result in the independent assembly of the SSU and LSU (Davis and Williamson, 2017). In bacteria, approximately 100 auxiliary factors that are involved in rRNA processing and the integration of RPs have been identified (Shajani et al., 2011). Some of these have been shown to mediate similar functions in chloroplasts (for review, see Bohne, 2014; Liu et al., 2015; Jeon et al., 2017; Janowski et al., 2018). Despite the dual genetic origin of plastid RPs, which necessitates spatiotemporal orchestration of RP assembly, and significant structural differences with respect to bacterial ribosomes, few chloroplast-specific ribosome biogenesis factors have been identified to date (Bohne, 2014; Wang et al., 2016; Meurer et al., 2017; Paieri et al., 2018; Pulido et al., 2018).

Here, we report the functional characterization of CONSERVED ONLY IN THE GREEN LINEAGE20 (CGL20) in *Arabidopsis* (*Arabidopsis thaliana*; AtCGL20). CGL20s are small, Pro-rich proteins that are conserved in photosynthetic eukaryotes. Their loss is associated with a general reduction in chloroplast protein content, which leads to a virescent growth phenotype. Our analyses of mutant lines strongly support the notion that AtCGL20 proteins are required for efficient ribosomal biogenesis in plastids.

RESULTS

The GreenCut Protein CGL20 Is a Small Pro- and Glu-Rich Protein

In a search for previously uncharacterized factors required for chloroplast biogenesis, proteins were considered as candidates if they (1) are shared by photosynthetic eukaryotes from the green lineage but

are not found in nonphotosynthetic eukaryotes (the so-called GreenCut proteins; Merchant et al., 2007; Grossman et al., 2010) and (2) were identified as recently segmentally duplicated genes in *Arabidopsis* (Bolle et al., 2013). One of these gene pairs comprises At2G17240 and At3G24506 (the *Arabidopsis* equivalents of the *Chlamydomonas reinhardtii* gene CGL20; Karpowicz et al., 2011); hence, At2G17240 and At3G24506 are designated hereafter as AtCGL20A and AtCGL20B, respectively. These genes code for proteins of 140 (AtCGL20A) and 149 (AtCGL20B) amino acids (Fig. 1), and each contains a predicted N-terminal chloroplast transit peptide, such that the mature proteins have a calculated molecular mass of ~10 kD and a calculated pI of 4.3. All of the CGL20 proteins examined in the green lineage contained Pro-rich N-terminal sequences, whereas the C-terminal regions were characterized by a high proportion of acidic amino acids (Fig. 1; Supplemental Table S1).

Lack of AtCGL20 Affects Plant Growth, Pigment Composition, and Photosynthesis

Arabidopsis T-DNA insertion lines for AtCGL20A and AtCGL20B were identified (*atcgl20a* and *atcgl20b*) and crossed to generate the double mutant line *atcgl20ab* (Fig. 2). To analyze transcript abundance in *atcgl20* mutants, reverse transcription quantitative PCR analyses were carried out (Fig. 2B). In the wild-type Columbia-0 (Col-0) ecotype, AtCGL20A transcripts were found to be fourfold more abundant than their AtCGL20B counterparts. As expected, AtCGL20A and AtCGL20B transcripts failed to accumulate in the respective single mutant lines and in the double mutant *atcgl20ab*. No obvious growth phenotype was observed for *atcgl20b*, but *atcgl20a* had slightly paler leaves than the wild type (Fig. 2C). However, growth rate and leaf pigmentation of the double mutant *atcgl20ab* differed clearly from those of wild-type plants (Fig. 2, C and D; Supplemental Table S2), producing a virescent phenotype. Growth rates of *atcgl20* mutants were also investigated at low temperature (Supplemental Fig. S1A). All mutants germinated at 4°C, but *atcgl20ab* stopped growing during the seedling stage and failed to assemble functional PSII complexes, as indicated by the lack of any detectable maximal quantum yield of PSII (F_v/F_m) signal.

To test whether the disruption of AtCGL20A and AtCGL20B affects photosynthetic performance, chlorophyll *a* fluorescence and P_{700} parameters were determined (Table 1) using the Dual-PAM-100 system (Walz). The double mutant exhibited only a moderate decrease in PSII functionality ($F_v/F_m = 0.76 \pm 0.01$) but showed remarkably lower nonphotochemical quenching (NPQ) values (0.27 ± 0.05) than wild-type plants (0.90 ± 0.13). Interestingly, a significant but less pronounced decline in NPQ was detected in *atcgl20a* plants (0.66 ± 0.13). Moreover, Y(ND) values were increased in *atcgl20ab* plants, which reflects a donor-side

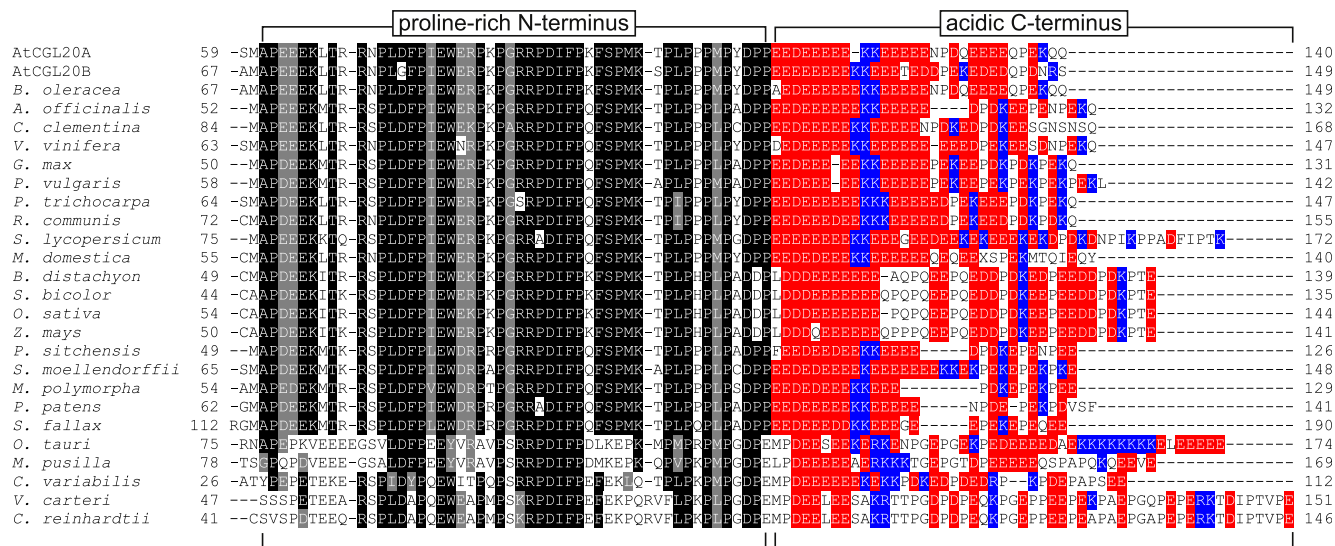


Figure 1. Sequence alignment of Arabidopsis CGL20A (AtCGL20A), CGL20B (AtCGL20B), and homologs from other species in the green lineage. Predicted chloroplast transit peptides are not included in the alignment. Stretches of sequence similarity/identity conserved in the Pro-rich N-terminal region in at least 80% of the proteins are highlighted by gray/black shading. At the C-terminal end, acidic (E and D) and basic (K and R) amino acids are marked in red and blue, respectively. Sequence identifiers and further features of these proteins are listed in Supplemental Table S1.

limitation of PSI in photosynthetic electron transport. We also tested for NAD(P)H dehydrogenase-like (NDH) complex activity in *atcgl20* mutant lines as described by Armbruster et al. (2013). The typical fluorescence rise after a light-dark switch, which can be mainly attributed to NDH-dependent cyclic electron transport, was observed in Col-0, *atcgl20a*, and *atcgl20b* but not in *atcgl20ab* (Supplemental Fig. S1C).

To confirm that the *atcgl20ab* phenotype resulted from the double knockout, the *AtCGL20A* or *AtCGL20B*

gene was fused to the eGFP-encoding reporter gene, placed under the control of the cauliflower mosaic virus 35S promoter, and transformed into the *atcgl20ab* background (Supplemental Fig. S1B). Each GFP fusion construct was able to complement the double mutant phenotype, indicating that *AtCGL20A* and *AtCGL20B* have redundant functions.

In summary, *atcgl20ab* has a *pgr* (proton gradient regulation) phenotype similar to that of the Arabidopsis mutant line *pgr1*, which is deficient in the cytochrome

Figure 2. Characterization of Arabidopsis *atcgl20ab* knockout mutants. A, Structures and T-DNA insertion sites in the *AtCGL20A* and *AtCGL20B* genes. Left (LB) and right (RB) T-DNA borders are indicated. Exons are numbered and shown as white rectangles, untranslated regions as black rectangles. B, Quantification of At2G127240 and At3G24506 transcripts by real-time PCR analyses using transcripts of the actin-encoding gene *ACT8* (At1G49240) as a reference. Means \pm SD were calculated from three technical replicates. C, Growth phenotypes of the genotypes analyzed. Plants were grown for 5 weeks under a 12/12-h light/dark regime. D, Leaf-area measurements of the genotypes shown in C. Means \pm SD were calculated from data for 12 leaf areas per genotype.

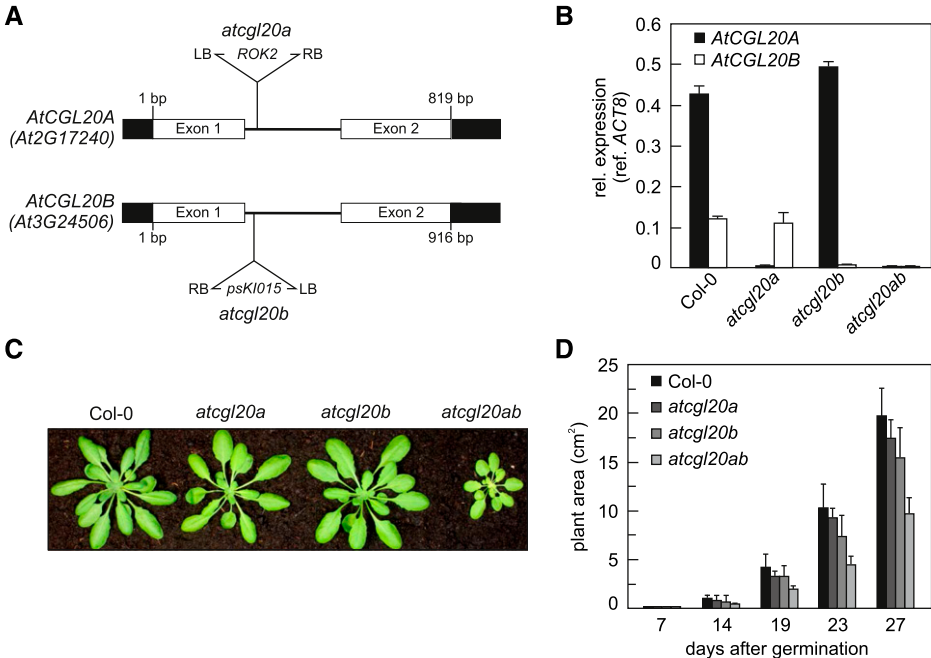


Table 1. Chlorophyll *a* fluorescence and P_{700} parameters of wild-type (*Col-0*), *atcgl20a*, *atcgl20b*, *atcgl20ab*, *oeAtCGL20A-eGFP*, and *oeAtCGL20B-eGFP* plants

Leaves were exposed to $130 \mu\text{E m}^{-2} \text{s}^{-1}$ for 15 min. The dark-relaxation phase lasted 10 min. Mean values ($n = 5$) \pm SD are provided. Φ_{II} , Effective quantum yield of PSII at $100 \mu\text{E m}^{-2} \text{s}^{-1}$; 1-qP, excitation pressure; qE, energy-dependent quenching of chlorophyll fluorescence; qI, photoinhibitory quenching; Y(I), photochemical quantum yield of PSI; Y(ND), nonphotochemical quantum yield of PSI, donor-side limited; Y(NA) nonphotochemical quantum yield of PSI, acceptor-side limited.

Parameter	<i>Col-0</i>	<i>atcgl20a</i>	<i>atcgl20b</i>	<i>atcgl20ab</i>	<i>oeAtCGL20A-eGFP</i>	<i>oeAtCGL20B-eGFP</i>
F_v/F_m	0.80 ± 0.00	0.80 ± 0.01	0.81 ± 0.00	0.76 ± 0.01	0.81 ± 0.00	0.81 ± 0.00
Φ_{II}	0.41 ± 0.04	0.43 ± 0.03	0.39 ± 0.04	0.45 ± 0.04	0.40 ± 0.02	0.38 ± 0.04
1-qP	0.41 ± 0.06	0.39 ± 0.04	0.43 ± 0.05	0.37 ± 0.05	0.42 ± 0.03	0.44 ± 0.06
NPQ	0.90 ± 0.13	0.66 ± 0.13	0.92 ± 0.11	0.27 ± 0.05	0.97 ± 0.07	1.00 ± 0.10
qE	0.75 ± 0.13	0.50 ± 0.11	0.76 ± 0.10	0.15 ± 0.05	0.81 ± 0.07	0.84 ± 0.10
qI	0.35 ± 0.04	0.33 ± 0.05	0.39 ± 0.04	0.26 ± 0.01	0.40 ± 0.02	0.41 ± 0.03
Y(I)	0.70 ± 0.03	0.69 ± 0.03	0.71 ± 0.03	0.65 ± 0.04	0.70 ± 0.02	0.69 ± 0.04
Y(ND)	0.19 ± 0.04	0.21 ± 0.04	0.21 ± 0.04	0.29 ± 0.03	0.21 ± 0.03	0.23 ± 0.05
Y(NA)	0.10 ± 0.02	0.10 ± 0.02	0.08 ± 0.01	0.07 ± 0.01	0.09 ± 0.02	0.08 ± 0.01

(Cyt) *b₆f* complex (Munekage et al., 2001), and this phenotype is present in a milder form in the single mutant *atcgl20a*. However, *atcgl20ab* shows additional defects in photosynthesis, such as a lower level of PSII functionality, lack of detectable NDH activity, and substantially altered chloroplast pigment composition even under normal growth conditions.

AtCGL20A and AtCGL20B Are Targeted to Chloroplasts and Mitochondria

In previous studies, AtCGL20A, AtCGL20B, and their *C. reinhardtii* homolog were identified as chloroplast proteins (Bayer et al., 2011; Narsai et al., 2011; Terashima et al., 2011). To confirm protein localization, protoplasts of *oeAtCGL20A*-enhanced GFP (eGFP) and *oeAtCGL20B*-eGFP plants were isolated and examined by confocal laser scanning microscopy (Fig. 3A). In both cases, strong eGFP signals were exclusively detectable in chloroplasts. We also examined the subcellular localization of CGL20 homologs in the green lineage using TargetP (Supplemental Table S1). Chloroplast localization could be predicted for 41 CGL20 homologs, whereas a mitochondrial or an ambiguous localization was predicted for four homologs from Chlorophyta (CGL20 of *C. reinhardtii*, *Volvox carterii*, *Chlorella variabilis*, and *Ostreococcus lucimarinus*). To identify even small amounts of AtCGL20, which might be targeted to mitochondria and are below the eGFP detection threshold of fluorescence microscopy, we performed cell fractionation and immunodetection assays (Fig. 3B). To this end, an antibody was raised against a synthetic peptide found in both AtCGL20 proteins (see “Materials and Methods” for details). We were able to detect AtCGL20A- and AtCGL20B-eGFP fusion proteins in whole-leaf extracts of overexpression plants. Thus, chloroplasts and mitochondria were isolated from *oeAtCGL20A*-eGFP and *oeAtCGL20B*-eGFP plants and subjected to SDS-PAGE and immunodetection assays of marker proteins (Fig. 3B). Both fusion proteins could be detected in mitochondria and were

present in both the soluble and insoluble chloroplast fractions.

Since both eGFP fusion proteins showed the same pattern of localization and *atcgl20ab* plants overexpressing either *AtCGL20A-eGFP* or *AtCGL20B-eGFP* complemented the wild-type phenotype (Supplemental Fig. S1B), subsequent biochemical experiments were carried out exclusively with *atcgl20ab* plants overexpressing *AtCGL20A-eGFP*. Next, the association of AtCGL20A-eGFP with high-molecular-mass (HMM) complexes in the chloroplast stroma was analyzed (Fig. 3C). Most of AtCGL20A-eGFP was found in the free protein fraction in Suc step-gradient experiments. However, a significant portion was located in the HMM fraction, together with the ribosomal subunits Rpl2 and Rps1. The fact that neither Rubisco nor the stromal chaperonin Cpn60 was significantly enriched in the HMM fraction indicated that AtCGL20A-eGFP associates with a stromal complex that is larger than the Cpn60 complex (~800 kD). Thus, AtCGL20 proteins are found in mitochondria but predominantly in chloroplasts, where they are part of a stromal complex with a molecular mass greater than 800 kD.

Loss of AtCGL20 Function Alters the Composition of the Chloroplast Proteome and Thylakoid Membrane Complexes

The dual localization of AtCGL20A and AtCGL20B and multiple alterations in chloroplast function prompted us to investigate changes at the transcriptomic and proteomic levels in *atcgl20ab* (Fig. 4; Supplemental Fig. S2; Supplemental Tables S3–S7). RNA sequencing analysis revealed that 1,254 genes were significantly differentially expressed (adjusted $P < 0.05$) in *atcgl20ab* relative to the wild type. Of these, 880 gene transcripts were down-regulated (\log_2 fold change [FC] < -0.59) and 374 were up-regulated (\log_2 FC > 0.59 ; Supplemental Table S3). In addition, the relative abundance of 1,920 protein groups was quantified in *atcgl20ab* with respect to the wild-type

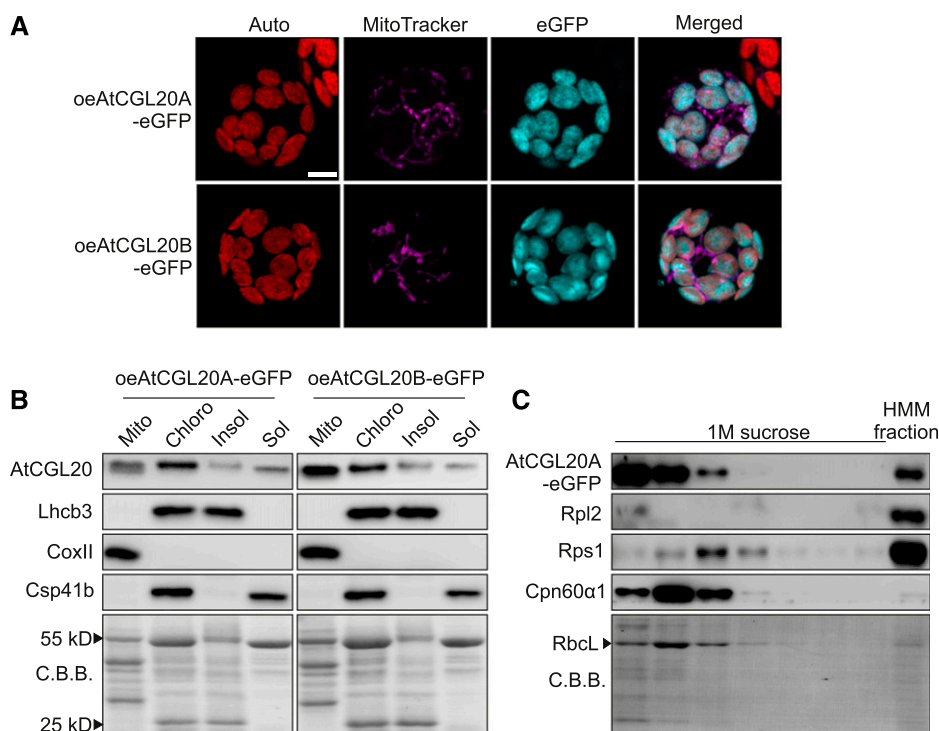


Figure 3. Subcellular localization of AtCGL20A and AtCGL20B. A, Chlorophyll autofluorescence (Auto), MitoTracker, and eGFP fluorescence emission (eGFP) of protoplasts isolated from oeAtCGL20A-eGFP and oeAtCGL20B-eGFP plants. Protoplasts were analyzed by confocal laser scanning microscopy and overlaid in a single image (Merged). Bar = 5 μ m. B, Immunodetection of AtCGL20A-eGFP and AtCGL20B-eGFP in cell fractionation experiments. Mitochondria (Mito) and chloroplasts (Chlro) were isolated from oeAtCGL20A-eGFP and oeAtCGL20B-eGFP plants, and chloroplasts were further separated into insoluble (Insol) and soluble (Sol) fractions. The purity of the mitochondrial fraction was examined by immunodetection of CoxII, whereas Lhcb3 and Csp41b served as marker proteins for the insoluble and soluble chloroplast fractions, respectively. To control for loading, polyvinylidene difluoride (PVDF) membranes were stained with Coomassie Brilliant Blue G-250 (C.B.B.). C, Accumulation of AtCGL20A-eGFP in the HMM fraction isolated by Suc step-gradient centrifugation from stroma extracts of oeAtCGL20A-eGFP chloroplasts. Fractions were characterized by SDS-PAGE. Cpn60 α 1, Rps1, and Rpl2 were immunodetected as marker subunits for the stromal protein complex chaperonin 60 and the SSU and LSU of chloroplast ribosomes, respectively. Coomassie Brilliant Blue staining is shown as a loading control. The position of the large Rubisco subunit RbcL is highlighted.

control. Of these, 208 and 216 proteins showed a \log_2 FC < -0.59 (adjusted P < 0.05) and a \log_2 FC > 0.59 (adjusted P < 0.05), respectively (Supplemental Table S4). We further addressed the question of whether any particular cellular compartment is specifically affected in *atcgl20ab* by examining the subcellular targeting of proteins with altered gene expression or abundance (Fig. 4B). Indeed, plastid components were overrepresented among those affected at the transcript and protein levels. For instance, 27% and 6% of the up- and down-regulated transcripts encode plastid proteins, respectively. At the protein level, the effect was even more obvious: 30% of proteins with significantly higher and 72% with significantly lower abundances in *atcgl20ab* are localized to the plastid. By contrast, only a small number of mitochondrion-targeted proteins showed significant alterations at the transcript or protein level in *atcgl20ab*.

In light of the pronounced photosynthetic defects in *atcgl20ab* (Table 1; Supplemental Table S2), we investigated transcript and subunit levels of thylakoid protein

complexes in more detail (Fig. 4C; Supplemental Table S5). Overall, only minor changes in the amounts of transcripts coding for thylakoid complex subunits were detected in *atcgl20ab*. By contrast, PSII and PSI subunit levels were clearly reduced in *atcgl20ab*. Remarkably, NDH and Cyt *b₆f* complexes exhibited the most pronounced reductions, together with subunit D1 of PSII (encoded by *psbA*), which is known to exhibit a high turnover rate (Sundby et al., 1993).

To verify the outcome of the proteome analysis, we compared membrane complex integrity and subunit abundance in mitochondria (Supplemental Fig. S3A) and thylakoid membranes isolated from wild-type and *atcgl20ab* plants (Supplemental Fig. S3, B and C) by 2D blue native (BN)/SDS-PAGE analysis. In line with the proteome data (Supplemental Table S4), no obvious differences in respiratory complex abundance could be detected. Moreover, the analysis of thylakoid complexes confirmed the specific impact of *atcgl20ab* mutations on NDH-PSI and Cyt *b₆f* (Supplemental Fig. S3B). Since the NDH-PSI and the Cyt *b₆f* complexes are

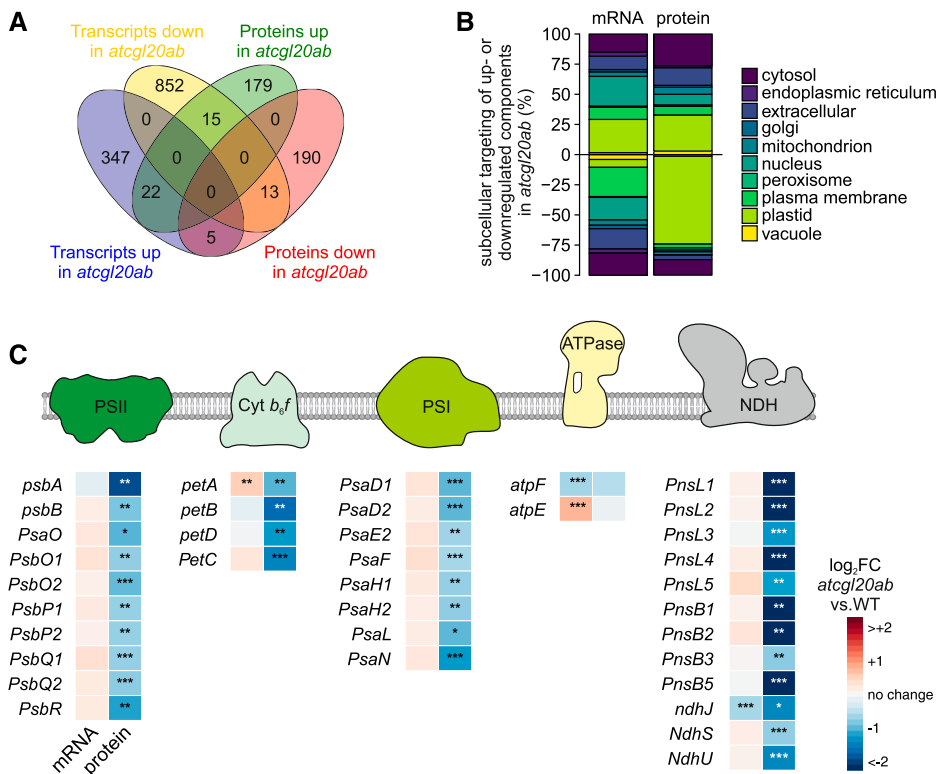


Figure 4. Comparative transcriptomic and proteomic analyses of Col-0 and *atcgl20ab*. **A**, Venn diagram of up-regulated (\log_2 FC > 0.59) and down-regulated (\log_2 FC < -0.59) transcripts and proteins in *atcgl20ab* compared with the wild type. **B**, Subcellular distribution of the proteins that are up-regulated (\log_2 FC > 0.59) or down-regulated (\log_2 FC < -0.59) in *atcgl20ab* at the transcriptional (mRNA) or protein (protein) level. **C**, Impact of *AtCGL20* disruption on the transcriptional and protein-level expression of thylakoid complex subunits. Asterisks indicate the following values: *, P < 0.05; **, P < 0.01; and ***, P < 0.001. Colors, which represent down- or up-regulated components in *atcgl20ab*, range from dark blue (\log_2 FC < -2) to dark red (\log_2 FC > 2). WT, Wild type.

less abundant than other thylakoid complexes on Coomassie blue-stained 2D gels, these reductions were verified by immunodetection assays (Supplemental Fig. S3, B and C). We also examined the integrity of thylakoid membrane complexes in the single mutants *atcgl20a* and *atcgl20b*. Interestingly, NDH-PSI and Cyt *b₆f* complex formation was clearly affected in *atcgl20a* but not in *atcgl20b* (Supplemental Fig. S3B), as was confirmed by immunodetection of marker subunits for the different thylakoid complexes (Supplemental Fig. S3D). Thus, the *pgr* phenotype (Table 1) and the lack of the postillumination fluorescence rise in *atcgl20ab* plants (Supplemental Fig. S1C) can be attributed to substantially reduced levels of Cyt *b₆f* and NDH-PSI complexes, respectively. In spite of the fact that *AtCGL20A* and *AtCGL20B* are also localized to mitochondria (Fig. 3B), their absence appears to have no measurable effect on protein complex abundances in these organelles (Supplemental Fig. S3A).

Loss of *AtCGL20* Function Affects the Chloroplast Translational Machinery

AtCGL20A and *AtCGL20B* are coexpressed with genes involved in plastid gene expression, in particular with genes coding for chloroplast RPs (Supplemental Table S8). Given that *atcgl20ab* shows a virescent phenotype (Fig. 2C), which is often associated with disruptions in chloroplast protein homeostasis (Koussevitzky et al., 2007) and reductions in chloroplast protein level (Fig. 4B) and thylakoid complex amounts (Fig. 4C),

we investigated perturbations in chloroplast gene expression in more detail. To this end, we compared plastome-encoded transcript and protein levels of 31 RNA-protein pairs between *atcgl20ab* and the wild-type control (Fig. 5A). Only moderate changes were observed at the transcript level; 11 transcripts were significantly (adjusted P < 0.05) up-regulated (\log_2 FC > 0.59), but only two were down-regulated (\log_2 FC < 0.59). Remarkably, at the protein level, the opposite trend was apparent: the abundances of 10 plastid-encoded proteins derived from different plastid operons were reduced (\log_2 FC > 0.59), whereas only three proteins were increased in amount (Rpl20, Rpl22, and Ycf3).

To test plastid translation in *atcgl20ab*, we investigated in vivo incorporation of [³⁵S]Met into de novo plastid proteins of wild-type and *atcgl20ab* plants grown either under 22°C or shifted to 4°C (Fig. 5B). Mutant plants grown under moderate temperature showed ~50% labeling efficiency, whereas *atcgl20ab* plants subjected to 4°C incorporated only ~25% of [³⁵S]Met compared with wild-type plants. To further determine whether *atcgl20ab* is defective in chloroplast translation initiation or termination, we examined the association of several plastid-encoded RNAs with chloroplast ribosomes. To this end, polysome-enriched samples were isolated from wild-type and *atcgl20ab* leaves under polysome-preserving conditions (Barkan, 1993) and further fractionated by Suc density-gradient centrifugation (Fig. 5C). Subsequently, total RNAs were isolated from 12 fractions and subjected to denaturing gel electrophoresis and RNA gel-blot analyses using

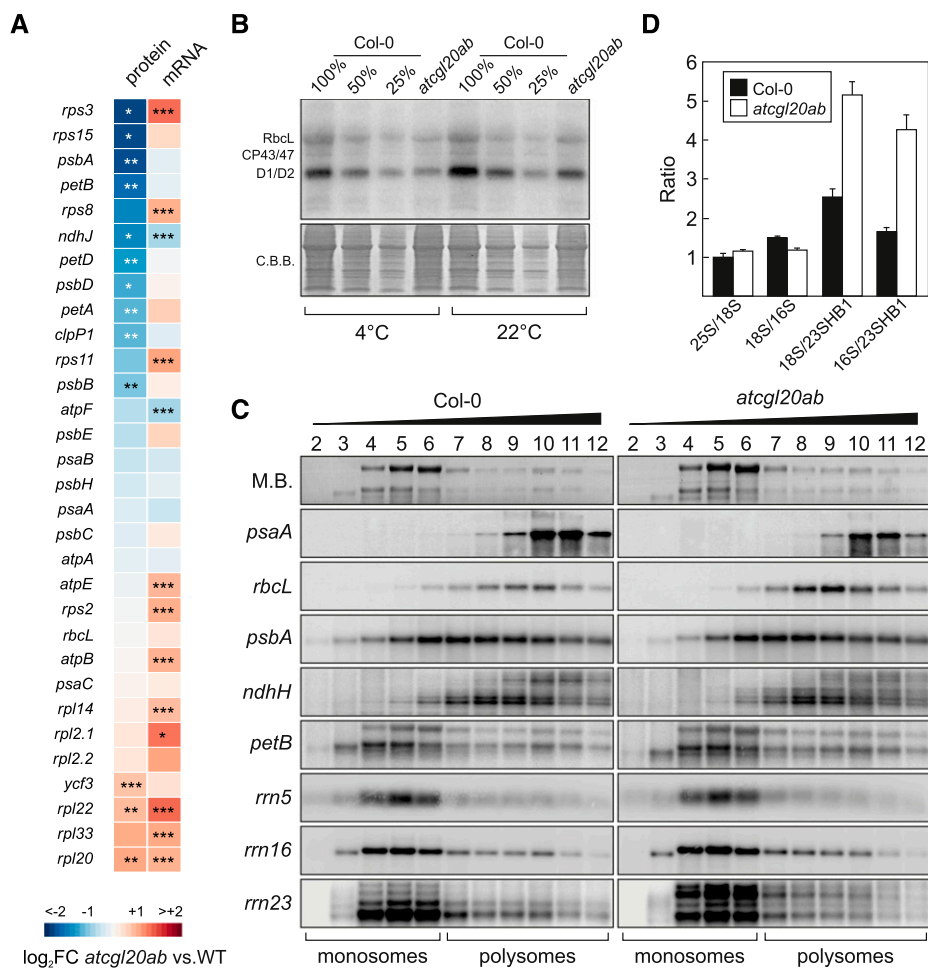


Figure 5. Chloroplast gene expression and polysome loading in *AtCGL20* loss-of-function mutants. **A**, Relative abundances of selected plastome-encoded mRNAs and proteins in *atcg120ab* compared with the wild type (WT). Asterisks indicate the following values: *, $P < 0.05$; **, $P < 0.01$; and ***, $P < 0.001$. Colors, which represent down- or up-regulated components in *atcg120ab*, range from dark blue (\log_2 FC < -2) to dark red (\log_2 FC > 2). **B**, Pulse-labeling analysis of de novo synthesized plastid proteins in 20-d-old seedlings of Col-0 and *atcg120ab* grown under 22°C or shifted for 7 d to 4°C prior to the experiment. Labeling was performed with [³⁵S]Met for 40 min under moderate light intensity in the presence of cycloheximide. Whole leaf extracts corresponding to equal amounts of fresh weight were separated by SDS-PAGE, stained with Coomassie Brilliant Blue (C.B.B.), and subjected to autoradiography. Abundant signals were identified as RbcL, CP43/CP47, and D1/D2 according to Rühle et al. (2014) and Pulido et al. (2018). **C**, RNA gel-blot hybridization of fractions obtained following Suc density-gradient centrifugation under polysome-preserving conditions. Free ribosomes (monosomes) are found in fractions 2 to 6, whereas fractions 7 to 12 contain mRNA-polysome complexes. Membranes were hybridized with probes specific for *psaA*, *rbcL*, *psbA*, *ndhH*, *petB*, *rrn5*, *rrn16*, and *rrn23*. Methylene Blue (M.B.) staining is shown as a loading control. **D**, Microfluidics-based quantification of rRNA abundance in *atcg120ab* compared with the wild-type control (Col-0). Means \pm SD were calculated from three biological replicates. Relative amounts of large cytosolic (25S), small cytosolic (18S), small chloroplast (16S), and the 1.3-kb hidden-break product of the 23S species (23S HB1) in Col-0 were compared with the values for *atcg120ab*.

selected plastid transcript probes. Transcripts of *psaA*, *psbA*, *rbcL*, *ndhH*, and *petB* did not show a shift to lower or higher density fractions, indicating that plastid translation initiation or termination is not perturbed in *atcg120ab*. Similarly, the distribution of plastid rRNAs (*rrn5*, *rrn16*, and *rrn23*) was unchanged. However, we detected nonprocessed 23S rRNAs of the LSU in fractions 4 to 11, implying that, in the double mutant, both free and actively translating chloroplast ribosomes contain unprocessed 23S rRNAs.

Relative amounts of rRNAs are sensitive indicators of plastid SSU and LSU abundances, since their steady-state levels largely depend on their efficient association with ribosomal subunits. In addition, rRNA quantification allows the assignment of a biogenesis defect either to the SSU or LSU, as the subunits are assembled independently and only form an SSU/LSU complex during translation (Walter et al., 2010; Tiller et al., 2012; Fristedt et al., 2014). Thus, we monitored the accumulation of the SSUs and LSUs of cytosolic and chloroplast ribosomes by quantifying their rRNA

species using a microfluidics-based approach (Fig. 5D). The ratios of cytosolic LSU to cytosolic SSU (25S/18S), cytosolic SSU to chloroplast SSU (18S/16S), cytosolic SSU to chloroplast LSU (18S/23SHB1), and chloroplast SSU to chloroplast LSU (16S/23SHB1) were determined from wild-type and *atcgl20ab* plants (Fig. 5D). In contrast to the 25S/18S and 18S/16S ratios, which were only slightly altered in *atcgl20ab*, the 18S/23SHB1 and 16S/23SHB1 ratios were twofold higher in *atcgl20ab* plants than in the wild type.

From these results, we deduced that lack of AtCGL20A and AtCGL20B alters chloroplast LSU biogenesis. However, the defect seems not to interfere with translation initiation or termination (Fig. 5C) but affects the elongation step (Fig. 5B), leading to lower accumulation of plastome-encoded proteins in *atcgl20ab* (Fig. 5A). The fact that the ratio of free to RNA-associated ribosomes is unchanged in *atcgl20ab* is also consistent with previous studies, which revealed that defects in plastid ribosome biogenesis do not

necessarily lead to significant changes in polysome loading patterns (Pesaresi et al., 2001; Nishimura et al., 2010; Chi et al., 2012).

AtCGL20 Is Required for LSU Biogenesis in Chloroplasts

To investigate the influence of AtCGL20 on chloroplast rRNA maturation, RNA gel-blot experiments were carried out with probes specific for 16S, 4.5S, 5S, and 23S rRNAs, which were hybridized to size-fractionated RNA samples isolated from wild-type, *atcgl20a*, *atcgl20b*, and *atcgl20ab* plants (Fig. 6A). In contrast to the wild-type-like levels of 16S, 4.5S, and 5S rRNAs, hybridization experiments with probes specific for 23S rRNAs detected clear changes in the single mutant *atcgl20a*, which were even more pronounced in the double mutant *atcgl20ab*. Unprocessed precursors of 2.9 and 2.4 kb accumulated to significant levels, whereas processed products of the 23S rRNA with

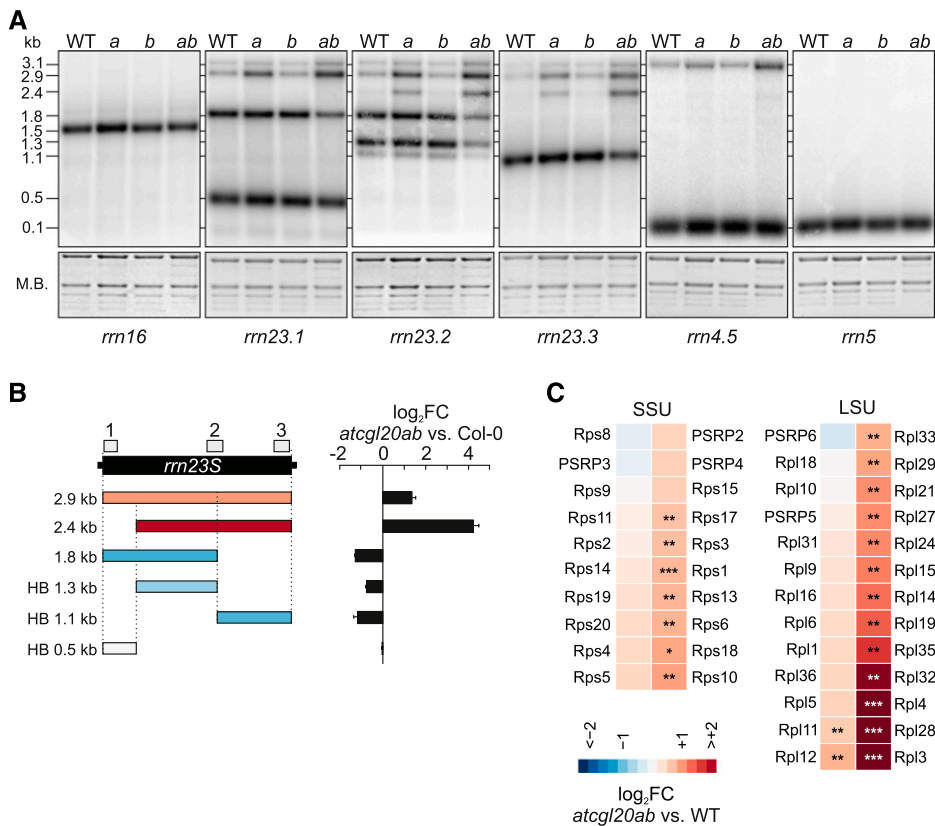


Figure 6. RNA gel-blot hybridization of plastid rRNAs and quantification of ribosomal proteins in the HMM fraction of *atcgl20ab* stroma. A, Total RNA isolated from 20-d-old wild-type (WT), *atcgl20a* (a), *atcgl20b* (b), and *atcgl20ab* (ab) plants was fractionated by denaturing agarose gel electrophoresis and blotted onto nylon membranes. Membranes were hybridized with probes specific for the 16S rRNA (*rrn16*), hidden-break fragments of 0.5 kb (*rrn23.1*), 1.3 kb and 1.1 kb (*rrn23.2*), and 1.1 kb (*rrn23.3*) of the 23S rRNA, as well as the 4.5S (*rrn4.5*) and 5S rRNA (*rrn5*). M.B., Methylene Blue. B, Quantification of 23S hidden-break (HB) products. RNA gel-blot hybridization signals for *atcgl20ab* and wild-type (Col-0) samples were quantified (Supplemental Table S9). Means \pm SD were calculated from three technical replicates. Probes for *rrn23S* used in A are depicted in gray, and subspecies of processed 23S rRNA are colored according to their abundance in *atcgl20ab* as per a scale extending from dark blue (\log_2 FC < -2) to dark red (\log_2 FC > 2). C, SSU and LSU protein abundance in the HMM fraction isolated from *atcgl20ab* chloroplast stroma (Supplemental Table S10). Asterisks indicate the following values: *, $P < 0.05$; **, $P < 0.01$; and ***, $P < 0.001$.

lower molecular masses (1.8, 1.3, and 1.1 kb) were markedly reduced (Fig. 6B; Supplemental Table S9). Notably, levels of the smallest hidden-break product (0.5 kb) of the mature 23S rRNA were not affected in *atcgl20ab*.

In light of our observations that a portion of AtCGL20A-eGFP comigrates with ribosomal subunits in the HMM fraction (>800 kD) in Suc step-gradient experiments (Fig. 3C) and that chloroplast LSU biogenesis is impaired in *atcgl20ab* (Figs. 5, C and D, and 6A), we performed a comparative proteomic study of the HMM fractions isolated from wild-type and *atcgl20ab* stromal extracts (Fig. 6C; Supplemental Table S10). A MapMan analysis of the data (Supplemental Table S11) showed that the levels of chloroplast LSU proteins (Bin 29.2.1.1.2) were significantly changed in *atcgl20ab* ($P = 2.8 \times 10^{-4}$). Thus, an in-depth comparison of SSU and LSU protein amounts between wild-type and *atcgl20ab* HMM stromal fractions was carried out (Fig. 6C). No significant reduction in the amounts of any chloroplast RP could be identified in *atcgl20ab*. Although several chloroplast SSU proteins were slightly more abundant in *atcgl20ab* than in the wild-type control, the most pronounced increases ($\log_2 \text{FC} > 2$) in the double mutant were

observed for the LSU subunits Rpl32, Rpl4, Rpl28, and Rpl3 (Fig. 6C).

Taken together, these data confirm that absence of AtCGL20 has a specific impact on chloroplast LSU biogenesis, whereas chloroplast SSU biogenesis is unaffected. This conclusion is corroborated by the finding that only 23S rRNA maturation is clearly altered in *atcgl20ab* (Fig. 6, A and B). In addition, several chloroplast LSU proteins are more prominently represented in the stromal HMM fraction (>800 kD) from *atcgl20ab* than are constituents of the SSU (Fig. 6C).

AtCGL20A-eGFP Comigrates with Chloroplast Ribosomes

Several factors involved in rRNA processing have been shown to be physically associated with ribosomes or ribosomal precursor complexes (Chi et al., 2012; Meurer et al., 2017; Paieri et al., 2018). Since a portion of AtCGL20A-eGFP had been found in the HMM fraction in Suc step-gradient experiments (Fig. 3C), we extended our comigration analysis by performing Suc density-gradient centrifugation of stromal fractions isolated under conditions in which SSU and LSU were partially dissociated from each other (Fig. 7A). Rps1, a marker

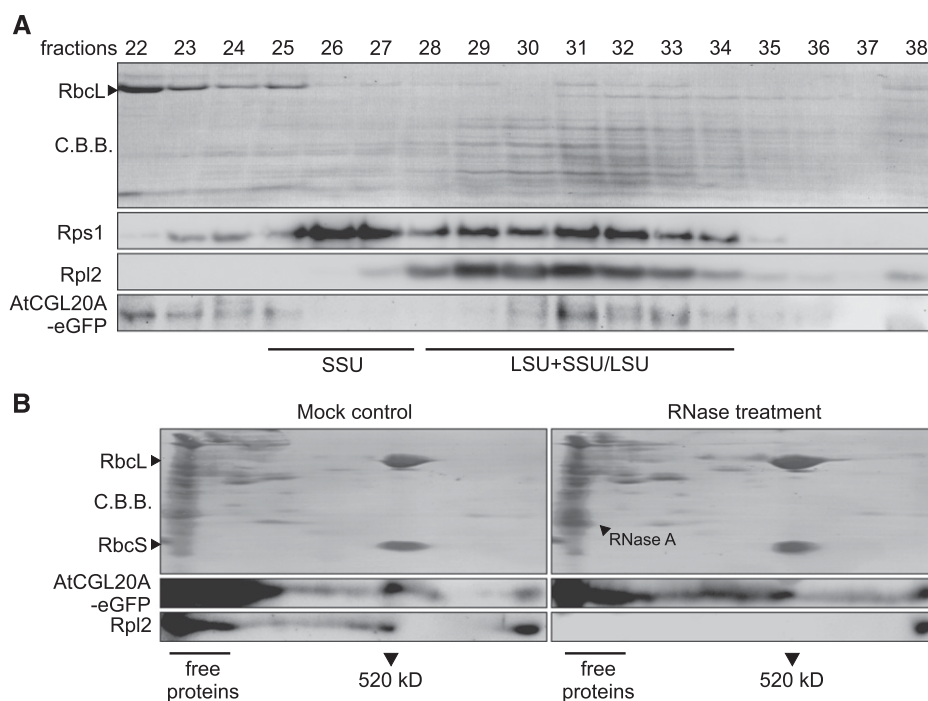


Figure 7. Comigration studies of AtCGL20A-eGFP. A, Suc density-gradient centrifugation of stromal extracts containing AtCGL20A-eGFP. Stromal extracts of AtCGL20A-eGFP plants were prepared with reduced amounts Mg^{2+} and subjected to Suc density-gradient centrifugation. Suc fractions were collected, and proteins were separated by SDS-PAGE. After protein transfer, PVDF membranes were decorated with antibodies specific for Rps1, Rpl2, AtCGL20, and GFP. Coomassie Brilliant Blue (C.B.B.) staining is shown as a loading control, and the position of the large Rubisco subunit RbcL is indicated. B, BN/SDS-PAGE analysis of stromal extracts isolated from AtCGL20A-eGFP plants. Stroma was either treated with RNase A or an RNase inhibitor as a mock control (RNasin; Promega) and subjected to BN/SDS-PAGE analyses. After protein transfer, PVDF membranes were probed with antibodies specific for AtCGL20 and Rpl2. Coomassie Brilliant Blue staining is shown as a loading control. Positions of Rubisco (~520 kD) and RNase A are indicated.

subunit for the chloroplast SSU, was immunodetected in fractions 22 to 35, with two distinct peaks in fractions 26/27 and 31/32 (Fig. 7A). By contrast, the marker subunit Rpl2 for the LSU was detected in fractions 27 to 38 and predominantly in fractions 29 to 33. These results indicated that the SSU could be partially dissociated from the LSU and was enriched in fractions 26 and 27, whereas a mixture of dissociated LSU and fully assembled ribosomes was found in fractions 28 to 35. The fusion protein AtCGL20A-eGFP was found in fractions 22 to 25, 29 to 36, and 38 but did not appear in fractions 26 to 28. Consequently, AtCGL20A-eGFP does not comigrate with the dissociated SSU but together with either the detached chloroplast LSU or as part of fully assembled ribosomes (Fig. 7A).

A specific characteristic of rRNAs in ribosomal pre-complexes is their susceptibility to RNase treatments, whereas rRNAs in fully assembled ribosomes are tightly packed with RPs and are protected from degradation (Williams and Barkan, 2003; Meurer et al., 2017). As a consequence, biogenesis factors that interact with ribosomal precomplexes tend to lose their association with rRNAs when treated with RNase (Meurer et al., 2017; Paieri et al., 2018). To investigate an association of AtCGL20A-eGFP with ribosomal pre-complexes, isolated stromal extracts of *oeAtCGL20A-eGFP* overexpression lines were either treated with RNase A or an RNase inhibitor (control) and subsequently subjected to 2D BN/SDS-PAGE analysis (Fig. 7B). After protein transfer, PVDF membranes were probed with AtCGL20- and Rpl2-specific antibodies. Although most of the AtCGL20A-eGFP fusion and Rpl2 were detected in the free protein fraction, a significant portion of both proteins comigrated with the HMM fraction (>800 kD) in the control, which was previously shown to contain ribosomal subunits (Bučinská et al., 2018). Strikingly, Rpl2 and AtCGL20A-eGFP signals increased in the HMM fraction after RNase treatment. Therefore, we conclude that AtCGL20 is involved in late steps in the biogenesis of the chloroplast LSU, since AtCGL20A-eGFP comigrates with LSU complexes (Fig. 7A) that are resistant to RNase treatment (Fig. 7B).

DISCUSSION

CGL20 Function Emerged in the Green Lineage

Although the core structures and functions of bacterial and chloroplast ribosomes are conserved, considerable changes have occurred over the course of chloroplast ribosome evolution. These include differences in rRNA processing and the addition of five new subunits (PSRP2–PSRP6) as well as several structural features unique to chloroplast ribosomes (Bieri et al., 2017), which might have evolved as a consequence of the need to translate a substantially reduced number of chloroplast-encoded proteins (Tiller and Bock, 2014; Sun and Zerges, 2015; Graf et al., 2017). Furthermore, the massive transfer of genes to the nuclear genome has

increased the complexity of organellar ribosome biogenesis, as both auxiliary factors and RPs have to be imported into chloroplasts and correctly assembled with plastome-encoded rRNAs and RPs. It is therefore evident that, owing to the relocation of genetic information to the nucleus, additional auxiliary factors became necessary in order to maintain efficient ribosome biogenesis. Indeed, several factors required for chloroplast LSU biogenesis, such as DCL, RH39, RH22, or RH50, have no orthologs in bacteria (Bellaoui et al., 2003; Nishimura et al., 2010; Chi et al., 2012; Paieri et al., 2018) and, like CGL20, first emerged in the green lineage.

Plants That Lack AtCGL20 Show a Characteristic Perturbation in Chloroplast Biogenesis

A large number of virescent *Arabidopsis* mutants with impaired chloroplast biogenesis have been described in the literature (Pesaresi et al., 2001; Sugimoto et al., 2004; Koussevitzky et al., 2007; Tillich et al., 2009; Chi et al., 2012; Janowski et al., 2018). Their defects are often associated with perturbations in chloroplast protein homeostasis (Sugimoto et al., 2004; Koussevitzky et al., 2007; Yu et al., 2008; Chi et al., 2012). Since pronounced pleiotropic effects usually accompany their disruption, the precise molecular functions of chloroplast biogenesis factors are often difficult to derive from analyses of mutant lines. Moreover, this study was complicated by the low abundance of AtCGL20 proteins and the absence of a clear domain prediction (Fig. 1). For these reasons, we turned to large-scale transcriptome and proteome analyses to compare *atcgl20ab* plants with their wild-type counterpart (Fig. 4). In line with observations made with other virescent *Arabidopsis* mutants (Kim et al., 2009; Janowski et al., 2018), *atcgl20ab* exhibited a general reduction in chloroplast protein content (Fig. 4B) as well as diminished abundance of thylakoid membrane complexes (Fig. 4C). Remarkably, Cyt *b₆f* and NDH complexes were those most affected in *atcgl20ab* (Fig. 4C; Supplemental Fig. S3B), which were reduced to ~30% and ~10% of wild-type levels, respectively. This finding effectively accounts for the combined *pgr* and chlororespiratory reduction phenotype of *atcgl20ab* (Table 1; Supplemental Fig. S2). A similar photosynthetic phenotype has been reported for the *Arabidopsis* mutant *pgr3-1*, which is disrupted in a chloroplast pentatricopeptide-repeat protein required for post-transcriptional steps in organellar gene expression (Yamazaki et al., 2004). However, selective disruption of Cyt *b₆f* and NDH complexes in *pgr3-1* mutants did not result in any significant changes in PSII and PSI levels or photosynthetic growth rates under moderate light intensities. Accordingly, we can exclude a specific role for AtCGL20 in Cyt *b₆f* or NDH complex biogenesis, and we therefore interpret their low levels as an indirect consequence of impaired chloroplast translation in the double mutant (Fig. 5).

Despite the dual localization (Fig. 3), transcript and protein levels of mitochondrial components (Fig. 4B) and respiratory complexes (Supplemental Fig. S3) were essentially unaffected in *atcgl20ab*. Notably, about 500 proteins with ambiguous transit peptides are predicted in Arabidopsis to be dual targeted to mitochondria and chloroplasts (Mitschke et al., 2009). However, a function in both organelles could only be attributed to some of them (Kmieć et al., 2014; Mazzoleni et al., 2015) and seems unlikely for others (Rödiger et al., 2011; Baudisch et al., 2014). It is therefore assumed that a certain degree of mistargeting is tolerated and might be the consequence of the evolution of the plastid import machinery (Sharma et al., 2018). On the other hand, a large group of proteins that were experimentally shown to be dual targeted are involved in organellar gene expression and in particular in translation (for review, see Carrie and Small, 2013). We therefore conclude that AtCGL20 is critical for chloroplast processes, although we cannot exclude the possibility that AtCGL20 might mediate mitochondrial functions in other developmental stages, plant organs, or specific growth conditions.

AtCGL20 Functions in Chloroplast LSU Biogenesis

Our current knowledge of chloroplast ribosome biogenesis is scant and mostly inferred from bacterial ribosome biogenesis, in which the two subunits are assembled independently in a dynamic process through coordinated folding of rRNAs and association of sets of RPs (Davis and Williamson, 2017). The order of bacterial RP binding is highly flexible, and several parallel assembly pathways have been identified (Mulder et al., 2010; Davis et al., 2016). However, LSU assembly is more complex, owing to a more intricate rRNA folding pathway, a larger number of RPs, and the need to form a functional peptidyl transfer center as well as the polypeptide tunnel exit. Chloroplast SSUs and LSUs are assembled independently, as has been demonstrated in studies of mutants altered in chloroplast LSU and SSU structure (Nishimura et al., 2010; Chi et al., 2012; Tiller et al., 2012; Janowski et al., 2018). In addition, several auxiliary chloroplast ribosome biogenesis factors have been identified, a significant number of which are DEAD-box RNA helicases, GTPases, or rRNA methylases (for review, see Böhne, 2014). Recent proteome (Majeran et al., 2012) and several GFP-fusion-based localization studies have shown that many of these factors are enriched in plastid nucleoids, which supports the assumption that ribosome assembly takes place in this intra-organellar subcompartment (Böhne, 2014). By contrast, protoplast studies (Fig. 3) showed that AtCGL20A- and AtCGL20B-eGFP did not display typical nucleoid localizations (Meurer et al., 2017). The uniform distribution of eGFP signals in the chloroplast might be explained by the overaccumulation of fusion proteins in the free stromal fraction (Figs. 3C and 7B), masking nucleoid-associated AtCGL20A- and

AtCGL20B-eGFP signals. Furthermore, it cannot be excluded that the large eGFP tag might interfere with nucleoid association.

Our study provides four lines of evidence that AtCGL20 is involved in late steps in the assembly of the chloroplast LSU: (1) 23S rRNA maturation is specifically impaired in *atcgl20ab* mutants, whereas 16S rRNA processing is not affected (Fig. 6); (2) several of the protein constituents of the chloroplast LSU overaccumulate in the stromal HMM fraction of *atcgl20ab*; (3) AtCGL20A-eGFP comigrates with LSU complexes (Fig. 7A); and (4) a subfraction of AtCGL20A-eGFP associates with an RNase-insensitive stromal HMM complex (Fig. 7B). Specific impairment of the LSU was reported also by Chi et al. (2012), and other defects in plastid protein homeostasis or chloroplast gene expression can lead to disturbances in 23S rRNA processing (Koussevitzky et al., 2007; Yu et al., 2008). However, the lack of AtCGL20 resulted in a distinct alteration in the 23S rRNA processing pattern (Fig. 6, A and B), which has also been observed in *nara1-2* and *dcl-1* mutants (Bellaoui et al., 2003; Nishimura et al., 2010). The absence of RH39 in *nara1-2* mutants led to a specific disruption in the processing of the second hidden-break site in 23S rRNAs. As a consequence, *nara1-2* plants showed normal levels of the 0.5-kb hidden-break product, whereas 1.1- and 1.3-kb fragments were markedly reduced (Fig. 6B). RH39 was proposed to be directly involved in introducing the hidden break by binding to the 23S rRNA close to an exposed stem-loop structure. This suggestion was further supported by structural analysis, which confirmed the accessibility of the putative RH39-binding site (Bieri et al., 2017). However, a function as an RNA chaperone or a direct involvement of AtCGL20 in hidden-break processing is unlikely, since the protein does not contain a canonical RNA-binding domain (Fig. 1). Intriguingly, the mutant line *dcl-1*, which is disrupted in the chloroplast ribosome biogenesis factor DCL, displayed an altered 23S rRNA processing pattern similar to that seen in *atcgl20ab* (Bellaoui et al., 2003). DCL does not possess obvious RNA-binding capacity either, but it was suggested to enable 4.5S cleavage after binding to the assembled LSU. Likewise, AtCGL20 might be involved in late LSU assembly steps and promote efficient RH39-mediated 23S processing.

Notably, AtCGL20 function seems to be essential for the formation of translationally active chloroplast ribosomes after germination under cold stress, since *atcgl20ab* plants failed to synthesize chlorophyll or PSII complexes at 4°C and soon stopped growing (Supplemental Fig. S1A). In addition, chloroplast translation is more severely affected in mutant plants shifted to low temperature (Fig. 5B). Pronounced effects at low temperature have also been observed in several other Arabidopsis mutants that are impaired in chloroplast protein synthesis (Sugimoto et al., 2004; Paieri et al., 2018; Pulido et al., 2018) as well as in bacterial strains with defects in ribosome biogenesis (Davis and Williamson, 2017). Thus, alternative LSU assembly

pathways might exist that bypass AtCGL20 function. However, its presence becomes crucial under cold stress, and LSU intermediates might be blocked in kinetic traps, leading to the growth arrest of *atcgl20ab* plants.

Besides specific alterations in 23S rRNA processing, a significant accumulation of several LSU subunits could be observed in the stromal HMM fraction (>800 kD) of *atcgl20ab* plants, which might be due to the accumulation of chloroplast LSU precomplexes (Fig. 6C). On the other hand, no detailed RP compositions of chloroplast ribosome assembly intermediates have yet been described. Reasons for this are technical difficulties in resolving assembly intermediates over their entire molecular mass range and in detecting low-abundance, short-living ribosomal precomplexes. Moreover, in analogy to the bacterial assembly process, several chloroplast ribosome assembly pathways might exist that run in parallel or are dynamically regulated during different plant developmental stages. Future work using a combination of Suc gradient experiments, mass spectrometry, and cryo-electron microscopy-based technologies (Davis et al., 2016) may provide a deeper understanding about the structure of chloroplast ribosome intermediates and the precise function of AtCGL20 in LSU assembly.

MATERIALS AND METHODS

Bioinformatics Sources

Arabidopsis (*Arabidopsis thaliana*) protein and gene sequences were downloaded from TAIR (<http://www.arabidopsis.org>), Phytozome (<https://phytozome.jgi.doe.gov/pz/portal.html>), and the National Center for Biotechnology Information (<http://www.ncbi.nlm.nih.gov/>). Protein sequence alignments were performed using the Vector NTI software (Invitrogen). Chloroplast transit peptides were predicted by ChloroP (<http://www.cbs.dtu.dk/services/ChloroP/>) and TargetP (<http://www.cbs.dtu.dk/services/TargetP/>). Information about sequences used in the alignment (Fig. 1) is listed in Supplemental Table S1. Alignments were formatted with Boxshade (http://www.ch.embnet.org/software/BOX_form.html). Coexpression analysis was carried out with the ATTED-II web server (<http://atted.jp/>; Obayashi et al., 2018). Enrichment analyses of differentially expressed genes and of proteins with altered abundance were carried out with MapMan (Thimm et al., 2004).

Plant Material and Growth Conditions

T-DNA insertion lines for *AT2G17240* (*atcgl20a*; SALK_133989) and *AT3G24506* (*atcgl20b*; SAIL_71_A01) were obtained from the SALK (Alonso et al., 2003) and SAIL (Sessions et al., 2002) collections, respectively. The double mutant *atcgl20ab* was generated by crossing the single mutant lines *atcgl20a* and *atcgl20b*. Plants were grown on potting soil (A210; Stender) under controlled greenhouse conditions (70–90 $\mu\text{E m}^{-2} \text{s}^{-1}$, 16/8-h light/dark cycles) or on a 12-h-light/12-h-dark cycle in climate chambers for biochemical and physiological analyses. Fertilizer was added to plants grown under greenhouse conditions in accordance with the supplier's recommendations (Osmocote Plus: 15% [w/v] nitrogen, 11% [w/v] P_2O_5 , 13% [w/v] K_2O , and 2% [w/v] MgO; Scotts Deutschland). Growth kinetics were analyzed on the basis of leaf area, which was determined from photographs taken at different times after germination (7–27 d) and quantified using the ImageJ software (Schneider et al., 2012). For cold-stress treatment, surface-sterilized mutant and wild-type seeds were plated on Murashige and Skoog (1962) medium (pH 5.8) supplemented with 0.7% (w/v) plant agar (Duchefa). Seeds were allowed to germinate at 4°C under long-day conditions (16 h of light/8 h of dark) in low light

(30 $\mu\text{E m}^{-2} \text{s}^{-1}$) for 6 weeks. Control plates were grown at 22°C under moderate light levels (100 $\mu\text{E m}^{-2} \text{s}^{-1}$).

To restore the wild-type phenotype, *AtCGL20A* and *AtCGL20B* coding regions were cloned into the binary Gateway vector pB7FWG2.0 (Karimi et al., 2002), placing the genes under the control of the 35S promoter and fused to the 5' end of the *EGFP* gene to generate *AtCGL20A-eGFP* and *AtCGL20B-eGFP* fusions. Both constructs were first transformed into *Agrobacterium tumefaciens* strain GV3101 and then into *atcgl20ab* plants by the floral dip method (Clough and Bent, 1998). T1 plants were selected using a stereomicroscope (Lumar.V12; Zeiss) based on a wild-type-like growth phenotype and high eGFP signals. After selection of homozygous progeny (annotated as *oeAtCGL20A-eGFP* and *oeAtCGL20B-eGFP*), complementation of the *atcgl20ab* mutant phenotype was verified by Dual-PAM analyses.

Leaf Pigment Analysis

Leaves were harvested from 5-week-old plants grown in climate chambers at 4 h after onset of the light period and homogenized in liquid nitrogen. The samples were extracted with 100% (v/v) acetone and centrifuged (16,000g) for 20 min at 4°C. Pigment compositions in the supernatants were analyzed as described by Färber et al. (1997).

Chlorophyll *a* Fluorescence and P_{700} Measurements

Chlorophyll *a* fluorescence and P_{700} measurements were performed using the DUAL-PAM-100 system (Walz) in the dual-channel measuring mode. After 5-week-old plants had been dark adapted for 20 min, single leaves were exposed to probe light to measure minimal chlorophyll fluorescence (F_0) and then to a saturating light pulse (10,000 $\mu\text{E m}^{-2} \text{s}^{-1}$, 800 ms) for determination of maximal chlorophyll fluorescence (F_m). After steady-state fluorescence yields (F_s) had been measured during a 10-min exposure to actinic red light (126 $\mu\text{E m}^{-2} \text{s}^{-1}$), a saturating light pulse (10,000 $\mu\text{E m}^{-2} \text{s}^{-1}$, 800 ms) was applied to determine the maximal fluorescence yield in the light (F_m'). F_m'' and F_0'' were measured by applying a saturating light pulse (10,000 $\mu\text{E m}^{-2} \text{s}^{-1}$, 800 ms) after a dark relaxation phase of 10 min. Parameters were calculated as described by Rühle et al. (2014). P_{700} measurements were carried out using the default settings of the DUAL-PAM software (version 1.19). The parameters $Y(I)$, $Y(ND)$, and $Y(NA)$ were calculated as described in the DUAL-PAM manual.

In vivo chlorophyll *a* fluorescence of whole plants was measured using an imaging chlorophyll fluorometer (Imaging PAM; Walz). Plants were dark adapted for 20 min and exposed to a pulsed, blue probe beam and a saturating light flash to calculate F_v/F_m . The postillumination rise in fluorescence was determined as previously described by Shikanai et al. (1998). A saturating light pulse was applied to determine F_m , which was followed by a 5-min exposure to actinic light (80 $\mu\text{E m}^{-2} \text{s}^{-1}$) and a dark incubation for 5 min to analyze the postillumination chlorophyll *a* fluorescence rise.

Confocal Laser Scanning Microscopy and Organelle Isolation

Protoplasts were isolated as described by Rühle et al. (2014) from 20-d-old *oeAtCGL20A-eGFP* and *oeAtCGL20B-eGFP* plants. Mitochondria were stained with MitoTracker Red (Thermo Scientific) according to the supplier's instructions. eGFP signals, MitoTracker, and chlorophyll autofluorescence were detected simultaneously with a Leica SP8 confocal microscope. Maximum projections of Z stacks were processed using the Lightning adaptive deconvolution approach. Chloroplast isolation was performed according to Kunst (1998). Intact chloroplasts were ruptured in a buffer containing 20 mM HEPES, pH 7.5 (KOH), and 10 mM EDTA for 30 min on ice. Soluble proteins were separated from the insoluble fraction by centrifugation (35,000g) for 30 min at 4°C. Mitochondria were isolated according to Escobar et al. (2006).

AtCGL20 Antibody Generation

Rabbit antibodies were raised against a synthesized peptide sequence (73-PLDFPIEWERPKEG-86) that is conserved in both AtCGL20 proteins. Peptide synthesis, immunization, and affinity purification were performed by Bio-Genes. Antiserum was employed in dilutions of 1:200 to 1:1,000.

Suc Step-Gradient Centrifugation

Suc step-gradient centrifugation was performed according to Rivera et al. (2015). Crude stroma was prepared from leaves of 20-d-old seedlings grown under climate-controlled chamber conditions. Plant material was first homogenized in chloroplast isolation buffer (330 mM D-sorbitol, 20 mM Tricine/NaOH, pH 7.6, 10 mM NaHCO₃, 0.1% [w/v] bovine serum albumin, and 0.03% [w/v] ascorbate). The homogenate was then filtered through two layers of Miracloth (Calbiochem) and centrifuged (2,000g) for 5 min at 4°C. The pellet was resuspended in chloroplast lysis buffer (10 mM Tris-HCl, pH 7.5, 10 mM MgOAc, 50 mM KCl, and 6 mM β-mercaptoethanol). After centrifugation (35,000g) for 30 min at 4°C, 500 μL of the supernatant (~1.5 mg total protein content) was layered onto 3 mL of a high-salt Suc solution (10 mM Tris-HCl, pH 7.5, 10 mM MgOAc, 150 mM KCl, 6 mM β-mercaptoethanol, and 1 M Suc). Samples were centrifuged for 12 h (55,000g) in a TL100.3 fixed-angle rotor. Seven fractions were recovered from the top, and the pellet was resuspended in 100 μL of the residual volume. Samples (20 μL) of each fraction were fractionated by Tricine-SDS-PAGE (Schägger, 2006) containing 10% (w/v) acrylamide, blotted, and probed with antibodies against AtCGL20, Rps1, Rpl2, and Cpn60α as described below (see Supplemental Table S13 for information on the latter antibodies).

Transcriptome Analysis

Total RNA was extracted from 4-week-old wild-type and 5-week-old *atcgl20ab* plants, grown under climate-controlled chamber conditions, using the RNeasy Mini Kit (Qiagen). RNA quality was tested by agarose gel electrophoresis. Additional quality checks, RNA sequencing library preparation, and long noncoding RNA sequencing were performed at Novogene Biotech using standard Illumina protocols. The RNA sequencing libraries were sequenced on an Illumina HiSeq 2500 system using the paired-end mode. Three biological replicates were used for each analysis. RNA sequencing reads were analyzed on the Galaxy platform (<https://usegalaxy.org/>). After grooming FASTQ files, adaptors were removed with Trimmomatic (Bolger et al., 2014) and sequencing quality was assessed with FastQC (<http://www.bioinformatics.babraham.ac.uk/projects/fastqc/>). Reads were mapped to the Arabidopsis genome (TAIR10) with the gapped-read mapper TopHat 2.1.1 (Kim et al., 2013) set for Forward Read unstranded libraries and adjusting the maximum intron length to 5,000 bp. Reads were counted with featureCounts (Liao et al., 2014) with the help of the gene annotation in Araport11 (www.araport.org/data/araport11). Differentially expressed genes were obtained with DESeq2 (Love et al., 2014) running with the fit type set to parametric and applying a 1.5-fold change cutoff and an adjusted $P < 0.05$. Sequencing data have been deposited in the National Center for Biotechnology Information's Gene Expression Omnibus (Edgar et al., 2002) and are accessible through GEO Series accession number GSE134415.

Proteome Analysis

Label-free shotgun proteomics was performed with the same plant material as was used for transcriptome analysis. Leaf samples (100 mg, five biological replicates per genotype) were snap frozen in liquid nitrogen and ground into fine powder. The powder was resuspended in 1 mL of extraction buffer (100 mM HEPES, pH 7.5, 150 mM NaCl, 10 mM dithiothreitol [DTT], 1% [w/v] SDS, and 1× Roche cOmplete Protease Inhibitor Cocktail), and samples were disrupted by sonication (three 10-s on/off cycles) with a Branson Sonifier B-12 (Branson Ultrasonics). After removing cell debris by centrifugation at 10,000g for 30 min, proteins were precipitated in chloroform-methanol (Wessel and Flügge, 1984) and solubilized in 6 M guanidine hydrochloride. Protein concentration was determined by the bicinchoninic assay (Thermo Fisher Scientific). Proteome aliquots (100 μg) were reduced in 10 mM DTT for 30 min at 37°C and alkylated with 50 mM iodoacetamide for 30 min at room temperature in the dark. After purification by chloroform-methanol precipitation, samples were digested with trypsin (protease:enzyme ratio of 100:1 [w/w]) at 37°C overnight. Peptides were desalted with homemade C18 stage tips (Rappsilber et al., 2003), vacuum dried until nearly dry, and stored at -80°C.

The peptide mixture was fractionated on a nano-liquid chromatography (LC) system (Ultimate 3000 RSLC; Thermo Fisher Scientific) equipped with an Acclaim Pepmap nano-trap column (C18, 100 Å, 100 μm × 2 cm; Thermo Fisher Scientific) and an Acclaim Pepmap RSLC analytical column (C18, 100 Å, 75 μm × 50 cm; Thermo Fisher Scientific). Chromatographic separation was carried out using a 150-min linear gradient of 5% to 45% acetonitrile at a flow rate of 250 nL min⁻¹. The column temperature was set to 50°C. An Impact II high-resolution quadrupole time-of-flight device (Bruker Daltonics) was directly

coupled to the LC device using a CaptiveSpray nano-electrospray ionization source (Bruker Daltonics). MS1 spectra were acquired at 3 Hz with a mass range from mass-to-charge ratio 200 to 2,000, with the 18 most intense peaks being selected for tandem mass spectrometry (MS/MS) analysis using an intensity-dependent spectrum acquisition time of between 4 and 16 Hz. The dynamic exclusion duration was set to 0.5 min.

The MaxQuant software (version 1.6.1.0; Cox and Mann, 2008) was used to process the raw MS files. The built-in Andromeda search engine (Cox et al., 2011) was employed to search MS/MS spectra against the Arabidopsis UniProt database (version February 2017). Enzyme specificity was set to trypsin, allowing up to two missed cleavages. Cys carbamidomethylation was set as static modification, and N-terminal acetylation and Met oxidation were set as variable modifications. During the search, sequences of 248 common contaminant proteins and decoy sequences were automatically added. A false discovery rate of 1% was applied at the peptide and protein levels. Proteins were quantified across samples using the label-free quantification algorithm (Cox et al., 2014) with default settings. Downstream bioinformatics and statistical analyses were performed using Perseus (version 1.6.1.1; Tyanova et al., 2016) and R (version 3.5.0; R Core Team, 2018). Potential contaminants, reverse hits, and proteins identified only by site modification were excluded from further analysis. Protein groups were retained if they had been quantified in at least three of the five total replicates in at least one genotype. Protein label-free quantification intensities were log₂ transformed, and missing values were imputed from a normal distribution within Perseus. The resulting matrix was exported, and data were quantile normalized using the R/Bioconductor package Process (Bolstad, 2018). Protein groups with statistically significant differential abundances were determined employing the R/Bioconductor package limma (Ritchie et al., 2015), with P values that were adjusted for multiple comparisons according to the approach of Benjamini and Hochberg (1995). Proteins with a log₂(ratio) relative to the wild-type (Col-0) larger than 0.59 and with false discovery rate-adjusted $P < 0.05$ were considered to be significantly changed. The MS proteomics data have been deposited with the ProteomeXchange consortium via the PRIDE partner repository (Vizcaino et al., 2014) with the data set identifier PXD014514 and can be accessed during reviewing at www.ebi.ac.uk/pride/ with the following username and password: reviewer25980@ebi.ac.uk and kW0erj7.

Nucleic Acid Analysis

Arabidopsis DNA was isolated from 3-week-old leaves as described by Ihnatowicz et al. (2004). The T-DNA insertion sites in *atcgl20a* and *atcgl20b* were determined by PCR using combinations of insertion- and gene-specific primers (Supplemental Table S12), which were also employed for screening of homozygous double mutants.

Total RNA was extracted from snap-frozen leaves with the TRIzol reagent (Invitrogen) according to the supplier's instructions. RNA for reverse transcription quantitative PCR analysis was isolated using the RNeasy Mini Kit (Qiagen). Arabidopsis cDNA was synthesized with the iScript cDNA synthesis kit (Bio-Rad). The reaction mixtures contained iQ SYBR Green Supermix (Bio-Rad), cDNA as template, and gene-specific primers. Levels of the *ACT8* actin gene (*AT1G49240*) transcript served as a reference. DNA amplification was monitored on the basis of the SYBR Green fluorescence signal in an IQ5 Multicolor Real Time PCR Detection system (Bio-Rad). Levels of gene expression were calculated using the standard-curve method implemented in the IQ5 Optical System software.

RNA gel-blot hybridizations were performed under stringent conditions according to standard protocols (Sambrook and Russell, 2001). Samples equivalent to 1 to 5 μg of total RNA were fractionated by electrophoresis on formaldehyde-containing agarose gels (1.2% [w/v]), blotted onto nylon membranes (Hybond-N+; Amersham Bioscience), and fixed by UV irradiation (Stratalkiner UV Crosslinker 1800). To control for equal loading, abundant RNAs on nylon membranes were stained with Methylene Blue solution (0.02% [w/v] Methylene Blue and 0.3 M sodium acetate, pH 5.5). To detect gene- and rRNA-specific transcripts, amplified DNA fragments from cDNA templates were labeled with radioactive [α -³²P]dCTP and subsequently used as probes in hybridization experiments (see Supplemental Table S12 for primer information). Signals were detected with the Typhoon Phosphor Imager System (GE Healthcare). Polysome-associated mRNAs were isolated as described before (Barkan, 1993).

Microfluidics-based quantification of rRNA species was carried out in initial quality-control experiments for RNA sequencing at Novogene Biotech using an Agilent 2100 Bioanalyzer (Agilent) system. Ratios of rRNA species were

calculated from three biological replicates of Col-0 and *atcgl20ab* as described previously (Walter et al., 2010; Tiller et al., 2012).

In Vivo Translation Assay

In vivo incorporation of [³⁵S]Met was performed according to Meurer et al. (2017). Col-0 and *atcgl20ab* were either grown under climate-controlled chamber conditions for 20 d or shifted to 4°C conditions for 7 d prior to the experiment. Plant material (200 mg) was incubated for 30 min in labeling buffer (1 mM KH₂PO₄/K₂HPO₄, pH 6.3, 20 μg mL⁻¹ cycloheximide, and 0.1% [w/v] Tween 20). [³⁵S]Met was added and plants were vacuum infiltrated. Samples were exposed to 50 μmol photons m⁻² s⁻¹ for 40 min at room temperature. Plants were washed three times in labeling buffer and snap frozen. Whole-protein extract was isolated from ground tissue by resuspension in loading buffer (see below). Samples were adjusted according to equal fresh weight and subjected to Tricine-SDS-PAGE. Gels were stained with Coomassie Brilliant Blue G-250, and signals were detected with the Typhoon Phosphor Imager System (GE Healthcare).

Protein Analysis

Leaves from 5-week-old plants grown under climate-controlled chamber conditions were harvested 4 h after the onset of the light period and directly homogenized in loading buffer (100 mM Tris-HCl, pH 6.8, 50 mM DTT, 8% [w/v] SDS, 24% [w/v] glycerol, and 0.02% [w/v] Bromophenol Blue). Denaturation for 5 min at 70°C and protein fractionation on Tricine-SDS-PAGE gels (10% gels) were carried out according to Schagger (2006).

Sample preparation for BN-PAGE was performed as described by Peng et al. (2008) using freshly prepared thylakoids. BN-PAGE gels (4%–12% gradient) were prepared as described by Schagger et al. (1994). Solubilized samples corresponding to 80 μg of chlorophyll were loaded per lane, and gels were run at 4°C overnight. To separate complexes into their subunits, strips of the BN-polyacrylamide gel were treated with denaturing buffer (0.2 M Na₂CO₃, 5% [w/v] SDS, and 50 mM DTT) for 30 min at room temperature and layered on 10% Tricine-SDS-PAGE gels. In the case of stromal extract analyses, chloroplast-enriched pellets were resuspended directly in BN washing buffer (25 mM Bis-Tris-HCl, pH 7, and 20% [w/v] glycerol) and passed 20 times through a 0.45-mm syringe to mechanically disrupt intact chloroplasts. The supernatant was separated from the membranous pellet by centrifugation at 35,000g. Protein concentration was determined using the Bradford Protein Assay (Bio-Rad). RNase A (Qiagen) was added (one-tenth of total protein content) to isolated stroma and incubated for 15 min at room temperature. BN sample buffer (one-tenth of sample volume, 100 mM Bis-Tris-HCl, pH 7, 750 mM aminocaproic acid, and 5% [w/v] Coomassie Brilliant Blue G-250) was added to the supernatant, and samples (150 μg of total protein content) were separated on 4% to 12% BN gradient gels (Schagger et al., 1994). Isolated mitochondria equivalent to 150 μg of total protein content were solubilized in BN washing buffer containing 1.5% (w/v) *n*-dodecyl-β-maltoside. After centrifugation (35,000g for 30 min at 4°C), BN sample buffer (one-tenth of sample volume) was added and mitochondrial complexes were separated on 5% to 12% BN gradient gels. Second-dimension electrophoresis was performed as described earlier.

Proteins fractionated by gel electrophoresis were transferred to PVDF membranes (Immobilon-P; Millipore) using a semidry blotting system (Bio-Rad) as described in the supplier's instructions. After blocking with 10 mM Tris-HCl, pH 8, 150 mM NaCl, and 0.1% [v/v] Tween 20 supplemented with 3% (w/v) skim milk powder, the membranes were first incubated with primary antibodies at 4°C overnight and then with secondary antibodies for 2 to 3 h. Signals were detected by enhanced chemiluminescence (Pierce, Thermo Scientific) using an enhanced chemiluminescence reader system (Fusion FX7; PeqLab). Antibodies used in this study are listed in Supplemental Table S13.

Proteome Analysis of the HMM Fraction in the Chloroplast Stroma

Stroma fractions of three biological replicates of Col-0 and *atcgl20ab* plants were isolated from 20-d-old plants as described earlier and subjected to Suc step-gradient centrifugation with 50 mM KCl (instead of 150 mM) in the cushion. The protein concentration of the last fraction was appropriately adjusted with chloroplast lysis buffer. Aliquots (30 μg) of protein were reduced, alkylated, and digested with trypsin (0.4 μg) as described above. Peptides were desalted with homemade C18 stage tips, vacuum dried to near dryness, and stored at –80°C. LC-MS/MS and data analysis were performed as described above.

Suc Density-Gradient Centrifugation

Crude stromal extracts were prepared as described above. Chloroplast-enriched pellets were resuspended in chloroplast lysis buffer (10 mM Tris-HCl, pH 7.5, 50 mM KCl, 1 mM MgOAc, and 6 mM β-mercaptoethanol). After centrifugation (35,000g) for 30 min at 4°C, 500 μL of the supernatant (~2 mg of total protein content) was layered onto a continuous (10%–40%) Suc gradient (2 mL) prepared in lysis buffer. The gradients were centrifuged at 45,000 rpm (~273,000g) in an SW60 Ti rotor (Beckman Coulter) for 3 h at 4°C. Samples were separated into 38 fractions, subjected to 10% Tricine-SDS-PAGE, blotted, and probed with antibodies against AtCGL20, Rps1, Rpl2, and GFP.

Accession Numbers

Sequence data from this article can be found in the GenBank/EMBL data libraries under the accession numbers listed in Supplemental Table S1.

Supplemental Data

The following supplemental materials are available.

Supplemental Figure S1. Cold treatment, complementation, and NDH activity analyses of *atcgl20* mutants.

Supplemental Figure S2. Graphical illustration of MapMan enrichment analyses.

Supplemental Figure S3. BN/SDS-PAGE analysis of mitochondrial and thylakoid complexes.

Supplemental Table S1. CGL20 homologs in the green lineage.

Supplemental Table S2. Pigment analysis.

Supplemental Table S3. Transcriptomic analysis (RNA sequencing) of wild-type and *atcgl20ab* plants.

Supplemental Table S4. Shotgun proteome analysis of wild-type and *atcgl20ab* plants.

Supplemental Table S5. Combined proteome and transcriptome data.

Supplemental Table S6. MapMan pathway analysis of the *atcgl20ab* transcriptome.

Supplemental Table S7. MapMan pathway analysis of the *atcgl20ab* proteome.

Supplemental Table S8. AtCGL20A coexpression analysis.

Supplemental Table S9. Quantification of processed 23S rRNA products in the wild type and *atcgl20ab*.

Supplemental Table S10. Proteome analysis of the HMM fraction in the chloroplast stroma of the wild type and *atcgl20ab*.

Supplemental Table S11. MapMan pathway analysis of the HMM proteome in the chloroplast stroma of the wild type and *atcgl20ab*.

Supplemental Table S12. Primers used in this study.

Supplemental Table S13. Antibodies used in this study.

ACKNOWLEDGMENTS

We thank Daniel Smeets and Alexander Fahrner for their excellent support in confocal fluorescence imaging as well as Paul Hardy for critical reading of the article. Furthermore, we thank Toshiharu Shikanai for providing antibodies against NdhH and NdhL, Jörg Meurer for the antibody against AtpF, and David Stern for the antibody against Csp41b.

Received December 5, 2019; accepted December 22, 2019; published January 14, 2020.

LITERATURE CITED

Ahmed T, Yin Z, Bhushan S (2016) Cryo-EM structure of the large subunit of the spinach chloroplast ribosome. *Sci Rep* 6: 35793

- Alonso JM, Stepanova AN, Leisse TJ, Kim CJ, Chen H, Shinn P, Stevenson DK, Zimmerman J, Barajas P, Cheuk R, et al (2003) Genome-wide insertional mutagenesis of *Arabidopsis thaliana*. *Science* **301**: 653–657
- Armbruster U, Rühle T, Kreller R, Strotbek C, Zühlke J, Tadini L, Blunder T, Hertle AP, Qi Y, Rengstl B, et al (2013) The photosynthesis affected mutant68-like protein evolved from a PSII assembly factor to mediate assembly of the chloroplast NAD(P)H dehydrogenase complex in *Arabidopsis*. *Plant Cell* **25**: 3926–3943
- Barkan A (1993) Nuclear mutants of maize with defects in chloroplast polysome assembly have altered chloroplast RNA metabolism. *Plant Cell* **5**: 389–402
- Baudisch B, Langner U, Garz I, Klösgen RB (2014) The exception proves the rule? Dual targeting of nuclear-encoded proteins into endosymbiotic organelles. *New Phytol* **201**: 80–90
- Bayer RG, Stael S, Csaszar E, Teige M (2011) Mining the soluble chloroplast proteome by affinity chromatography. *Proteomics* **11**: 1287–1299
- Bellaoui M, Keddie JS, Grissem W (2003) DCL is a plant-specific protein required for plastid ribosomal RNA processing and embryo development. *Plant Mol Biol* **53**: 531–543
- Benjamini Y, Hochberg Y (1995) Controlling the false discovery rate: A practical and powerful approach to multiple testing. *J R Stat Soc B* **57**: 289–300
- Bieri P, Leibundgut M, Saurer M, Boehringer D, Ban N (2017) The complete structure of the chloroplast 70S ribosome in complex with translation factor pY. *EMBO J* **36**: 475–486
- Bohne AV (2014) The nucleoid as a site of rRNA processing and ribosome assembly. *Front Plant Sci* **5**: 257
- Bolger AM, Lohse M, Usadel B (2014) Trimmomatic: A flexible trimmer for Illumina sequence data. *Bioinformatics* **30**: 2114–2120
- Bolle C, Huep G, Kleinbölting N, Haberer G, Mayer K, Leister D, Weisshaar B (2013) GABI-DUPLO: A collection of double mutants to overcome genetic redundancy in *Arabidopsis thaliana*. *Plant J* **75**: 157–171
- Bolstad B (2018) preprocessCore: A collection of pre-processing functions. R package version 1.42.0. <https://github.com/bmbolstad/preprocessCore>
- Bučinská L, Kiss É, Koník P, Knoppová J, Komenda J, Sobotka R (2018) The ribosome-bound protein Pam68 promotes insertion of chlorophyll into the CP47 subunit of photosystem II. *Plant Physiol* **176**: 2931–2942
- Carrie C, Small I (2013) A reevaluation of dual-targeting of proteins to mitochondria and chloroplasts. *Biochim Biophys Acta* **1833**: 253–259
- Chi W, He B, Mao J, Li Q, Ma J, Ji D, Zou M, Zhang L (2012) The function of RH22, a DEAD RNA helicase, in the biogenesis of the 50S ribosomal subunits of *Arabidopsis* chloroplasts. *Plant Physiol* **158**: 693–707
- Clough SJ, Bent AF (1998) Floral dip: A simplified method for *Agrobacterium*-mediated transformation of *Arabidopsis thaliana*. *Plant J* **16**: 735–743
- Cox J, Hein MY, Lubner CA, Paron I, Nagaraj N, Mann M (2014) Accurate proteome-wide label-free quantification by delayed normalization and maximal peptide ratio extraction, termed MaxLFQ. *Mol Cell Proteomics* **13**: 2513–2526
- Cox J, Mann M (2008) MaxQuant enables high peptide identification rates, individualized p.p.b.-range mass accuracies and proteome-wide protein quantification. *Nat Biotechnol* **26**: 1367–1372
- Cox J, Neuhauser N, Michalski A, Scheltema RA, Olsen JV, Mann M (2011) Andromeda: A peptide search engine integrated into the MaxQuant environment. *J Proteome Res* **10**: 1794–1805
- Davis JH, Tan YZ, Carragher B, Potter CS, Lyumkis D, Williamson JR (2016) Modular assembly of the bacterial large ribosomal subunit. *Cell* **167**: 1610–1622
- Davis JH, Williamson JR (2017) Structure and dynamics of bacterial ribosome biogenesis. *Philos Trans R Soc Lond B Biol Sci* **372**: 20160181
- Edgar R, Domrachev M, Lash AE (2002) Gene Expression Omnibus: NCBI gene expression and hybridization array data repository. *Nucleic Acids Res* **30**: 207–210
- Escobar MA, Geisler DA, Rasmusson AG (2006) Reorganization of the alternative pathways of the *Arabidopsis* respiratory chain by nitrogen supply: Opposing effects of ammonium and nitrate. *Plant J* **45**: 775–788
- Färber A, Young AJ, Ruban AV, Horton P, Jahns P (1997) Dynamics of xanthophyll-cycle activity in different antenna subcomplexes in the photosynthetic membranes of higher plants (The relationship between zeaxanthin conversion and nonphotochemical fluorescence quenching). *Plant Physiol* **115**: 1609–1618
- Fristedt R, Scharff LB, Clarke CA, Wang Q, Lin C, Merchant SS, Bock R (2014) RBF1, a plant homolog of the bacterial ribosome-binding factor RbfA, acts in processing of the chloroplast 16S ribosomal RNA. *Plant Physiol* **164**: 201–215
- Germain A, Hottel AM, Barkan A, Stern DB (2013) RNA processing and decay in plastids. *Wiley Interdiscip Rev RNA* **4**: 295–316
- Graf M, Arenz S, Huter P, Dönhöfer A, Nováček J, Wilson DN (2017) Cryo-EM structure of the spinach chloroplast ribosome reveals the location of plastid-specific ribosomal proteins and extensions. *Nucleic Acids Res* **45**: 2887–2896
- Grossman AR, Karpowicz SJ, Heinnickel M, Dewez D, Hamel B, Dent R, Niyogi KK, Johnson X, Alric J, Wollman FA, et al (2010) Phylogenomic analysis of the *Chlamydomonas* genome unmasks proteins potentially involved in photosynthetic function and regulation. *Photosynth Res* **106**: 3–17
- Ihnatowicz A, Pesaresi P, Varotto C, Richly E, Schneider A, Jahns P, Salamini F, Leister D (2004) Mutants for photosystem I subunit D of *Arabidopsis thaliana*: Effects on photosynthesis, photosystem I stability and expression of nuclear genes for chloroplast functions. *Plant J* **37**: 839–852
- Janowski M, Zoschke R, Scharff LB, Martinez Jaime S, Ferrari C, Proost S, Ng Wei Xiong J, Omranian N, Musialak-Lange M, Nikoloski Z, et al (2018) AtKsgA from *Arabidopsis thaliana* is important for maturation of the small subunit of the chloroplast ribosome. *Plant J* **96**: 404–420
- Jeon Y, Ahn HK, Kang YW, Pai HS (2017) Functional characterization of chloroplast-targeted RbgA GTPase in higher plants. *Plant Mol Biol* **95**: 463–479
- Karimi M, Inzé D, Depicker A (2002) GATEWAY vectors for *Agrobacterium*-mediated plant transformation. *Trends Plant Sci* **7**: 193–195
- Karpowicz SJ, Prochnik SE, Grossman AR, Merchant SS (2011) The GreenCut2 resource, a phylogenomically derived inventory of proteins specific to the plant lineage. *J Biol Chem* **286**: 21427–21439
- Keus RJA, Dekker AF, Kreuk KCJ, Groot GSP (1984) Transcription of ribosomal DNA in chloroplasts of *Spirodela oligorhiza*. *Curr Genet* **9**: 91–97
- Kim D, Perte G, Trapnell C, Pimentel H, Kelley R, Salzberg SL (2013) TopHat2: Accurate alignment of transcriptomes in the presence of insertions, deletions and gene fusions. *Genome Biol* **14**: R36
- Kim J, Rudella A, Ramirez Rodriguez V, Zybailov B, Olinares PDB, van Wijk KJ (2009) Subunits of the plastid ClpPR protease complex have differential contributions to embryogenesis, plastid biogenesis, and plant development in *Arabidopsis*. *Plant Cell* **21**: 1669–1692
- Kmiec B, Teixeira PF, Glaser E (2014) Phenotypical consequences of expressing the dually targeted presequence protease, AtPreP, exclusively in mitochondria. *Biochimie* **100**: 167–170
- Kössel H, Natt E, Strittmatter G, Fritzche E, Gozdzička-Jozefiak A, Przybyl D (1985) Structure and expression of rRNA operons from plastids of higher plants. In L van Vloten-Doting, G Groot, and T Hall, eds, *Molecular Form and Function of the Plant Genome*. Plenum Publishing, New York, pp 183–198
- Koussevitzky S, Stanne TM, Peto CA, Giap T, Sjögren LLE, Zhao Y, Clarke AK, Chory J (2007) An *Arabidopsis thaliana* virescent mutant reveals a role for ClpR1 in plastid development. *Plant Mol Biol* **63**: 85–96
- Kunst L (1998) Preparation of physiologically active chloroplasts from *Arabidopsis*. *Methods Mol Biol* **82**: 43–48
- Leal-Klevezas DS, Martínez-Soriano JP, Nazar RN (2000) Transcription and processing map of the 4.5S-5S rRNA intergenic region (ITS3) from rapeseed (*Brassica napus*) chloroplasts. *Plant Cell Rep* **19**: 667–673
- Leister D (2003) Chloroplast research in the genomic age. *Trends Genet* **19**: 47–56
- Liao Y, Smyth GK, Shi W (2014) featureCounts: An efficient general purpose program for assigning sequence reads to genomic features. *Bioinformatics* **30**: 923–930
- Liu J, Zhou W, Liu G, Yang C, Sun Y, Wu W, Cao S, Wang C, Hai G, Wang Z, et al (2015) The conserved endoribonuclease YbeY is required for chloroplast ribosomal RNA processing in *Arabidopsis*. *Plant Physiol* **168**: 205–221
- Love MI, Huber W, Anders S (2014) Moderated estimation of fold change and dispersion for RNA-seq data with DESeq2. *Genome Biol* **15**: 550

- Majeran W, Friso G, Asakura Y, Qu X, Huang M, Ponnala L, Watkins KP, Barkan A, van Wijk KJ (2012) Nucleoid-enriched proteomes in developing plastids and chloroplasts from maize leaves: A new conceptual framework for nucleoid functions. *Plant Physiol* **158**: 156–189
- Mazzoleni M, Figuet S, Martin-Laffon J, Mininno M, Gilgen A, Leroux M, Brugière S, Tardif M, Alban C, Ravanel S (2015) Dual targeting of the protein methyltransferase PrmA contributes to both chloroplastic and mitochondrial ribosomal protein L11 methylation in Arabidopsis. *Plant Cell Physiol* **56**: 1697–1710
- Merchant SS, Prochnik SE, Vallon O, Harris EH, Karpowicz SJ, Witman GB, Terry A, Salamov A, Fritz-Laylin LK, Maréchal-Drouard L, et al (2007) The *Chlamydomonas* genome reveals the evolution of key animal and plant functions. *Science* **318**: 245–250
- Meurer J, Schmid LM, Stoppel R, Leister D, Brachmann A, Manavski N (2017) PALE CRESS binds to plastid RNAs and facilitates the biogenesis of the 50S ribosomal subunit. *Plant J* **92**: 400–413
- Miller OL Jr., Hamkalo BA, Thomas CA Jr. (1970) Visualization of bacterial genes in action. *Science* **169**: 392–395
- Mitschke J, Fuss J, Blum T, Höglund A, Reski R, Kohlbacher O, Rensing SA (2009) Prediction of dual protein targeting to plant organelles. *New Phytol* **183**: 224–235
- Mulder AM, Yoshioka C, Beck AH, Bunner AE, Milligan RA, Potter CS, Carragher B, Williamson JR (2010) Visualizing ribosome biogenesis: Parallel assembly pathways for the 30S subunit. *Science* **330**: 673–677
- Munekage Y, Takeda S, Endo T, Jahns P, Hashimoto T, Shikanai T (2001) Cytochrome *b₆f* mutation specifically affects thermal dissipation of absorbed light energy in Arabidopsis. *Plant J* **28**: 351–359
- Murashige T, Skoog F (1962) A revised medium for rapid growth and bioassays with tobacco tissue cultures. *Physiol Plant* **15**: 473–497
- Narsai R, Law SR, Carrie C, Xu L, Whelan J (2011) In-depth temporal transcriptome profiling reveals a crucial developmental switch with roles for RNA processing and organelle metabolism that are essential for germination in Arabidopsis. *Plant Physiol* **157**: 1342–1362
- Nishimura K, Ashida H, Ogawa T, Yokota A (2010) A DEAD box protein is required for formation of a hidden break in Arabidopsis chloroplast 23S rRNA. *Plant J* **63**: 766–777
- Obayashi T, Aoki Y, Tadaka S, Kagaya Y, Kinoshita K (2018) ATTED-II in 2018: A plant coexpression database based on investigation of the statistical property of the mutual rank index. *Plant Cell Physiol* **59**: e3
- Paieri F, Tadini L, Manavski N, Kleine T, Ferrari R, Morandini P, Pesaresi P, Meurer J, Leister D (2018) The DEAD-box RNA helicase RH50 is a 23S-4.5S rRNA maturation factor that functionally overlaps with the plastid signaling factor GUN1. *Plant Physiol* **176**: 634–648
- Peng L, Shimizu H, Shikanai T (2008) The chloroplast NAD(P)H dehydrogenase complex interacts with photosystem I in Arabidopsis. *J Biol Chem* **283**: 34873–34879
- Perez Boerema A, Aibara S, Paul B, Tobiasson V, Kimanius D, Forsberg BO, Wallden K, Lindahl E, Amunts A (2018) Structure of the chloroplast ribosome with chl-RRF and hibernation-promoting factor. *Nat Plants* **4**: 212–217
- Pesaresi P, Varotto C, Meurer J, Jahns P, Salamini F, Leister D (2001) Knock-out of the plastid ribosomal protein L11 in Arabidopsis: Effects on mRNA translation and photosynthesis. *Plant J* **27**: 179–189
- Pfannschmidt T, Blanvillain R, Merendino L, Courtois F, Chevalier F, Liebers M, Grübler B, Hommel E, Lerbs-Mache S (2015) Plastid RNA polymerases: Orchestration of enzymes with different evolutionary origins controls chloroplast biogenesis during the plant life cycle. *J Exp Bot* **66**: 6957–6973
- Pulido P, Zagari N, Manavski N, Gawronski P, Matthes A, Scharff LB, Meurer J, Leister D (2018) CHLOROPLAST RIBOSOME ASSOCIATED supports translation under stress and interacts with the ribosomal 30S subunit. *Plant Physiol* **177**: 1539–1554
- R Core Team (2018) R: A language and environment for statistical computing. R Foundation for Statistical Computing. <https://www.R-project.org/> (June 28, 2018)
- Rappsilber J, Ishihama Y, Mann M (2003) Stop and go extraction tips for matrix-assisted laser desorption/ionization, nanoelectrospray, and LC/MS sample pretreatment in proteomics. *Anal Chem* **75**: 663–670
- Ritchie ME, Phipson B, Wu D, Hu Y, Law CW, Shi W, Smyth GK (2015) limma powers differential expression analyses for RNA-sequencing and microarray studies. *Nucleic Acids Res* **43**: e47
- Rivera MC, Maguire B, Lake JA (2015) Isolation of ribosomes and polyosomes. *Cold Spring Harb Protoc* **2015**: 293–299
- Rödiger A, Baudisch B, Langner U, Klösgen RB (2011) Dual targeting of a mitochondrial protein: The case study of cytochrome c1. *Mol Plant* **4**: 679–687
- Rühle T, Razeghi JA, Vamvaka E, Viola S, Gandini C, Kleine T, Schünemann D, Barbato R, Jahns P, Leister D (2014) The Arabidopsis protein CONSERVED ONLY IN THE GREEN LINEAGE160 promotes the assembly of the membranous part of the chloroplast ATP synthase. *Plant Physiol* **165**: 207–226
- Sambrook J, Russell DW (2001) Molecular Cloning: A Laboratory Manual. Ed 3. Cold Spring Harbor Laboratory Press, Cold Spring Harbor, NY
- Schägger H (2006) Tricine-SDS-PAGE. *Nat Protoc* **1**: 16–22
- Schägger H, Cramer WA, von Jagow G (1994) Analysis of molecular masses and oligomeric states of protein complexes by blue native electrophoresis and isolation of membrane protein complexes by two-dimensional native electrophoresis. *Anal Biochem* **217**: 220–230
- Schneider CA, Rasband WS, Eliceiri KW (2012) NIH Image to ImageJ: 25 years of image analysis. *Nat Methods* **9**: 671–675
- Sessions A, Burke E, Presting G, Aux G, McElver J, Patton D, Dietrich B, Ho P, Bacwaden J, Ko C, et al (2002) A high-throughput Arabidopsis reverse genetics system. *Plant Cell* **14**: 2985–2994
- Shajani Z, Sykes MT, Williamson JR (2011) Assembly of bacterial ribosomes. *Annu Rev Biochem* **80**: 501–526
- Sharma M, Bennewitz B, Klösgen RB (2018) Rather rule than exception? How to evaluate the relevance of dual protein targeting to mitochondria and chloroplasts. *Photosynth Res* **138**: 335–343
- Sharma MR, Dönhöfer A, Barat C, Marquez V, Datta PP, Fucini P, Wilson DN, Agrawal RK (2010) PSRP1 is not a ribosomal protein, but a ribosome-binding factor that is recycled by the ribosome-recycling factor (RRF) and elongation factor G (EF-G). *J Biol Chem* **285**: 4006–4014
- Shikanai T, Endo T, Hashimoto T, Yamada Y, Asada K, Yokota A (1998) Directed disruption of the tobacco *ndhB* gene impairs cyclic electron flow around photosystem I. *Proc Natl Acad Sci USA* **95**: 9705–9709
- Sugimoto H, Kusumi K, Tozawa Y, Yazaki J, Kishimoto N, Kikuchi S, Iba K (2004) The *virescent-2* mutation inhibits translation of plastid transcripts for the plastid genetic system at an early stage of chloroplast differentiation. *Plant Cell Physiol* **45**: 985–996
- Sun Y, Zerges W (2015) Translational regulation in chloroplasts for development and homeostasis. *Biochim Biophys Acta* **1847**: 809–820
- Sundby C, McCaffery S, Anderson JM (1993) Turnover of the photosystem II D1 protein in higher plants under photoinhibitory and non-photoinhibitory irradiance. *J Biol Chem* **268**: 25476–25482
- Terashima M, Specht M, Hippler M (2011) The chloroplast proteome: A survey from the *Chlamydomonas reinhardtii* perspective with a focus on distinctive features. *Curr Genet* **57**: 151–168
- Thimm O, Bläsing O, Gibon Y, Nagel A, Meyer S, Krüger P, Selbig J, Müller LA, Rhee SY, Stitt M (2004) MAPMAN: A user-driven tool to display genomics data sets onto diagrams of metabolic pathways and other biological processes. *Plant J* **37**: 914–939
- Tiller N, Bock R (2014) The translational apparatus of plastids and its role in plant development. *Mol Plant* **7**: 1105–1120
- Tiller N, Weingartner M, Thiele W, Maximova E, Schöttler MA, Bock R (2012) The plastid-specific ribosomal proteins of *Arabidopsis thaliana* can be divided into non-essential proteins and genuine ribosomal proteins. *Plant J* **69**: 302–316
- Tillich M, Hardel SL, Kupsch C, Armbruster U, Delannoy E, Gualberto JM, Lehwark P, Leister D, Small ID, Schmitz-Linneweber C (2009) Chloroplast ribonucleoprotein CP31A is required for editing and stability of specific chloroplast mRNAs. *Proc Natl Acad Sci USA* **106**: 6002–6007
- Tyanova S, Temu T, Sinitcyn P, Carlson A, Hein MY, Geiger T, Mann M, Cox J (2016) The Perseus computational platform for comprehensive analysis of (prote)omics data. *Nat Methods* **13**: 731–740
- Vizcaíno JA, Deutsch EW, Wang R, Csordas A, Reisinger F, Ríos D, Dienes JA, Sun Z, Farrah T, Bandeira N, et al (2014) ProteomeXchange provides globally coordinated proteomics data submission and dissemination. *Nat Biotechnol* **32**: 223–226
- Walter M, Piepenburg K, Schöttler MA, Petersen K, Kahlau S, Tiller N, Drechsel O, Weingartner M, Kudla J, Bock R (2010) Knockout of the plastid RNase E leads to defective RNA processing and chloroplast ribosome deficiency. *Plant J* **64**: 851–863
- Wang Y, Wang C, Zheng M, Lyu J, Xu Y, Li X, Niu M, Long W, Wang D, Wang H, et al (2016) WHITE PANICLE1, a Val-tRNA synthetase

- regulating chloroplast ribosome biogenesis in rice, is essential for early chloroplast development. *Plant Physiol* **170**: 2110–2123
- Wessel D, Flügge UI** (1984) A method for the quantitative recovery of protein in dilute solution in the presence of detergents and lipids. *Anal Biochem* **138**: 141–143
- Williams PM, Barkan A** (2003) A chloroplast-localized PPR protein required for plastid ribosome accumulation. *Plant J* **36**: 675–686
- Yamaguchi K, Subramanian AR** (2000) The plastid ribosomal proteins: Identification of all the proteins in the 50 S subunit of an organelle ribosome (chloroplast). *J Biol Chem* **275**: 28466–28482
- Yamaguchi K, Subramanian AR** (2003) Proteomic identification of all plastid-specific ribosomal proteins in higher plant chloroplast 30S ribosomal subunit. *Eur J Biochem* **270**: 190–205
- Yamaguchi K, von Knoblauch K, Subramanian AR** (2000) The plastid ribosomal proteins: Identification of all the proteins in the 30 S subunit of an organelle ribosome (chloroplast). *J Biol Chem* **275**: 28455–28465
- Yamazaki H, Tasaka M, Shikanai T** (2004) PPR motifs of the nucleus-encoded factor, PGR3, function in the selective and distinct steps of chloroplast gene expression in Arabidopsis. *Plant J* **38**: 152–163
- Yu F, Liu X, Alsheikh M, Park S, Rodermeil S** (2008) Mutations in *SUPPRESSOR OF VARIEGATION1*, a factor required for normal chloroplast translation, suppress *var2*-mediated leaf variegation in Arabidopsis. *Plant Cell* **20**: 1786–1804
- Zoschke R, Bock R** (2018) Chloroplast translation: Structural and functional organization, operational control, and regulation. *Plant Cell* **30**: 745–770

5 Chlorophyll fluorescence video imaging: A versatile tool for identifying factors related to photosynthesis

Rühle T, **Reiter B**, Leister D (2018) Chlorophyll fluorescence video imaging: A versatile tool for identifying factors related to photosynthesis. *Front Plant Sci* **9**: 55

DOI: <https://doi.org/10.3389/fpls.2018.00055>



Chlorophyll Fluorescence Video Imaging: A Versatile Tool for Identifying Factors Related to Photosynthesis

Thilo Rühle*, Bennet Reiter and Dario Leister

Plant Molecular Biology, Department of Biology, Ludwig Maximilian University of Munich, Munich, Germany

OPEN ACCESS

Edited by:

Juliette Jouhet,
UMR5168 Laboratoire de Physiologie
Cellulaire Végétale (LPCV), France

Reviewed by:

Dimitris Petroustos,
Univ. Grenoble Alpes, CNRS, CEA,
INRA, BIG-LPCV, Grenoble, France
Katarzyna Glowacka,
University of Illinois
at Urbana-Champaign, United States

*Correspondence:

Thilo Rühle
thilo.ruehle@biologie.
uni-muenchen.de;
thiloruehle@hotmail.com

Specialty section:

This article was submitted to
Plant Physiology,
a section of the journal
Frontiers in Plant Science

Received: 26 October 2017

Accepted: 10 January 2018

Published: 30 January 2018

Citation:

Rühle T, Reiter B and Leister D
(2018) Chlorophyll Fluorescence
Video Imaging: A Versatile Tool
for Identifying Factors Related
to Photosynthesis.
Front. Plant Sci. 9:55.
doi: 10.3389/fpls.2018.00055

Measurements of chlorophyll fluorescence provide an elegant and non-invasive means of probing the dynamics of photosynthesis. Advances in video imaging of chlorophyll fluorescence have now made it possible to study photosynthesis at all levels from individual cells to entire crop populations. Since the technology delivers quantitative data, is easily scaled up and can be readily combined with other approaches, it has become a powerful phenotyping tool for the identification of factors relevant to photosynthesis. Here, we review genetic chlorophyll fluorescence-based screens of libraries of *Arabidopsis* and *Chlamydomonas* mutants, discuss its application to high-throughput phenotyping in quantitative genetics and highlight potential future developments.

Keywords: photosynthesis, *Arabidopsis*, *Chlamydomonas*, chloroplast, screening, chlorophyll fluorescence, forward genetic screen, reverse genetic screen

INTRODUCTION

Since the discovery of the rapid fluorescence transient associated with the initial exposure of dark-adapted leaves to light (the Kautsky effect) in 1931, chlorophyll (Chl) fluorescence has emerged as an indispensable probe in photosynthesis research. There are several reasons for this remarkable development: (i) measurements of Chl fluorescence dynamics can be carried out on intact plants or algal cell cultures in an essentially non-invasive manner, (ii) multiple quantitative photosynthetic parameters can be extracted in short measuring times, (iii) Chl fluorescence measurements can be easily combined with other analytical tools, (iv) instrumentation capable of automated quantification and analysis of Chl fluorescence is now commercially available to a broad range of plant scientists and the technique is no longer restricted to a small group of experts, (v) technical advances achieved in recent decades now permit investigations from the single-cell level (Oxborough and Baker, 1997; Küpper et al., 2000; Tseng and Chu, 2017) to crop plants in the field (Virlet et al., 2017), and open up numerous applications, such as the use of Chl fluorescence-derived parameters as indicators of abiotic (Baker, 2008; Rungrat et al., 2016) or biotic stress (reviewed in: Chaerle et al., 2009). A particularly important technological breakthrough in this field was the development of video imaging systems (Omasa et al., 1987; Fenton and Crofts, 1990), which not only paved the way for the examination of the spatial heterogeneity within a sample, but also made it possible to assess large numbers of samples (e.g., individual plants or cell colonies) in a

single experimental run. Thus, Chl fluorescence video imaging (CFVI) can be regarded as an ideal phenotyping technology for the identification of mutants affected in photosynthesis.

In the following, we will give an overview of CFVI-based screens which have been carried out on plant and green algal mutant libraries in the past, discuss recent progress and consider how the technology may be further developed in the future. Technical and theoretical aspects of Chl fluorescence imaging have been described in detail in Nedbal and Whitmarsh (2004), as well as in Oxborough (2004). The interested reader is also referred to several excellent review articles for introductions to the biophysical basis and biochemical implications of Chl fluorescence-derived photosynthetic parameters (Maxwell and Johnson, 2000; Roháček, 2002; Baker, 2008; Kalaji et al., 2017).

In brief, a typical state-of-the-art CFVI analysis is based on the application of pulse-amplitude-modulated (PAM), measuring light (ML), which is generated by a powerful array of LEDs placed in a defined working distance to the sample. Those LEDs can also serve for the generation of short saturation pulses (SPs) and for actinic illumination (AL) of the samples to drive photosynthesis. Emitted red Chl fluorescence is detected by a computer-connected charge-coupled device (CCD) video camera which is protected from excitation light or near-infrared radiation by appropriate color glass filters. Custom software allows the conversion of Chl fluorescence signals into false color images, calculation of different photosynthetic parameters and quantitative analyses of the results. In general, plant or algal samples are dark-adapted prior to the measurements to open all PSII reaction centers. Then, samples are exposed to ML for dark fluorescence yield (F_0) determination and to a short SP for maximum fluorescence yield (F_m) measurement, respectively (see also **Figure 1A**). In this state, the PSII quantum yield (F_v/F_m) is maximal and can be calculated according to the equation $F_v/F_m = (F_m - F_0)/F_m$. AL is switched on and application of SPs provides maximum fluorescence yields (F_m') of illuminated samples. Effective PSII quantum yields (Φ_{II}) are calculated by the equation $\Phi_{II} = (F_m' - F)/F_m'$ (Genty et al., 1989), whereas the fluorescence yield (F) is recorded every time shortly before a SP and represents an average of several current fluorescence yield (F_t) pictures. Electron transport rates through PSII [ETR(II)] at a given photosynthetically active radiation (PAR) can be calculated according to Schreiber et al. (1995), using the equation $ETR(II) = \Phi_{II} \times PAR \times 0.84 \times 0.5$. Maximum ETR(II) measured at saturating light intensity provides an estimate of the maximum photosynthesis rate (P_{max}). F_m' values of illuminated samples are in general lowered compared to F_m by non-photochemical quenching (NPQ), which can be quantified according to the equation $NPQ = (F_m - F_m')/F_m'$ (Bilger and Björkman, 1990). NPQ mechanisms can be further examined in dark relaxation experiments. To this end, actinic light is switched off after a period of actinic light exposure and minimum fluorescence (F_0'') and maximum fluorescence yields (F_m'') are determined by application of SPs in the dark relaxation phase (**Figure 1A**). The two NPQ components qE (ΔpH -dependent feedback de-excitation, the major component of

NPQ), and qI (photo-inhibitory quenching) can be calculated according to the equations $qE = F_m/F_m' - F_m/F_m''$ (Thiele et al., 1997) and $qI = (F_v - F_v'')/F_v$ (Björkman and Demmig, 1987).

Chl FLUORESCENCE VIDEO IMAGING IN FORWARD GENETIC APPROACHES

Screens for Chlamydomonas and Arabidopsis Mutants Defective in Photochemical Quenching

The first instance of the successful use of Chl fluorescence imaging to identify photosynthetic mutants was the detection of a '*high-chlorophyll-fluorescence*' (*hcf*) phenotype in a population of methyl-methane sulfonate-mutagenized *Chlamydomonas reinhardtii* cells by Bennoun and Levine (1967) (**Table 1**). The screen was based on the fact that severe perturbations in photosynthetic electron transport, such as those caused by incubating algal cells in the presence of the photosynthetic electron transport inhibitor 3-(3,4-dichlorophenyl)-1,1-dimethylurea (DCMU), lead to high steady-state levels of Chl fluorescence. Following its application for screening of *Chlamydomonas* mutant libraries (see for example Harris, 1989) the concept was tested in higher plants (Miles and Daniel, 1973) and employed for the screening of maize (Miles and Daniel, 1974; Barkan et al., 1986; Taylor et al., 1987) and *Arabidopsis* mutant libraries (Dinkins et al., 1994; Meurer et al., 1996b). Several factors involved in chloroplast biogenesis were identified using the *hcf* phenotyping method, including the maize proteins HCF106, HCF60, and HCF136 (reviewed in: Belcher et al., 2015) and the *Arabidopsis* proteins HCF5 (Dinkins et al., 1997), HCF101 (Lezhneva et al., 2004), HCF107 (Felder et al., 2001), HCF109 (Meurer et al., 1996a), HCF145 (Lezhneva and Meurer, 2004; Manavski et al., 2015), HCF152 (Meierhoff et al., 2003) and LPA1 (Peng et al., 2006).

Even though such *hcf* mutant screens can be performed rapidly and efficiently, and have significantly enhanced our knowledge of the molecular repertoire required for photosynthesis and chloroplast biogenesis, only mutants with severe defects can be unequivocally detected, and these are often lethal under photoautotrophic conditions. However, technological progress in Chl fluorescence analyses during the 1980s and 1990s allowed the technique to be employed for more elaborate modes of screening, and led to the identification of algal or plant mutants with relatively modest alterations in photosynthetic performance. For example, Varotto et al. (2000a,b) identified '*photosynthesis affected mutants*' (*pam*) in *Arabidopsis* on the basis of their lower effective quantum yields (Φ_{II}) (Genty et al., 1989) using a combination of a pulse-amplitude-modulation fluorometer (Schreiber et al., 1986) and an automated screening system. This set-up facilitated the screening of large *En* transposon or T-DNA mutagenized *Arabidopsis* populations, and *pam* mutants disrupted in the nucleus-encoded photosystem I subunits PsaE1 (*pam4*) (Varotto et al., 2000b) and PsaD1 (*pam62*)

TABLE 1 | Chronology of Chl fluorescence phenotyping based gene discovery studies.

Phenotype/principle	Organism	Authors
<i>hcf</i>	Chlamydomonas	Bennoun and Levine, 1967
<i>hcf</i>	Maize	Miles and Daniel, 1974
<i>hcf</i>	Maize	Barkan et al., 1986
<i>hcf</i>	Maize	Taylor et al., 1987
<i>hcf</i>	Arabidopsis	Dinkins et al., 1994
<i>hcf</i>	Arabidopsis	Meurer et al., 1996b
Low NPQ after high light treatment	Chlamydomonas	Niyogi et al., 1997
Low NPQ after high light treatment	Arabidopsis	Niyogi et al., 1998
Deficiency in state transition	Chlamydomonas	Fleischmann et al., 1999
Deficiency in state transition	Chlamydomonas	Kruse et al., 1999
Low NPQ after high light treatment	Arabidopsis	Shikanai et al., 1999
Alterations in Φ_{II}	Arabidopsis	Varotto et al., 2000a
Lack of NDH complex activity	Arabidopsis	Hashimoto et al., 2003
Identification of mutants with unchanged Φ_{II} after acclimation to high light	Arabidopsis	Walters et al., 2003
Low NPQ after high light treatment	Arabidopsis	Kalituho et al., 2006
<i>hcf</i>	Arabidopsis	Peng et al., 2006
Identification of photorespiration mutants by comparison of F_v/F_m values under varying CO_2 concentrations	Arabidopsis	Badger et al., 2009
Identification of NDH complex mutants in a guilt-by-association approach	Arabidopsis	Takabayashi et al., 2009
Quantitative genetic analysis of thermal dissipation	Arabidopsis	Jung and Niyogi, 2009
Identification of CEF mutants with a high qE	Arabidopsis	Livingston et al., 2010
Affected Chl fluorescence transients	Chlamydomonas	Houille-Vernes et al., 2011
Affected Chl fluorescence transients	Chlamydomonas	Tolletier et al., 2011
Identification of hydrogenase-deficient mutants using Φ_{II} measurements under anaerobiosis	Chlamydomonas	Godaux et al., 2013
Suppressor screen of mutants with a high NPQ in the absence of PsbS	Arabidopsis	Brooks et al., 2013
Identification of mutants with altered mitochondrial respiration using F_v/F_m measurements	Chlamydomonas	Massoz et al., 2015
Quantitative genetic analysis of variations in Φ_{II} acclimation to irradiance changes in different natural Arabidopsis accessions	Arabidopsis	van Rooijen et al., 2015
High transient NPQ after a dark-light shift	Arabidopsis	Zhang et al., 2016
Identification of mutants with emergent photosynthetic phenotypes under dynamic environmental conditions	Arabidopsis	Cruz et al., 2016
Identification of mitochondrial complex I mutants in a Φ_{II} -based screening of a mutagenized <i>pgr1</i> library	Chlamydomonas	Massoz et al., 2017
Identification of mutants affected in the slowly reversible photoprotective form of NPQ termed qH	Arabidopsis	Malnoë et al., 2017

hcf, high chlorophyll fluorescence; NPQ, non-photochemical quenching; Φ_{II} , effective quantum yield of PSII; NDH complex, NADH dehydrogenase-like complex; F_v/F_m , maximal quantum yield of PSII; qE, energy-dependent quenching; CEF, cyclic electron flow.

(Ihnatowicz et al., 2004), the metal-ion transporter IRT1 (*pam25*) (Varotto et al., 2002), and the cytoplasmic *N*-acetyltransferase AtMAK3 (*pam21*) (Pesaresi et al., 2003), as well as the PSII assembly factor PAM68 (*pam68*) (Armbruster et al., 2010), were isolated and functionally characterized in subsequent studies.

Screens for Chlamydomonas and Arabidopsis Mutants Affected in Non-Photochemical Quenching (NPQ)

Due to their sessile lifestyle, many multicellular photosynthetic organisms have evolved various strategies to cope with light stress (Ort, 2001). When the photosynthetic machinery is exposed to excessively high levels of light, short- and long-term adaptive responses are triggered at the molecular level, which allow for the thermal dissipation of excited energy by NPQ mechanisms to prevent over-reduction of the electron transport chain. At least

four processes contribute to NPQ: qE (zeaxanthin-dependent quenching), qT (state-transition-dependent quenching) and qI (reviewed in: Ruban, 2016). Several CFVI-based screens have been performed on mutagenized Chlamydomonas and Arabidopsis populations with the aim of dissecting the genetics of NPQ (Table 1). Mutant identification was essentially based on the comparison of two video images of Chl fluorescence captured under different illumination conditions. The first picture was taken in the dark-adapted state during a saturating light pulse (F_m), or shortly after the onset of high-light treatment (F). The second image was recorded after several minutes of exposure to high light either during a saturating light pulse (F_m') or not (F'). The NPQ values derived using the equation $(F - F')/F'$ or $(F_m - F_m')/F_m'$ were then visualized as false-color images, and several Chlamydomonas and Arabidopsis mutants affected in NPQ of excited Chl states could be identified. Subsequent analyses revealed three distinct groups of mutants with aberrant

NPQ (reviewed in: Golan et al., 2004). Mutants in the first group were impaired in the generation of a proton gradient across the thylakoid membrane, which is a prerequisite for the induction of qE (the Δ pH-dependent quenching component of NPQ), and were consequently defined as ‘*proton gradient regulation*’ mutants (*pgr*). One such mutant, *pgr1*, was further characterized, and shown to be defective in the photosynthetic electron transfer C (*PETC*) gene, which encodes the Rieske subunit of the cytochrome *b₆f* complex (Munekage et al., 2001). Another mutant line impaired in the build-up of the proton gradient is *pgr5* (Shikanai et al., 1999; Munekage et al., 2002). It lacks a component of the antimycin A-sensitive cyclic electron flow (CEF) pathway, which is mediated by the ferredoxin-plastoquinone reductase *PGRL1/PGR5* (Hertle et al., 2013). The second group with aberrant NPQ comprised the mutants *npq1* and *npq2*, which display defects in the xanthophyll cycle and are disrupted in the violaxanthin de-epoxidase and zeaxanthin epoxidase, respectively (Niyogi et al., 1997). The third type of mutant (*npq4*) showed normal pigment composition, xanthophyll cycle activity and photosynthetic electron transport, but this mutant was nevertheless specifically affected at the level of qE (Li et al., 2000). It turned out that the *npq4* mutant lacks the PSII-associated protein S (PsbS), which is now known to be the luminal pH sensor that triggers NPQ within the PSII antenna in plants (Li et al., 2000). In a subsequent study, which was designed to isolate Arabidopsis lines affected in other slowly reversible NPQ components, CFVI was used to screen mutagenized seedlings for suppressors of the *npq4* phenotype (Brooks et al., 2013). This screen yielded the *suppressor of quenching 1* (*soq1*), which has a high NPQ even in the absence of PsbS and lacks a thylakoid membrane protein (SOQ1) that harbors a thioredoxin-like, a β -propeller and a haloacid-dehalogenase domain. SOQ1 maintains light-harvesting efficiency and prevents formation of a slow, reversible NPQ mechanism that is independent of qE, qZ, and qT, but participates in a photoprotective, ‘qI-like’ mechanism termed qH (Malnoë et al., 2017). To identify factors involved in qH, suppressors of *soq1 npq4* were screened for by CFVI and two mutants affected either in chlorophyllide *a* oxygenase (CAO) or the plastid lipocalin (LCNP) showed a reversion to the low NPQ phenotype of *npq4*. In-depth analyses of both mutants provided evidence that qH operates under high-light and cold stress, and can be localized to the peripheral LHCII antenna of PSII and requires LCNP (Malnoë et al., 2017).

A further step toward an understanding of the molecular basis of NPQ was the identification of so-called ‘*state transition*’ (*stt*) mutants with alterations in qT. State transitions involve the reversible association of the mobile pool of light-harvesting-complex II proteins (LHCIIIs) with either PSII (state 1) or PSI (state 2) and re-establish a balanced distribution of light energy between the photosystems. Several studies (Fleischmann et al., 1999; Kruse et al., 1999) took advantage of the fact that the green alga *Chlamydomonas* undergoes large changes in Chl fluorescence during state transitions, which can be attributed to its significantly higher fraction of mobile LHCIIIs (about 80%, Delosme et al., 1996) compared to land plants (15–20%) (Allen, 1992). Mutants affected in state transitions were identified by

comparing fluorescence images taken under state-1 and state-2 conditions, and this type of differential fluorescence screen enabled Fleischmann et al. (1999) to isolate four *stt* mutants (*stt2*, *stt3*, *stt5*, and *stt7*). These mutants were characterized by high Chl fluorescence levels at room temperature even under state-2 conditions, indicating that they were physiologically locked in state 1. Further analyses showed that *stt7* lacks the thylakoid serine-threonine protein kinase Stt7, which is required for phosphorylation of LHCII in response to state-2 conditions (Depège et al., 2003).

Screening for Chlororespiratory Arabidopsis Mutants

In addition to the predominant linear electron flow pathway, which results in the production of both NADPH and ATP, two CEF routes around PSI have been described that are important for balancing the ATP/NADPH budget of photosynthesis, as well as for protecting the photosystems from photodamage in plants (reviewed in: Yamori and Shikanai, 2016). One of these pathways is mediated by the NADH-like dehydrogenase (NDH) complex, which is also responsible for chlororespiration in the dark. To identify ‘*chlororespiratory reduction*’ mutants (*crr*) which are disrupted in NDH function, Hashimoto et al. (2003) established a CFVI-based screening system, in which the post-illumination rise of Chl fluorescence (PIF) after a low-light treatment was monitored in an Arabidopsis mutant population. Under such conditions, the fluorescence signal is almost proportional to the reduction state of the plastoquinone pool (Krause and Weis, 1991), so that the chlororespiratory activity of the NDH complex can be derived from the degree to which the PIF is depressed in mutants with a dysfunctional NDH complex (Shikanai et al., 1998). Screening of over 50,000 M2 seedlings for aberrant PIFs led to the identification of 17 *crr* mutants in Arabidopsis. These could be assigned to at least 11 loci, and further analyses revealed the existence of novel NDH subunits and allowed the functional characterization of factors required for efficient NDH complex biogenesis (reviewed in: Peng et al., 2011).

Screening for Arabidopsis Mutants Affected in Acclimation of Photosynthesis to the Environment

Plants and algae can undergo photosynthetic acclimation processes which take place over periods of hours or days and entail substantial changes in plastid and nuclear gene expression, as well as adjustments of the photosynthetic apparatus. For instance, the long-term response to high light levels has been thoroughly studied and, instead of reducing the demands on light harvesting, it actually enhances the capacity for electron transport and carbon dioxide fixation. To investigate the molecular mechanisms behind the signal cascades that activate the acclimation response to high light, Walters et al. (2003) screened an Arabidopsis mutant population for alterations in ‘*acclimation of photosynthesis to the environment*’ (*ape*). Their CFVI screen was based on the observation that in wild-type Arabidopsis plants a 3-day exposure to high light raises effective quantum yields (Φ_{II}), and its goal was to

identify mutants that were unable to increase P_{\max} under these conditions. Among the three *ape* mutants obtained, which showed distinct acclimation-defective phenotypes, *ape2* exhibited a lower P_{\max} under all light regimes, and was disrupted in the chloroplast envelope triose-phosphate/phosphate translocator (TPT). Subsequent studies using Arabidopsis double and triple mutants altered in the day and night modes of photoassimilate export from the chloroplast provided evidence that carbohydrates act as chloroplast-to-nucleus retrograde signals and modulate the acclimation response to high light (Schmitz et al., 2012, 2014).

Screening for Arabidopsis Mutants Affected in Photorespiration

Ribulose-1,5-bisphosphate carboxylase/oxygenase (RuBisCO) not only fixes atmospheric CO_2 but also oxygen. The phosphoglycolate generated by the latter reaction must be degraded via a complex mechanism which is known as photorespiration, because CO_2 is released during the process. The photorespiratory pathway is distributed between four compartments (chloroplasts, cytosol, peroxisomes and mitochondria) and requires the action of several transporters and enzymes. Most of the early mutants affected in photorespiration were identified by their ability to grow normally in a high concentration (1%) of CO_2 , while becoming chlorotic when shifted to ambient air (Somerville, 1986). Recently, it was shown that mutations in components involved in the photorespiratory pathway also impair photosynthetic light reactions, as revealed by the observation that photorespiratory mutants transferred from high to ambient CO_2 concentrations showed a decline in PSII functionality (Takahashi et al., 2007). Thus, Badger et al. (2009) set up a CFVI screen designed to detect mutants with more subtle photorespiratory phenotypes. To this end, levels of PSII function in mutagenized Arabidopsis seedlings grown under high concentrations of CO_2 , and in its absence, were compared. Two major mutant phenotype classes could be distinguished. One group comprised 'photorespiration-like' mutants, which were characterized by F_v/F_m values that were close to those of wild-type plants under high CO_2 concentrations, but significantly lower than normal in the absence of CO_2 . The second group consisted of lines in which F_v/F_m values were depressed even under high concentrations of CO_2 . Remarkably, some members of the second group were able to partially recover PSII functionality after exposure to zero CO_2 concentrations, and were therefore named for this 'reverse photorespiration' phenotype (Badger et al., 2009).

Screening for Chlamydomonas Mutants Impaired in Hydrogenase Activity

As aquatic organisms, many unicellular green algae are characterized by a remarkably flexible metabolism, and can acclimate rapidly to anaerobic conditions (Terashima et al., 2010; Grossman et al., 2011). As part of an extensive response to anaerobiosis, expression and synthesis of oxygen-labile [Fe-Fe] hydrogenases are induced in *C. reinhardtii* and hydrogen production is linked to photosynthesis by ferredoxin-mediated electron supply. Several factors required for expression,

maturation and activity of [Fe-Fe] hydrogenases have been identified, most of them through a H_2 -sensing, chemochromic screening system that can discriminate *Chlamydomonas* mutants with aberrant H_2 production capacities (reviewed in: Hemschemeier et al., 2009). An alternative, less time-consuming approach has been demonstrated by Godaux et al. (2013), and takes advantage of the observation that mutants with defects in [Fe-Fe] hydrogenase activity exhibit low effective PSII quantum yields shortly after a shift from dark anaerobiosis to saturating light conditions. As a proof of concept, screening of a small *Chlamydomonas* population of about 3000 strains generated by insertional mutagenesis yielded five mutants with a Chl fluorescence signature similar to that of the [Fe-Fe] hydrogenase-deficient control strain, and one of them turned out to be defective in the previously characterized [Fe-Fe] hydrogenase assembly factor G (HydG) (Posewitz et al., 2004). Moreover, in various mutants affected in anaerobic energy metabolism, the effective quantum yield of PSII was shown to be correlated with the level of [Fe-Fe] hydrogenase activity. Thus, the screening system represents a time-saving, alternative approach to the chemochromic method, and is capable of detecting mutants impaired in [Fe-Fe] hydrogenase biogenesis, regulation or activity.

Screening for Chlamydomonas Mutants Altered in Mitochondrial Respiration

Although respiration and photosynthesis take place in different organelles in photosynthetic eukaryotes, the energy metabolisms of mitochondria and chloroplasts are intertwined at multiple levels. Not only do these organelles share over 100 dual-targeted proteins (reviewed in: Carrie and Small, 2013), provide both ATP and contribute to photorespiration, chloroplasts can shuttle reducing power to mitochondria via the malate valve (reviewed in: Scheibe, 2004; Kramer and Evans, 2011). Functional cooperation between mitochondria and chloroplasts in balancing the cellular ATP/NADPH ratio becomes even more obvious when compensatory acclimation processes are studied in mutants affected in photosynthesis or respiration. For instance, in *Chlamydomonas* mutants defective in different complexes of the respiratory electron transport chain, the resulting ATP deficiency is counterbalanced by increased non-photochemical reduction of the plastoquinone pool mediated by the chlororespiratory pathway, LHCII protein association to PSI and cyclic photophosphorylation (Cardol et al., 2003). Furthermore, the *Chlamydomonas* strain *pgrl1* disrupted in the proton regulation 5 like 1 protein (PGRL1), which was identified as a CEF mutant in CFVI-based screen (Tolte et al., 2011), compensates for ATP deficiency by increasing oxygen photoreduction downstream of PSI and shows higher susceptibility to mitochondrial inhibitors (Dang et al., 2014). These results are consistent with the finding that overall fitness and yields of photosynthesis were only significantly reduced when state transitions and mitochondrial respiration were concomitantly impaired in the *Chlamydomonas* double mutant *stt7-9 dum22* (Cardol et al., 2009). Thus, increased cyclic electron transport rates induced by state 2 transitions can supply extra ATP when respiratory ATP production becomes

limiting and, conversely, mitochondrial cooperation is increased when CEF is downregulated in *Chlamydomonas*. One important conclusion that could be drawn from these studies was that PSII efficiencies were reduced in respiratory mutants and was explained by enhanced rates of non-photochemical reduction of plastoquinone mediated by the chlororespiratory pathway and preferential association of LHCII proteins with PSI (Cardol et al., 2003). Massoz et al. (2015) therefore used F_v/F_m values as an initial criterion to select mutants affected in mitochondrial respiration. Several mutants disrupted in subunits of the respiratory complex I or the isocitrate lyase were isolated from a collection of about 2900 insertional mutants generated in either a wild-type or a state transition-defective strain (*stt7-9*). A later refinement of the screening procedure used the CEF mutant *pgrl1* as the starting strain with a view to isolating mutants impaired in mitochondrial complex I (Massoz et al., 2017). As proof of concept, the double mutant *pgrl1Δnd4*, which is deficient in both CEF and complex I, was generated and shown to exhibit a lower PSII efficiency than either of the single mutants. Subsequent screening of about 3000 insertional mutants created in the *pgrl1* background resulted in 46 mutants with reduced PSII efficiency, of which three were complex I mutants. Further analyses revealed that one of these was disrupted in NADH dehydrogenase [ubiquinone] 1 alpha subcomplex assembly factor 3 (NDUFAF3), a complex I assembly factor also conserved in humans (Massoz et al., 2017).

Chl FLUORESCENCE VIDEO IMAGING IN REVERSE GENETIC APPROACHES

Forward genetic approaches still dominated mutant searches in the late 1990s and early 2000s (Lloyd and Meinke, 2012), but thanks to advances in genome sequencing technologies, the establishment of large mutant libraries and the development of new genetic tools such as RNA silencing techniques (Mohr et al., 2014), and more recently genome editing tools (Yin et al., 2017), reverse genetics has since come to the fore. Indeed, in conjunction with the tremendous rise in the availability of myriad ‘omics’ datasets, reverse genetic strategies have become the more practicable choice, since laborious screens of large mutant libraries are circumvented and the underlying genetic defects are already known. Relative to classical forward genetic approaches, reverse genetic screens start with a significantly reduced number of lines or strains, which are generally disrupted in genes with poorly characterized or unknown functions. Depending on the stringency of preselection criteria (e.g., coregulation or phylogenomic studies), ‘the starting material’ can be narrowed down to a reasonable number of candidates which is compatible with the complexity of the required screening procedure. One example for the power of such ‘guilt-by-association’ approaches is the identification of three subunits of the NDH complex – NDF1, NDF2, and NDF4 (Takabayashi et al., 2009) now called photosynthetic NDH subcomplex B subunit PnsB1, PnsB2, and PnsB3 (Ifuku et al., 2011). In that study, genes of unknown function were selected on the basis of their co-expression with

nucleus-encoded NDH subunits L, N, and O (NDHL, NDHN, and NDHO). In addition, Arabidopsis genes (of unknown function) were considered together with homologs found in cyanobacteria but not in green algae, since *C. reinhardtii* lacks a plant-type NDH complex. Insertion lines were identified for 21 of the 36 genes pre-selected by means of the bioinformatics screen, and these were tested for NDH activity. Remarkably, four of them (nearly 20%) failed to exhibit the post-illumination rise in fluorescence. Further studies provided evidence that the respective genes indeed code for the NDH subunits NDF1 (PnsB1), NDF2 (PnsB2), and NDF4 (PnsB3), whereas NDF3 corresponds to the chlororespiratory reduction protein 6 (CRR6), which is involved in NDH subcomplex A assembly (Munshi et al., 2006).

Chl Fluorescence Image Analyses in Combined Screening Protocols

Since Chl fluorescence-based phenotyping is no longer as time-consuming as it once was, and manageable numbers of candidates can be examined in reverse genetics projects, contemporary screening approaches can be extended to more elaborate protocols in which subtle or multiple photosynthetic phenotypes can be detected in a single, albeit longer, experimental run. Commercial Chl video imaging systems now make it possible to set up automated measuring routines composed of several analytical blocks that can last for days. One example of such a combined screening protocol is shown in **Figure 1**, which we use routinely for initial phenotyping of selected Arabidopsis mutant lines.

In principle, the approach comprises six phases, in which most of the previously described Chl fluorescence signatures of photosynthetic mutants can be identified (**Figure 1A**). In the first block, the F_v/F_m measurement allows one to assess PSII functionality and pinpoint mutants with an *hcf* phenotype, such as the Arabidopsis PSII subunit O (PsbO) knockdown mutant *psbO1 psbO2* (**Figure 1B**) (Steinberger et al., 2015). The second analytical block was designed to identify mutant lines with a *crr* phenotype, and detects NDH activity by means of a PIF measurement (**Figure 1C**). Block 3 implements a standard slow induction experiment, which is carried out under moderate actinic light intensities. Several informative parameters can be extracted in block 3 which reveal aspects of the transient dynamics of photosynthesis upon a dark-light shift. For instance, *pgr* mutants can be already identified at this stage by their low transient NPQ phenotype (DalCorso et al., 2008). Conversely, mutants affected in chloroplast F_1F_0 -ATP synthase activity can be identified on the basis of their high NPQ (**Figure 1D**) (Rühle et al., 2014; Grahl et al., 2016; Zhang et al., 2016). The increased NPQ in such mutants can be attributed to a high operating qE, which is established as a result of proton accumulation in the thylakoid lumen already under moderate light intensities. Parameters determined at the end of block 3 reflect photosynthetic performance in the steady state, and an analysis of effective quantum yields (Φ_{II}) uncovers *pam* mutants (**Figure 1E**). Samples in block 4 are shifted back into the dark and NPQ relaxation kinetics provide values of qI

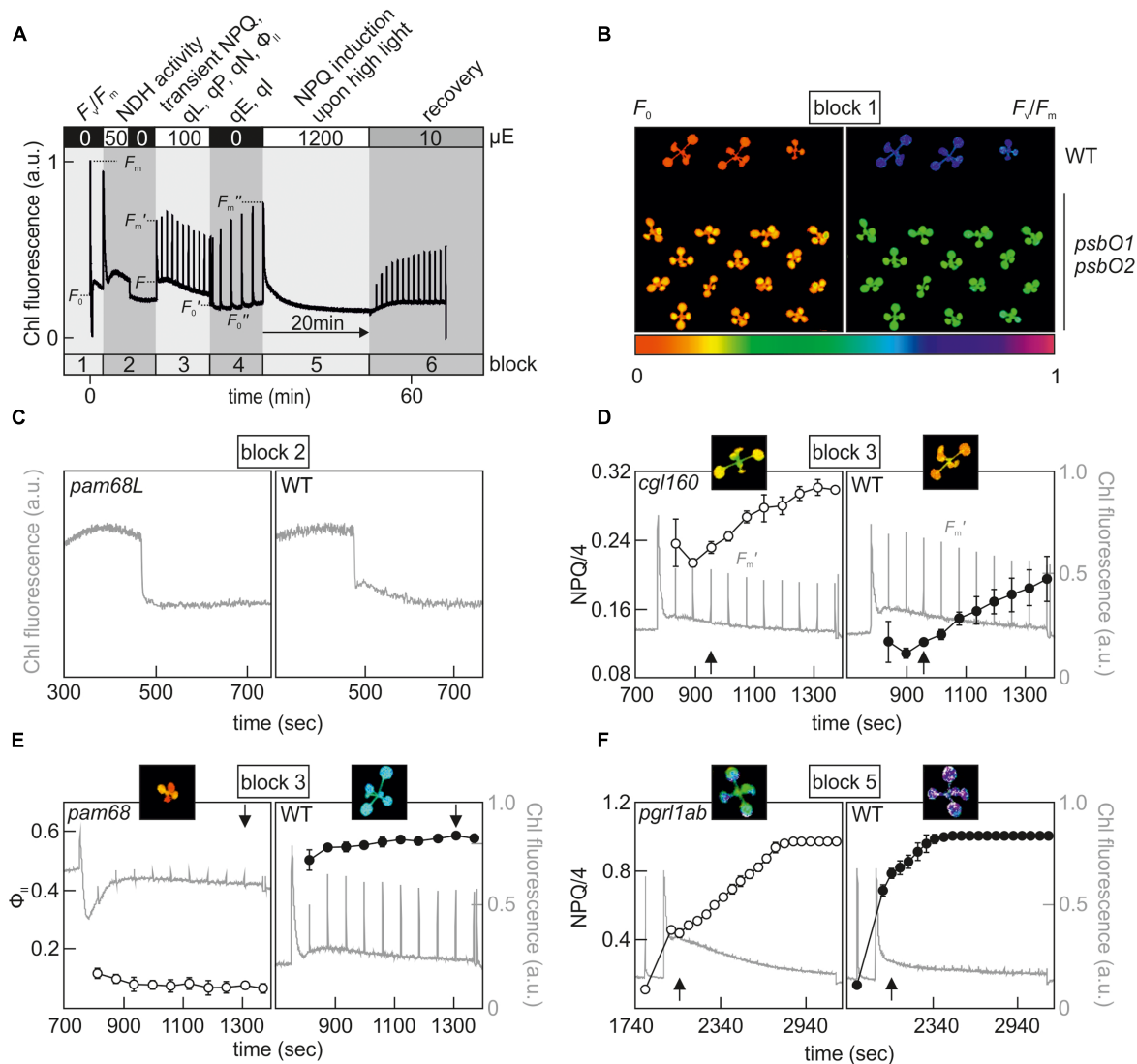


FIGURE 1 | Example of a combined screening protocol based on Chl fluorescence video imaging which is able to identify *hcf*, *crr*, *npq*, *pam* and PSII repair mutants. **(A)** Chl fluorescence was monitored using an Imaging PAM system (Walz®) and the indicated sequence of actinic light conditions was executed in series to determine, in a single experimental run, the various photosynthetic parameters listed at the top. Plants were dark-adapted for 20 min and acclimated to measuring light for 5 min prior to the analysis. For further explanations, see the main text. F_0/F_m , maximum quantum yield of PSII; NPQ, non-photochemical quenching; q_L , fraction of open PSII centers; q_P , photochemical quenching coefficient; q_N non-photochemical quenching coefficient; Φ_{II} , effective quantum yield of PSII; q_E , energy-dependent quenching; q_I , photo-inhibitory quenching. **(B)** Example of an *hcf* mutant phenotype, which can be detected in measurement block 1. F_0 and F_v/F_m images of wild-type and *psbO1 psbO2* (Steinberger et al., 2015) Arabidopsis plants. **(C)** Identification of a *crr* mutant phenotype in block 2. Detail of the post-illumination fluorescence rise (PIF) analysis of *pam68L* (Armbruster et al., 2013), which is disrupted in NDH complex assembly. **(D)** Detection of a high NPQ phenotype in block 3. F_m' values were recorded every minute by applying saturating light pulses after a dark-light transition ($100 \mu\text{E m}^{-2} \text{s}^{-1}$) and calculated NPQ values of the chloroplast ATP synthase-deficient mutant *cgl160* (Rühle et al., 2014) were compared to a wild-type control. **(E)** Example of a *pam* mutant phenotype, which can be distinguished at the end of block 3. Φ_{II} values of the PSII assembly mutant *pam68* (Armbruster et al., 2010) were compared to a wild-type control. **(F)** Detection of an *npq* phenotype in measurement block 5. NPQ analyses were carried out with the CEF mutant *pgr1ab* (DalCorso et al., 2008) and compared to a wild-type control. False-color images for F_0 , F_v/F_m , NPQ/4, and Φ_{II} depicted at the time points highlighted by a black arrow represent values on a rainbow scale from 0 to 1 shown below **(B)**. Note that NPQ parameters in **(D,F)** are displayed in NPQ/4 to fit the standard color code ranging from 0 to 1. Chl fluorescence signals were normalized to F_m and are shown in gray on a scale from 0 to 1 in **(D-F)**.

and q_E , which was recently determined in an initial screening step to identify 'high cyclic electron flow around PSI' (*hcef*) mutants with altered CEF (Livingston et al., 2010). Block 5 also implements a dark-light shift experiment, but using excessive light intensities ($1200 \mu\text{E m}^{-2} \text{s}^{-1}$) and longer exposure times

(20 min), which allow the detection of *npq* mutants due to their aberrant NPQ induction patterns under high light (Niyogi et al., 1998). After the photodamage-inducing high-light treatment in block 5, the protocol ends with a recovery phase from high light (block 6) under low light intensities ($10 \mu\text{E m}^{-2} \text{s}^{-1}$) and

was designed to pick up mutants that are defective in the PSII repair mechanism (Schroda et al., 1999; Malnoe et al., 2014). Overall, the CFVI protocol outlined above can already uncover a wide range of phenotypes, but can be further expanded to cover a larger collection of photosynthetic parameters, such as the determination of P_{\max} from light saturation curves (van Rooijen et al., 2015) and measurements of qT in state transitions (Pribil et al., 2010) or effective quantum yields/NPQ parameters under fluctuating light conditions (Cruz et al., 2016).

Chl Fluorescence Image Phenotyping under Simulated Environmental Conditions

The photosynthetic lifestyle of plants and algae requires a high degree of flexibility and the ability to adapt to rapidly fluctuating environments. However, for reasons of scalability and reproducibility most of the screening studies referred to here were conducted with small *Arabidopsis* plants or algae grown in stable, standardized laboratory settings and would have been impossible with fully developed crops under field conditions. Furthermore, phenotyping of mutant collections involved measurements of only one or a few photosynthetic parameters, which were determined at one or more time points, thus providing a rather static picture of the highly dynamic process of photosynthesis. It is therefore obvious that many factors that contribute to the fine tuning of photosynthesis in response to dynamic environmental changes will have not been identified by previous screening procedures (Cruz et al., 2016). This assertion is also supported by the observation that plant lines lacking PsbS (Külheim et al., 2002), the LHCII serine/threonine-protein kinase STN7 (Grieco et al., 2012) or PGR5 (Suorsa et al., 2012) showed higher levels of photodamage and notable reductions in their growth rates (or lethality) only under fluctuating light conditions that were not observed under unchanging conditions. One logical and straightforward way to bypass this limitation would be to carry out phenotyping of mutant collections in the field, and suitable large-scale Chl fluorescence image analyzers are now available for this task (e.g., Field Scanalyzer) (Virlet et al., 2017). However, besides the fact that in several countries the cultivation of genetically modified plants in the field is either prohibited or subject to legal restrictions, such studies are complicated by a multitude of overlapping, unpredictable abiotic and biotic stress factors, and statistical evaluation of the results become particularly challenging. For these reasons, the dynamic environmental photosynthesis imager (DEPI) platform was developed for replication of natural, fluctuating growth conditions in the laboratory (Cruz et al., 2016). Several parameters can be controlled (light intensity, CO₂ concentration, humidity and temperature) in the growth chamber, and rapid responses as well as long-term acclimation processes of photosynthesis can be assessed *in situ* by the integrated CFVI system in more than two hundred plants simultaneously. As a proof of concept, a library of over 300 T-DNA *Arabidopsis* lines disrupted in nuclear genes coding for chloroplast-targeted proteins (Ajajawi et al., 2010) was exposed to a 5-day regime of fluctuating light levels

and screened for alterations in photosynthetic performance. As a result, *psb33* plants lacking PSII protein 33 (PSB33) (Fristedt et al., 2015) and several other conditional mutant lines showed transient, spatiotemporal-dependent phenotypes which could not be detected or were not reliably expressed under standard growth conditions. PSB33 is a green-lineage-specific protein (Merchant et al., 2007) predominantly found in non-appressed thylakoids of *Arabidopsis* chloroplasts and sustains D1 of PSII under fluctuating light conditions (Fristedt et al., 2017). Thus, the DEPI system can reveal new, complex and previously unseen phenotypes, and provides a versatile experimental platform with which to identify factors required for remodeling and regulation of photosynthesis under dynamic environmental conditions.

Chl FLUORESCENCE VIDEO IMAGING IN QUANTITATIVE GENETIC APPROACHES

Forward and reverse genetics are efficient strategies for elucidating the functions of a single gene or of small gene families, but these approaches reach their limits when the genetic architecture of a quantitative trait and its interaction with the environment needs to be determined. Most agronomically important traits (e.g., grain yield, grain size, ripening or flowering time) are controlled by multiple genes which have to be analyzed by quantitative genetic approaches, such as classical linkage mapping or genome-wide association studies (GWAS) (reviewed in: Bazakos et al., 2017). Natural variation also exists for photosynthetic traits and can be roughly divided into morphological and physiological variations, which have been investigated in several studies with different plant species (reviewed in: Flood et al., 2011). For instance, Jung and Niyogi (2009) examined natural NPQ variation in different *Arabidopsis* accessions and provided evidence that thermal dissipation is a quantitative trait that depends on multiple, nucleus-encoded genetic factors. Two high-NPQ QTLs (*HQE1* and *HQE2*) were identified in a quantitative trait locus (QTL) analysis which was performed with a F2 mapping population generated from a cross between a low-NPQ and a high-NPQ *Arabidopsis* accession (Jung and Niyogi, 2009). Remarkably, *HQE1* and *HQE2* were not mapped to previously characterized factors identified in forward genetic approaches, indicating that quantitative genetics can serve as a complementary strategy to dissect the genetic architecture of thermal dissipation.

Even though quantitative genetic approaches have a long history in plant science, their potential for photosynthesis research has not yet been fully explored. This may simply reflect the high complexity of the genetic architecture of photosynthesis, which not only comprises the several hundred genes directly involved in biogenesis processes, regulation or acclimation of photosynthesis, but also involves two quite distinct genetic systems (plastid and nuclear genome) with different inheritance modes. Moreover, successful quantitative genetic approaches in photosynthesis research require reproducible, non-invasive, high-throughput phenotyping pipelines that were not available until recently. However, several platforms have been developed

in recent years. Examples include FluorImager (Barbagallo et al., 2003), GROWSCREEN FLUORO (Jansen et al., 2009), PlantScreen (Humplík et al., 2015), Phenovator (Flood et al., 2016), the DEPI system (Cruz et al., 2016) or the crop population growth information detection system (Wang et al., 2017), which now integrate CFVI analyses into their phenotyping facilities. As an example for the combination of a GWAS and a high-throughput Chl fluorescence phenotyping approach, van Rooijen et al. (2015) have explored the natural genetic variation for acclimation of photosynthetic light use efficiency (Φ_{II}) in 344 *Arabidopsis* accessions. Of 63 newly identified gene candidates, 13 encode chloroplast-localized proteins, most of which are either associated with abiotic stress responses or have unknown functions.

GENE DISCOVERY THROUGH CHLOROPHYLL FLUORESCENCE VIDEO IMAGING – A BRIEF OUTLOOK

Due to the advances in imaging and data acquisition technologies in the last two decades, Chl fluorescence-based analyses have entered the ‘phenomics’ field and promise to increase our knowledge of photosynthesis substantially. Modern phenotyping systems are highly flexible and will allow the identification of new genotype-phenotype-environment relationships and accelerate gene discovery studies significantly.

The next obvious step will be to determine photosynthetic parameters of large-scale, indexed mutant collections like the *Arabidopsis* unimutant (O’Malley and Ecker, 2010), the *Arabidopsis* Chloroplast 2010 Project (Ajjawi et al., 2010) and the GABI-DUPLO double mutant (Bolle et al., 2013) collections, or the recently generated *Chlamydomonas* mutant collection CLiP (Li et al., 2016). Consequently, with the exception of screening approaches under highly specialized conditions, tedious forward genetic screening procedures, which were carried out by single researchers or research groups in the past, will become obsolete. A major task in the future will lie in the processing, handling, quality control, maintenance, storage, analysis and sharing of the vast amount of data collected by CFVI-based phenotyping studies, which will become even more challenging when such screens are combined with other non-invasive phenotyping technologies (Walter et al., 2015; Tardieu et al., 2017). But computational techniques for assessing the quality of phenotypic data (Xu et al., 2015) and analyzing massive amounts of data in order to reveal dynamic relationships between phenotypes and environment (Yang et al., 2017) have already been developed, and these will eventually replace manual evaluation methods.

Chl fluorescence video imaging also has the potential to be an important technological driver in crop science, since it offers an efficient screening technology for rapid evaluation of plant performance under stress conditions such as drought, salinity, freezing, chilling, high temperature or nutrient deficiency (reviewed in: Baker and Rosenqvist, 2004). CFVI is of particular interest in plant breeding programs, since low-cost and precise high-throughput phenotyping technologies have been regarded as one of the major bottleneck in the postgenomic era of

plant breeding (reviewed in: Araus and Cairns, 2014). A further challenge is the difficulty to extrapolate results gained under a strictly controlled environment (such as a growth chamber or greenhouse) to field conditions. It is therefore inevitable to establish high throughput phenotyping technologies under heterogeneous field conditions to analyze quantitative traits and to elucidate their underlying genetic architecture for future breeding efforts. Significant progress in non-invasive sensor and imaging technology has been made (reviewed in: White et al., 2012; Fiorani and Schurr, 2013) and the Field Scanalyzer system installed at Rothamsted Research (United Kingdom) by LemnaTec GmbH (Germany) is one example, which now employs Chl fluorescence based measurements for high-throughput phenotyping in the field (Virlet et al., 2017).

While recent work has mainly focused on scaling up CFVI screening systems for simultaneous evaluation of large sample collections, a future direction might be to explore the potential of screening single cells by exploiting their Chl fluorescence fingerprints. Flow cytometry technologies are well established for unicellular microalgae in environmental and toxicological studies (reviewed in: Hyka et al., 2013) and several flow cytometry studies with plant protoplasts have been reported (Harkins et al., 1990; Galbraith, 2007; Berendzen et al., 2012; You et al., 2015). Flow cytometry is generally coupled to fluorescence-activated cell sorting, which permits the isolation of a desired cell population with specific physiological properties. Recently, this technique has been successfully employed to screen high-lipid *Chlamydomonas* mutants that were stained with the lipid-sensitive dye Nile Red prior to screening (Xie et al., 2014; Terashima et al., 2015) or to identify protein-protein interactions in plant protoplasts by combining bimolecular fluorescence complementation with flow cytometry (Berendzen et al., 2012). Moreover, Chl autofluorescence has been used in flow cytometry studies as an endogenous probe to sort tobacco mesophyll protoplasts (Harkins et al., 1990) and to discriminate between different phytoplankton species by cytometric approaches (Hildebrand et al., 2016). Although implementation will be challenging, the combination of flow cytometry and Chl fluorescence kinetics-based cell sorting can provide a fast means of screening mutagenized cell populations for specific Chl fluorescence phenotypes.

AUTHOR CONTRIBUTIONS

TR designed and wrote the article. BR and DL wrote the article.

FUNDING

This work was funded by the German Science Foundation (DFG, Research Unit FOR2092, grant RU 1945/2-1).

ACKNOWLEDGMENTS

We thank Paul Hardy for critical comments on the manuscript.

REFERENCES

- Ajjawi, I., Lu, Y., Savage, L. J., Bell, S. M., and Last, R. L. (2010). Large-scale reverse genetics in Arabidopsis: case studies from the Chloroplast 2010 Project. *Plant Physiol.* 152, 529–540. doi: 10.1104/pp.109.148494
- Allen, J. F. (1992). Protein phosphorylation in regulation of photosynthesis. *Biochim. Biophys. Acta* 1098, 275–335. doi: 10.1016/S0005-2728(09)91014-3
- Araus, J. L., and Cairns, J. E. (2014). Field high-throughput phenotyping: the new crop breeding frontier. *Trends Plant Sci.* 19, 52–61. doi: 10.1016/j.tplants.2013.09.008
- Armbruster, U., Rühle, T., Kreller, R., Strotbek, C., Zühlke, J., Tadini, L., et al. (2013). The photosynthesis affected mutant68-like protein evolved from a PSII assembly factor to mediate assembly of the chloroplast NAD(P)H dehydrogenase complex in Arabidopsis. *Plant Cell* 25, 3926–3943. doi: 10.1105/tpc.113.114785
- Armbruster, U., Zühlke, J., Rengstl, B., Kreller, R., Makarenko, E., Rühle, T., et al. (2010). The Arabidopsis thylakoid protein PAM68 is required for efficient D1 biogenesis and photosystem II assembly. *Plant Cell* 22, 3439–3460. doi: 10.1105/tpc.110.077453
- Badger, M. R., Fallahi, H., Kaines, S., and Takahashi, S. (2009). Chlorophyll fluorescence screening of *Arabidopsis thaliana* for CO₂ sensitive photorespiration and photoinhibition mutants. *Funct. Plant Biol.* 36, 867–873. doi: 10.1071/FP09199
- Baker, N. R. (2008). Chlorophyll fluorescence: a probe of photosynthesis in vivo. *Annu. Rev. Plant Biol.* 59, 89–113. doi: 10.1146/annurev.arplant.59.032607.092759
- Baker, N. R., and Rosenqvist, E. (2004). Applications of chlorophyll fluorescence can improve crop production strategies: an examination of future possibilities. *J. Exp. Bot.* 55, 1607–1621. doi: 10.1093/jxb/erh196
- Barbagallo, R. P., Barbagallo, R. P., Oxborough, K., Oxborough, K., Pallett, K. E., Pallett, K. E., et al. (2003). Rapid noninvasive screening for perturbations of metabolism and plant growth using chlorophyll fluorescence imaging. *Plant Physiol.* 132, 485–493. doi: 10.1104/pp.102.018093
- Barkan, A., Miles, D., and Taylor, W. C. (1986). Chloroplast gene expression in nuclear, photosynthetic mutants of maize. *EMBO J.* 5, 1421–1427. doi: 10.1002/j.1460-2075.1986.tb04378.x
- Bazakos, C., Hanemian, M., Trontin, C., Jiménez-Gómez, J. M., and Loudet, O. (2017). New strategies and tools in quantitative genetics: How to go from the phenotype to the genotype. *Annu. Rev. Plant Biol.* 68, 435–455. doi: 10.1146/annurev-arplant-042916-40820
- Belcher, S., Williams-Carrier, R., Stiffler, N., and Barkan, A. (2015). Large-scale genetic analysis of chloroplast biogenesis in maize. *Biochim. Biophys. Acta* 1847, 1004–1016. doi: 10.1016/j.bbabi.2015.02.014
- Bennoun, P., and Levine, R. P. (1967). Detecting mutants that have impaired photosynthesis by their increased level of fluorescence. *Plant Physiol.* 42, 1284–1287.
- Berendzen, K. W., Bohmer, M., Wallmeroth, N., Peter, S., Vesic, M., Zhou, Y., et al. (2012). Screening for in planta protein-protein interactions combining bimolecular fluorescence complementation with flow cytometry. *Plant Methods* 8:25. doi: 10.1186/1746-4811-8-25
- Bilger, W., and Björkman, O. (1990). Role of the xanthophyll cycle in photoprotection elucidated by measurements of light-induced absorbance changes, fluorescence and photosynthesis in leaves of *Hedera canariensis*. *Photosynth. Res.* 25, 173–185. doi: 10.1007/BF00033159
- Björkman, O., and Demmig, B. (1987). Photon yield of O₂ evolution and chlorophyll fluorescence characteristics at 77 K among vascular plants of diverse origins. *Planta* 170, 489–504. doi: 10.1007/BF00402983
- Bolle, C., Huep, G., Kleinbölting, N., Haberer, G., Mayer, K., Leister, D., et al. (2013). GABI-DUPLO: A collection of double mutants to overcome genetic redundancy in *Arabidopsis thaliana*. *Plant J.* 75, 157–171. doi: 10.1111/tpj.12197
- Brooks, M. D., Sylak-Glassman, E. J., Fleming, G. R., and Niyogi, K. K. (2013). A thioredoxin-like/β-propeller protein maintains the efficiency of light harvesting in Arabidopsis. *Proc. Natl. Acad. Sci. U.S.A.* 110, E2733–E2740. doi: 10.1073/pnas.1305443110
- Cardol, P., Alric, J., Girard-Bascou, J., Franck, F., Wollman, F.-A., and Finazzi, G. (2009). Impaired respiration discloses the physiological significance of state transitions in *Chlamydomonas*. *Proc. Natl. Acad. Sci. U.S.A.* 106, 15979–15984. doi: 10.1073/pnas.0908111106
- Cardol, P., Gloire, G., Havaux, M., Remacle, C., Matagne, R., and Franck, F. (2003). Photosynthesis and state transitions in mitochondrial mutants of *Chlamydomonas reinhardtii* affected in respiration. *Plant Physiol.* 133, 2010–2020. doi: 10.1104/pp.103.028076
- Carrie, C., and Small, I. (2013). A reevaluation of dual-targeting of proteins to mitochondria and chloroplasts. *Biochim. Biophys. Acta* 1833, 253–259. doi: 10.1016/j.bbamcr.2012.05.029
- Chaerle, L., Lenk, S., Leinonen, I., Jones, H. G., Van Der Straeten, D., and Buschmann, C. (2009). Multi-sensor plant imaging: towards the development of a stress-catalogue. *Biotechnol. J.* 4, 1152–1167. doi: 10.1002/biot.200800242
- Cruz, J. A., Savage, L. J., Zegarac, R., Hall, C. C., Satoh-Cruz, M., Davis, G. A., et al. (2016). Dynamic environmental photosynthetic imaging reveals emergent phenotypes. *Cell Syst.* 2, 365–377. doi: 10.1016/j.cels.2016.06.001
- DalCorso, G., Pesaresi, P., Masiero, S., Aseeva, E., Schünemann, D., Finazzi, G., et al. (2008). A complex containing PGRL1 and PGR5 is involved in the switch between linear and cyclic electron flow in Arabidopsis. *Cell* 132, 273–285. doi: 10.1016/j.cell.2007.12.028
- Dang, K.-V., Plet, J., Tolleter, D., Jokel, M., Cuiné, S., Carrier, P., et al. (2014). Combined increases in mitochondrial cooperation and oxygen photoreduction compensate for deficiency in cyclic electron flow in *Chlamydomonas reinhardtii*. *Plant Cell* 26, 3036–3050. doi: 10.1105/tpc.114.126375
- Delosme, R., Olive, J., and Wollman, F. A. (1996). Changes in light energy distribution upon state transitions: an in vivo photoacoustic study of the wild type and photosynthesis mutants from *Chlamydomonas reinhardtii*. *Biochim. Biophys. Acta* 1273, 150–158. doi: 10.1016/0005-2728(95)00143-3
- Depège, N., Bellafiore, S., and Rochaix, J. D. (2003). Role of chloroplast protein kinase Stt7 in LHClI phosphorylation and state transition in *Chlamydomonas*. *Science* 299, 1572–1575. doi: 10.1126/science.1081397
- Dinkins, R. D., Bandaranayake, H., Baeza, L., Griffiths, A. J., and Green, B. R. (1997). *hcf5*, a nuclear photosynthetic electron transport mutant of *Arabidopsis thaliana* with a pleiotropic effect on chloroplast gene expression. *Plant Physiol.* 113, 1023–1031. doi: 10.1104/pp.113.4.1023
- Dinkins, R. D., Bandaranayake, H., Green, B. R., and Griffiths, A. J. (1994). A nuclear photosynthetic electron transport mutant of *Arabidopsis thaliana* with altered expression of the chloroplast petA gene. *Curr. Genet.* 25, 282–288. doi: 10.1007/BF00357174
- Felder, S., Meierhoff, K., Sane, A. P., Meurer, J., Driemel, C., Plücken, H., et al. (2001). The nucleus-encoded HCF107 gene of Arabidopsis provides a link between intercistronic RNA processing and the accumulation of translation-competent *psbH* transcripts in chloroplasts. *Plant Cell* 13, 2127–2141. doi: 10.1105/TPC.010090
- Fenton, J. M., and Crofts, A. R. (1990). Computer aided fluorescence imaging of photosynthetic systems - Application of video imaging to the study of fluorescence induction in green plants and photosynthetic bacteria. *Photosynth. Res.* 26, 59–66. doi: 10.1007/BF00048977
- Fiorani, F., and Schurr, U. (2013). Future scenarios for plant phenotyping. *Annu. Rev. Plant Biol.* 64, 267–291. doi: 10.1146/annurev-arplant-050312-120137
- Fleischmann, M. M., Ravel, S., Delosme, R., Olive, J., Zito, F., Wollman, F.-A., et al. (1999). Isolation and characterization of photoautotrophic mutants of *Chlamydomonas reinhardtii* deficient in state transition. *J. Biol. Chem.* 274, 30987–30994. doi: 10.1074/jbc.274.43.30987
- Flood, P. J., Harbinson, J., and Aarts, M. G. M. (2011). Natural genetic variation in plant photosynthesis. *Trends Plant Sci.* 16, 327–335. doi: 10.1016/j.tplants.2011.02.005
- Flood, P. J., Kruijer, W., Schnabel, S. K., van der Schoor, R., Jalink, H., Snel, J. F. H., et al. (2016). Phenomics for photosynthesis, growth and reflectance in *Arabidopsis thaliana* reveals circadian and long-term fluctuations in heritability. *Plant Methods* 12:14. doi: 10.1186/s13007-016-0113-y
- Fristedt, R., Herdean, A., Blaby-Haas, C. E., Mamedov, F., Merchant, S. S., Last, R. L., et al. (2015). PHOTOSYSTEM II PROTEIN33, a protein conserved in the plastid lineage, is associated with the chloroplast thylakoid membrane and provides stability to photosystem II supercomplexes in Arabidopsis. *Plant Physiol.* 167, 481–492. doi: 10.1104/pp.114.253336
- Fristedt, R., Trotta, A., Suorsa, M., Nilsson, A. K., Croce, R., Aro, E.-M., et al. (2017). PSB33 sustains photosystem II D1 protein under fluctuating light conditions. *J. Exp. Bot.* 68, 4281–4293. doi: 10.1093/jxb/erx218

- Galbraith, D. W. (2007). *Protoplast Analysis Using Flow Cytometry and Sorting. Flow Cytometry with Plant Cells*. Weinheim: Wiley-VCH, 231–250. doi: 10.1002/9783527610921.ch10
- Genty, B., Briantais, J.-M., and Baker, N. R. (1989). The relationship between the quantum yield of photosynthetic electron transport and quenching of chlorophyll fluorescence. *Biochim. Biophys. Acta* 990, 87–92. doi: 10.1016/S0304-4165(89)80016-9
- Godaux, D., Emonds-Alt, B., Berne, N., Ghysels, B., Alric, J., Remacle, C., et al. (2013). A novel screening method for hydrogenase-deficient mutants in *Chlamydomonas reinhardtii* based on in vivo chlorophyll fluorescence and photosystem II quantum yield. *Int. J. Hydrogen Energy* 38, 1826–1836. doi: 10.1016/j.ijhydene.2012.11.081
- Golan, T., Li, X.-P., Muller-Moule, P., and Niyogi, K. K. (2004). “Using mutants to understand light stress acclimation in plants,” in *Chlorophyll a Fluorescence: A Signature of Photosynthesis*, eds G. C. Papageorgiou and Govindjee (Dordrecht: Springer Netherlands), 525–554.
- Grahl, S., Reiter, B., Gügel, I. L., Vamvaka, E., Gandini, C., Jahns, P., et al. (2016). The Arabidopsis protein CGLD11 is required for chloroplast ATP synthase accumulation. *Mol. Plant* 9, 885–899. doi: 10.1016/j.molp.2016.03.002
- Grieco, M., Tikkanen, M., Paakkari, V., Kangasjarvi, S., and Aro, E.-M. (2012). Steady-state phosphorylation of light-harvesting complex II proteins preserves photosystem I under fluctuating white light. *Plant Physiol.* 160, 1896–1910. doi: 10.1104/pp.112.206466
- Grossman, A. R., Catalanotti, C., Yang, W., Dubini, A., Magneschi, L., Subramanian, V., et al. (2011). Multiple facets of anoxic metabolism and hydrogen production in the unicellular green alga *Chlamydomonas reinhardtii*. *New Phytol.* 190, 279–288. doi: 10.1111/j.1469-8137.2010.03534.x
- Harkins, K. R., Jefferson, R. A., Kavanagh, T. A., Bevan, M. W., and Galbraith, D. W. (1990). Expression of photosynthesis-related gene fusions is restricted by cell type in transgenic plants and in transfected protoplasts. *Proc. Natl. Acad. Sci. U.S.A.* 87, 816–820. doi: 10.1073/pnas.87.2.816
- Harris, E. H. (1989). “Nuclear mutations described in *C. reinhardtii*,” in *The Chlamydomonas Sourcebook: A Comprehensive Guide to Biology and Laboratory Use*, ed. E. H. Harris (San Diego, CA: Academic Press, Inc.), 461–542.
- Hashimoto, M., Endo, T., Peltier, G., Tasaka, M., and Shikanai, T. (2003). A nucleus-encoded factor, CRR2, is essential for the expression of chloroplast *ndhB* in Arabidopsis. *Plant J.* 36, 541–549. doi: 10.1046/j.1365-313X.2003.01900.x
- Hemschemeier, A., Melis, A., and Happe, T. (2009). Analytical approaches to photobiological hydrogen production in unicellular green algae. *Photosynth. Res.* 102, 523–540. doi: 10.1007/s11120-009-9415-5
- Hertle, A. P., Blunder, T., Wunder, T., Pesaresi, P., Pribil, M., Armbruster, U., et al. (2013). PGRL1 is the elusive ferredoxin-plastoquinone reductase in photosynthetic cyclic electron flow. *Mol. Cell* 49, 511–523. doi: 10.1016/j.molcel.2012.11.030
- Hildebrand, M., Davis, A., Abbriano, R., Pugsley, H. R., Traller, J. C., Smith, S. R., et al. (2016). “Applications of imaging flow cytometry for microalgae,” in *Imaging Flow Cytometry*, eds N. Barteneva and I. Vorobjev (New York, NY: Humana Press), 47–67.
- Houille-Vernes, L., Rappaport, F., Wollman, F.-A., Alric, J., and Johnson, X. (2011). Plastid terminal oxidase 2 (PTOX2) is the major oxidase involved in chlororespiration in *Chlamydomonas*. *Proc. Natl. Acad. Sci. U.S.A.* 108, 20820–20825. doi: 10.1073/pnas.1110518109
- Humplik, J. F., Lázár, D., Fürst, T., Husíčková, A., Hýbl, M., and Spíchal, L. (2015). Automated integrative high-throughput phenotyping of plant shoots: a case study of the cold-tolerance of pea (*Pisum sativum* L.). *Plant Methods* 11:20. doi: 10.1186/s13007-015-0063-9
- Hyka, P., Lickova, S., Přibyl, P., Melzoch, K., and Kovar, K. (2013). Flow cytometry for the development of biotechnological processes with microalgae. *Biotechnol. Adv.* 31, 2–16. doi: 10.1016/j.biotechadv.2012.04.007
- Ifuku, K., Endo, T., Shikanai, T., and Aro, E.-M. (2011). Structure of the chloroplast NADH dehydrogenase-like complex: nomenclature for nuclear-encoded subunits. *Plant Cell Physiol.* 52, 1560–1568. doi: 10.1093/pcp/pcr098
- Ihnatowicz, A., Pesaresi, P., Varotto, C., Richly, E., Schneider, A., Jahns, P., et al. (2004). Mutants for photosystem I subunit D of *Arabidopsis thaliana*: effects on photosynthesis, photosystem I stability and expression of nuclear genes for chloroplast functions. *Plant J.* 37, 839–852. doi: 10.1111/j.1365-313X.2003.02011.x
- Jansen, M., Gilmer, F., Biskup, B., Nagel, K. A., Rascher, U., Fischbach, A., et al. (2009). Simultaneous phenotyping of leaf growth and chlorophyll fluorescence via Growscreen Fluoro allows detection of stress tolerance in *Arabidopsis thaliana* and other rosette plants. *Funct. Plant Biol.* 36, 902–914. doi: 10.1071/FP09095
- Jung, H.-S., and Niyogi, K. K. (2009). Quantitative genetic analysis of thermal dissipation in Arabidopsis. *Plant Physiol.* 150, 977–986. doi: 10.1104/pp.109.137828
- Kalaji, H. M., Schansker, G., Brestic, M., Bussotti, F., Calatayud, A., Ferroni, L., et al. (2017). Frequently asked questions about chlorophyll fluorescence, the sequel. *Photosynth. Res.* 132, 13–66. doi: 10.1007/s11120-016-0318-y
- Kalituho, L., Graßes, T., Graf, M., Rech, J., and Jahns, P. (2006). Characterization of a nonphotochemical quenching-deficient Arabidopsis mutant possessing an intact PsbS protein, xanthophyll cycle and lumen acidification. *Planta* 223, 532–541. doi: 10.1007/s00425-005-0093-z
- Kramer, D. M., and Evans, J. R. (2011). The importance of energy balance in improving photosynthetic productivity. *Plant Physiol.* 155, 70–78. doi: 10.1104/pp.110.166652
- Krause, G. H., and Weis, E. (1991). Chlorophyll fluorescence and photosynthesis: the basics. *Annu. Rev. Plant Physiol. Plant Mol. Biol.* 42, 313–349. doi: 10.1146/annurev.pp.42.060191.001525
- Kruse, O., Nixon, P. J., Schmid, G. H., and Mullineaux, C. W. (1999). Isolation of state transition mutants of *Chlamydomonas reinhardtii* by fluorescence video imaging. *Photosynth. Res.* 61, 43–51. doi: 10.1023/A:1006229308606
- Külheim, C., Agren, J., and Jansson, S. (2002). Rapid regulation of light harvesting and plant fitness in the field. *Science* 297, 91–93. doi: 10.1126/science.1072359
- Küpper, H., Šetlík, I., Trtílek, M., and Nedbal, L. (2000). A microscope for two-dimensional measurements of in vivo chlorophyll fluorescence kinetics using pulsed measuring radiation, continuous actinic radiation, and saturating flashes. *Photosynthetica* 38, 553–570. doi: 10.1023/A:1012461407557
- Lezhneva, L., Amann, K., and Meurer, J. (2004). The universally conserved HCF101 protein is involved in assembly of [4Fe-4S]-cluster-containing complexes in *Arabidopsis thaliana* chloroplasts. *Plant J.* 37, 174–185. doi: 10.1046/j.1365-313X.2003.01952.x
- Lezhneva, L., and Meurer, J. (2004). The nuclear factor HCF145 affects chloroplast *psaA-psaB-rps14* transcript abundance in *Arabidopsis thaliana*. *Plant J.* 38, 740–753. doi: 10.1111/j.1365-313X.2004.02081.x
- Li, X., Zhang, R., Patena, W., Gang, S. S., Blum, S. R., Ivanova, N., et al. (2016). An indexed, mapped mutant library enables reverse genetics studies of biological processes in *Chlamydomonas reinhardtii*. *Plant Cell* 28, 367–387. doi: 10.1105/tpc.16.00465
- Li, X. P., Björkman, O., Shih, C., Grossman, A. R., Rosenquist, M., Jansson, S., et al. (2000). A pigment-binding protein essential for regulation of photosynthetic light harvesting. *Nature* 403, 391–395. doi: 10.1038/35000131
- Livingston, A. K., Cruz, J. A., Kohzuma, K., Dhingra, A., and Kramer, D. M. (2010). An Arabidopsis mutant with high cyclic electron flow around photosystem I (hcef) involving the NADPH dehydrogenase complex. *Plant Cell* 22, 221–233. doi: 10.1105/tpc.109.071084
- Lloyd, J., and Meinke, D. (2012). A comprehensive dataset of genes with a loss-of-function mutant phenotype in Arabidopsis. *Plant Physiol.* 158, 1115–1129. doi: 10.1104/pp.111.192393
- Malnoë, A., Schultink, A., Shahrasbi, S., Rumeau, D., Havaux, M., and Niyogi, K. K. (2017). The plastid lipocalin LCNP is required for sustained photoprotective energy dissipation in Arabidopsis. *Plant Cell* doi: 10.1105/tpc.17.00536 [Epub ahead of print].
- Malnoë, A., Wang, F., Girard-Bascou, J., Wollman, F.-A., and de Vitry, C. (2014). Thylakoid FtsH protease contributes to photosystem II and cytochrome *b6f* remodeling in *Chlamydomonas reinhardtii* under stress conditions. *Plant Cell* 26, 373–390. doi: 10.1105/tpc.113.120113
- Manavski, N., Torabi, S., Lezhneva, L., Arif, M. A., Frank, W., and Meurer, J. (2015). HIGH CHLOROPHYLL FLUORESCENCE145 binds to and stabilizes the *psaA* 5' UTR via a newly defined repeat motif in Embryophyta. *Plant Cell* 27, 2600–2615. doi: 10.1105/tpc.15.00234
- Massoz, S., Hanikenne, M., Bailleul, B., Coosemans, N., Radoux, M., Miranda-Astudillo, H., et al. (2017). In vivo chlorophyll fluorescence screening allows the isolation of a *Chlamydomonas* mutant defective for NDUFAF3, an assembly factor involved in mitochondrial complex I assembly. *Plant J.* 17, 2045–2054. doi: 10.1111/tpj.13677

- Massoz, S., Larosa, V., Horrion, B., Matagne, R. F., Remacle, C., and Cardol, P. (2015). Isolation of *Chlamydomonas reinhardtii* mutants with altered mitochondrial respiration by chlorophyll fluorescence measurement. *J. Biotechnol.* 215, 27–34. doi: 10.1016/j.jbiotec.2015.05.009
- Maxwell, K., and Johnson, G. N. (2000). Chlorophyll fluorescence—a practical guide. *J. Exp. Bot.* 51, 659–668. doi: 10.1093/jxb/51.345.659
- Meierhoff, K., Felder, S., Nakamura, T., Bechtold, N., and Schuster, G. (2003). HCF152, an Arabidopsis RNA binding pentatricopeptide repeat protein involved in the processing of chloroplast *psbB-psbT-psbH-petB-petD* RNAs. *Plant Cell* 15, 1480–1495. doi: 10.1105/tpc.010397
- Merchant, S. S., Prochnik, S. E., Vallon, O., Harris, E. H., Karpowicz, S. J., Witman, G. B., et al. (2007). The Chlamydomonas genome reveals the evolution of key animal and plant functions. *Science* 318, 245–250. doi: 10.1126/science.1143609
- Meurer, J., Berger, A., and Westhoff, P. (1996a). A nuclear mutant of Arabidopsis with impaired stability on distinct transcripts of the plastid *psbB*, *psbD/C*, *ndhH*, and *ndhC* operons. *Plant Cell* 8, 1193–1207. doi: 10.1105/tpc.8.7.1193
- Meurer, J., Meierhoff, K., and Westhoff, P. (1996b). Isolation of high-chlorophyll-fluorescence mutants of *Arabidopsis thaliana* and their characterisation by spectroscopy, immunoblotting and northern hybridisation. *Planta* 198, 385–396. doi: 10.1007/BF00620055
- Miles, C. D., and Daniel, D. J. (1973). A rapid screening technique for photosynthetic mutants of higher plants. *Plant Sci. Lett.* 1, 237–240. doi: 10.1016/0304-4211(73)90025-4
- Miles, C. D., and Daniel, D. J. (1974). Chloroplast reactions of photosynthetic mutants in *Zea mays*. *Plant Physiol.* 53, 589–595. doi: 10.1104/pp.53.4.589
- Mohr, S. E., Smith, J. A., Shamu, C. E., Neumüller, R. A., and Perrimon, N. (2014). RNAi screening comes of age: improved techniques and complementary approaches. *Nat. Rev. Mol. Cell Biol.* 15, 591–600. doi: 10.1038/nrm3860
- Munekage, Y., Hojo, M., Meurer, J., Endo, T., Tasaka, M., and Shikanai, T. (2002). PGR5 is involved in cyclic electron flow around photosystem I and is essential for photoprotection in Arabidopsis. *Cell* 110, 361–371. doi: 10.1016/S0092-8674(02)00867-X
- Munekage, Y., Takeda, S., Endo, T., Jahns, P., Hashimoto, T., and Shikanai, T. (2001). Cytochrome b6f mutation specifically affects thermal dissipation of absorbed light energy in Arabidopsis. *Plant J.* 28, 351–359. doi: 10.1046/j.1365-3113.2001.01178.x
- Munshi, M. K., Kobayashi, Y., and Shikanai, T. (2006). CHLORORESPIRATORY REDUCTION 6 is a novel factor required for accumulation of the chloroplast NAD(P)H dehydrogenase complex in Arabidopsis. *Plant Physiol.* 141, 737–744. doi: 10.1104/pp.106.080267.1
- Nedbal, L., and Whitmarsh, J. (2004). “Chlorophyll fluorescence imaging of leaves and fruits,” in *Chlorophyll a Fluorescence: A Signature of Photosynthesis*, eds G. C. Papageorgiou and Govindjee (Dordrecht: Springer Netherlands), 389–407. doi: 10.1007/978-1-4020-3218-9
- Niyogi, K., Bjorkman, O., and Grossman, A. (1997). Chlamydomonas xanthophyll cycle mutants identified by video imaging of chlorophyll fluorescence quenching. *Plant Cell* 9, 1369–1380. doi: 10.1105/tpc.9.8.1369
- Niyogi, K. K., Grossman, A. R., and Bjorkman, O. (1998). Arabidopsis mutants define a central role for the xanthophyll cycle in the regulation of photosynthetic energy conversion. *Plant Cell* 10, 1121–1134. doi: 10.1105/tpc.10.7.1121
- O'Malley, R. C., and Ecker, J. R. (2010). Linking genotype to phenotype using the Arabidopsis unimutant collection. *Plant J.* 61, 928–940. doi: 10.1111/j.1365-3113.2010.04119.x
- Omasa, K., Shimazaki, K., Aiga, I., Larcher, W., and Onoe, M. (1987). Image analysis of chlorophyll fluorescence transients for diagnosing the photosynthetic system of attached leaves. *Plant Physiol.* 84, 748–752. doi: 10.1104/pp.84.3.748
- Ort, D. R. (2001). When there is too much light. *Plant Physiol.* 125, 29–32. doi: 10.1104/pp.125.1.29
- Oxborough, K. (2004). “Using chlorophyll a fluorescence imaging to monitor photosynthetic performance,” in *Chlorophyll a Fluorescence: A Signature of Photosynthesis*, eds G. C. Papageorgiou and Govindjee (Dordrecht: Springer Netherlands), 409–428.
- Oxborough, K., and Baker, N. R. (1997). An instrument capable of imaging chlorophyll a fluorescence from intact leaves at very low irradiance and at cellular and subcellular levels of organization. *Plant Cell Environ.* 20, 1473–1483. doi: 10.1046/j.1365-3040.1997.d01-42.x
- Peng, L., Ma, J., Chi, W., Guo, J., Zhu, S., Lu, Q., et al. (2006). LOW PSII ACCUMULATION1 is involved in efficient assembly of photosystem II in *Arabidopsis thaliana*. *Plant Cell* 18, 955–969. doi: 10.1105/tpc.105.037689
- Peng, L., Yamamoto, H., and Shikanai, T. (2011). Structure and biogenesis of the chloroplast NAD(P)H dehydrogenase complex. *Biochim. Biophys. Acta* 1807, 945–953. doi: 10.1016/j.bbabo.2010.10.015
- Pesaresi, P., Gardner, N. A., Masiero, S., Dietzmann, A., Eichacker, L., Wickner, R., et al. (2003). Cytoplasmic N-terminal protein acetylation is required for efficient photosynthesis in Arabidopsis. *Plant Cell* 15, 1817–1832. doi: 10.1105/tpc.012377.NatA
- Posewitz, M. C., King, P. W., Smolinski, S. L., Zhang, L., Seibert, M., and Ghirardi, M. L. (2004). Discovery of two novel radical S-adenosylmethionine proteins required for the assembly of an active [Fe] hydrogenase. *J. Biol. Chem.* 279, 25711–25720. doi: 10.1074/jbc.M403206200
- Pribil, M., Pesaresi, P., Hertle, A., Barbato, R., and Leister, D. (2010). Role of plastid protein phosphatase TAP38 in LHCII dephosphorylation and thylakoid electron flow. *PLoS Biol.* 8:e1000288. doi: 10.1371/journal.pbio.1000288
- Roháček, K. (2002). Chlorophyll fluorescence parameters: the definitions, photosynthetic meaning, and mutual relationships. *Photosynthetica* 40, 13–29. doi: 10.1023/A:1020125719386
- Ruban, A. V. (2016). Nonphotochemical chlorophyll fluorescence quenching: mechanism and effectiveness in protecting plants from photodamage. *Plant Physiol.* 170, 1903–1916. doi: 10.1104/pp.15.01935
- Rühle, T., Razeghi, J. A., Vamvaka, E., Viola, S., Gandini, C., Kleine, T., et al. (2014). The Arabidopsis protein CONSERVED ONLY IN THE GREEN LINEAGE160 promotes the assembly of the membranous part of the chloroplast ATP synthase. *Plant Physiol.* 165, 207–226. doi: 10.1104/pp.114.237883
- Rungrat, T., Awlia, M., Brown, T., Cheng, R., Sirault, X., Fajkus, J., et al. (2016). Using phenomic analysis of photosynthetic function for abiotic stress response gene discovery. *Arabidopsis Book* 14:e0185. doi: 10.1199/tab.0185
- Scheibe, R. (2004). Malate valves to balance cellular energy supply. *Physiol. Plant.* 120, 21–26. doi: 10.1111/j.0031-9317.2004.0222.x
- Schmitz, J., Heinrichs, L., Scossa, F., Fernie, A. R., Oelze, M. L., Dietz, K. J., et al. (2014). The essential role of sugar metabolism in the acclimation response of *Arabidopsis thaliana* to high light intensities. *J. Exp. Bot.* 65, 1619–1636. doi: 10.1093/jxb/eru027
- Schmitz, J., Schöttler, M., Krueger, S., Geimer, S., Schneider, A., Kleine, T., et al. (2012). Defects in leaf carbohydrate metabolism compromise acclimation to high light and lead to a high chlorophyll fluorescence phenotype in *Arabidopsis thaliana*. *BMC Plant Biol.* 12:8. doi: 10.1186/1471-2229-12-8
- Schreiber, U., Bilger, W., and Neubauer, C. (1995). “Chlorophyll fluorescence as a noninvasive indicator for rapid assessment of *In Vivo* photosynthesis,” in *Ecophysiology of Photosynthesis*, eds E. D. Schulze and M. Caldwell (Berlin: Springer), 49–70.
- Schreiber, U., Schliwa, U., and Bilger, W. (1986). Continuous recording of photochemical and non-photochemical chlorophyll fluorescence quenching with a new type of modulation fluorometer. *Photosynth. Res.* 10, 51–62.
- Schroda, M., Vallon, O., Wollman, F. A., and Beck, C. F. (1999). A chloroplast-targeted heat shock protein 70 (HSP70) contributes to the photoprotection and repair of photosystem II during and after photoinhibition. *Plant Cell Online* 11, 1165–1178. doi: 10.1105/tpc.11.6.1165
- Shikanai, T., Endo, T., Hashimoto, T., Yamada, Y., Asada, K., and Yokota, A. (1998). Directed disruption of the tobacco *ndhB* gene impairs cyclic electron flow around photosystem I. *Proc. Natl. Acad. Sci. U.S.A.* 95, 9705–9709.
- Shikanai, T., Munekage, Y., Shimizu, K., Endo, T., and Hashimoto, T. (1999). Identification and characterization of Arabidopsis mutants with reduced quenching of chlorophyll fluorescence. *Plant Cell Physiol.* 40, 1134–1142.
- Somerville, C. R. (1986). Analysis of photosynthesis with mutants of higher plants and algae. *Annu. Rev. Plant Physiol.* 37, 467–506. doi: 10.1146/annurev.pp.37.060186.002343
- Steinberger, I., Egidio, F., and Schneider, A. (2015). Chlorophyll fluorescence measurements in Arabidopsis wild-type and photosystem II mutant leaves. *Bio-protocol* 5:e1532. doi: 10.21769/BioProtoc.1532
- Suorsa, M., Jarvi, S., Grieco, M., Nurmi, M., Pietrzykowska, M., Rantala, M., et al. (2012). PROTON GRADIENT REGULATION5 is essential for proper acclimation of Arabidopsis photosystem I to naturally and artificially fluctuating light conditions. *Plant Cell* 24, 2934–2948. doi: 10.1105/tpc.112.097162

- Takabayashi, A., Ishikawa, N., Obayashi, T., Ishida, S., Obokata, J., Endo, T., et al. (2009). Three novel subunits of Arabidopsis chloroplastic NAD(P)H dehydrogenase identified by bioinformatic and reverse genetic approaches. *Plant J.* 57, 207–219. doi: 10.1111/j.1365-313X.2008.03680.x
- Takahashi, S., Bauwe, H., and Badger, M. (2007). Impairment of the photorespiratory pathway accelerates photoinhibition of photosystem II by suppression of repair but not acceleration of damage processes in Arabidopsis. *Plant Physiol.* 144, 487–494. doi: 10.1104/pp.107.097253
- Tardieu, F., Cabrera-Bosquet, L., Pridmore, T., and Bennett, M. (2017). Plant phenomics, from sensors to knowledge. *Curr. Biol.* 27, R770–R783. doi: 10.1016/j.cub.2017.05.055
- Taylor, W. C., Barkan, A., and Martienssen, R. A. (1987). Use of nuclear mutants in the analysis of chloroplast development. *Dev. Genet.* 8, 305–320. doi: 10.1002/dvg.1020080503
- Terashima, M., Freeman, E. S., Jinkerson, R. E., and Jonikas, M. C. (2015). A fluorescence-activated cell sorting-based strategy for rapid isolation of high-lipid *Chlamydomonas* mutants. *Plant J.* 81, 147–159. doi: 10.1111/tpj.12682
- Terashima, M., Specht, M., Naumann, B., and Hippler, M. (2010). Characterizing the anaerobic response of *Chlamydomonas reinhardtii* by quantitative proteomics. *Mol. Cell. Proteomics* 9, 1514–1532. doi: 10.1074/mcp.M900421-MCP200
- Thiele, A., Winter, K., and Krause, G. H. (1997). Low inactivation of D1 protein of photosystem II in young canopy leaves of *Anacardium excelsum* under high-light stress. *J. Plant Physiol.* 151, 286–292. doi: 10.1016/S0176-1617(97)80254-4
- Tolter, D., Ghysels, B., Alric, J., Petroutsos, D., Tolstygina, I., Krawietz, D., et al. (2011). Control of hydrogen photoproduction by the proton gradient generated by cyclic electron flow in *Chlamydomonas reinhardtii*. *Plant Cell* 23, 2619–2630. doi: 10.1105/tpc.111.086876
- Tseng, Y.-C., and Chu, S.-W. (2017). High spatio-temporal-resolution detection of chlorophyll fluorescence dynamics from a single chloroplast with confocal imaging fluorometer. *Plant Methods* 13:43. doi: 10.1186/s13007-017-0194-2
- van Rooijen, R., Aarts, M. G. M., and Harbinson, J. (2015). Natural genetic variation for acclimation of photosynthetic light use efficiency to growth irradiance in Arabidopsis. *Plant Physiol.* 167, 1412–1429. doi: 10.1104/pp.114.252239
- Varotto, C., Maiwald, D., Pesaresi, P., Jahns, P., Salamini, F., and Leister, D. (2002). The metal ion transporter IRT1 is necessary for iron homeostasis and efficient photosynthesis in *Arabidopsis thaliana*. *Plant J.* 31, 589–599. doi: 10.1046/j.1365-313X.2002.01381.x
- Varotto, C., Pesaresi, P., Maiwald, D., Kurth, J., Salamini, F., and Leister, D. (2000a). Identification of photosynthetic mutants of Arabidopsis by automatic screening for altered effective quantum yield of photosystem 2. *Photosynthetica* 38, 497–504. doi: 10.1023/A:1012445020761
- Varotto, C., Pesaresi, P., Meurer, J., Oelmüller, R., Steiner-Lange, S., Salamini, F., et al. (2000b). Disruption of the Arabidopsis photosystem I gene *psaE1* affects photosynthesis and impairs growth. *Plant J.* 22, 115–124. doi: 10.1046/j.1365-313X.2000.00717.x
- Virlet, N., Sabermanesh, K., Sadeghi-Tehran, P., and Hawkesford, M. J. (2017). Field Scanalyzer: An automated robotic field phenotyping platform for detailed crop monitoring. *Funct. Plant Biol.* 44, 143–153. doi: 10.1071/FP16163
- Walter, A., Liebisch, F., and Hund, A. (2015). Plant phenotyping: from bean weighing to image analysis. *Plant Methods* 11:14. doi: 10.1186/s13007-015-0056-8
- Walters, R. G., Shephard, F., Rogers, J. J. M., Rolfe, S. A., and Horton, P. (2003). Identification of mutants of Arabidopsis defective in acclimation of photosynthesis to the light environment. *Plant Physiol.* 131, 472–481. doi: 10.1104/pp.015479
- Wang, H., Qian, X., Zhang, L., Xu, S., Li, H., Xia, X., et al. (2017). Detecting crop population growth using chlorophyll fluorescence imaging. *Appl. Opt.* 56, 9762–9769. doi: 10.1364/AO.56.009762
- White, J. W., Andrade-Sanchez, P., Gore, M. A., Bronson, K. F., Coffelt, T. A., Conley, M. M., et al. (2012). Field-based phenomics for plant genetics research. *Field Crop Res.* 133, 101–112. doi: 10.1016/j.fcr.2012.04.003
- Xie, B., Stessman, D., Hart, J. H., Dong, H., Wang, Y., Wright, D. A., et al. (2014). High-throughput fluorescence-activated cell sorting for lipid hyperaccumulating *Chlamydomonas reinhardtii* mutants. *Plant Biotechnol. J.* 12, 872–882. doi: 10.1111/pbi.12190
- Xu, L., Cruz, J. A., Savage, L. J., Kramer, D. M., and Chen, J. (2015). Plant photosynthesis phenomics data quality control. *Bioinformatics* 31, 1796–1804. doi: 10.1093/bioinformatics/btu854
- Yamori, W., and Shikanai, T. (2016). Physiological functions of cyclic electron transport around photosystem I in sustaining photosynthesis and plant growth. *Annu. Rev. Plant Biol.* 67, 81–106. doi: 10.1146/annurev-arplant-043015-112002
- Yang, Y., Xu, L., Feng, Z., Cruz, J. A., Savage, L. J., Kramer, D. M., et al. (2017). PhenoCurve: capturing dynamic phenotype-environment relationships using phenomics data. *Bioinformatics* 33, 1370–1378. doi: 10.1093/bioinformatics/btw673
- Yin, K., Gao, C., and Qiu, J.-L. (2017). Progress and prospects in plant genome editing. *Nat. Plants* 3:17107. doi: 10.1038/nplants.2017.107
- You, M. K., Lim, S. H., Kim, M. J., Jeong, Y. S., Lee, M. G., and Ha, S. H. (2015). Improvement of the fluorescence intensity during a flow cytometric analysis for rice protoplasts by localization of a green fluorescent protein into chloroplasts. *Int. J. Mol. Sci.* 16, 788–804. doi: 10.3390/ijms16010788
- Zhang, L., Duan, Z., Zhang, J., and Peng, L. (2016). BIOGENESIS FACTOR REQUIRED FOR ATP SYNTHASE 3 facilitates assembly of the chloroplast ATP synthase complex in Arabidopsis. *Plant Physiol.* 171, 1291–1306. doi: 10.1104/pp.16.00248

Conflict of Interest Statement: The authors declare that the research was conducted in the absence of any commercial or financial relationships that could be construed as a potential conflict of interest.

Copyright © 2018 Rühle, Reiter and Leister. This is an open-access article distributed under the terms of the Creative Commons Attribution License (CC BY). The use, distribution or reproduction in other forums is permitted, provided the original author(s) and the copyright owner are credited and that the original publication in this journal is cited, in accordance with accepted academic practice. No use, distribution or reproduction is permitted which does not comply with these terms.

6 Discussion

6.1 Identification of auxiliary biogenesis factors

In the evolution of the photosynthetic eukaryotic cell, numerous light-dependent mechanisms for the regulation of chloroplast functions have emerged. Most of such mechanisms are coupled to the stromal redox poise, which is directly linked to photosynthetic electron transport rates (reviewed in Cejudo et al., 2019). In contrast to most bacterial plasma and mitochondrial respiratory membranes, which store energy predominantly as transmembrane electric field ($\Delta\Psi$), the *pmf* of the chloroplast thylakoid membrane additionally consists of a proton concentration gradient (ΔpH) component (Davis and Kramer, 2020). Elevated ΔpH triggers several protective mechanisms in photosynthesis, such as downregulation of the electron transport chain at the level of the Cytochrome (Cyt) *b6f* complex, the action of the photosystem II (PSII) subunit PsbS, and the activation of the xanthophyll cycle, leading to heat-dissipation of excitation energy (reviewed in Ruban, 2016; Armbruster et al., 2017). Monitoring of chlorophyll fluorescence parameters can not only be employed to probe for defects in the electron transport chain itself (Chapter 5), but also allows measuring of NPQ parameters, thus enabling the dissection of complex photosynthetic phenotypes (Chapter 4). Especially when combined with video imaging techniques that permit non-invasive high-throughput screening of young plants, measuring of chlorophyll fluorescence can be a powerful tool in identifying factors required for the functioning of the photosynthetic machinery.

Compared to mutants of other photosynthetic complexes, perturbations in the assembly of the cpATP synthase are easily overlooked, since most auxiliary factors are non-essential (Chapters 2 and 3; Benz et al., 2009; Rühle et al., 2014; Zhang et al., 2016; 2018) and only reductions of steady-state levels below a certain threshold lead to visible growth reductions under controlled conditions (Rott et al., 2011). Due to its specialized role in the thylakoid membrane, harvesting the trans-thylakoid proton gradient generated by the light-driven reactions of photosynthesis, perturbations in the activity of the cpATP synthase lead to an accumulation of protons in the lumen, thus triggering NPQ mechanisms (Maiwald et al., 2003; Dal Bosco et al., 2004). CpATP synthase activity is coupled to the redox status of the stroma through a chloroplast-specific regulatory loop in the γ -subunit, rapidly activating the enzyme in the light and deactivating it in the dark (reviewed in Hisabori et al., 2013). Recent evidence suggests that the γ -subunit may also play a crucial role in fine tuning ATP synthase activity in the light and participates in the regulation of electron transport rates in response to the availability of electron acceptors downstream of photosystem I (PSI) (Carrillo et al., 2016; Kanazawa et al., 2017; Takagi et al., 2017). Especially under low light intensities, NADPH thioredoxin reductase C (NTRC), plays a role in the activation of the cpATP synthase (Carrillo et al., 2016). Thus, monitoring NPQ parameters at lower light intensities is not only a powerful

tool for the identification of new factors (Chapter 2), but also allows the functional dissection of phenotypes generated by mutations that cause only mild disturbances in the accumulation of cpATP synthase (Chapter 3).

6.2 Assembly of organellar ATP synthases

The bacterial origin of organellar ATP synthase structure is apparent. Whereas the mitochondrial ATP synthase acquired several additional subunits, which also increased the complexity of its biogenesis process (reviewed in Rühle and Leister, 2015), the cpATP synthase is still remarkably similar to its bacterial ancestors, especially compared to cyanobacteria (Hahn et al., 2018). Nevertheless, emerging evidence suggests that also the assembly of chloroplast ATP synthases might be different from its bacterial counterpart (Chapters 2 and 3; Mao et al., 2015; Zhang et al., 2016; 2018).

6.2.1 CGLD11 is required for early CF₁ assembly

Assembly of bacterial F₁ could be achieved in vitro from purified components (Sternweis and Smith, 1977; Sternweis 1978) and no specialized auxiliary factor is known to assist in the assembly of non-photosynthetic bacterial F₁ (Rühle and Leister, 2015). In contrast, mitochondrial F₁ assembly is dependent on the chaperones Atp11p/Atp12p that bind to hydrophobic patches of the β - and α -subunits, respectively and prevent aggregation or unfavorable homodimerization (Wang et al., 2000; Wang and Ackermann 2000). CF₁ assembly has been shown to be dependent on the stromal chaperonin Cpn60 (Chen and Jagendorf, 1994). However, since Cpn60 alone was not sufficient to reconstitute CF₁ from denatured subunits the existence of additional chaperones was proposed. Whereas this was already shown to be true for the γ -subunit (Mao et al., 2015), corresponding α/β chaperones were still missing. Based on our results we concluded that CGLD11 (also known as BFA3) might exert a similar function as Atp11p, since it physically interacted with CF₁- β and its disruption led to reduced levels of cpATP synthase (Chapter 2). Consistently, Zhang et al. (2016) could demonstrate that CGLD11/BFA3, similar to Atp11p in mitochondria, binds close to the catalytic site, which harbors hydrophobic amino acids and shows the tendency to aggregate (Wang and Ackerman, 2000; Ackerman 2002). Moreover, they found that the amino acid residues required for binding of CGLD11/BFA3 were already present prior to its emergence in Chloroplastida and proposed that they might have evolved to confer an increased affinity for binding of inhibitory Mg⁺ADP to the catalytic site. Since $\alpha\beta$ -heterodimers already possess ATPase activity (Du and Gromet-Elhanan, 1999), increased binding affinity for inhibiting Mg⁺ADP might play a role in the assembly process to prevent wasteful ATP hydrolysis by assembly intermediates. Due to the diurnal fluctuation of the chloroplast ATP supply, this might be especially important during the night when the ATP pool is low (Rühle and Leister, 2015).

It is intriguing to speculate about why chloroplast and mitochondrial F_1 - β had to develop such a special protective mechanism independently of each other. Indeed, increased regulatory importance of $Mg^{+}ADP$ in inhibiting the ATP hydrolysis function of the F_1 part was proposed for both organellar ATP synthases (Fitin et al., 1979; Bar-Zvi et al., 1982). Moreover, β -subunits of chloroplasts and mitochondria are remarkably conserved (67% sequence identity) and the nucleotide binding sites are identical (Hahn et al., 2018). Interestingly, we found CGLD11 able to interact also with the (plant) mitochondrial β -subunit, in yeast two-hybrid experiments, suggesting that the site of interaction may be conserved across organelles (Chapter 2, Fig. 9). Since Atp11p is absent in chloroplasts, CGLD11 could carry out a similar function by masking the hydrophobic catalytic site and promoting the incorporation of the β -subunit into the CF_1 module.

Remarkably, we found CGLD11 also localized to mitochondria in organelle fractionation and subsequent immunodetection experiments (Chapter 2, Fig. 2), raising the question whether CGLD11 might act as a β -subunit chaperone in both organelles. However, subunit accumulation and ATP production of the mitochondrial ATP synthase were not impaired in *atcgld11* mutant plants (Chapter 2, Fig. 3), which renders an involvement of CGLD11 in the formation of the mitochondrial ATP synthase assembly questionable. Conversely, Arabidopsis Atp11p fused to a chloroplast transit peptide was not able to complement the CGLD11/BFA3 mutant phenotype, further contradicting an inter-organellar interchangeability of the chaperones (Zhang et al., 2016).

6.2.2 CGL160 acquired a central role in the assembly of CF_0 and linkage to CF_1

It is generally accepted that the assembly of CF_0 and subsequent joining to CF_1 is a critical step in the biogenesis of bacterial and organellar ATP synthases, since incorrect or premature formation of the proton translocating channel between the c-ring and the a-subunit (subunit 9 and 6 in mitochondria, respectively) leads to uncontrolled dissipation of the transmembrane *pmf* (Birkenhäger et al., 1999; Franklin et al., 2004). Whereas the final steps of bacterial ATP synthase assembly are not fully understood, they have been elegantly resolved in both yeast and human mitochondria (reviewed in Song et al., 2018). A key intermediate in human ATP synthase assembly consists of the ATP9-ring, F_1 and the peripheral stator (He et al., 2018), whereas in yeast the INA complex (INAC) was shown to assist in the addition of the ATP9-ring to an intermediate containing F_1 , the peripheral stator, as well as the subunits ATP6 and ATP8 (Naumenko et al., 2017). Although their exact assembly pathway and the order of addition of the subunits differ, the formation of the proton-translocating unit is the final step in the assembly of both the yeast and the human ATP synthase (Song et al., 2018). Given the crucial role of the cpATP synthase, not only in utilization, but also in the regulation of the *pmf*, it is conceivable that formation of the proton-conducting channel in chloroplasts might be tightly regulated.

Several lines of evidence support the notion that CGL160 might play a role in this process: (i) The membranous Atp1/Unc1-like domain and the soluble chloroplast-specific N-terminus separately accounted for the severe reduction of cpATP synthase amounts in mutants of AtCGL160 (Chapter 3, Fig. 3), (ii) AtCGL160 was associated to later cpATP synthase assembly stages (Chapter 3, Fig. 4), and (iii) AtCGL160 physically interacted with subunits of the c-ring and the peripheral stator (Rühle et al., 2014), as well as CF₁ (Chapter 3, Figs. 5 and 6).

Several auxiliary factors were shown to assist in the membrane insertion of bacterial CF_O components (Rühle and Leister, 2015). However, it is not clear how the final steps of ATP synthase assembly are mediated, since stable assembly intermediates, lacking the respective subunit, could be identified for both $\Delta\delta$ and Δa mutants (Ono et al., 2004; Kuruma et al., 2012; Brockmann et al., 2013; Hilbers et al., 2013). Whereas F_O intermediates were observed in bacteria and mitochondria, accumulation of CF_O is strictly dependent on the presence of CF₁ (Chapter 2; Lemaire and Wollman, 1989; Mao et al., 2015; Zhang et al., 2016; 2018). Conversely, the presence of the c-ring was shown to be an essential prerequisite for accumulation of CF₁ in *Chlamydomonas* (Lemaire and Wollman, 1989). However, knockouts of CF_O-a and -b led to the accumulation of residual amounts of CF₁, suggesting that their presence is not strictly required for the membrane association of CF₁. In addition, in the *Arabidopsis* mutant deficient of AEF1, a PPR protein required for splicing and editing of the plastome-encoded *atpF* (CF_O-b), b-subunits were present sub-stoichiometrically, whereas CF₁- δ seems to be strictly required for accumulation of ATP synthase subunits (Maiwald et al., 2003). Intriguingly, CF_O-a was not enriched to the same extent ($\log_2FC \sim 2.8$) as the other ATP synthase subunits ($\log_2FC > \sim 4.4$), including CF₁- δ , in oeAtCGL160 colP fractions (Chapter 3, Fig. 4A, Supplemental Table S1), implying that AtCGL160 might be associated to an intermediate lacking CF_O-a. Analogous to the proposed model for human mitochondria (He et al., 2018), addition of subunit a and formation of the proton-translocating unit could be the last step of cpATP synthase assembly. In summary, a central role for CGL160 in the assembly of the cpATP synthase by mediating c-ring assembly and facilitating the joining of CF₁ to CF_O is proposed in Figure 6. Like INAC in yeast mitochondria, CGL160 could act as a “placeholder” by interacting with CF_O-c, CF_O-b and CF₁- β , thus preventing the premature formation of the proton-translocating unit (Fig. 6).

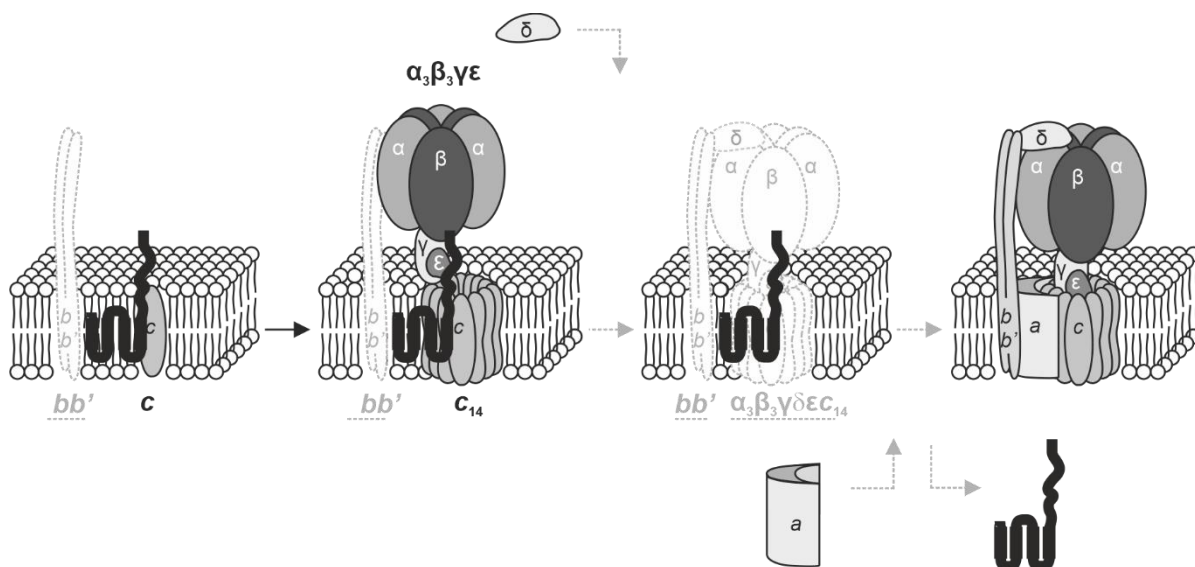


Figure 6. Model of CGL160-mediated cpATP synthase assembly. CF₁ assembly is omitted for clarity. The membranous Atp1/Unc1-like domain of CGL160 initially interacts with CF₀-c and facilitates c-ring assembly. Stator subunits b and b' might already be associated by CGL160/CF₀-b mediated interaction. The chloroplast-specific soluble domain recruits CF₁ by interaction with the membrane-proximal domain of CF₁-β. Establishment of the proton-translocating unit through addition of CF₀-a and dissociation of CGL160 might be the final step of assembly. Figure was adapted and modified from Rühle and Leister (2015).

6.2.3 ATP synthase regulation by night

The oxidation of the γ -subunit and subsequent inactivation of the cpATP synthase upon prolonged dark incubation (e.g. by night) was proposed to prevent futile depletion of the ATP pool by the hydrolysis function of the enzyme (Ort and Oxborough, 1992). However, analysis of the constitutively redox-activated γ -subunit mutant *gamera* revealed increased stability of photosynthetic complexes upon prolonged darkness, suggesting that a certain degree of ATPase activity may be beneficial during the night to maintain a baseline *pmf*, which might be needed to support proton gradient-dependent import and repair mechanisms (Kohzuma et al., 2017). The proposed central role of CGL160 in the assembly of the ATP synthase might thus also be important during the night to prevent uncoupled proton efflux by assembly intermediates and preserving the *pmf* in darkness. Remarkably, *atcg160* mutants exhibited a variegated leaf phenotype when grown under short-day conditions, whereas mutant plants grown in conditions with a shortened night-period did not display variegation (Fristedt et al., 2015). This phenotype could not be observed in *atcg1d11* mutants, although cpATP synthase accumulation is reduced comparably (Chapter 2, Fig. 1; Chapter 3, Figs. 1, 3), indicating that this might not be a general phenotype of mutants defective in cpATP synthase assembly.

Variegation is defined as the presence of chlorotic sections with abnormally developed chloroplasts in otherwise normal green tissue (reviewed in Aluru et al., 2006). The two best characterized mutants with a variegated leaf phenotype are *immutans*, defective in the plastid terminal oxidase (PTOX) and *var2* a knockout of the thylakoid FtsH2 protease (reviewed in

Putarjunan et al., 2013). PTOX is a homologue of the mitochondrial alternative oxidase (AOX) and transfers electron from plastoquinol to stromal oxygen, creating water and plastoquinone (reviewed in Foudree et al., 2012). PTOX was therefore proposed to act as an electron “safety valve” by relieving excitation pressure from the plastoquinone pool and protecting photosynthetic complexes from overreduction. Whereas the primary cause for the white sectors in *immutans* might be the impairment of the plastoquinone-dependent phytoene desaturase and consequently lack of photoprotective pigments, overaccumulation of phytoene was not observed in *var2* (Liu et al. 2010). The FtsH2 protease is predominantly involved in the repair cycle of PSII by degrading photooxidatively damaged D1 proteins, but has also other targets in the thylakoid membrane (Liu et al. 2010). As both *immutans* and *var2* variegation increased with higher light intensities, it has been proposed that variegation in general might be caused by mutations that predispose chloroplasts to photooxidation under high excitation pressure (Putarjunan et al., 2013). Considering that variegation in *atcgl160* only emerges during prolonged night, the underlying mechanism causing chlorotic lesions might be independent of photosynthetic excitation pressure. Interestingly, overexpression of the membranous part of CGL160 in *oeAtCGL160C* lines could not rescue variegation of the mutant background (Chapter 3, Fig. 1B), indicating that the function of the soluble chloroplast-specific domain may play a role in this process. Nevertheless, further genetic and biochemical studies, such as monitoring of phytoene desaturase activity and targeted second-site suppressor analysis, are required to dissect the mechanism of variegation caused by disruption of CGL160.

Besides the already mentioned light-dependent thiol modification of the γ -subunit, the cpATP synthase is subjected to other posttranslational modifications, including acetylation and phosphorylation (Kanekatsu et al., 1998; Schmidt et al., 2013; 2017). Schmidt et al. (2013) could show that phosphorylation affects the stability and nucleotide affinity of the complex. Given the very slow turnover rate of the cpATP synthase compared to other thylakoid complexes (reviewed in Schöttler et al., 2015), posttranslational modifications may thus provide an elegant mechanism to control the accumulation of the enzyme in response to environmental stimuli. Indeed, differential phosphorylation of the β -subunit by the chloroplast calmodulin kinase II during the night was shown in a phosphoproteomics screen (Reiland et al., 2009). Interestingly, also peptides of the soluble domain of AtCGL160 could be identified as targets for phosphorylation by Reiland et al. (2009). Adjacent to the identified serine, CGL160 harbors several additional putative phosphorylation sites, including two sites that are strictly conserved throughout the green lineage (Chapter 3, Supplemental Fig. S1). Since CGL160 might be target for regulatory modulation, it is tempting to speculate that also the assembly of the ATP synthase could be regulated in response to diurnal fluctuations. Genetic approaches, such as the exchange of putative phosphorylation sites by phospho-ablative/-

mimetic amino acids combined with targeted phospho-proteomics under different conditions (e. g. day vs. night) might help to elucidate a possible regulatory role for CGL160.

6.3 Assembly of chloroplast ribosomes

6.3.1 Consequences of chloroplast-to-nucleus gene transfer

Early in the evolution from endosymbiont to organelle, most of the former (cyano)bacterial genes were transferred to the host nucleus, leaving the chloroplast with a highly conserved gene-set of around 100 protein coding genes (reviewed in Timmis et al., 2004). Due to the massive reduction of the chloroplast genome, the translational diversity of plastid ribosomes changed from roughly 4000 different proteins to a small set of mostly membrane-targeted components of the photosynthetic machinery (Tiller and Bock, 2014; Sun and Zerges, 2015). Since biogenesis of the translation machinery in bacteria markedly limits cell division rates, it was proposed that prokaryotic ribosomes are optimized to translate their own proteinaceous components (Reuveni et al., 2017). However, most chloroplast ribosomal proteins (cpRPs) are encoded in the nucleus and translated on cytosolic ribosomes, reducing the need for extensive autocatalytic specialization (Zoschke and Bock, 2018). Conceivably, this shift in translational specialization might be one reason for the structural changes that occurred during evolution of chloroplast ribosomes, including differences in rRNA processing, addition of protein extensions, loss of RPs and acquisition of novel RPs (Ahmed et al., 2016; Graf et al., 2016; Bieri et al., 2017; Perez-Boerema et al., 2018).

Most structural changes in cpRP content occurred in the peripheral regions of the LSU (Ahmed et al., 2016; Graf et al., 2016; Bieri et al., 2017). Especially the later stages of higher plant 50S biogenesis diverge from *E. coli*, mostly due to changes in rRNA processing, like cleavage of the former 3' end of the 23S rRNA to yield a 4.5S rRNA (Whitfield et al., 1978; Keus et al., 1984; Leal-Klevezas et al., 2000). Moreover, processing of the 23S rRNA at two sites, so called "hidden breaks" occurs after maturation of the 23S rRNA (Kössel et al., 1985). Consequently, new auxiliary components had to be acquired to sustain efficient plastid ribosome biogenesis. Indeed, several factors, required for 50S biogenesis do not possess clear bacterial orthologs (Bellaoui et al., 2003; Nishimura et al., 2010; Paieri et al., 2018).

6.3.2 CGL20 is required for late assembly steps of chloroplast LSU

The structural defects identified in *atcg/20ab* in 23S rRNA processing and RP composition of the LSU provide evidence that CGL20 could also have been recruited in the green lineage to support later stages of 50S biogenesis (Chapter 4). Due to the highly dynamic character of ribosome biogenesis, it is not possible to define an exact sequence of late 50S assembly. However, based on rRNA processing patterns of identified auxiliary factors, a rough hierarchy of rRNA processing events is proposed in Figure 7.

Defects in the formation of hidden breaks, observed in mutants of factors required for early 23S and 4.5S rRNA processing events like DCL, RHON1, RH22, SOT1, or RH50, suggest that it might occur prior to the cleavage of the 23S rRNA (Bellaoui et al., 2003; Stoppel et al., 2012; Chi et al., 2012; Wu et al., 2016; Paieri et al., 2018). Conversely, the 4.5S rRNA was processed efficiently in mutants of factors involved in the formation of hidden breaks (Beligni and Mayfield 2008; Nishimura et al., 2010). Likewise, 4.5S rRNA processing was not perturbed in *atcg/20ab*, implying that it may act in later steps (Chapter 4, Fig. 6).

Post-maturation processing of the 23S rRNA occurs at two sites, yielding fragments of 0.5 kb (5' fragment), 1.3 kb (middle fragment), and 1.1 kb (3' fragment) (Fig. 7). CSP41 and RH39 were proposed to be required for formation of hidden breaks close to the 5' and 3' ends of the 23S rRNA, respectively (Beligni and Mayfield, 2008; Nishimura et al., 2010). Based on the observation that 5' and 3' specific hidden break products as well as their respective precursors (1.8 kb and 2.4 kb) accumulated independently in mutants of CSP41 and RH39, it was suggested that both processing events occur autonomously (Nishimura et al., 2010). This is consistent with the 23S rRNA pattern of *dcl*, which showed normal accumulation of the 5' fragment, but reduced abundance of 1.3 and 1.1 hidden break products (Bellaoui et al., 2003). Likewise, only the 1.3 and 1.1 hidden break products were reduced in *atcg/20ab*, whereas the 0.5 kb product accumulated normally (Chapter 4, Fig. 6). Taken together, our results provide evidence that the presence of CGL20 is not required for 4.5S processing or 5' hidden break processing, but promotes RH39-mediated 3' cleavage, corroborating the independence of the processing events (Fig. 7).

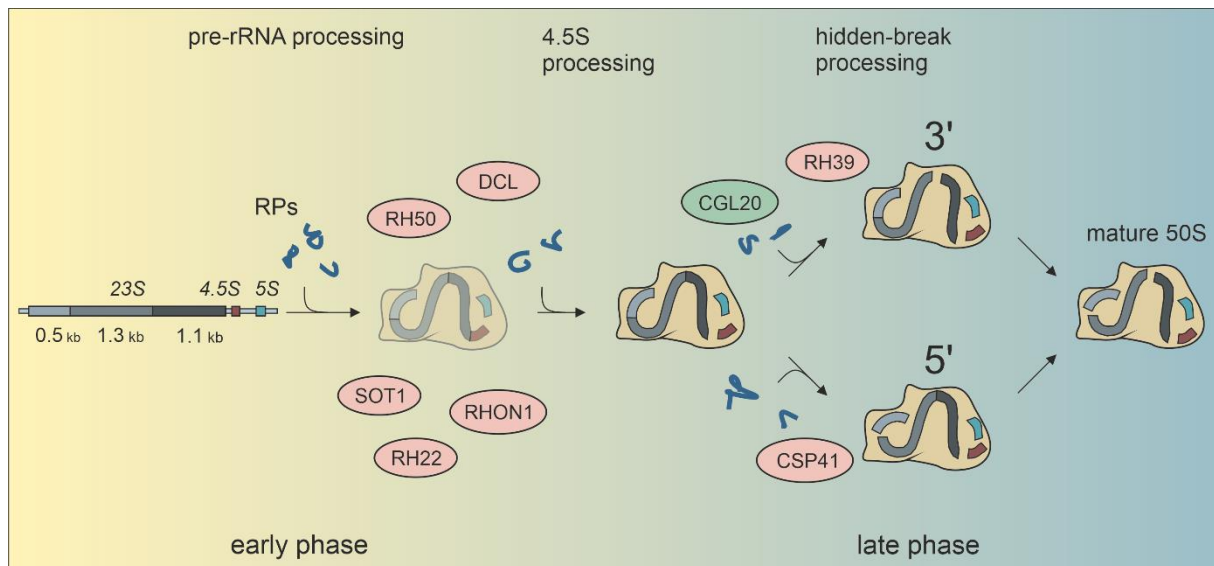


Figure 7. Assembly of the chloroplast 50S ribosomal subunit. LSU assembly is initiated by cotranscriptional binding of ribosomal proteins (blue) to the rRNA (colored in cyan for 5S, amber for 4.5S, and shades of grey for 23S rRNA). In the early phase, RH50 (Paieri et al., 2018), RH22 (Chi et al., 2012), DCL (Bellaoui et al., 2003), RHON1 (Stoppel et al., 2012), and SOT1 (Wu et al., 2016) are involved in various stages of 4.5S and 23S rRNA preprocessing. CSP41 (Beligni and Mayfield, 2008) and RH39 (Nishimura et al., 2010) carry out independent processing of the 5' and 3' hidden break site, respectively. CGL20 (green) promotes RH39 mediated processing of the 3' hidden break site.

6.3.3 Adaptations to membrane targeting

Post-maturation processing of the LSU rRNA is common in nature and was found to occur in multiple biological groups, including (cyano)bacteria (reviewed in Evguenieva-Hackenberg, 2005), fungi, insects, and mammals (Winnebeck et al., 2010; Azpurua et al., 2013; Navarro-Ródenas et al., 2018). Since post-maturation rRNA processing seems to be absent in the SSU, proposed functions of hidden-break induced structural changes of the LSU include the promotion of translational fidelity in naked mole rat (Azpurua et al., 2013), but also regulation of translational elongation in response to light in the cyanobacterium *Synechococcus elongatus* (Doolittle, 1973). Accordingly, the exact purpose of hidden break processing in higher plant chloroplasts is not clear. However, the severe phenotype of the RH39 knockout in *Arabidopsis* indicates that the post-maturation separation of the 23S rRNA might be required for efficient chloroplast translation in higher plants (Nishimura et al., 2010).

The absence of 3' post-maturation processing of the 23S rRNA in *Chlamydomonas* chloroplasts (Turmel et al., 1993) as well as the lack of a canonical RNA binding domain suggest that CGL20 is not directly involved in introducing the hidden break (Chapter 4). Due to their RNA binding properties, ribosomal proteins often contain positively charged stretches, making them susceptible for aggregation (Jäkel et al., 2002). Studies in yeast could establish that ribosomal proteins are therefore often associated to dedicated chaperones that can bind newly synthesized RPs cotranslationally (reviewed in Pillet et al., 2017). These specialized

chaperones harbour structurally distinct domains (for example negatively charged), enabling them to bind and protect aggregation-prone regions on ribosomal proteins (Pausch et al., 2015). Remarkably, the C-terminus of AtCGL20 is predominantly negatively charged, a feature, which is conserved throughout the green lineage (Chapter 4, Fig. 1), potentially enabling CGL20 to mask positively charged, aggregation-prone patches on ribosomal proteins.

Due to N- and C-terminal extensions and the acquisition of novel ribosomal proteins, the protein-to-RNA ratio changed from ~1:3 in bacteria to ~2:3 in chloroplasts (Yamaguchi and Subramanian, 2000; Yamaguchi et al., 2000), thus following the general trend of replacing RNA in chloroplast ribonucleoproteins by proteinaceous components (Barbrook et al., 2006). As mentioned earlier, cpRP extensions in general were mainly acquired in the LSU (Graf et al., 2016). Consistent with the highly conserved rRNA core, containing the peptidyl transfer centre, most changes can be observed in the peripheral regions of LSU (Graf et al., 2016; Bieri et al., 2017). A remarkable architectural alteration is the – as compared to bacteria – narrowed polypeptide exit-tunnel of the chloroplast LSU, which is due to extensions of several cpRPs (Ahmed et al., 2016; Graf et al., 2016; Bieri et al., 2017). Moreover, a conglomerate of cpRP extensions adjacent to the polypeptide exit-tunnel could be identified (Graf et al., 2016). These structural adaptations were proposed to have coevolved with the considerably changed cotranslational membrane targeting mechanism of chloroplasts as compared to bacteria (Graf et al., 2016; Bieri et al., 2017). CpSRP54, a chloroplast-specific component of the targeting machinery has recently been shown to bind to uL4, which is not directly adjacent to the tunnel-exit (Hristou et al., 2019). Nevertheless, it is conceivable that the structural changes of the chloroplast LSU periphery enable ribosomes to bind to the thylakoid membrane or other components of the targeting and membrane insertion machinery, such as SecY/E and ALB3 (Graf et al., 2016; Hristou et al., 2019).

Intriguingly, although the abundance of the soluble chloroplast-encoded RuBisCO large subunit (RbcL) was drastically reduced in *nara12* (Necessary for the Achievement of RuBisCO Accumulation 12, RH39), it was not among the proteins that were reduced significantly in *atcgl20ab* shotgun proteomics (Chapter 4, Fig. 5A). In contrast, the steady-state accumulation of chloroplast-encoded membrane components of PSII (*psbA/B*) and the Cyt *b6f* complex (*petB/D*) were reduced significantly. Moreover, de novo synthesis of RbcL was drastically reduced in *nara12* compared to that of D1, whereas this difference could not be observed in newly synthesized RbcL and D1 of *atcgl20ab* (Chapter 4, Fig. 5B). Finally, the specific reduction of the Cyt *b6f* and NDH complexes observed in *atcgl20ab* was not described in other mutants impaired in ribosome assembly. It is tempting to speculate that CGL20 may function in the integration of divergent LSU cpRPs that were acquired as an adaptation to cotranslational membrane targeting. Further experiments should therefore not only focus on

finding the exact binding partner of CGL20, but also investigate if membrane association of ribosome footprints, as observed in Hristou et al. (2019), might be disturbed in *atcgl20ab*.

6.4 Conclusion and future perspectives

Identification and characterization of auxiliary proteins is crucial in understanding the principles of protein complex biogenesis. As demonstrated in this thesis, large scale phylogenetic classifications such as the GreenCut2 can provide a valuable basis for the identification of factors involved in the biogenesis of chloroplast complexes. The recent advances in genome editing allow for rapid and targeted manipulation and can thus be a powerful tool in the identification of new factors, especially when combined with high throughput phenotyping techniques like chlorophyll fluorescence video imaging.

We were able to identify two new components of chloroplast-specific ATP synthase assembly: CGLD11/BFA3 is a CF₁- β chaperon presumably involved in very early steps of CF₁ assembly by shielding the hydrophobic catalytic site of the β -subunit and preventing aggregation, comparable to mitochondrial Atp11p. CGL160, additionally to its conserved role in facilitating c-ring assembly, acquired a central role in late steps of ATP synthase assembly, mediating joining of the submodules. Both factors may have evolved in the green lineage as a response to an increased regulatory control of ATP synthase activity depending on environmental cues. It has become evident that assembly and regulation are tightly interconnected, thus both aspects must be considered in order to elucidate the biogenesis of the thylakoid-bound rotary machine.

Biogenesis of thylakoid complexes like the ATP synthase is strictly dependent on the chloroplast gene expression machinery. Structural data revealed that chloroplast ribosome architecture, particularly the periphery of the LSU may have adapted as consequence of translational specialization to mostly membrane-targeted proteins of the photosynthetic machinery. The proposed role of CGL20 in late 50S assembly steps may thus have been selected for to ensure rapid biogenesis of a structural divergent LSU. The remarkable exactness of structural data provided by recent advances in cryo-EM combined with mutant analysis may help to further elucidate the mechanisms of how ribosomes are built in the chloroplast.

The general mechanisms of tightly coordinated assembly of the ATP synthase to prevent harmful intermediates and the dynamic biogenesis of ribosomes in both sequential and parallel steps remained largely unchanged. However, both pathways adapted to the structural and regulatory rearrangements following the specialization of the endosymbiont on photosynthesis. The factors presented in this thesis are examples of how those adaptations may have been achieved in the green lineage.

References for Chapters 1 and 6

- Ackerman SH** (2002) Atp11p and Atp12p are chaperones for F_1 -ATPase biogenesis in mitochondria. *Biochim Biophys Acta* **1555**: 101-105
- Ahmed T, Yin Z, Bhushan S** (2016) Cryo-EM structure of the large subunit of the spinach chloroplast ribosome. *Sci Rep* **6**: 35793
- Akiyama K, Kurotoi A, Iida K, Kuromori T, Shinozaki K, Sakurai T** (2014) RARGE II: an integrated phenotype database of Arabidopsis mutant traits using a controlled vocabulary. *Plant Cell Physiol* **55**: e4
- Allen JF** (2015) Why chloroplasts and mitochondria retain their own genomes and genetic systems: Colocation for redox regulation of gene expression. *Proc Natl Acad Sci U S A* **112**: 10231–10238
- Alonso JM, Stepanova AN, Leisse TJ, Kim CJ, Chen HM, Shinn P, Stevenson DK, Zimmerman J, Barajas P, Cheuk R, et al.** (2003) Genome-wide insertional mutagenesis of *Arabidopsis thaliana*. *Science* **301**: 653-657
- Aluru MR, Yu F, Fu A, Rodermeier S** (2006) Arabidopsis variegation mutants: New insights into chloroplast biogenesis. *J Exp Bot* **57**: 1871–1881
- Arana JL, Vallejos RH** (1982) Involvement of sulfhydryl groups in the activation mechanism of the ATPase activity of chloroplast coupling factor 1. *J Biol Chem* **257**: 1125–1127
- Archibald JM** (2015) Endosymbiosis and eukaryotic cell evolution. *Curr Biol* **25**: 911–921
- Armbruster U, Correa Galvis V, Kunz HH, Strand DD** (2017) The regulation of the chloroplast proton motive force plays a key role for photosynthesis in fluctuating light. *Curr Opin Plant Biol* **37**: 56–62
- Armbruster U, Labs M, Pribil M, Viola S, Xu W, Scharfenberg M, Hertle AP, Rojahn U, Jensen PE, Rappaport F, et al** (2013) Arabidopsis CURVATURE THYLAKOID1 proteins modify thylakoid architecture by inducing membrane curvature. *Plant Cell* **25**: 2661–2678
- Azpurua J, Ke Z, Chen IX, Zhang Q, Ermolenko DN, Zhang ZD, Gorbunova V, Seluanov A** (2013) Naked mole-rat has increased translational fidelity compared with the mouse, as well as a unique 28S ribosomal RNA cleavage. *Proc Natl Acad Sci U S A* **110**: 17350–17355
- Ballhausen B, Altendorf K, Gabriele DH** (2009) Constant c_{10} Ring Stoichiometry in the *Escherichia coli* ATP Synthase Analyzed by Cross-Linking. *J Bacteriol* **191**: 2400–2404
- von Ballmoos C, Wiedenmann A, Dimroth P** (2009) Essentials for ATP Synthesis by F_1F_0 ATP Synthases. *Annu Rev Biochem* **78**: 649–672
- Bang WY, Chen J, Jeong IS, Kim SW, Kim CW, Jung HS, Lee KH, Kweon HS, Yoko I, Shiina T, et al** (2012) Functional characterization of ObgC in ribosome biogenesis during chloroplast development. *Plant J* **71**: 122–134
- Bar-Zvi D, Shavit N** (1982) Modulation of the chloroplast ATPase by tight ADP binding. Effect of uncouplers and ATP. *J Bioenerg Biomembr* **14**: 467–478
- Barbrook AC, Howe CJ, Purton S** (2006) Why are plastid genomes retained in non-photosynthetic organisms? *Trends Plant Sci* **11**: 101-108
- Bédard J, Trösch R, Wu F, Ling Q, Flores-Pérez Ú, Töpel M, Nawaz F, Jarvis P** (2017) Suppressors of the chloroplast protein import mutant *tic40* reveal a genetic link between protein import and thylakoid biogenesis. *Plant Cell* **29**: 1726–1747
- Beligni MV, Mayfield SP** (2008) Arabidopsis thaliana mutants reveal a role for CSP41a and CSP41b, two ribosome-associated endonucleases, in chloroplast ribosomal RNA metabolism. *Plant Mol Biol* **67**: 389–401
- Bellaoui M, Keddie JS, Grussem W** (2003) DCL is a plant-specific protein required for plastid ribosomal RNA processing and embryo development. *Plant Mol Biol* **53**: 531–543

- Benz M, Bals T, Gügel IL, Piotrowski M, Kuhn A, Schünemann D, Soll J, Ankele E** (2009) Alb4 of Arabidopsis promotes assembly and stabilization of a non chlorophyll-binding photosynthetic complex, the CF₁CF₀-ATP synthase. *Mol Plant* **2**: 1410–1424
- Bieri P, Leibundgut M, Saurer M, Boehringer D, Ban N** (2017) The complete structure of the chloroplast 70S ribosome in complex with translation factor pY. *EMBO J* **36**: 475–486
- Birkenhäger R, Greie JC, Altendorf K, Deckers-Hebestreit G** (1999) F₀ complex of the *Escherichia coli* ATP synthase: Not all monomers of the subunit c oligomer are involved in F₁ interaction. *Eur J Biochem* **264**: 385–396
- Bohne A** (2014) The nucleoid as a site of rRNA processing and ribosome assembly and ribosome assembly. *Front Plant Sci* **5**: 257
- Bolle C, Huep G, Kleinbölting N, Haberer G, Mayer K, Leister D, Weisshaar B** (2013) GABI-DUPLO: A collection of double mutants to overcome genetic redundancy in Arabidopsis thaliana. *Plant J* **75**: 157–171
- Bollenbach TJ, Lange H, Gutierrez R, Erhardt M, Stern DB, Gagliardi D** (2005) RNR1, a 3′-5′ exoribonuclease belonging to the RNR superfamily, catalyzes 3′ maturation of chloroplast ribosomal RNAs in *Arabidopsis thaliana*. *Nucleic Acids Res* **33**: 2751–2763
- Bölter B, Soll J** (2016) Once upon a Time – Chloroplast Protein Import Research from Infancy to Future Challenges. *Mol Plant* **9**: 798–812
- Boyer PD** (1993) Boyer P.D. (1993). The binding change mechanism for ATP synthase - some probabilities and possibilities. *Biochim Biophys Acta* **1140**: 215–250
- Brockmann B, Koop DK, Strahl H, Deckers-Hebestreit G** (2013) Time-delayed in vivo assembly of subunit a into preformed *Escherichia coli* F₀F₁ atp synthase. *J Bacteriol* **195**: 4074–4084
- Carrillo LR, Froehlich JE, Cruz JA, Savage LJ, Kramer DM** (2016) Multi-level regulation of the chloroplast ATP synthase: the chloroplast NADPH thioredoxin reductase C (NTRC) is required for redox modulation specifically under low irradiance. *Plant J* **87**: 654–663
- Cejudo FJ, Ojeda V, Delgado-Requerrey V, González M, Pérez-Ruiz JM** (2019) Chloroplast redox regulatory mechanisms in plant adaptation to light and darkness. *Front Plant Sci* **10**: 380
- Chen GG, Jagendorf AT** (1994) Chloroplast molecular chaperone-assisted refolding and reconstitution of an active multisubunit coupling factor CF₁ core. *Proc Natl Acad Sci U S A* **91**: 11497–11501
- Chen SS, Sperling E, Silverman JM, Davis JH, Williamson JR** (2012) Measuring the dynamics of *E. coli* ribosome biogenesis using pulse-labeling and quantitative mass spectrometry. *Mol Biosyst* **8**: 3325–3334
- Chi W, He B, Mao J, Li Q, Ma J, Ji D, Zou M, Zhang L** (2012) The Function of RH22, a DEAD RNA Helicase, in the Biogenesis of the 50S Ribosomal Subunits of Arabidopsis Chloroplasts. *Plant Physiol* **158**: 693–707
- Chorev DS, Baker LA, Wu D, Beilstein-Edmands V, Rouse SL, Zeev-Ben-Mordehai T, Jiko C, Samsudin F, Gerle C, Khalid S, et al** (2018) Protein assemblies ejected directly from native membranes yield complexes for mass spectrometry. *Science* **362**: 829–834
- Connolly K, Culver G** (2009) Deconstructing ribosome construction. *Trends Biochem Sci* **34**: 256–263
- Cruz JA, Harfe B, Radkowski CA, Dann MS, McCarty RE** (1995) Molecular dissection of the epsilon subunit of the chloroplast ATP synthase of spinach. *Plant Physiol* **109**: 1379–1388
- Cruz JA, Sacksteder CA, Kanazawa A, Kramer DM** (2001) Contribution of electric field ($\Delta\psi$) to steady-state transthylakoid proton motive force (*pmf*) in vitro and in vivo. Control of *pmf* parsing into $\Delta\psi$ and ΔpH by ionic strength. *Biochemistry* **40**: 1226–1237
- Dal Bosco C, Lezhneva L, Bieh A, Leister D, Strotmann H, Wanner G, Meurer J** (2004) Inactivation of the Chloroplast ATP Synthase γ Subunit Results in High Non-photochemical Fluorescence Quenching and Altered Nuclear Gene Expression in Arabidopsis thaliana. *J Biol Chem* **279**: 1060–1069

- Daum B, Nicastro D, Austin J, Richard McIntosh J, Kühlbrandt W** (2010) Arrangement of photosystem II and ATP synthase in chloroplast membranes of spinach and pea. *Plant Cell* **22**: 1299–1312
- Davis GA, Kramer DM** (2020) Optimization of ATP Synthase c-Rings for Oxygenic Photosynthesis. **10**: 1778
- Davis JH, Tan YZ, Carragher B, Potter CS, Lyumkis D, Williamson JR** (2016) Modular Assembly of the Bacterial Large Ribosomal Subunit. *Cell* **167**: 1610–1622
- Davis JH, Williamson JR** (2017) Structure and dynamics of bacterial ribosome biogenesis. *Philos Trans R Soc Lond B Biol Sci* **372**: 1716
- Deckers-Hebestreit G** (2013) Assembly of the *Escherichia coli* F₀F₁ ATP synthase involves distinct subcomplex formation. *Biochem Soc Trans* **41**: 1288–1293
- Doolittle WF** (1973) Postmaturation cleavage of 23S ribosomal ribonucleic acid and its metabolic control in the blue-green alga *Anacystis nidulans*. *Biochem Soc Trans* **41**: 1288–1293
- Du Z, Gromet-Elhanan Z** (1999) Refolding of recombinant α and β subunits of the *Rhodospirillum rubrum* F₀F₁ ATP synthase into functional monomers that reconstitute an active $\alpha_1\beta_1$ -dimer. *Eur J Biochem* **263**: 430–437
- Duss O, Stepanyuk GA, Puglisi JD, Williamson JR** (2019) Transient Protein-RNA Interactions Guide Nascent Ribosomal RNA Folding. *Cell* **179**: 1357–1369
- Eberhard S, Loisel C, Drapier D, Bujaldon S, Girard-Bascou J, Kuras R, Choquet Y, Wollman FA** (2011) Dual functions of the nucleus-encoded factor TDA1 in trapping and translation activation of *atpA* transcripts in *Chlamydomonas reinhardtii* chloroplasts. *Plant J* **67**: 1055–1066
- Evguenieva-Hackenberg E** (2005) Bacterial ribosomal RNA in pieces. *Mol Microbiol* **57**: 318–325
- Fitin AF, Vasilyeva EA, Vinogradov AD** (1979) An inhibitory high affinity binding site for ADP in the oligomycin-sensitive ATPase of beef heart submitochondrial particles. *Biochem Biophys Res Commun* **86**: 434–439
- Foudree A, Putarjuna A, Kambakam S, Nolan T, Fussell J, Pogorelko G, Rodermeier S** (2012) The mechanism of variegation in *immutans* provides insight into chloroplast biogenesis. *Front Plant Sci* **3**: 260
- Franklin MJ, Brusilow WSA, Woodbury DJ** (2004) Determination of proton flux and conductance at pH 6.8 through single F₀ sectors from *Escherichia coli*. *Biophys J* **87**: 3594–3599
- Fristedt R** (2017) Chloroplast function revealed through analysis of GreenCut2 genes. *J Exp Bot* **68**: 2111–2120
- Fristedt R, Martins NF, Strenkert D, Clarke CA, Suchoszek M, Thiele W, Schöttler MA, Merchant SS** (2015) The Thylakoid Membrane Protein CGL160 Supports CF₁CF₀ ATP Synthase Accumulation in *Arabidopsis thaliana*. *PLoS One* **10**: e0121658
- Fristedt R, Scharff LB, Clarke CA, Wang Q, Lin C, Merchant SS, Bock R** (2014) RBF1, a Plant Homolog of the Bacterial Ribosome-Binding Factor RbfA, Acts in Processing of the Chloroplast 16S Ribosomal RNA. *Plant Physiol* **164**: 201–215
- Gilchrist E, Haughn G** (2010) Reverse genetics techniques: Engineering loss and gain of gene function in plants. *Briefings Funct Genomics Proteomics* **9**: 103–110
- Graf M, Arenz S, Huter P, Dönhöfer A, Nováček J, Wilson DN** (2017) Cryo-EM structure of the spinach chloroplast ribosome reveals the location of plastid-specific ribosomal proteins and extensions. *Nucleic Acids Res* **45**: 2887–2896
- Gotta SL, Miller Jr OL, French SL** (1991) rRNA transcription rate in *Escherichia coli*. *J Bacteriol* **173**: 6647–6649
- Groth G, Pohl E** (2001) The structure of the chloroplast F₁-ATPase at 3.2 Å resolution. *J Biol Chem* **276**: 1345–1352
- Guo H, Suzuki T, Rubinstein JL** (2019) Structure of a bacterial ATP synthase. *Elife* **8**: 1–17
- Hahn A, Vonck J, Mills DJ, Meier T, Kühlbrandt W** (2018) Structure, mechanism, and regulation of the chloroplast ATP synthase. *Science* **360**: 4318

- He J, Ford HC, Carroll J, Douglas C, Gonzales E, Ding S, Fearnley IM, Walker JE** (2018) Assembly of the membrane domain of ATP synthase in human mitochondria. *Proc Natl Acad Sci U S A* **115**: 2988–2993
- Hermolin J, Fillingame RH** (1995) Assembly of F_0 Sector of *Escherichia coli* H^+ ATP Synthase Interdependence of subunit insertion into the membrane. *J Biol Chem* **270**: 2815–2817
- Herold M, Nierhaus KH** (1987) Incorporation of six additional proteins to complete the assembly map of the 50S subunit from *Escherichia coli* ribosomes. *J Biol Chem* **262**: 8826–8833
- Hilbers F, Eggers R, Pradela K, Friedrich K, Herkenhoff-Hesselmann B, Becker E, Deckers-Hebestreit G** (2013) Subunit δ Is the Key Player for Assembly of the H^+ -translocating Unit of *Escherichia coli* F_0F_1 ATP Synthase. *J Biol Chem* **288**: 25880–25894
- Hisabori T, Sunamura EI, Kim Y, Konno H** (2013) The chloroplast ATP synthase features the characteristic redox regulation machinery. *Antioxidants Redox Signal* **19**: 1846–1854
- Hohmann-Marriott MF, Blankenship RE** (2011) Evolution of Photosynthesis. *Annu Rev Plant Biol* **62**: 515–548
- Hristou A, Gerlach I, Stolle DS, Neumann J, Bischoff A, Dünschede B, Nowaczyk MM, Zoschke R, Schünemann D** (2019) Ribosome-Associated Chloroplast SRP54 Enables Efficient Cotranslational Membrane Insertion of Key Photosynthetic Proteins. *Plant Cell* **31**: 2734–2750
- Jagendorf AT** (2002) Photophosphorylation and the chemi-osmotic hypothesis. *Photosynth Res* **73**: 215–245
- Jäkel S, Mingot JM, Schwarzmaier P, Hartmann E, Görlich D** (2002) Importins fulfil a dual function as nuclear import receptors and cytoplasmic chaperones for exposed basic domains. *EMBO J* **21**: 377–386
- Janowski M, Zoschke R, Scharff L, Martinez Jaime S, Ferrari C, Proost S, Ng Wei Xiong J, Omranian N, Musialak-Lange M, Nikoloski Z, et al** (2018) *AtRsgA* from *Arabidopsis thaliana* is important for maturation of the small subunit of the chloroplast ribosome. *Plant J* **96**: 404–420
- Jensen PE, Leister D** (2014) Chloroplast evolution, structure and functions. *F1000Prime Rep* **6**: 40
- Jeon Y, Ahn HK, Kang YW, Pai HS** (2017) Functional characterization of chloroplast-targeted RbgA GTPase in higher plants. *Plant Mol Biol* **95**: 463–479
- Junge W, Nelson N** (2015) ATP synthase. *Annu Rev Biochem* **84**: 631–557
- Kanazawa A, Ostendorf E, Kohzuma K, Hoh D, Strand DD, Sato-Cruz M, Savage L, Cruz JA, Fisher N, Froehlich JE, et al** (2017) Chloroplast ATP synthase modulation of the thylakoid proton motive force: implications for photosystem I and photosystem II photoprotection. *Front Plant Sci* **8**: 719
- Kanekatsu M, Saito H, Motohashi K, Hisabori T** (1998) The beta subunit of chloroplast ATP synthase (CF_0CF_1 -ATPase) is phosphorylated by casein kinase II. *Biochem Mol Biol Int* **46**: 99–105
- Karpowicz SJ, Prochnik SE, Grossman AR, Merchant SS** (2011) The GreenCut2 resource, a phylogenomically derived inventory of proteins specific to the plant lineage. *J Biol Chem* **286**: 21427–21439
- Kato-Yamada Y, Bald D, Koike M, Motohashi K, Hisabori T, Yoshida M** (1999) ϵ Subunit, an Endogenous Inhibitor of Bacterial F_1 -ATPase, Also Inhibits F_0F_1 -ATPase. *J Biol Chem* **274**: 33991–33994
- Keus RJA, Dekker AF, Kreuk KCJ, Groot GSP** (1984) Transcription of ribosomal DNA in chloroplasts of *Spirodela oligorhiza*. *Curr Genet* **9**: 91–97
- Khusainov I, Vicens Q, Bochler A, Grosse F, Myasnikov A, Meñetret JF, Chicher J, Marzi S, Romby P, Yusupova G, et al** (2016) Structure of the 70S ribosome from human pathogen *Staphylococcus aureus*. *Nucleic Acids Res* **44**: 10491–10504
- Kleinbölting N, Hüp G, Klötgen A, Viehöver P, Weisshaar B** (2012) GABI-Kat SimpleSearch: new features of the *Arabidopsis thaliana* T-DNA mutant database. *Nucleic Acids Res* **40**: 1211–1215

- Kleine T, Leister D** (2016) Retrograde signaling: Organelles go networking. *Biochim Biophys Acta - Bioenerg* **1857**: 1313–1325
- Kössel H, Natt E, Strittmatter G, Fritzsche E, Gozdicka-Jozefiak A, Przybyl D** (1985) Structure and expression of rRNA operons from plastids of higher plants. In *Molecular form and function of the plant genome*, L. van Vloten-Doting, G. Groot, and T. Hall, eds (Plenum Publishing Corporation), pp. 183–198
- Kol S, Majczak W, Heerlien R, van der Berg JP, Nouwen N, Driessen AJM** (2009) Subunit a of the F_1F_0 ATP Synthase Requires YidC and SecYEG for Membrane Insertion. *J Mol Biol* **390**: 893–901
- Komatsu T, Kawaide H, Saito C, Yamagami A, Shimada S, Nakazawa M, Matsui M, Nakano A, Tsujimoto M, Natsume M, et al** (2010) The chloroplast protein BPG2 functions in brassinosteroid-mediated post-transcriptional accumulation of chloroplast rRNA. *Plant J* **61**: 409–422
- Kong MM, Wang FF, Yang ZN, Mi HL** (2013) ATPG is required for the accumulation and function of chloroplast ATP synthase in Arabidopsis. *Chinese Sci Bull* **58**: 3224–3232
- Krupinska K, Melonek J, Krause K** (2013) New insights into plastid nucleoid structure and functionality. *Planta* **237**: 653–664
- Kuruma Y, Suzuki T, Ono S, Yoshida M, Ueda T** (2012) Functional analysis of membranous F_0 -a subunit of F_1F_0 -ATP synthase by *in vitro* protein synthesis. *Biochem J* **442**: 631–638
- Van Der Laan M, Bechduft P, Kol S, Nouwen N, Driessen AJM** (2004) F_1F_0 ATP synthase subunit c is a substrate of the novel YidC pathway for membrane protein biogenesis. *J Cell Biol* **165**: 213–222
- Leal-Klevezas DS, Martínez-Soriano JP, Nazar RN** (2000) Transcription and processing map of the 4.5S-5S rRNA intergenic region (ITS3) from rapeseed (*Brassica napus*) chloroplasts. *Plant Cell Rep* **19**: 667–673
- Lemaire C, Wollman F** (1989) The Chloroplast ATP Synthase in *Chlamydomonas reinhardtii*. *Biochemistry* **264**: 10235–10242
- Liu J, Zhou W, Liu G, Yang C, Sun Y, Wu W, Cao S, Wang C, Hai G, Wang Z, et al** (2015) The Conserved Endoribonuclease YbeY Is Required for Chloroplast Ribosomal RNA Processing in Arabidopsis. *Plant Physiol* **168**: 205–221
- Liu X, Yu F, Rodermel S** (2010) Arabidopsis Chloroplast FtsH, *var2* and Suppressors of *var2* Leaf Variegation: A Review. *J Integr Plant Biol* **52**: 750–761
- Maiwald D, Dietzmann A, Jahns P, Pesaresi P, Joliot P, Joliot A, Levin JZ, Salamini F, Leister D** (2003) Knock-out of the genes coding for the rieske protein and the ATP-synthase δ -subunit of Arabidopsis. Effects on photosynthesis, thylakoid protein composition, and nuclear chloroplast gene expression. *Plant Physiol* **133**: 191–202
- Majeran W, Friso G, Asakura Y, Qu X, Huang M, Ponnala L, et al.** (2012) Nucleoid-enriched proteomes in developing plastids and chloroplasts from maize leaves: a new conceptual framework for nucleoid functions. *Plant Physiol* **158**: 156–189
- Manuell AL, Quispe J, Mayfield SP** (2007) Structure of the chloroplast ribosome: Novel domains for translation regulation. *PLoS Biol* **5**: 1785–1797
- Mao J, Chi W, Ouyang M, He B, Chen F, Zhang L** (2015) PAB is an assembly chaperone that functions downstream of chaperonin 60 in the assembly of chloroplast ATP synthase coupling factor 1. *Proc Natl Acad Sci U S A* **112**: 4152–4157
- Martin W, Kowallik KV** (1999) Annotated English translation of Mereschkowsky's 1905 paper "Über Natur und Ursprung der Chromatophoren im Pflanzenreiche". *Eur J Phycol* **34**: 287–295
- Melnikov S, Ben-Shem A, Garreau De Loubresse N, Jenner L, Yusupova G, Yusupov M** (2012) One core, two shells: Bacterial and eukaryotic ribosomes. *Nat Struct Mol Biol* **19**: 560–567

- Merchant SS, Prochnik SE, Vallon E, Harris EH, Karpowicz SJ, Witman GB, Terry A, Salamov A, Fritz-Laylin LK, Meréchal-Drouard L, Marshall WF, et al.** (2007) The *Chlamydomonas* genome reveals the evolution of key animal and plant functions. *Science* **318**: 245-250
- Meurer J, Schmid LM, Stoppel R, Leister D, Brachmann A, Manavski N** (2017) PALE CRESS binds to plastid RNAs and facilitates the biogenesis of the 50S ribosomal subunit. *Plant J* **92**: 400–413
- Miller Jr OL, Hamkalo BA, Thomas Jr CA** (1970) Visualization of Bacterial Genes in Action. *Science* **169**: 392-395
- Mizushima S, Nomura M** (1970) Assembly mapping of 30S ribosomal proteins from *E. coli*. *Nature* **226**: 1214–1218
- Mulder MA, Yoshioka C, Beck AH, Bunner AE, Milligan RA, et al.** (2010) Visualizing ribosome biogenesis: parallel assembly pathways for the 30S subunit. *Science* **330**: 673-677
- Nalin CM, McCarty RE** (1984) Role of a disulfide bond in the gamma subunit in activation of the ATPase of chloroplast coupling factor 1. *J Biol Chem* **259**: 7275–7280
- Naumenko N, Morgenstern M, Rucktäschel R, Warscheid B, Rehling P** (2017) INA complex liaises the F₁F₀-ATP synthase membrane motor modules. *Nat Commun* **8**: 1237
- Navarro-Ródenas A, Carra A, Morte A** (2018) Identification of an alternative rRNA post-transcriptional maturation of 26S rRNA in the Kingdom Fungi. *Front Microbiol* **9**: 994
- Niehaus TD, Thamm AMK, De Crécy-Lagard V, Hanson AD** (2015) Proteins of unknown biochemical function: A persistent problem and a roadmap to help overcome it. *Plant Physiol* **169**: 1436–1442
- Nishimura K, Ashida H, Ogawa T, Yokota A** (2010) A DEAD box protein is required for formation of a hidden break in Arabidopsis chloroplast 23S rRNA. *Plant J* **63**: 766–777
- Nishio JN, Whitmarsh J** (1993) Dissipation of the proton electrochemical potential in intact chloroplasts. *Plant Physiol* **101**: 89-96
- Niyogi KK, Truong TB** (2013) Evolution of flexible non-photochemical quenching mechanisms that regulate light harvesting in oxygenic photosynthesis. *Curr Opin Plant Biol* **16**: 307-314
- Nowak KF, McCarty RE** (2004) Regulatory Role of the C-Terminus of the ϵ Subunit from the Chloroplast ATP Synthase. *Biochemistry* **43**: 3273–3279
- Nowak KF, Tabidze V, McCarty RE** (2002) The C-terminal domain of the ϵ subunit of the chloroplast ATP synthase is not required for ATP synthesis. *Biochemistry* **41**: 15130–15134
- Okegawa Y, Kobayashi Y, Shikanai T** (2010) Physiological links among alternative electron transport pathways that reduce and oxidize plastoquinone in Arabidopsis. *Plant J* **63**: 458–468
- Okuno D, Iino R, Noji H** (2011) Rotation and structure of F₀F₁-ATP synthase. *J Biochem* **149**: 655–664
- Ono S, Sone N, Yoshida M, Suzuki T** (2004) ATP synthase that lacks F₀a-subunit. Isolation, properties, and indication of F₀b₂-subunits as an anchor rail of a rotating c-ring. *J Biol Chem* **279**: 33409–33412
- Ort DR, Oxborough K** (1992) In situ regulation of chloroplast coupling factor activity. *Annu Rev Plant Physiol Plant Mol Biol* **43**: 269–291
- Ozaki Y, Suzuki T, Kuruma Y, Ueda T, Yoshida M** (2008) Unc1 protein can mediate ring-assembly of c-subunits of F₀F₁-ATP synthase in vitro. *Biochem Biophys Res Commun* **367**: 663-666
- Paieri F, Tadini L, Manavski N, Kleine T, Ferrari R, Morandini PA, Pesaresi P, Meurer J, Leister D** (2018) The DEAD-box RNA helicase RH50 is a 23S-4.5S rRNA maturation factor that functionally overlaps with the plastid signaling factor GUN1. *Plant Physiol* **176**: 634-648
- Pausch P, Singh U, Ahmed YL, Pillet B, Murat G, Altegoer F, Stier G, Thoms M, Hurt E, Sinning I, et al** (2015) Co-translational capturing of nascent ribosomal proteins by their dedicated chaperones. *Nat Commun* **6**: 7494

- Perez Boerema A, Aibara S, Paul B, Tobiasson V, Kimanius D, Forsberg BO, Wallden K, Lindahl E, Amunts A** (2018) Structure of the chloroplast ribosome with chl-RRF and hibernation-promoting factor. *Nat Plants* **4**: 212–217
- Pfalz J, Bayraktar OA, Prikryl J, Barkan A** (2009) Site-specific binding of a PPR protein defines and stabilizes 5' and 3' mRNA termini in chloroplasts. *EMBO J* **28**: 2042–2052
- Pícková A, Potocký M, Houštěk J** (2005) Assembly factors of F₁F₀-ATP synthase across genomes. *Proteins Struct Funct Genet* **59**: 393–402
- Pillet B, Mitterer V, Kressler D, Pertschy B** (2017) Hold on to your friends: Dedicated chaperones of ribosomal proteins: Dedicated chaperones mediate the safe transfer of ribosomal proteins to their site of pre-ribosome incorporation. *BioEssays* **39**: 1–12
- Pribil M, Labs M, Leister D** (2014) Structure and dynamics of thylakoids in land plants. *J Exp Bot* **65**: 1955–1972
- Pulido P, Zagari N, Manavski N, Gawronski P, Matthes A, Scharff LB, Meurer J, Leister D** (2018) CHLOROPLAST RIBOSOME ASSOCIATED supports translation under stress and interacts with the ribosomal 30S subunit. *Plant Physiol* **177**: 1539–1554
- Putarjunan A, Liu X, Nolan T, Yu F, Rodermeel S** (2013) Understanding chloroplast biogenesis using second-site suppressors of *immutans* and *var2*. *Photosynth Res* **116**: 437–453
- Reiland S, Messerli G, Baerenfaller K, Gerrits B, Endler A, Grossmann J, Grussem W, Baginsky S** (2009) Large-scale Arabidopsis phosphoproteome profiling reveals novel chloroplast kinase substrates and phosphorylation networks. *Plant Physiol* **150**: 889–903
- Reiter B** (2015) Characterization of novel proteins involved in the biosynthesis of the chloroplast ATP-synthase. Masterarbeit, LMU München: Fakultät für Biologie
- Renato M, Boronat A, Azcón-Bieto J** (2015) Respiratory processes in non-photosynthetic plastids. *Front Plant Sci* **6**: 496
- Reuveni S, Ehrenberg M, Paulsson J** (2017) Ribosomes are optimized for autocatalytic production. *Nature* **547**: 293–297
- Rott M, Martins NF, Thiele W, Lein W, Bock R, Kramer DM, Schöttler MA** (2011) ATP synthase repression in tobacco restricts photosynthetic electron transport, CO₂ assimilation, and plant growth by overacidification of the thylakoid lumen. *Plant Cell* **23**: 304–321
- Ruban A V.** (2015) Evolution under the sun: Optimizing light harvesting in photosynthesis. *J Exp Bot* **66**: 7–23
- Ruban A V.** (2016) Nonphotochemical chlorophyll fluorescence quenching: Mechanism and effectiveness in protecting plants from photodamage. *Plant Physiol* **170**: 1903–1916
- Rühle T, Leister D** (2015) Assembly of F₁F₀-ATP synthases. *Biochim Biophys Acta* **1847**: 849–860
- Rühle T, Razeghi JA, Vamvaka E, Viola S, Gandini C, Kleine T, Schünemann D, Barbato R, Jahns P, Leister D** (2014) The Arabidopsis protein CONSERVED ONLY IN THE GREEN LINEAGE160 promotes the assembly of the membranous part of the chloroplast ATP synthase. *Plant Physiol* **165**: 207–26
- Rühle T, Reiter B, Leister D** (2018) Chlorophyll fluorescence video imaging: A versatile tool for identifying factors related to photosynthesis. *Front Plant Sci* **9**: 55
- Sakurai T, Satou M, Akiyama K, Iida K, Seki M, Kuromori T, Ito T, Konagaya A, Toyoda T, Shinozaki K** (2005) RARGE: a large-scale database of RIKEN Arabidopsis resources ranging from transcriptome to phenome. *Nucleic Acids Res* **33**: 647–650
- Schmidt C, Beilstein-edmands V, Mohammed S, Robinson C V** (2017) Acetylation and phosphorylation control both local and global stability of the chloroplast F₁ ATP synthase. *Sci Rep* **7**: 44068
- Schmidt C, Zhou M, Marriott H, Morgner N, Politis A, Robinson CV** (2013) Comparative cross-linking and mass spectrometry of an intact F-type ATPase suggest a role for phosphorylation. *Nat Commun* **4**: 1985

- Schöttler MA, Tóth SZ, Boulouis A, Kahlau S** (2015) Photosynthetic complex stoichiometry dynamics in higher plants: Biogenesis, function, and turnover of ATP synthase and the cytochrome b6f complex. *J Exp Bot* **66**: 2373–2400
- Sessions A, Burke E, Presting G, Aux G, McElver J, Patton D, Dietrich B, Ho P, Bacwaden J, Ko C, et al.** (2002) A high-throughput Arabidopsis reverse genetics system. *Plant Cell* **14**: 2985–2994
- Shajani Z, Sykes MT, Williamson JR** (2011) Assembly of Bacterial Ribosomes. *Annu Rev Biochem* **80**: 501–526
- Sharma MR, Dönhöfer A, Barat C, Marquez V, Datta PP, Fucini P, Wilson DN, Agrawal RK** (2010) PSRP1 is not a ribosomal protein, but a ribosome-binding factor that is recycled by the Ribosome-recycling Factor (RRF) and Elongation Factor G (EF-G). *J Biol Chem* **285**: 4006–4014
- Sharma MR, Wilson DN, Datta PP, Barat C, Schlutzen F, Fucini P, Agrawal RK** (2007) Cryo-EM study of the spinach chloroplast ribosome reveals the structural and functional roles of plastid-specific ribosomal proteins. *Proc Natl Acad Sci U S A* **104**: 19315–19320
- Shi XB, Wei JM, Shen YK** (2001) Effects of sequential deletions of residues from the N- or C-terminus on the functions of ϵ subunit of the chloroplast ATP synthase. *Biochemistry* **40**: 10825–10831
- Song J, Pfanner N, Becker T** (2018) Assembling the mitochondrial ATP synthase. *Proc Natl Acad Sci U S A* **115**: 2850–2852
- Sternweis PC** (1978) The epsilon subunit of *Escherichia coli* coupling factor 1 is required for its binding to the cytoplasmic membrane. *J Biol Chem* **253**: 3123–3128
- Sternweis PC, Smith JB** (1977) Characterization of the purified membrane attachment (δ) subunit of the proton translocating adenosine triphosphatase from *Escherichia coli*. *Biochemistry* **16**: 4020–4025
- Stoppel R, Manavski N, Schein A, Schuster G, Teubner M, Schmitz-Linneweber C, Meurer J** (2012) RHON1 is a novel ribonucleic acid-binding protein that supports RNase e function in the Arabidopsis chloroplast. *Nucleic Acids Res* **40**: 8593–8606
- Strand DD, Kramer DM** (2014) "Control of non-photochemical escitonquencing by the proton circuit of photosynthesis" in *Non-Photochemical Quenching and Energy Dissipation in Plants, Algae and Cyanobacteria*, edsB. Demmig-Adams, G. Garab, W.W. Adams III, and Govindjee (Dorbrecht: Springer), 387–408. doi: 10.1021/ac950914h
- Sugimoto H, Kusumi K, Tozawa Y, Yazaki J, Kishimoto N, Kikuchi S, Iba K** (2004) The *virescent-2* mutation inhibits translation of plastid transcripts for the plastid genetic system at an early stage of chloroplast differentiation. *Plant Cell Physiol* **45**: 985–996
- Sun Y, Zerges W** (2015) Translational regulation in chloroplasts for development and homeostasis. *Biochim Biophys Acta - Bioenerg* **1847**: 809–820
- Suzuki T, Ozaki Y, Sone N, Feniouk BA, Yoshida M** (2007) The product of *uncI* gene in F_1F_0 -ATP synthase operon plays a chaperone-like role to assist c-ring assembly. *Proc Natl Acad Sci U S A* **104**: 20776–20781
- Takabayashi A, Takabayashi S, Takahashi K, Watanabe M, Uchida H, Murakami A, Fujita T, Ikeuchi M, Tanaka A** (2017) PCoM-DB Update: A Protein Co-Migration Database for Photosynthetic Organisms. *Plant Cell Physiol* **58**: e10
- Takagi D, Amako K, Hashiguchi M, Fukaki H, Ishizaki K, Goh T, Fukao Y, Sano R, Kurata T, Demura T, et al.** (2017) Chloroplastic ATP synthase builds up a proton motive force preventing production of reactive oxygen species in photosystem I. *Plant J* **91**: 306–324
- Takizawa K, Cruz J, Kanazawa A, Kramer DM** (2007) The thylakoid proton motive force *in vivo*. Quantitative, non-invasive probes, energetics, and regulatory consequences of light-induced pmf. *Biochim Biophys Acta* **1767**: 1233–1244
- Tiller N, Bock R** (2014) The translational apparatus of plastids and its role in plant development. *Mol Plant* **7**: 1105–1120

- Tiller N, Weingartner M, Thiele W, Maximova E, Schöttler MA, Bock R** (2012) The plastid-specific ribosomal proteins of *Arabidopsis thaliana* can be divided into non-essential proteins and genuine ribosomal proteins. *Plant J* **69**: 302–316
- Timmis JN, Ayliff MA, Huang CY, Martin W** (2004) Endosymbiotic gene transfer: Organelle genomes forge eukaryotic chromosomes. *Nat Rev Genet* **5**: 123–135
- Trösch R, Töpel M, Flores-Pérez Ú, Jarvis P** (2015) Genetic and physical interaction studies reveal functional similarities between ALBINO3 and ALBINO4 in *Arabidopsis*. *Plant Physiol* **169**: 1292–1306
- Turmel M, Gutell RR, Mercier JP, Otis C, Lemieux C** (1993) Analysis of the chloroplast large subunit ribosomal RNA gene from 17 *Chlamydomonas* taxa: Three internal transcribed spacers and 12 group I intron insertion sites. *J Mol Biol* **232**: 446–467
- Vamvaka E** (2016) Metabolic engineering of *Synechocystis* sp. PCC6803 for plant type pigment productions and identification of new splicing factors in *Arabidopsis thaliana*. Dissertation, LMU München: Fakultät für Biologie.
- Vojta A, Alavi M, Becker T, Hörmann F, Küchler M, Soll J, Thomson R, Schleiff E** (2004) The protein translocon of the plastid envelopes. *J Biol Chem* **279**: 21401–21405
- de Vries J, Stanton A, Archibald JM, Gould SB** (2016) Streptophyte Terrestrialization in Light of Plastid Evolution. *Trends Plant Sci* **21**: 467–476
- Walter M, Piepenburg K, Schöttler MA, Petersen K, Kahlau S, Tiller N, Drechsel O, Weingartner M, Kudla J, Bock R** (2010) Knockout of the plastid RNase e leads to defective RNA processing and chloroplast ribosome deficiency. *Plant J* **64**: 851–863
- Wang P, Dalbey RE** (2011) Inserting membrane proteins: The YidC/Oxa1/Alb3 machinery in bacteria, mitochondria, and chloroplasts. *Biochim Biophys Acta - Biomembr* **1808**: 866–875
- Wang Y, Wang C, Zheng M, Lyu J, Xu Y, Li X, Niu M, Long W, Wang D, Wang H, et al** (2016) WHITE PANICLE1, a Val-tRNA Synthetase Regulating Chloroplast Ribosome Biogenesis in Rice, Is Essential for Early Chloroplast Development. *Plant Physiol* **170**: 2110–2123
- Wang ZG, Ackerman SH** (2000) The assembly factor Atp11p binds to the β -subunit of the mitochondrial F₁-ATPase. *J Biol Chem* **275**: 5767–5772
- Wang ZG, Sheluho D, Gatti DL, Ackerman SH** (2000) The α -subunit of the mitochondrial F₁ ATPase interacts directly with the assembly factor Atp12p. *EMBO J* **19**: 1486–1493
- Westhoff P, Alt J, Nelson N, Herrmann RG** (1985) Genes and transcripts for the ATP synthase CF₀ subunits I and II from spinach thylakoid membranes. *MGG Mol Gen Genet* **199**: 290–299
- Whitfield PR, Leaver CJ, Bottomley W, Atchison B** (1978) Low-molecular-weight (4.5S) ribonucleic acid in higher-plant chloroplast ribosomes. *Biochem J* **175**: 1103–1112
- Williamson JR** (2003) After the ribosome structures: How are the subunits assembled? *RNA* **9**: 165–167
- Wittig I, Meyer B, Heide H, Steger M, Bleier L, Wumaier Z, Karas M, Schägger H** (2010) Assembly and oligomerization of human ATP synthase lacking mitochondrial subunits a and A6L. *Biochim Biophys Acta - Bioenerg* **1797**: 1004–1011
- Wu W, Liu S, Ruwe H, Zhang D, Melonek J, Zhu Y, Hu X, Gusewski S, Yin P, Small ID, et al** (2016) SOT1, a pentatricopeptide repeat protein with a small MutS-related domain, is required for correct processing of plastid 23S-4.5S rRNA precursors in *Arabidopsis thaliana*. *Plant J* **85**: 607–621
- Yamaguchi K, Von Knoblauch K, Subramanian AR** (2000) The plastid ribosomal proteins. *J Biol Chem* **275**: 28455–28465
- Yamaguchi K, Subramanian AR** (2000) The plastid ribosomal proteins. Identification of all the proteins in the 50S subunit of an organelle ribosome (chloroplast). *J Biol Chem* **275**: 28466–28482

- Yamaguchi K, Subramanian AR** (2003) Proteomic identification of all plastid-specific ribosomal proteins in higher plant chloroplast 30s ribosomal subunit. *Eur J Biochem* **270**: 190–205
- Yap A, Kindgren P, Colas Des Francs-Small C, Kazama T, Tanz SK, Toriyama K, Small I** (2015) AEF1/MPR25 is implicated in RNA editing of plastid *atpF* and mitochondrial *nad5*, and also promotes *atpF* splicing in Arabidopsis and rice. *Plant J* **81**: 661–669
- Yi L, Celebi N, Chen M, Dalbey RE** (2004) Sec/SRP requirements and energetics of membrane insertion of subunits a, b, and c of the *Escherichia coli* F₁F₀ ATP synthase. *J Biol Chem* **279**: 39260–39267
- Yu F, Liu X, Alsheikh M, Park S, Rodermeier S** (2008) Mutations in SUPPRESSOR OF VARIEGATION1, a Factor Required for Normal Chloroplast Translation, Suppress *var2*-Mediated Leaf Variegation in Arabidopsis. *Plant Cell* **20**: 1786–1804
- Zhang L, Duan Z, Zhang J, Peng L** (2016) Biogenesis factor required for ATP synthase 3 facilitates assembly of the chloroplast ATP synthase complex. *Plant Physiol* **171**: 1291–1306
- Zhang L, Pu H, Duan Z, Li Y, Liu B, Zhang Q, Li W, Rochaix JD, Liu L, Peng L** (2018) Nucleus-encoded protein BFA1 promotes efficient assembly of the chloroplast ATP synthase coupling factor 1. *Plant Cell* **30**: 1770–1788
- Zhang L, Zhou W, Che L, Rochaix JD, Lu C, Li W, Peng L** (2019) PPR protein BFA2 is essential for the accumulation of the *AtpH/F* transcript in chloroplasts. *Front Plant Sci* **10**: 446
- Zoschke R, Bock R** (2018) Chloroplast Translation: Structural and Functional Organization, Operational Control and Regulation. *Plant Cell* **30**: 745–770
- Zoschke R, Kroeger T, Belcher S, Schöttler MA, Barkan A, Schmitz-Linneweber C** (2012) The pentatricopeptide repeat-SMR protein ATP4 promotes translation of the chloroplast *atpB/E* mRNA. *Plant J* **72**: 547–558

Supplemental information – Chapter 2

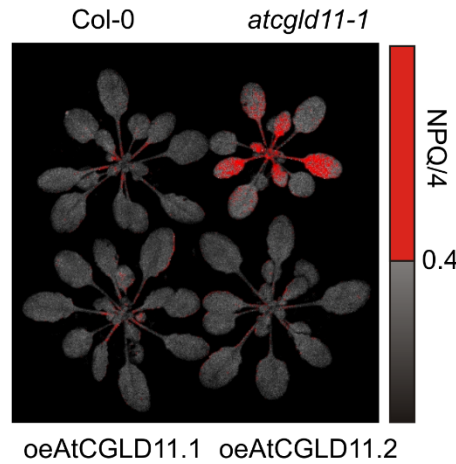
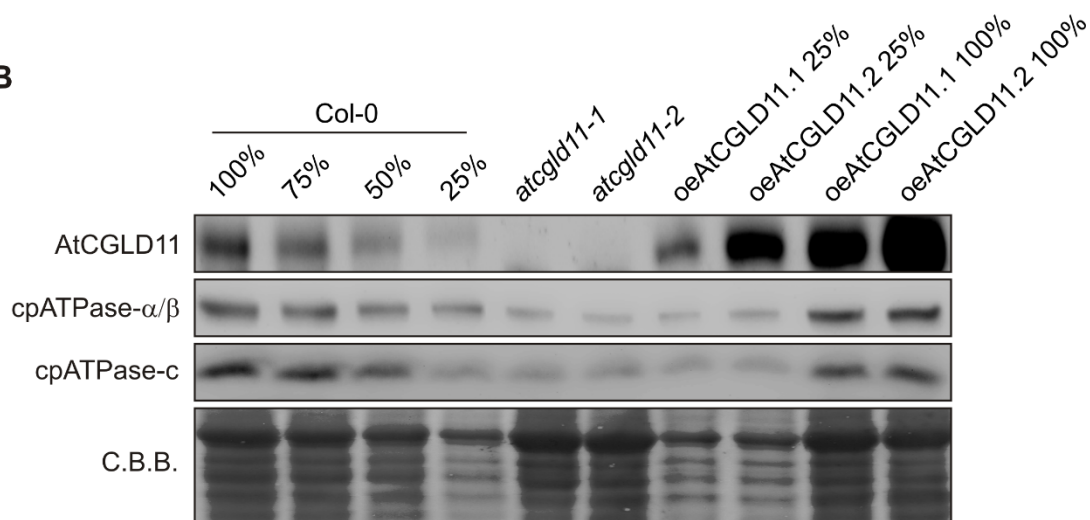
The following section contains Supplemental Figures S1 – 4 and Supplemental Table S1.

Supplemental Information

AtCGLD11	1maaispvqclfs.....cnsllhhqregsgslwrlgsrvlssslwklslfsglhlhrrrtlicavkgdpedafkktv	
<i>V. vinifera</i>	1	...mathlailslspvpayss.....ssslhfrsllpr...wtigmeklkafsssalmgyn....krrrtlicavqndaeaklfoktve	
<i>O. sativa</i>	1mstaaaaaastslrp.....asqsalrlagspr...rwcwgapalsparrafhadtr....rrktllyatdkgeeslkkktie	
<i>Z. mays</i>	1mattaaaastslrp.....lspcpriaslpr...rwcwgipvqssqrsafhaqr....rrstllcaadkapeeslkkktie	
<i>P. sitchensis</i>	1	mgpvsaifvghwlpthcfts.....slsqgilqysfpakglnqcklglsrfgrndvssflpssnrgrrkaliyagkgdvekslqstme	
<i>P. patens</i>	1msagcamasvslssrvvptvvearpvhsssrqawsrvcgsafdfgrlwapflstsssssfssrk....stvhvaassteikifktve	
<i>S. moellendorffii</i>	1matmAAAAAFAFCIRS.....S.....NGNGHWASGVVTPRPWALRIHSIAEPNLRMCSETRSN.....FCICAAAADSSQASQSSKE	
<i>C. reinhardtii</i>	1mqvgsraavcarss.....fvrvqafsscpvrvstcarvrnsacrSAAQPRQR.....PSRFVGARSELSDSLKETAADE	
<i>T. pseudonana</i>	1mrffillfthlsaclafap.....paslhtitlspstftstgsssslylsdndrrq.....srfegmqrepsq..delsi	
AtCGLD11	80	LDAMRDANPRQ.VEKIVVENI..AFDEVEFWIRLARS..TCKSEDDKKDYEEELATTVTI..DCVVKTKREK..ETSTDI..KGR..RPAIDGVE..EIS..PPRPDE	
<i>V. vinifera</i>	77	LDVMEANEAN..LQIVVENV..AFNESFWIRLARS..TCKSEDDKKDYEEELATTVTI..DRLVHKTKQK..ESATDV..KET..RPVVDEEE..EIS..PPRPDE	
<i>O. sativa</i>	76	LDAMRDANPRE..LDQIVVENV..AFDEGFWIRLARS..LCKSDDDKKDYEEELATTVTI..DRLVHKTKDEK..EQSTDV..KATISFVMHEGE..NAT..PPRPDE	
<i>Z. mays</i>	74	LDAMRDANPRE..LDQIVVENV..AFDAFGFWIRLARS..LCKSDDDKKDYEEELATTVTI..DRLVHKTKQK..EQSTDV..KATISFVMHEG..DVKK..PPRPDP	
<i>P. sitchensis</i>	88	LDKRGINEQQ..LPKIVAENI..AFDSAFMRMRARS..ELCESKDDKEDFEDR..SSLSM..MDRFVKKTTDE..ESATDI..KAT..KPKITEVDE..EIA..PPPKPE	
<i>P. patens</i>	90	LDNRSTYHN..MAQIVAENV..AFDAFWIRLARS..LCTSDDDGGEYEELASQHSI..ERIVSKTKK..ESSTDV..KATIKPLTEDDN..EIV..PPRNEA	
<i>S. moellendorffii</i>	79	LDKIRSTDSQL..LPQIVAENV..AFDSKFWIRLARS..LCKSEDDKKDYEEELASQHSI..ERIVQKTEEK..ETSTDV..MAI..EPVAGSKNEI..V..PPRPDP	
<i>C. reinhardtii</i>	74	LDKLSAKSQQLAQ..VAENV..AVDTKFWIRLARS..TAASKEDDKLQGLATS..VVL..DTVRRRT..EQQLADSGAV..QDD..VAAADDKG..EW..LPLTD	
<i>T. pseudonana</i>	72	LDTKSSAKPYELPNA..SRATRVSSPRFF..LRTAFRAAATDP..DEKERRLSA..PDNT..QAVVSMTE..DS..DERAKD..ERVVKAASEPES..GELVPLSK	
AtCGLD11	178	AINLMKREIIQ..REKEGQLDEGFLSEVNAQLRQAKESDKDKPG..LAL..CKVLQ..LYSATTI..SKRSYAKKG.....NEVVKAEE	
<i>V. vinifera</i>	175	ALSLMKEEIIQ..REKEGQLDEGFLAEVSAQLRQAKESDRDKPG..EAM..CKVLQ..DYASRV..SKRSYAKKG.....DEILKAE	
<i>O. sativa</i>	174	ALKLMKEEISNREKEGQLDEGFLSEVNAQLRQAKESGDKPG..QAM..CKVLQ..LYASNF..LQKRSYAYKG.....GEVIVPE	
<i>Z. mays</i>	171	TLKLMKEEITREKEGQLDEGFLSEVSAQLRQAKESGDKPG..QAM..CKVLQ..LYASKS..LQKRSYAYKG.....GQVVVPE	
<i>P. sitchensis</i>	186	SMILMRKELVOREKEGQLDEGFLSEVNAQLRQAKESGDKPG..VAT..CKVLQ..YASKVL..SRRSYAFKD.....GQVIKAE	
<i>P. patens</i>	183	SLIEMRREVEKRELEENFLDEGFLSEVSAQLRQAKESDKDKPG..VAT..CKVLQ..YACL..SKRSYAMKD.....GVVDKAE	
<i>S. moellendorffii</i>	178	ALQVRVRKELMHRESSGYLDGFLAEVNAQLRQAKESADKPG..LAL..CKVLQ..LYAATE..LAKTSYAKRD.....GVVDEAE	
<i>C. reinhardtii</i>	171	DQVESVRKALNRHRDR..LDGALLSNAFAALKKSSDEG..FDG..VQVLQ..LYLAARQ..AT.....GETEGVE	
<i>T. pseudonana</i>	170	ERVDAIRVEMERLEIGDLENGFLSTVDRAANKAHQG..MDSKVTHM..QVLQ..LYAGLV..SRARFQLQANVGAAISGEDQSAADAVAAAASEGDSVPNTAAS	
AtCGLD11	252	HFETLIIKAPEEQANKLFVDGLTIGKGDTIPDELSAVIKRRIERTLIRTEGSSYQQRILTEYLKIGIESRANEIMKLQG.....	similarity/ identity (%)
<i>V. vinifera</i>	249	YFETLIIKAPEEENKLLINGMTVGRGDVSPVEFYAVIKRRIERTLIRTEGSSYQQRILTEYLKIGIQSRAEEIVQVLQS.....	76/65
<i>O. sativa</i>	248	SFESVVIKAPENENKLLLDGLTVGKGNVSPPEFYAVIKRRIERTLIRTEGSSYQQRILVEYLKEIQARAEIVKVLQGPTI...	71/59
<i>Z. mays</i>	245	KFDECVIQAPENENKVLLDGLTVGKGDVSPDDLYAVIKRRIERTLIRTEGSSYQQRILVEYLKEIQARAEIVKVLQGPTI...	70/59
<i>P. sitchensis</i>	260	EFETLIIKGEDEENELLINGLTYGGEITLEDLNDVIOKRIERTLIRTEGSSYQQRILCEYLKIGILKVDDVQAFQNPQPS...	65/50
<i>P. patens</i>	262	ELPEKVMVDVEDKNDLLRNGFTYGGGEVPSDEFFKAVDRRIERTLIRTEGSSYQQRILAEYIREIEARAESPIAFAQSSPSSR...	59/44
<i>S. moellendorffii</i>	252	ELLENLISADSEADSMIRSGVDLGGGVPKSVDFRMAKRIERTLIRTEGSSYQQRILVEYLKEIERSVDMVAAFSS.....	60/47
<i>C. reinhardtii</i>	236	GANKLLGSQEKQITPLLRQLVAEG..QLTEAAMEALQKKEGVVILGQSSSYAQRVQAEYLKEAEARAKSYFQEIAASAPKQA	43/26
<i>T. pseudonana</i>	269	DLLEQLLRADTDADYEIRKGVNGEDSQCTKQDLVTEIQITVEGVILGLENSMAQRVQAEFLRELVTTRVEAV.....	36/20

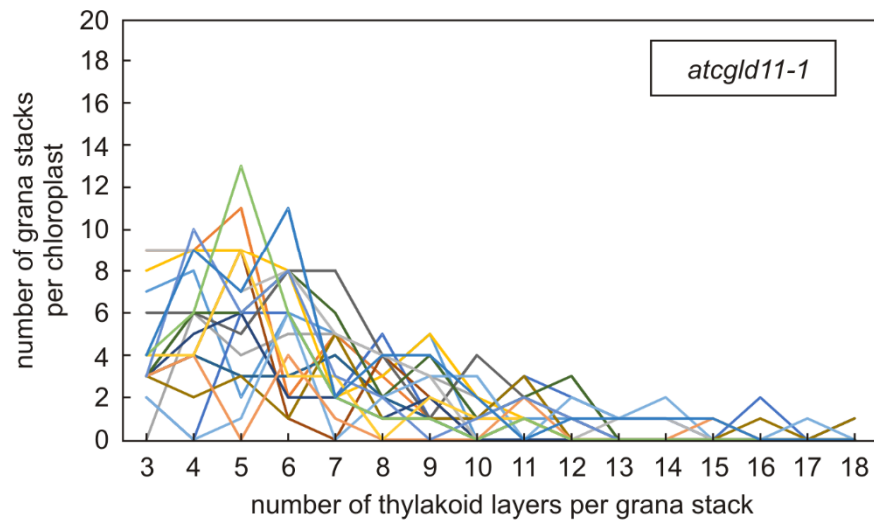
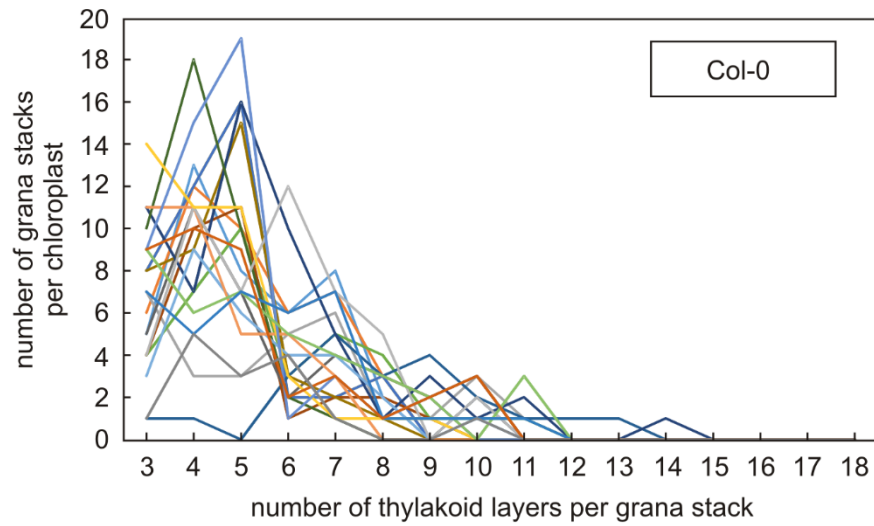
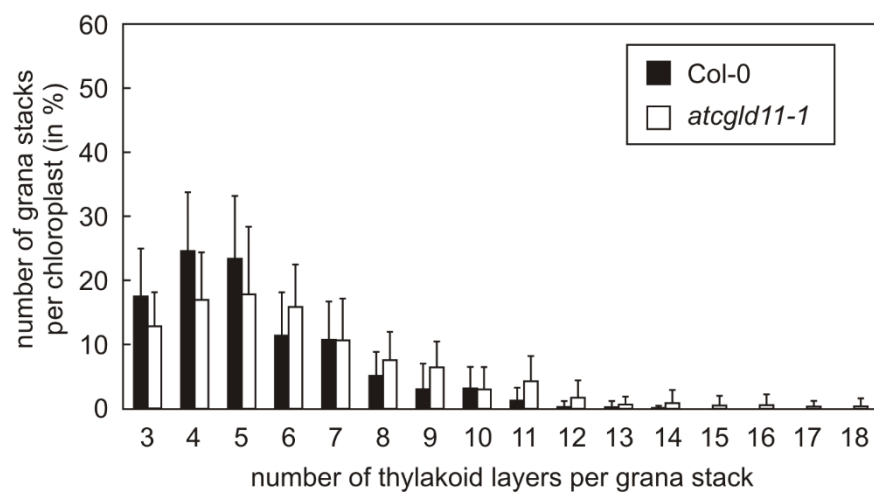
Supplemental Figure S1. Sequence alignment of AtCGLD11 (At2g21385.1) with its homologues from other eukaryotic species.

The sequence of AtCGLD11 was compared with those from grape (*Vitis vinifera*), rice (*Oryza sativa*), maize (*Zea mays*), *Picea sitchensis*, *Selaginella moellendorffii*, *Physcomitrella patens*, *Chlamydomonas reinhardtii* and *Thalassiosira pseudonana*. Transit peptides predicted by ChloroP are indicated in lowercase letters. Sequence similarity/identity is highlighted by grey/black shading. Similarity/identity scores relative to AtCGLD11 are given (in %) at the end of each protein sequence.

A**B****Supplemental Figure S2. Complementation analyses.**

(A) Two independent overexpressor lines (oeAtCGLD11.1 and oeAtCGLD11.2), WT (Col-0) and *atcgld11-1* plants were subjected to imaging PAM analyses, and NPQ/4 values were recorded in a false colour mode after a 15-min exposure to a flux of 100 $\mu\text{mol photons m}^{-2} \text{s}^{-1}$. Leaf areas exhibiting increased heat dissipation are visualized in red, with an NPQ/4 cut-off value of 0.4.

(B) Quantification of AtCGLD11 overexpression in oeAtCGLD11.1 and oeAtCGLD11.2. Serial dilutions of total WT leaf extract and extracts from the two knockout mutants *atcgld11-1* and *atcgld11-2* served as the reference and negative controls, respectively. Total leaf extracts from the two overexpressor lines were loaded in two different concentrations (25% and 100%). Chloroplast ATPase levels were examined in the two overexpressor lines by immunodetection of cpATPase- α/β and cpTPase-c. PVDF membranes were stained with Coomassie Brilliant Blue G-250 (C.B.B.).

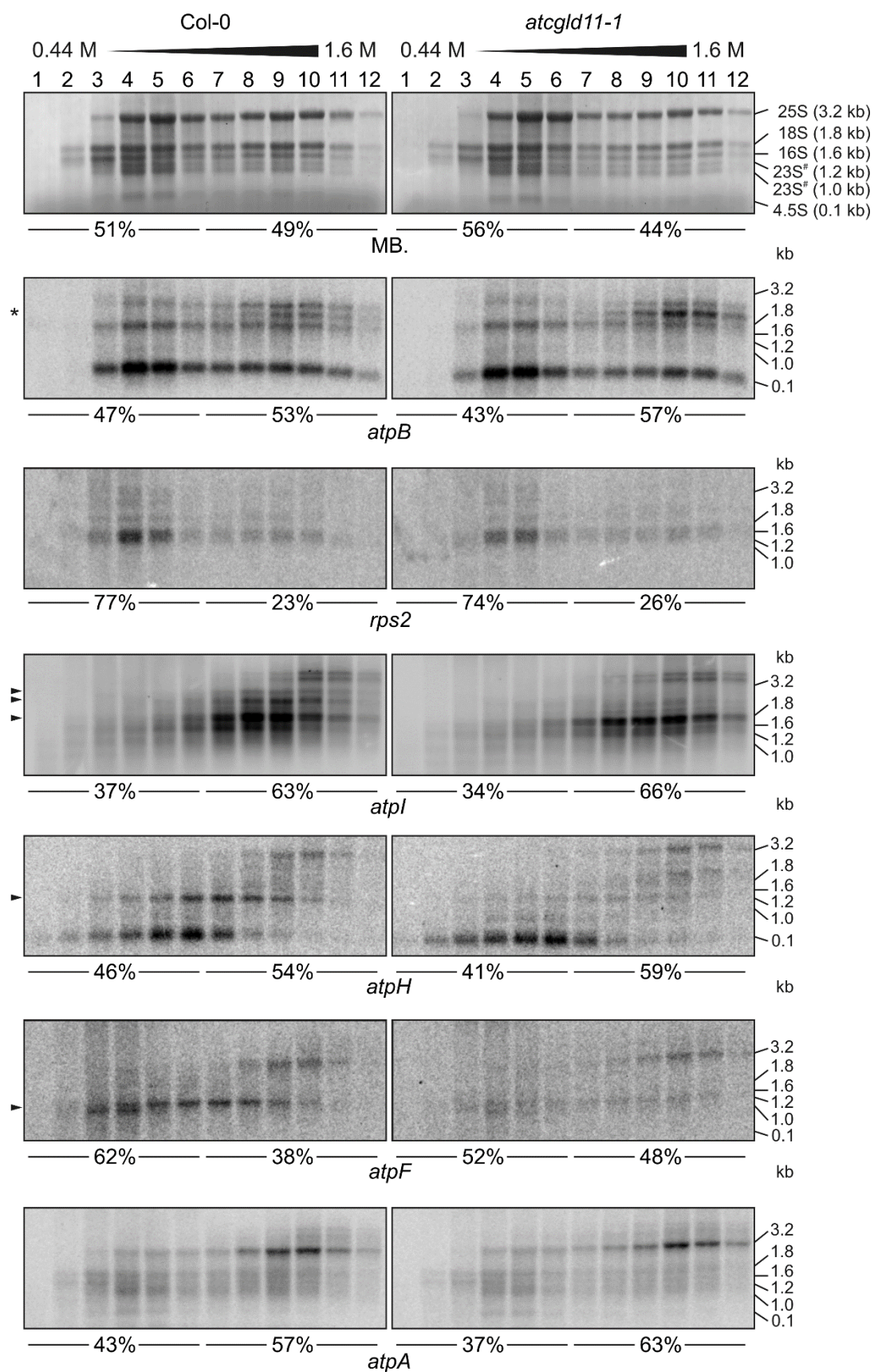
A**B**

Supplemental Figure S3. Quantification of thylakoid layers in grana stacks of Col-0 (n=21) and *atcgld11-1* (n=18) chloroplasts.

(A) Each lane represents the analysis of a single chloroplast. The number of grana stacks is plotted against the thylakoid layers per grana stack. The total number of grana stacks per chloroplast is 37.8 ± 9.6 for Col-0 and 32.9 ± 10.6 for *atcgld11-1*. The weighted means of number of thylakoid layers are 5.29 ± 0.74 (Col-0) and 6.28 ± 1.03 (*atcgld11-1*), respectively.

(B) The relative number of grana stacks (referred to the overall number of grana stacks in each chloroplast in %) versus the number of thylakoid layers per grana stack is shown for Col-0 and *atcgld11-1* samples.

(A, B) Note that variations in the calculated average and standard deviation values are also due to variations in sectional planes.



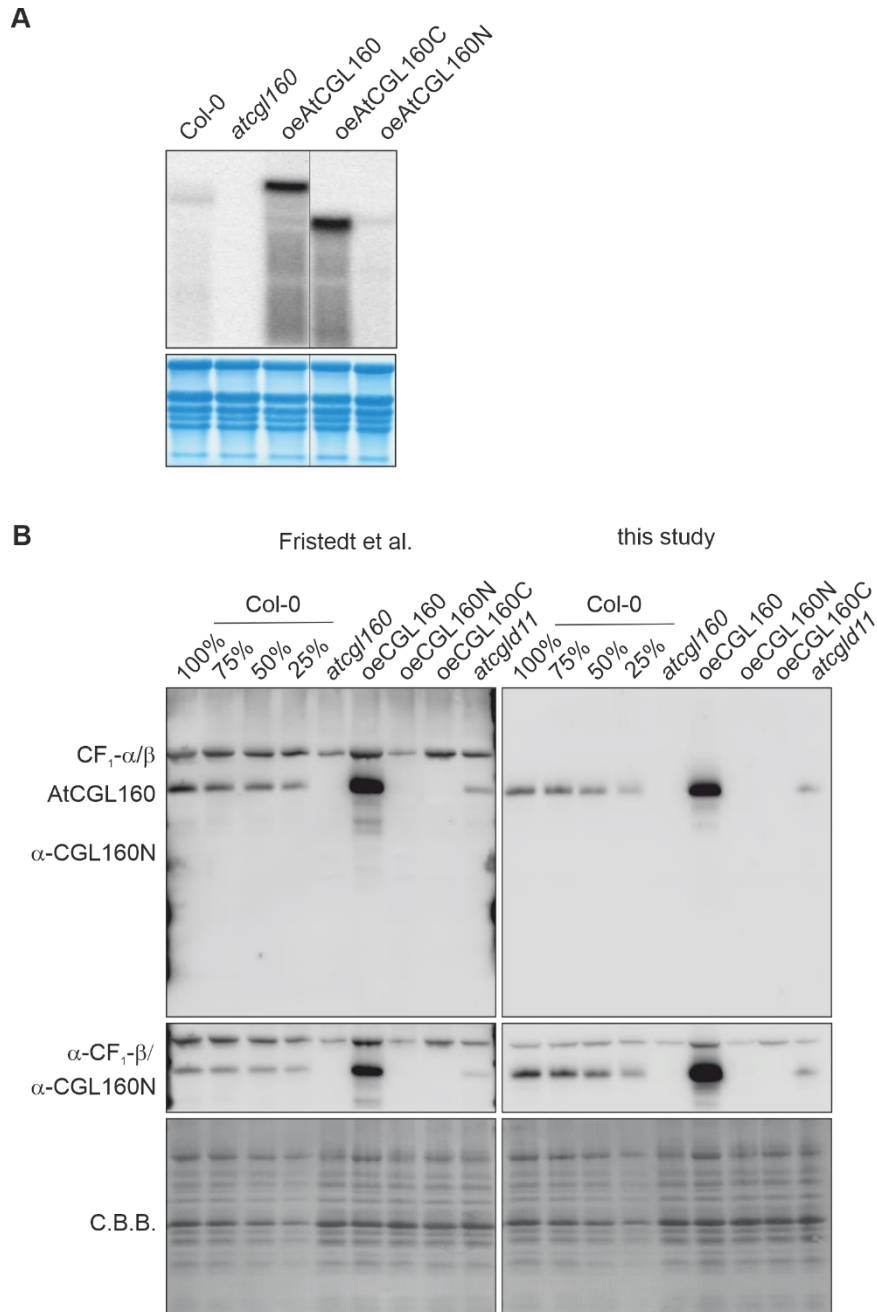
Supplemental Figure S4. Polysome association of cpATPase transcripts.

Polysome/RNA complexes were fractionated on sucrose gradients (0.44 to 1.66 M, fractions 1 to 12) and total RNA was isolated from each fraction, subjected to denaturing gel electrophoresis and blotted onto nylon membranes. Abundant rRNAs were visualised by staining with methylene blue (MB.) and used as molecular mass standards. Polysome loading of transcripts was examined by hybridizing radio-labelled probes (*atpB*, *rps2*, *atpI*, *atpH*, *atpF* and *atpA*) to size-fractionated, total RNAs. Non-associated (fraction 1-6) and polysome-associated transcripts (fraction 7-12) were quantified and corresponding percentages (relative to the total signal for fractions 1-12) are given below the corresponding lanes.

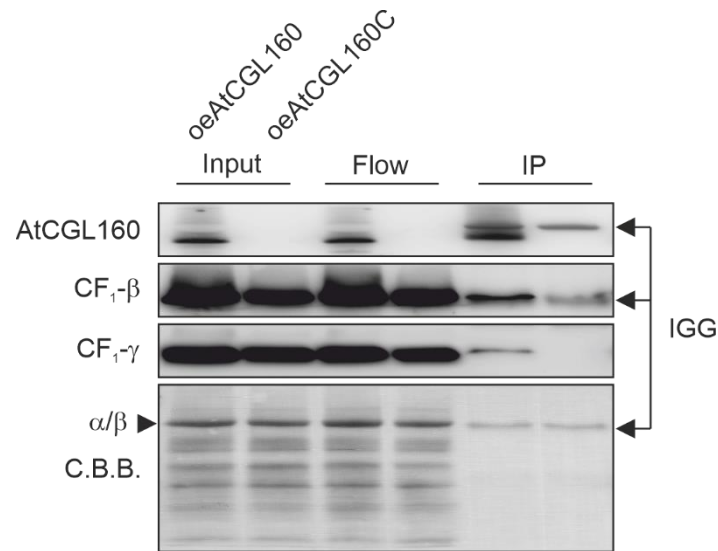
Supplemental Table S1. Primers used in this study.

Forward and reverse primer sequences (5' to 3'), the target gene and the application of each amplicon are listed. Sequence regions necessary for cloning are underlined.

Gene	Forward primer	Reverse primer	Application
<i>atcgld11-1</i> (T-DNA junction)	TTTTCCTGAAAACAATCGTC	TTGATTGCAATCTTTGGGTC	genotyping
<i>atcgld11-2</i> (T-DNA junction)	TCCGCTAATGCTTTGAATACG	TACAGTTGCAATCAGTGTGCG	genotyping
<i>AtCGLD11</i>	TCTCATCATCATCATCAACA	GCAAGGATATTTTCAACAAC	RT-PCR, Amplicon 1 (P1/P2)
<i>AtCGLD11</i>	AACCAGGGTTATTGGCTATG	CTTCAGTTGCAATCAGTGTG	RT-PCR, Amplicon 2 (P3/P4)
<i>Ubiquitin</i>	CTGTTACGGAACCC AATTC	GGAAAAAGGTCTGACCGACA	RT-PCR
<i>AtCGLD11</i>	<u>GGGGACAAGTTTGTACAAAAAGCAG</u> <u>GCTCAATGGCGGCAATATCCCCTGTT</u> CAATG	<u>GGGGACCACTTTGTACAGAAAGCT</u> <u>GGGTTTAACCCCTGGAGTAATTTCA</u>	AtCGLD11 cloning for complementation (Gateway cloning)
<i>AtCGLD11</i>	<u>CACCTCTTCGAGTCTATGGAAGCT</u>	TTAACCCCTGGAGTAATTTCA	AtCGLD11 TOPO cloning (pET151) for overexpression in <i>E. coli</i>
<i>AtCGLD11</i>	<u>ATATGTCGACATGATTGATGCTCTTA</u> GAGATGCA	<u>ATATTGCGGCCGCACCCTGGAGTAAT</u> TTCATAATTTTC	AtCGLD11 into pET51b(+) for overexpression in <i>E. coli</i>
<i>rps2</i>	AGATATTGGAACATCGATTGG	TAACATAATGACACCGAGCC	Northern probe
<i>atpA</i>	GACAGACAGACCGGTAAAC	AAACATCTCCTGACTGGGTC	Northern probe
<i>atpB</i>	TTAGGTCCTGTCGATACTCG	CCAATAAGGCGGATACCT	Northern probe
<i>atpE</i>	GTGTACTGACTCCGAATCGA	TATTGAGAGCCTCGACTCGT	Northern probe
<i>atpF</i>	TCGTTTACTTGGGTCAGTGG	TTGTTGGAAAACCCGTTTCGC	Northern probe
<i>atpH</i>	GAATCCACTGGTTTCTGCTG	AGCGCTAATGCTACAACCAG	Northern probe
<i>atpI</i>	TATCCAGTTACCTCAAGGGGAGTTA	TTAATGATGACCTCCATAGACTCA	Northern probe
<i>atpA</i>	ACAGATGGACAAATATTCTTATCCG	CAGCGGTTAATGTCTTGTA	Run-on assay
<i>atpB</i>	GCTCTGGTGGTTAAGGGTCGAG	GCAGGTGCGGGGTCAGT	Run-on assay
<i>atpE</i>	GTGTACTGACTCCGAATCGA	TATTGAGAGCCTCGACTCGT	Run-on assay
<i>atpF</i>	TCGTTTACTTGGGTCAGTGG	TTGTTGGAAAACCCGTTTCGC	Run-on assay
<i>atpH</i>	GAATCCACTGGTTTCTGCTG	AGCGCTAATGCTACAACCAG	Run-on assay
<i>atpI</i>	TATCCAGTTACCTCAAGGGGAGTTA	TTAATGATGACCTCCATAGACTCA	Run-on assay
<i>rbcl</i>	GATCTGCGAATCCCTCCTGC	CAGAGCTACTCGTTGGTACG	Run-on assay
<i>psbA</i>	CATTCAATTGCTGCTCCTCCAGTA	GAGCCTCAACAGCAGCTAGGTCT	Run-on assay
<i>AtCGLD11</i>	<u>GGTGGTCATATGCTTCGAGTCTATG</u> GAAGCT	<u>GGTCCTGAATTC</u> TTAACCCCTGGAGTA ATTTCA	yeast-two hybrid, pGBKT7 vector cloning
<i>atpA</i> (cpATPase)	<u>GGTGGTCATATG</u> GTAACCATTAGAGC CGACGA	<u>GGTCCTGAATTC</u> TTATACTTTCTCCTG AAGTA	yeast-two hybrid, pGADT7 vector cloning
<i>atpB</i> (cpATPase)	<u>GGTGGTCATATG</u> AACAACAAATCCTAC TACTTC	<u>GGTCCTGAATTC</u> TCATTTCTTCAATTT ACTCT	yeast-two hybrid, pGADT7 vector cloning
<i>ATPC</i>	<u>GGTGGTCATATG</u> GCTTCCTCTGTTTC ACCACT	<u>GGTCCTGAATTC</u> TCAAACCTGTGCAT TAGCTC	yeast-two hybrid, pGADT7 vector cloning
<i>ATPD</i>	<u>GGTGGTCATATG</u> GCCACCGCAGCAT CAAGCTA	<u>GGTCCTGAATTC</u> TCAAGTAGCTAATT GAATCT	yeast-two hybrid, pGADT7 vector cloning
<i>atpE</i>	<u>GGTGGTCATATG</u> ACCTTAAATCTTTG TGTACTGACTC	<u>GGTCCTGAATTC</u> TCAAATCGTATTGA GAGCCT	yeast-two hybrid, pGADT7 vector cloning
<i>atpA</i> (mtATPase)	<u>GGTGGTCATATG</u> GAATTATCTCCTAG AGC	<u>GGTGGTGAATTC</u> TAAATTAAGCTA AAGCTC	yeast-two hybrid, pGADT7 vector cloning
	<u>GGTGGTCATATG</u> GCGTCTCGGAGAG TCTTAT	<u>GGTGGTGAATTC</u> TTAAGCTGCTGACT CTTTAG	yeast-two hybrid, pGADT7 vector cloning



Supplemental Figure S2. AtCGL160 RNA and protein levels in oeAtCGL160, oeAtCGL160N and oeCGL160C plants. A, RNA-gel blot analysis of AtCGL160 domain-specific complementation constructs. Total RNA (20 µg) of 4-week-old Col-0, *atcgl160*, oeAtCGL160, oeAtCGL160C and oeAtCGL160N plants was separated on a denaturing formaldehyde gel and blotted on nylon membranes. Membranes were hybridized with radioactive probes specific for the *AtCGL160* cTP region. Methylene blue staining is shown as loading control. B, Comparison of the AtCGL160 antibody, generated in Fristedt et al. (2015) (AS12 1853), with the antibody generated in this study. Thylakoids of indicated genotypes were separated by denaturing SDS-PAGE and blotted onto PVDF membranes. Membranes were first probed with antibodies against AtCGL160N and then with antibodies against CF₁-β. Coomassie brilliant blue staining (C.B.B.) is shown as loading control.



Supplemental Figure S3. Immunoblot analysis of AtCGL160 coimmunoprecipitation. A, Coimmunoprecipitation with NP40 solubilized thylakoids of *oeAtCGL160* and *oeAtCGL160C* was repeated using reduced amounts of the AtCGL160 antibody. Protein A coupled magnetic beads (Dynabeads™, Thermo) with AtCGL160 antibody and coimmunoprecipitated proteins (IP) were boiled in SDS loading buffer, separated by denaturing SDS-PAGE, and blotted onto PVDF membranes. Samples before (Input) and after (Flow) incubation with AtCGL160 antibody were loaded as control. Membranes were probed with antibodies against AtCGL160N and CF₁-β/CF₁-γ, separately. Positions of the large chain of the AtCGL160 antibody are indicated (IGG). Coomassie brilliant blue staining (C.B.B.) is shown as loading control. Positions of CF₁-α/β are highlighted in the C.B.B. staining.

Supplemental Table S1. AtCGL160 coimmunoprecipitation experiments. Differential enriched proteins in oeAtCGL160 versus oeAtCGL160C sorted by log₂ fold change (-log₁₀ p-value > 1.5). Nuclear genes are written in capital letters.

Protein IDs	Gene names	log ₂ FC	-Log ₁₀ p-value
O82279	<i>AtCGL160</i>	6.495	4.644
P09468	<i>atpE</i>	6.380	2.301
Q42139	<i>ATPG</i>	5.231	4.747
P56760	<i>atpH</i>	4.886	3.176
Q9SSS9	<i>ATPD</i>	4.672	4.523
P19366	<i>atpB</i>	4.437	4.459
P56759	<i>atpF</i>	4.399	5.913
P56757	<i>atpA</i>	4.235	6.410
Q01908	<i>ATPC1</i>	4.156	4.772
Q2HIU0	<i>At3g15110</i>	3.333	3.508
P56758	<i>atpl</i>	2.799	4.104
O49445	<i>LECRK72</i>	2.346	3.115
Q67XC4	<i>TBL40</i>	2.268	2.402
Q8LCQ4	<i>LHCA6</i>	2.082	3.710
A0A1P8B288; Q39099	<i>XTH4</i>	1.983	4.126
Q41963	<i>TIP1-2</i>	1.907	2.821
O22957	<i>At2g34040</i>	1.632	2.829
Q9SRL2; Q9M9X0; F4J8G2; Q9SRL7; Q9S9U3	<i>RLP32; RLP33; RLP34; RLP35; RLP53</i>	1.564	3.162
P38418; A0A1I9LPH1	<i>LOX2</i>	1.544	2.047
Q8LBV4	<i>At1g78140</i>	1.515	2.171
F4IUJ0; F4IUI9	<i>At2g26340</i>	1.451	3.021
Q9SF53; A0A1I9LSB4; Q9M3D2	<i>RPL35A; RPL35C</i>	1.254	2.619
A0A1P8B6D0; Q9SUI4	<i>PSAL</i>	1.193	2.938
Q9FFW9; F4KBJ3	<i>At5g38520</i>	1.136	3.084
Q96242	<i>CYP74A</i>	1.078	2.371
Q9SYW8; F4K8I1	<i>Lhca2</i>	0.941	2.356
Q9SR92	<i>STR10</i>	0.839	2.913
P56777	<i>psbB</i>	0.807	2.072
Q9LHA6	<i>At3g28220</i>	0.731	2.315
Q9S7N7	<i>PSAG</i>	0.575	2.157

Supplemental Table S2. Primers used in this study.

Primer name	Primer sequence 5' to 3'	Comment
oeAtCGL160_s	GGGGACAAGTTTGTACAAAAAAGCA GGCTCA ATGGCGATTCTTAGTTACAT	Gateway primer
oeAtCGL160_as	GGGGACCACTTTGTACAAGAAAGCTG GGTTTAATCACTGGCCTGTGTGT	Gateway primer
oeAtCGL160C_s	GGGGACAAGTTTGTACAAAAAAGCAG GCTCAATGGAACAATATTTTAAGCTGAAAA	Gateway primer
TP-AtCGL160C_fus_s	GGTCCACCGGAGTTGCTCCCGAACAAT ATTTTAAGCTGAA	Fusion PCR
TP-AtCGL160C_fus_as	TTCAGCTTAAAAATATTGTTCTGGGAGCAA CTCCGGTGGACC	Fusion PCR
AtCGL160N_fusion_as	CCGTTGCAACCGGTAAAAGTCAGCCCTG TCTTTAGCAGCTTGTA	Fusion PCR
AtCGL160-MBP_s	AAAATCATTCTACCCAATAA	MBP cloning primer
AtCGL160N-MBP_as	GGTCCTGAATTCTTACCTGTCTTTAGCAG CTTGTA	MBP cloning primer
GST-AtCGL160N-s	GGGGACAAGTTTGTACAAAAAAGCAGGC TCAAAAATCATTCTACCCAATAAGAAACCTGA	Gateway primer (GST)
GST-AtCGL160N-as	GGGGACCACTTTGTACAAGAAAGCTGGG TCTTACCTGTCTTTAGCAGCTTGTAC	Gateway primer (GST)
AtCGL160cTP_probe_s	ATGGCGATTAGTTACATCTCAGC	Northern- probe
AtCGL160cTP_probe_as	GGGAGCAACTCCGGTG	Northern- probe
pGBKT7-AtCGL160N_s	GGTGGTCATATGAAAATCATTCTACCCAAT AAGA	Y2H cloning primer
pGBKT7-AtCGL160N_as	GGTCCTGAATTCTTACCTGTCTTTAGCAGCT TGTA	Y2H cloning primer
pGADT7-alpha_s	GGTGGTCATATGGTAACCATTAGAGCCGA CGA	Y2H cloning primer
pGADT7-alpha_as	GGTCCTGAATTCTTATACTTTCTCCTGAAGTA	Y2H cloning primer
pGADT7-beta_s	GGTGGTCATATGAGAACAAATCCTACTACTTC	Y2H cloning primer
pGADT7-beta_as	GGTCCTGAATTCTCATTCTTCAATTTACTCT	Y2H cloning primer
pGADT7-gamma_s	GGTGGTCATATGGCTTCTCTGTTTCACCACT	Y2H cloning primer
pGADT7-gamma_as	GGTCCTGAATTCTCAAACCTGTGCATTAG CTC	Y2H cloning primer
pGADT7-delta_s	GGTGGTCATATGGCCACCGCAGCATCAAG CTA	Y2H cloning primer
pGADT7-delta_as	GGTCCTGAATTCTCAAGTAGCTAATTGAATCT	Y2H cloning primer
pGADT7-epsilon_s	GGTGGTCATATGACCTTAAATCTTTGTGTAC TGA	Y2H cloning primer

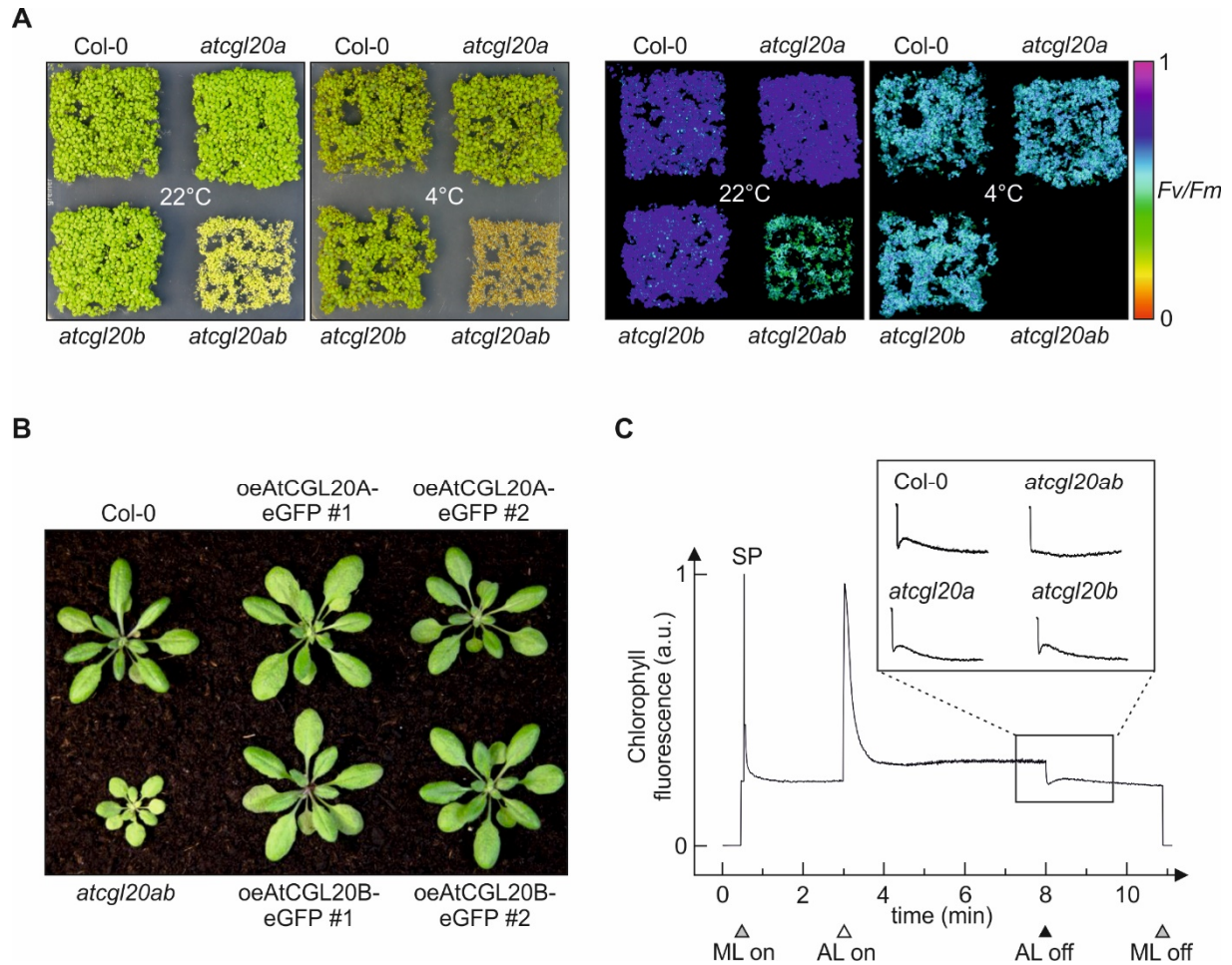
pGADT7-epsilon_as	GGTCCTGAATTCTCAAATCGTATTGAGAGCCT	Y2H cloning primer
pGADT7-atpFsoluble_s	GGTGGTCATATGTACTTTTTAAATT	Y2H cloning primer
pGADT7-atpFsoluble_as	GGTCCTGAATTCAATTAGTCA	Y2H cloning primer
pGADT7-atpGsoluble_s	GGTGGTCATATGCGCTACCTC	Y2H cloning primer
pGADT7-atpGsoluble_as	GGTCCTGAATTCAATTCTCCTTCTTGGA	Y2H cloning primer
pGADT7_AtpBI-AD_s	CGCGAATTCATGAGAACAAATCCTAC	Y2H cloning primer
pGADT7_AtpBI-AD_as	ACTCTCGAGTCAATTTCCCATATCAACCAC	Y2H cloning primer
pGADT7_AtpBII-AD_s	ATGGAATTCCCTCTAAGTGTCCAG	Y2H cloning primer
pGADT7_AtpBII-AD_as	AACCTCGAGTCAAGGTTGTAGCATAGTTG	Y2H cloning primer
pGADT7_AtpBIII-AD_s	CTAGAATTCCGAATCGTTGGCGAG	Y2H cloning primer
pGADT7_AtpBIII-AD_as	GCGCTCGAGTCATTTCTTCAATTTACTC	Y2H cloning primer
pGBKT7_AtCGL160N_del29_74_s	GACTTAATCTGGAACAGAGATTTTATGG	Y2H cloning primer
pGBKT7_AtCGL160N_del29_74_as	CATATGCAGGTCTCTCTCT	Y2H cloning primer
pGBKT7_AtCGL160N_del75_105_s	GTCTTCTGGGTTTCTGAG	Y2H cloning primer
pGBKT7_AtCGL160N_del75_105_as	GTGGAAGTAATGGGATCTTC	Y2H cloning primer
pGBKT7_AtCGL160N_del106_134_s	CGTTGTGAAAAATCGTCTTGACAC	Y2H cloning primer
pGBKT7_AtCGL160N_del106_134_as	GACTTTTCCTTTGAAGGAGATGG	Y2H cloning primer
pGBKT7_AtCGL160N_del135_160_s	GAAGCTGGCACCTACACG	Y2H cloning primer
pGBKT7_AtCGL160N_del135_160_as	CATTAGAAGACGATGCAAGCTCTTTAC TTAAATC	Y2H cloning primer
pGBKT7_AtCGL160N_del161_206_s	GAATCCCGGGGATCCG	Y2H cloning primer
pGBKT7_AtCGL160N_del161_206_as	CTATTTAGGAGACACAATAGCCTTACTC ATTTG	Y2H cloning primer

Supplemental information – Chapter 4

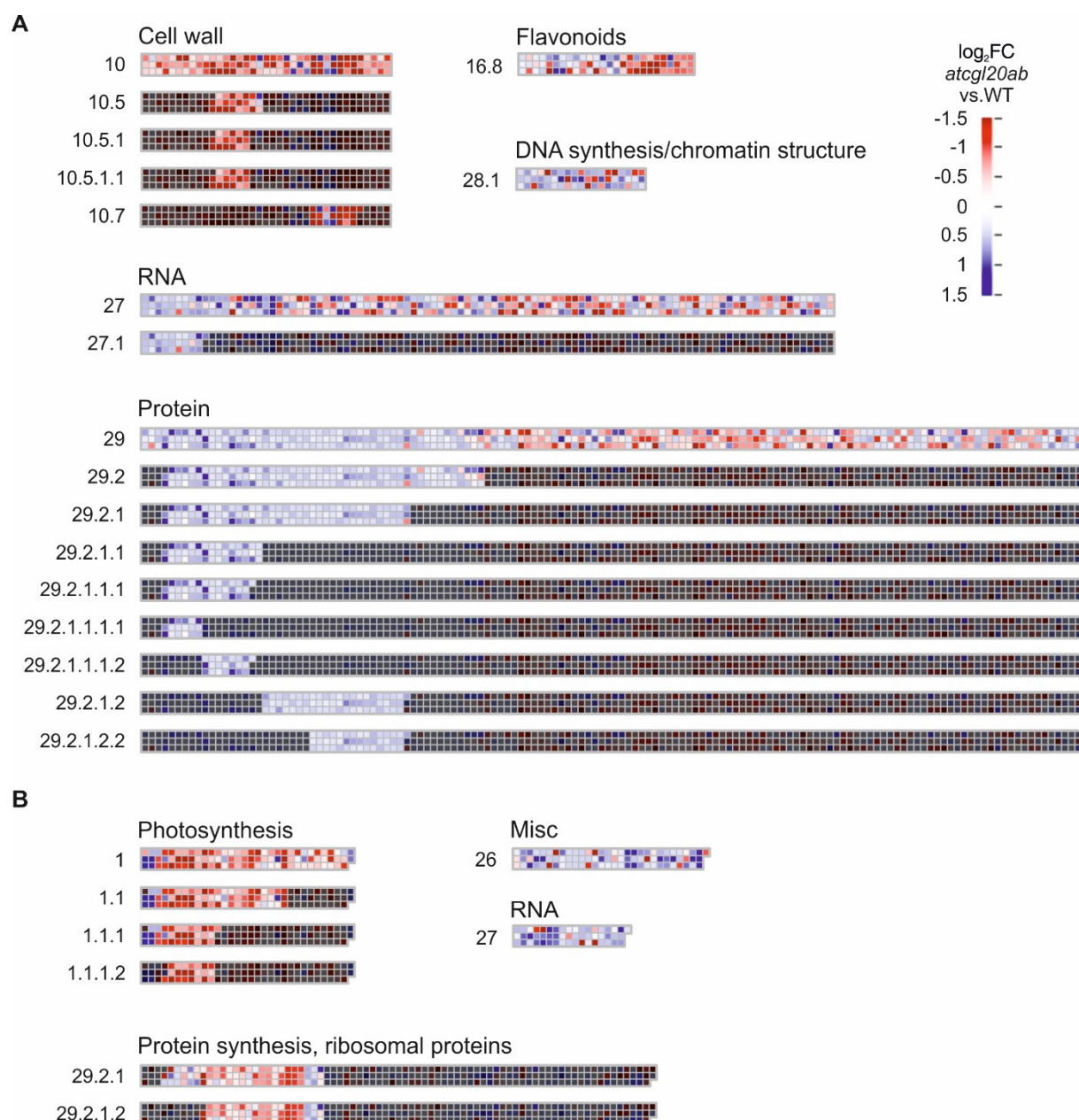
The following section contains Supplemental Figures S1 – 3 and Supplemental Tables S2, S9, S12, and S13.

Supplemental Tables S1, S3 – 8, and S10 – 11 are available online:

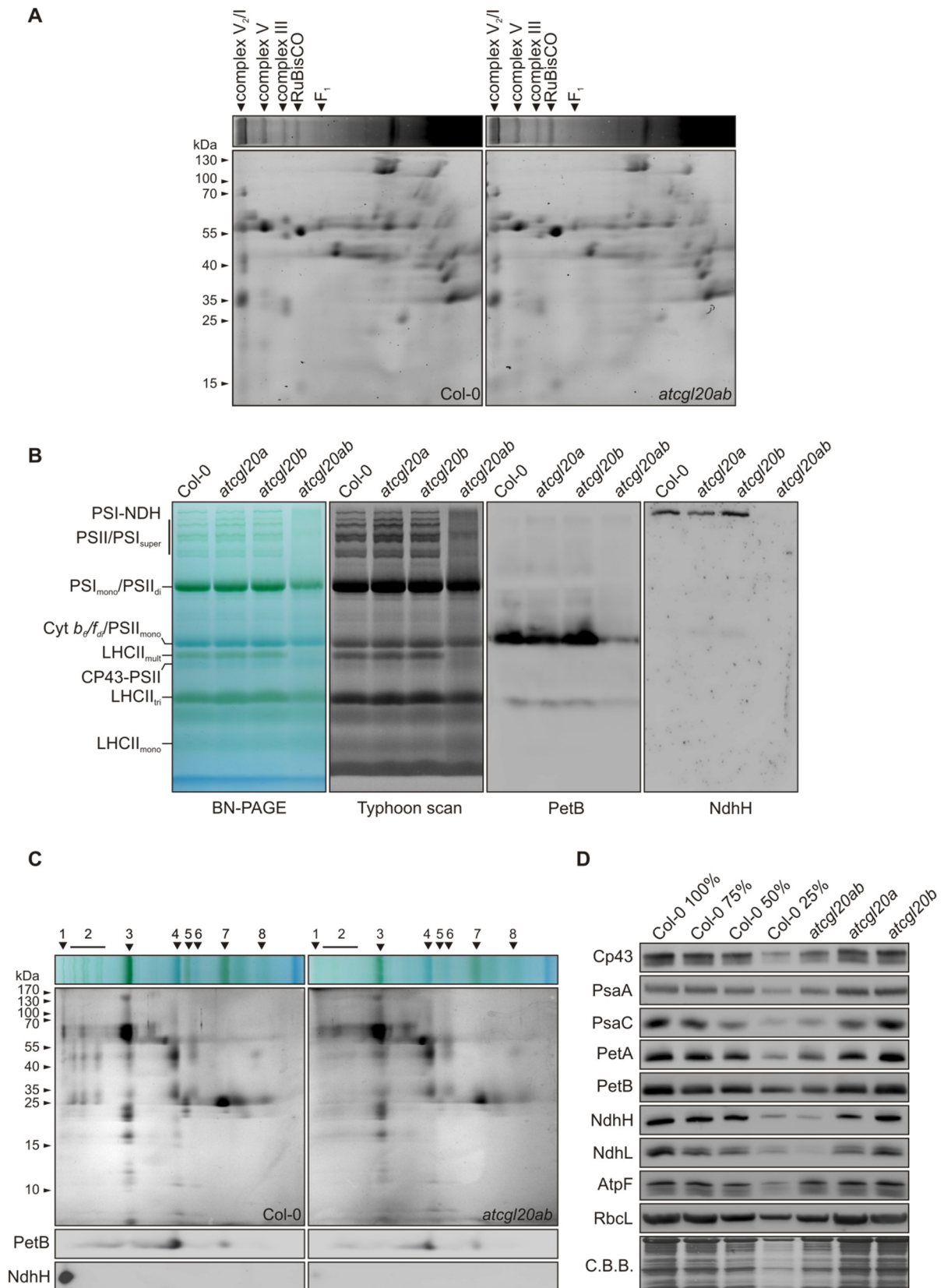
DOI: <https://doi.org/10.1104/pp.19.01502>



Supplemental Figure S1. Cold treatment, complementation and NDH activity analyses of *atcgl20* mutants. **A**, Growth and photosynthetic capacity of cold treated *atcgl20* mutant plants. Plants were germinated on Murashige and Skoog medium under ambient temperature (22 °C) and cold treatment (4 °C). Photosystem II functionality (F_v/F_m) was measured by Imaging-PAM (Walz). **B**, WT, *atcgl20ab* and complemented lines grown for six weeks under controlled climate chamber conditions. *Atcgl20ab* mutant plants were complemented with coding sequences of *AtCGL20A* and *AtCGL20B* which were fused to the 5' end of *eGFP* and under control of the constitutive 35S cauliflower mosaic virus promoter (CaMV). Two independent lines complementing the wild-type phenotype are shown. **C**, Analysis of the post illumination fluorescence rise of Col-0, *atcgl20a*, *atcgl20b* and *atcgl20ab*. Measuring light (ML), saturating pulse (SP), actinic light (AL).



Supplemental Figure S2. Graphical illustration of MapMan enrichment analyses. A, MapMan analysis of transcriptome data (*atcg120ab* vs. WT). B, MapMan analysis of proteome data (*atcg120ab* vs. WT). Each colored square represents the abundance of a single transcript (in A) or of a single protein (in B) on a $\log_2 FC$ scale. Only functional groups (bins) with significantly differently expressed terms ($p\text{-adj} < 0.05$) are displayed (see Supplemental Table 5 and 6).



Supplemental Figure S3. BN/SDS-PAGE analysis of mitochondria and thylakoid complexes. A, Coomassie brilliant blue (C.B.B.) staining of BN/SDS-PAGEs loaded with isolated mitochondria of Col-0 and *atcg120ab* plants which were solubilized with β -DM. Respiratory complexes and RuBisCO contamination are indicated according to the reference map of Arabidopsis mitochondria (www.gelmap.de/arabidopsis/). Sizes of the protein marker are

shown on the left. B, Immunoblot analysis of thylakoid membrane complexes separated on BN-PAGEs. Thylakoid membranes of Col-0, *atcgl20a*, *atcgl20b* and *atcgl20ab* were solubilized with β -DM, separated on BN-PAGEs and blotted directly on PVDF membranes, which were decorated with antibodies against PetB and NdhH. C, Immunoblot analyses of thylakoid membrane complexes separated by BN/SDS-PAGEs. After blotting, PVDF membranes were decorated with antibodies against PetB and NdhH. C.B.B. staining is shown as loading control. D, Immunoblots of selected chloroplast marker proteins. Leaf protein extracts of Col-0, *atcgl20a*, *atcgl20b* and *atcgl20ab* were separated by SDS-PAGE and blotted onto PVDF membranes. Blots were decorated with antibodies against PSII (Cp43), PSI (PsaA, PsaC), Cyt *b₆f* (PetA, PetB), NDH complex (NdhH, NdhL), the chloroplast ATP-synthase (AtpF) and RuBisCO (RbcL). C.B.B. staining is shown as loading control. Samples were adjusted to fresh weight. The bands detected in B and C were assigned to specific thylakoid protein complexes according to Armbruster et al. (2010) and Rühle et al. (2014): PSI-NAD(P)H dehydrogenase-like supercomplex (PSI-NDH = 1), PSII and PSI supercomplexes (PSII/PSI_{super} = 2), PSI monomers and PSII dimers (PSI_{mono}/PSII_{di} = 3), dimeric Cyt *b₆f* and PSII monomers (Cyt *b₆f_{di}*/PSII_{mono} = 4), multimeric LHCII (LHCII_{mult} = 5), CP43-free PSII monomers (CP43-PSII = 6), trimeric LHCII (LHCII_{tri} = 7), and monomeric LHCII (LHCII_{mono} = 8).

Supplemental Table S2. Pigment analyses of WT (Col-0), *atcgl20a*, *atcgl20b* and *atcgl20ab* leaves. Samples were harvested 4 h after beginning of the light phase (100 $\mu\text{E m}^{-2} \text{s}^{-1}$) from five-week-old plants grown under 12/12h dark/light conditions in a climate chamber. Pigments were extracted and quantified as described in Materials and Methods. Average values (n=5) and standard deviations were calculated, and values are given in pmol per mg fresh weight. VAZ, violaxanthin + antheraxanthin + zeaxanthin; n.d., not determined.

Pigment	Col-0	<i>atcgl20a</i>	<i>atcgl20b</i>	<i>atcgl20ab</i>	<i>cgl20ab/Col-0</i> (%)
Neoxanthin	28 \pm 6	23 \pm 4	29 \pm 5	11 \pm 1	39
Violaxanthin	25 \pm 5	24 \pm 5	26 \pm 4	21 \pm 1	84
Antheraxanthin	1 \pm 0	1 \pm 0	1 \pm 0	1 \pm 0	100
Zeaxanthin	0 \pm 0	0 \pm 0	0 \pm 0	0 \pm 0	n.d.
VAZ	26 \pm 6	25 \pm 6	27 \pm 5	22 \pm 2	85
Lutein	91 \pm 21	83 \pm 18	96 \pm 19	50 \pm 4	55
β -Carotene	71 \pm 15	63 \pm 9	74 \pm 11	31 \pm 2	44
Chl <i>a</i>	693 \pm 162	604 \pm 11	706 \pm 124	318 \pm 24	46
Chl <i>b</i>	218 \pm 53	185 \pm 34	226 \pm 38	92 \pm 7	42
Chl <i>a+b</i>	911 \pm 215	789 \pm 146	932 \pm 162	410 \pm 30	45
Chl <i>a/b</i>	3.19 \pm 0.07	3.26 \pm 0.03	3.13 \pm 0.02	3.44 \pm 0.04	108

Supplemental Table S9. Quantification of 23S rRNA processing products. Blots were hybridized with probes against *rnm23.1* (0.5 kb) and *rnm23.2* (3.1-1.1 kb). Signals of three technical replicates were quantified with ImageJ and normalized to the overall signal count.

23S rRNA species	WT #1	WT #2	WT #3	<i>atcg120ab</i> #1	<i>atcg120ab</i> #2	<i>atcg120ab</i> #3	<i>atcg120ab</i> /WT #1	<i>atcg120ab</i> /WT #2	<i>atcg120ab</i> /WT #3	log ₂ FC #1	log ₂ FC #2	log ₂ FC #3	Average FC	STDEV FC	P-value
3.1 kb	0.015	0.015	0.031	0.040	0.040	0.064	2.632	2.630	2.071	1.396	1.395	1.050	1.281	0.199	5.38E-02
2.9 kb	0.106	0.104	0.102	0.256	0.255	0.305	2.415	2.458	2.984	1.272	1.297	1.577	1.382	0.169	9.03E-03
2.4 kb	0.015	0.015	0.009	0.260	0.261	0.213	16.786	17.256	22.969	4.069	4.109	4.522	4.233	0.250	4.06E-03
1.8 kb	0.410	0.414	0.472	0.171	0.172	0.201	0.417	0.414	0.425	-1.263	-1.271	-1.235	-1.256	0.019	1.73E-03
1.3 kb	0.364	0.364	0.330	0.229	0.228	0.196	0.630	0.628	0.593	-0.667	-0.671	-0.754	-0.697	0.049	9.93E-04
1.1 kb	0.089	0.088	0.055	0.044	0.043	0.021	0.491	0.495	0.386	-1.025	-1.014	-1.373	-1.137	0.204	4.40E-02
0.5 kb	0.608	0.601	0.516	0.613	0.611	0.539	1.009	1.017	1.045	0.013	0.024	0.064	0.033	0.027	7.53E-01

Supplemental Table S12. Primers used in this study.

Primer name	Primer sequence 5' to 3'	Comment
atcgl20a_for	GAAGGTTCTGAATTCGAAAGG	Genotyping primer
atcgl20a_rev	ACTATCAAAACGCAAACGCAG	Genotyping primer
LBb1.3	ATTTTGCCGATTTTCGGAAC	SALK boarder primer
atcgl20b_for	TAGGAACCATCGAAGAACACG	Genotyping primer
atcgl20b_rev	AGCTTCCACTAAAGCGCTTTC	Genotyping primer
LB3	TAGCATCTGAATTTTCATAACCAATCTCGATACAC	SAIL boarder primer
atcgl20a_GW_for	GGGGACAAGTTTGTACAAAAAAGCAGGCTCAATGGCGTCGCTT TGCTCTG	Gateway primer
atcgl20a_GW_rev	GGGGACCACTTTGTACAAGAAAGCTGGGTCTTGCTGCTTCTCGG GTTGTT	Gateway primer
atcgl20a_stop_GW_rev	GGGGACCACTTTGTACAAGAAAGCTGGGTCTATTGCTGCTTCTC GGGTTGTT	Gateway primer + stop codon
atcgl20b_GW_for	GGGGACAAGTTTGTACAAAAAAGCAGGCTCAATGACGCCGCTT TCTATATC	Gateway primer
atcgl20b_GW_rev	GGGGACCACTTTGTACAAGAAAGCTGGGTTCGACCGGTTATCG GGTTG	Gateway primer
atcgl20b_stop_GW_rev	GGGGACCACTTTGTACAAGAAAGCTGGGTTCGACCGGTTATC GGGTTG	Gateway primer + stop codon
atcgl20a_qRT_for	GAATCAGCTGCAAGTTGTGTCT	qRT PCR primer
atcgl20a_qRT_rev	GGTTTAGGTCTTTCCCACTCAA	qRT PCR primer
atcgl20b_qRT_for	GCAATCCTCTCGATTTCCCTA	qRT PCR primer
atcgl20b_qRT_rev	GCAACGGTGACTTCATAGGAC	qRT PCR primer
Actin_8_for	GCAGCATGAAGATTAAGGTCGTG	qRT PCR primer
Actin_8_rev	TGTGGACAATGCCTGGACCTGCT	qRT PCR primer
probe_rn16_for	AGTCATCATGCCCTTATGC	Gel blot hybridization probe primer
probe_rn16_rev	CAGTCACTAGCCCTGCCTTC	Gel blot hybridization probe primer
probe_rn5_for	TATTCTGGTGTCTAGGCGTAG	Gel blot hybridization probe primer
probe_rn5_rev	ATCCTGGCGTCGAGCTATTTTTC	Gel blot hybridization probe primer
probe_rn23.1_for	GGAAAGGCTTACGGTGGATAC	Gel blot hybridization probe primer
probe_rn23.1_rev	CTAAGATGTTTCAGTTCGCCAGG	Gel blot hybridization probe primer
probe_rn23.2_for	GTTCGAGTACCAGGCGCTAC	Gel blot hybridization probe primer
probe_rn23.2_rev	CGGAGACCTGTGTTTTTGGT	Gel blot hybridization probe primer
probe_rn23.3_for	GGGCTGTTGCCCATTAAG	Gel blot hybridization probe primer
probe_rn23.3_rev	CTCATCTTGGGGTGGGCTTAC	Gel blot hybridization probe primer
probe_rn4.5_for	GAAGGTCACGGCGAGACGAGCC	Gel blot hybridization probe primer
probe_rn4.5_rev	GTTCAAGTCTACCGGTCTGTTAGG	Gel blot hybridization probe primer
probe_psaA_for	ACTCACATTGGACCTAGTGC	Gel blot hybridization probe primer
probe_psaA_rev	AAACTGTGGAAGCCTAGAAATATACA	Gel blot hybridization probe primer
probe_rbcL_for	CGTTGGAGAGACCGTTTCTT	Gel blot hybridization probe primer
probe_rbcL_rev	CAAAGCCCAAAGTTGACTCC	Gel blot hybridization probe primer
probe_psbA_for	CATTCAATTGCTGCTCCTCCAGTA	Gel blot hybridization probe primer
probe_psbA_rev	GAGCCTCAACAGCAGCTAGGTCT	Gel blot hybridization probe primer
probe_ndhH_for	GAGGATGTTGTTGACTGTGAACCCA	Gel blot hybridization probe primer
probe_ndhH_rev	TAAAACCCGGTGGTCGTATTTTC	Gel blot hybridization probe primer
probe_petB_for	TCGATGGTCGGCAAGTATGATGG	Gel blot hybridization probe primer
probe_petB_rev	GTGGATTGTCCAACACTAGCAC	Gel blot hybridization probe primer

Supplemental Table S13. Antibodies used in this study.

Name	Identifier	Supplier	Dilution	Product No./comment
α -AtCGL20	At2g17240/At3g24506	Biogenes	1:250-1:1000	generated in this study
α -Lhcb3	At5g54270	Agrisera	1:2000	AS01 002
α -Cp43	AtCg00280	Agrisera	1:3000	AS11 1787
α -PsaA	AtCg00350	Agrisera	1:1000	AS06 172
α -PsaC	AtCg01060	Agrisera	1:5000	AS10 939
α -PetB	AtCg00720	Agrisera	1:5000	AS18 4169
α -NdhH	AtCg01110	Toshiharu Shikanai	1:1000	
α -NdhL	At1g70760	Toshiharu Shikanai	1:1000	
α -AtpF	AtCg00130	Jörg Meurer	1:2000	
α -Csp41b	At1g09340	Rob Sharwood, David Stern	1:2000	
α -RbcL	AtCg00490	Agrisera	1:5000	AS01 017
α -Rps1	At5g30510	Agrisera	1:2000	AS15 2875
α -Rpl2	AtCg01310	Agrisera	1:2000	AS15 2876
α -CoxII	AtMg00160	Agrisera	1:1000	AS04 053A
α -Cpn60 α 1	At2g28000	Agrisera	1:1000	AS122613
α -GFP		Thermo Fisher	1:5000	A-6455

Danksagung

Für die freundschaftliche und unkomplizierte Aufnahme in seine hervorragende Arbeitsgruppe sowie für das stets entgegengebrachte Vertrauen und das Interesse an meiner Arbeit möchte ich mich herzlich bei Prof. Dr. Dario Leister bedanken!

Meine tiefe Dankbarkeit gilt PD Dr. Thilo Rühle für seine unermüdliche Begeisterung für das Vermitteln von Wissen, mit der er mich vor über 6 Jahren dazu ermutigte Teil seiner Forschung zu werden. Seither unterstützt, fördert und forderte er mich auf dem Weg, der letztlich zu dieser Dissertation führte. In dieser Zeit war er nicht nur ein hervorragender Lehrmeister, sondern auch ein Freund. Lieber Thilo, vielen Dank!

Mein herzlicher Dank gilt außerdem meinen Gutachtern, die sich bereit erklärt haben, meine Arbeit zu validieren. Insbesondere Herrn Prof. Dr. Nickelsen möchte ich danken für das Übernehmen meines Zweitgutachtens.

Ebenfalls bei Herrn Prof. Dr. Nickelsen, sowie allen weiteren Mitgliedern der Forschergruppe 2092, möchte ich mich für die herzliche Aufnahme und Unterstützung bedanken. Die gemeinsamen Treffen, geprägt von wissenschaftlicher Zusammenarbeit, ehrlichem Interesse und konstruktiver Kritik, habe ich als sehr lehrreich und angenehm empfunden. Die beiden internationalen Konferenzen auf dem wunderbaren Schloss Ringberg, auf denen es mir möglich war mit der globalen Forschungselite an einem Tisch zu sitzen, werden mir immer in Erinnerung bleiben.

Für die erfolgreiche und unkomplizierte Zusammenarbeit möchte ich mich bei meinen Kollaborationspartner(innen) und Ko-Autoren(innen), Prof. Dr. Jürgen Soll, Prof. Dr. Peter Jahns, PD Dr. Tatjana Kleine, PD Dr. Cordelia Bolle, Dr. Irene Gügel, Dr. Chiara Gandini, Dr. Sabine Bowman-Grahl, Dr. Evgenia Vamvaka, und Dr. Giada Marino bedanken. Ein besonderer Dank gilt dabei meinen Studenten, die an dieser Arbeit direkt oder indirekt beteiligt waren. Ihr wart klasse!

Der erste Stock im Gebäudeflügel F ist nun schon seit mehr als 6 Jahren mein Arbeits-Zuhause. Es lag und liegt nicht zuletzt an all den Mitarbeitern, Assistenten, Technischen Angestellten und Sekretärinnen, die mich auf dem Weg begleiteten, dass ich in dieser Zeit so gerne ins Labor gegangen bin. Vielen Dank für all die Hilfestellungen in unseren Mittwochsseminaren und Unterstützung im Labor! Mein spezieller Dank gilt dabei Angela Dietzmann, ohne deren unermüdliches Engagement wenig von unserer Arbeit im Labor möglich wäre. Vielen Dank, liebe Angie!

Ein spezielles und demütiges Dankeschön gilt außerdem unseren Gärtner(innen) Irmis, Anna, Ariel, Basti, und Ulli, die sich so hervorragend um all unsere Pflanzen kümmern und eine schier unendlich anmutende Zahl von Töpfen mit Erde bestücken. Ohne Euch wäre unsere Forschung in der Form nicht möglich. Vielen Dank, lieber Ariel für all die guten Gespräche in der Mensa oder beim Pflanzen eintüten!

Lieber Marcel, lieber Theo, unser Büro ist vielleicht nicht das ordentlichste, aber ich könnte mir kein besseres vorstellen! Danke für all die geschmacklosen Witze, Kaffee- und Teepausen, moralische Schützenhilfe, spannende Terrarien-Projekte und einfach alles was meinen Alltag als Doktorand so viel besser gemacht hat! Ich hoffe wir werden noch viele Smaragde aus dem Habachtal tragen!

Ein riesengroßes Dankeschön möchte ich meiner Familie, besonders meinen Eltern aussprechen. Vielen Dank für Eure Unterstützung und Begeisterung für meine Arbeit. Ihr habt mich immer ermutigt meinen Weg zu gehen, egal wohin er führt. Danke für alles.

Am allermeisten möchte ich meiner Frau Nicole danken. Ohne Deine Zusprache, Dein Verständnis und Deine Geduld hätte ich dieses Studium nie geschafft. Du hast immer an mich geglaubt, vor allem wenn ich an mir selbst gezweifelt habe (oft...). Ich weiß, dass wir zusammen alles meistern werden! Ich liebe Dich.

“True education is a kind of never ending story — a matter of continual beginnings, of habitual fresh starts, of persistent newness.”

— J.R.R. Tolkien —